Republic of Iraq
Ministry of Higher Education and Scientific Research
University of Babylon
College of Materials Engineering
Department of Engineering of Polymers and
Petrochemical Industries

Preparation and Characterization of Anti-bacterial Electrospun Nano fibers for Food Packaging Applications

A Thesis Submitted to the Council College of Materials Engineering / University of Babylon in Partial Fulfillment of the Requirements for the Degree of Doctorate of Philosophy in Materials Engineering / Polymer

Submitted by

Rusul Mohammed Abd Alradha Flaieh

B.Sc. Materials Engineering 2007

M.Sc. Materials Engineering/ Polymer 2011

Supervised by:

Prof. Dr. Hanaa Jawad Kadhim

Prof. Dr. Ali A. A. Al-Zubiedy

2022 A.D **1444 A.H**

وَيَرَى الَّذِينَ أُوتُوا
الْعِلْمَ الَّذِي أُنْزِلَ إِلَيْكَ
مِنْ رَبِّكَ هُوَ الْحَقَّ
وَيَهْدِي إِلَى صِرَاطِ
الْعَزِيزِ الْحَمِيدِ

٦ سبأ

Certification

We certify that we have read this Dissertation " **Preparation and Characterization of Anti-bacterial Electrospun Nano fibers for Food Packaging Applications**" and examining committee, we have examined the student (**Rusul Mohammed Abd Alradha**) in the content and that in our opinion it meets the stander of a Dissertation for the Degree of the Doctorate of Philosophy in Materials Engineering / Polymer.

Signature:
Prof. Dr. Zuhair Jabbar Abdul Ameer
Committee Chair
Date: / /2022

Signature:
Prof. Dr. Hanaa Jawad Kadhim
Committee member & Supervisor
Date: / /2022

Signature:
Prof. Dr. Ali A. Al- Zubiedy
Committee member & Supervisor
Date: / /2022

Signature:
Prof. Dr. Auda Jabbar Braihi
Committee member
Date: / /2022

Signature:
Prof. Dr. Nizar Jawad Hadi
Committee member
Date: / /2022

Signature:
Prof. Dr. Akram R. Jabur
Committee member
Date: / /2022

Signature:
Assist. Prof. Dr. Salih Abbas Habeeb
Committee member
Date: / /2022

Approval of the Department of Polymer and Engineering Petrochemical Industries Engineering
Head of Polymer and Petrochemical Industries Engineering Department

Prof. Dr. Zoalfokkar Kareem Mezaal
Date: / /2022

Approval of the Collage of Materials
Dean of Collage of Materials Engineering

Prof. Dr. Imad Ali Disher
Date: / /2022

Acknowledgement

*I Praise thank and gratitude to my lord, my path enlightener, my motivation in every step I took, I thank **ALLAH** very much and with sincere gratitude and devotion.*

I would like to express my gratitude to my supervisor Prof. Dr. Hanaa Jawad Kadhim for her guidance and advice.

I would like to thank the head of the department and all teaching staff and laboratories of materials engineering collage .

I finally would like to thank everyone in my family and every one helped me in any way possible towards completing my research work.

Rusul

2022

Dedication

I want to honor and give thanks to my mom soul for always being the infinite source of my support and power may her soul rest peacefully in heaven.

To my soulmate, my dear husband and my beloved kids for being patient and supportive during my hardest time.

To my family starting from my father, my step mother, my brothers and sisters, I want to thank you all for the encouragements and support you provided me with to finish my dissertation successfully.

I dedicate all my work to you and very greatful to have you all in my life.

Rusul

2022

Abstract

Nowadays, polymeric materials are widely used in the development of food packages, especially when increment demand for food quality and safety. So it was necessary to develop efficient packaging strategies for prolonging the shelf life of food. Meanwhile, packaging field has been focused on the production of functional materials able to reach such further protection as repression of microorganism growth, resistance to oxidation, and stability against environmental hazards. By using a new technique as electrospinning technique which different from traditional techniques.

So employing a bio-based functional layer/coating on a polymeric layer as food packaging material could be a potential way to available this protection for foods.

Hence in this thesis, the main objective was to used natural environmentally friendly materials and non- toxic solvent for purpose of sustainability and minimize the consumption of synthetic materials. Thus three parts were prepared in this thesis. The first part consists of utilization starch (ST) and cress seed mucilage (CSM) as a new source of bio macromolecules and natural polymers has piqued attention in food packaging as two separate blend with PVA (polyvinyl alcohol) which used as a spin ability aid.

Afterward, the two blend from PVA-ST-CSM were combined in various volume ratios and selected the ideal volume ratio based on the highest contact angle was (40:30:30) which was choice the basic blend to prepare the second part of nanofiber mats was strengthen by different filler additions from essential oils, such as ((moringa oil (MO), cardamom oil (CO), clove bud oil (CBO), thyme oil (TO), and fenugreek oil (FO)) in

various concentration (1, 5, and 10%). Furthermore, to another filler from walnut tree bark (WB) powder in different percentage (0.3, 0.5, 0.7 wt.%) and were examined by Field-Emission Scanning Electron Microscopy (FESEM), Wettability test, and Atomic Force Microscopy (AFM). As well as to biological tests as Anti-bacterial activity and Anti-oxidant activity.

Based on these findings was chosen the best percentage from these additions which was (10%) from essential oils and (0.5%) of (WB). These percentages was selected to prepare the third part which represent the final blend and was studied the structural and physical characteristics by (FESEM), Wettability test, Fourier Transform Infrared Spectroscopy (FTIR), Differential Scanning Calorimetry (DSC), (AFM), Ultraviolet-visible Spectrophotometer (UV), X-Ray Diffraction (XRD) and Thermogravimetric Analysis (TGA). As well as to biological tests as Anti-bacterial activity, Anti-oxidant activity and Anti-fungi activity and mechanical test such as Nano-indentation.

The results clarified that by increasing the WCA value from (74.049º to 105.358º) for basic sample and final sample respectively. While the average diameter and surface roughness increased from ((86.873 to 277.302 nm) and (159.012 to 210.046 nm) of basic and final sample respectively. In addition, the morphology of final sample consist of multi-layer strand that can fill pores of the membranes. Thus, affect on the air permeability of nanofiber web which can be considered as feasible for food packaging applications.

FTIR results showed that just physical reactions existed among the components and no chemical reactions occurred. The nanofibers of basic sample have not antibacterial and antifungal properties, while nanofibers

containing all additives (final sample) show antibacterial activity against E. coli about (37%) and S. aureus about (20%) and antifungal against candida bacteria about (18%). As well as, incorporating all additives in basic sample improved the antioxidant of the generated nanofibers. The amount of radical scavenging for the basic sample was (37%) and increasing up to (55%) for final sample. Observed the young modulus from nano-indentation test increased thus the tensile strength increasing and these properties necessary for the effective packaging to retain its shape under food loading and during their storage.

Different fruits and vegetables were packed in a plastic container and closed by nanofiber mats and without nanofiber. All samples were observed after a specific period of time which was 10 days in room temperature. The results observed that fruits and vegetables closed by nanofiber exhibited better freshness as compared to that without nanofiber. From the results of performed tests, it was observed that nanofiber mats possess enough morphological, structural, biological, mechanical and physical properties to be used as food packaging.

List of Contents

List of Figures

List of Tables

List of symbols

Symbol	***Meaning***	***Units***
ΔG_m	Gibbs energy	kJ mol^{-1}
ΔH_m	Change of enthalpy	kJ mol^{-1}
ΔS_m	Change of entropy	J/K
T	Absolute temperature	K
NIH/3T3	fibroblast cell	-
MTT	Colorimetric assay	-
TiO_2	Titanium Dioxide	-
ZnO	Zinc oxide	
D50	Median particle diameter	µm
Sa	Average Roughness	nm
Sq	Root Mean Square	nm
S_{bi}	Surface Bearing Index	-
Ssk	Surface skewness	-
Sy	Peak-to-peak	nm
Sz	Ten point height	nm
T_m	Melting Temperature	ºC
Er	Young's modulus	GPa
h.f	Residual Indentation Depth	-
CO_2	Carbon dioxide	-
K	Scherer's constant	-
β	Peak width	radian
A	Optical Density of Control	-
B	Optical Density of a Sample	-

List of Greek Symbols

Symbol	***Meaning***	***Units***
λ	X-Ray wave length	A°
θ	Bragg angle	(°)
η	Viscosity	cP
σ	Electrical Conductivity	µS/cm

List of Abbreviations

Abbreviate	***Meaning***
AEO	Angelica Essential Oil
AFM	*Atomic Force Microscopy*
Ag-NPs	Silver Nanoparticles
ASTM	American Society for Testing and Materials
CBO	Clove Bud Oil
CEO	Cinnamon Essential Oil
CI	Carbonyl Index
CMC	Carboxymethylcellulose
CMCS	Carboxymethyl Chitosan
CNPs	Chitosan Nanoparticles
CO	Cardamom Oil
CO	Chamomile Oil
CS	Chitosan
CSM	Cress Seed Mucilage
DLS	Dynamic Light Scattering
DPPH	2,2- diphenyl-1-picrylhydrazyl
DSC	Differential Scanning Calorimetry
EDX	Energy Dispersive X-Ray Analyzer
EE	Encapsulation Efficiency
EHD	Electrohydrodynamic
EOs	Essential Oils
FCNLs	Fibrous Composite Nano-Layers
FESEM	Field Emission Scanning Electron Microscopy
FO	Fenugreek Oil
FPM	Food Packaging Material
FTIR	Fourier Transform Infrared
GCEOs	Green Cardamonmum Essential Oils
GC-MS	Gas Chromatography–Mass Spectrometry
GEL	Gelatin
GRAS	Generally Recognized As Safe
^{1}H-NMR	Proton Nuclear Magnetic Resonance
HPLC	High Performance Liquid

	Chromatography
ICP-MS	Inductively Coupled Plasma Mass Spectrometry
IR	Infrared
LB	lysogeny Broth
MH	Muller–Hinton
MO	Moringa Oil
W_{loss}	Weight Loss
N/CEO	Nanophytosomes Cinnamon Essential Oil
NFs	Nanofibers
NMR	Nuclear Magnetic Resonance
O/W	Oil-in-Water
OR	Black Pepper Oleoresin
PAN	Polyacrylonitrile
PCL	polycaprolactone
PDI	Polydispersity Index
PE	Polyethylene
PEG	poly(ethylene glycol)
PEO	Poly(ethylene oxide)
PET	Poly (ethylene terephthalate)
PLA	Polylactic acid
PO	Peppermint Oil
PP	Polypropylene
PPC	poly (propylene carbon)
PPE	Pomegranate Peel Extract
PU	*Polyurethane*
PVA	Polyvinyl alcohol
PVAc	polyvinyl acetate
PVC	Polyvinyl chloride
PVP	Polyvinylpyrrolidone
RSA	Radical-Scavenging Activity
SD	Sodium Dehydroacetate
SEM	Scanning Electron Microscopy
SNF	Starch Nanofiber
STA	Corn Starch
T	Temperature
TEM	Transmission Electron Microscopy
TEO	Thyme Essential Oil

TGA	Thermogravimetric Analysis
TO	Thyme Oil
TP	Tea Polyphenol
UNHT	Ultra Nano Hardness Tester
US	United States
US-FDA	United States Food and Drug Administration
UV	Ultraviolet
UV–vis	Ultraviolet-visible
WB	Walnut Bark
WCA	Water Contact Angle
XRD	X-Ray Diffraction
β-CD	β-cyclodextrin

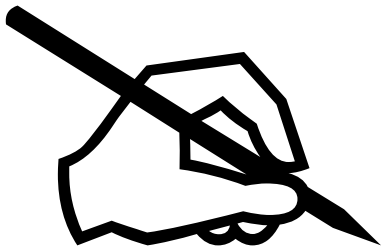

CHAPTER ONE

INTRODUCTION

1.1 Introduction

Food packaging materials (FPM) have an essential role in the food supply chain, such as in storage, handling, transport and protection of food from external contamination and product preservation. Thus it is necessary to attend to their demands by developing novel, cost-effective, eco-friendly and versatile materials and processes for protecting and monitoring the quality of food products, guaranteeing food safety and improving the traceability of products [1].

Most of the food contamination and physical harm occur during transportation. Thus, food packaging plays an integral role in extending the shelf-life of a product without compromising its quality. In addition to protecting and providing safe and nutritious food, minimizing food losses and preventing microbes are the characteristics of a good packaging material [2].

In general, the primary aims of food packaging involve the following aspects: (1) suppression of microorganism growth, resistance to oxidation, and stability against environmental hazards; (2) masking of unpleasant odors and preservation of flavor and (3) acting as carriers of biosensors for detection [3].

Many parameters are involved in maximizing food preservation, for example, improving the barrier properties of the packaging materials used. Several materials have been produced toward these goals to provide an effective barrier against oxygen, water vapor, and carbon dioxide [4].

This packaging not only can provide protection but also can be named active. Active packaging is enhancing of the protection function of traditional food packaging. It is designed to include a component that permits the absorption or release of substances from the packaged food or the environment surrounding the food. Thus, active packaging can be defined as a system in which the product, the package and the

environment interact to extend the shelf-life and improve the condition of packaged food to achieve some characteristics that cannot be obtained otherwise [5].

Materials currently used for food packaging are mostly non-biodegradable petrochemical-based plastics, one of the leading causes of environmental issues [6].

Nowadays, natural and edible materials are drawing more and more attention in the food packaging field due to their environment-friendly and biodegradable characteristics, as well as the effective controlling of the surface microbial by applying directly to the surface of food [7].

However, for the functional packaging materials applied in the food field, some additional features must be considered, such as degradable, superhydrophobic, edible, antibacterial and high barrier. In this regard, in the last decade, there has been a growing demand given to the extension of shelf-life of food, product safety, environmental issues, and cost-efficiency. For this purpose, many different material systems have been developed and exploited to fabricate high-efficiency food packaging materials. In recent years, particular interest has been given to the electrospinning technique for preparing nanostructured food packaging materials or the surface functionalization of the packaging materials with functional electrospun nanofibers [8].

Electrospinning has been known since the 1930s', but its applications in the food science field are new. Electrospinning exhibits several advantages over other production methods, such as (1) the relative ease of use, facile and cost-effective method for production of nanofibers. (2) easy incorporation of bioactive compounds into nanofibers. (3) a decreased size requirement for bioactive compounds, allowing their incorporation into food systems without affecting the sensory qualities of

products; and (4) the absence of heat during the electrospinning process, which can be of the key importance, especially for sensitive compounds.

In addition, nanofibers produced by electrospinning possess various structural and functional merits, such as submicron to nanoscale diameters, high surface to volume ratio, suitable porosity, tunable fiber diameters and high encapsulation efficiency for bioactive compounds. Under these structural advantages, the bioactive compounds encapsulated in electrospun fibers exhibit enhanced stability and bioavailability and can achieve targeted delivery and sustained release [9].

Based on these advantages, electrospinning showed potential application in the field of food science as shown in figure (1.1). Furthermore, electrospinning is a promising technique for fabricating active packaging materials or producing nanostructured layers for food packaging Fig. (1.2), which has applications ranging from controlling microbial growth to inhibiting oxidative degradation reactions to achieving targeted biocatalysis. Apart from these applications, a less explored potential application of electrospun fibers is as filtration membranes in food and beverage processing. Regarding the matrixes for encapsulation of bioactive compounds in the food industry, food-grade polymers (proteins and polysaccharides) are of great interest because they are nontoxic, biocompatible, biodegradable, renewable, and sustainable [10, 11].

The development of functional packaging materials based on electrospinning technology has become a hot spot in the food packaging field. Different approaches for preparing functional electrospun fiber will be introduced, and their applications to functional package materials will be described in Figure (1.3) [12].

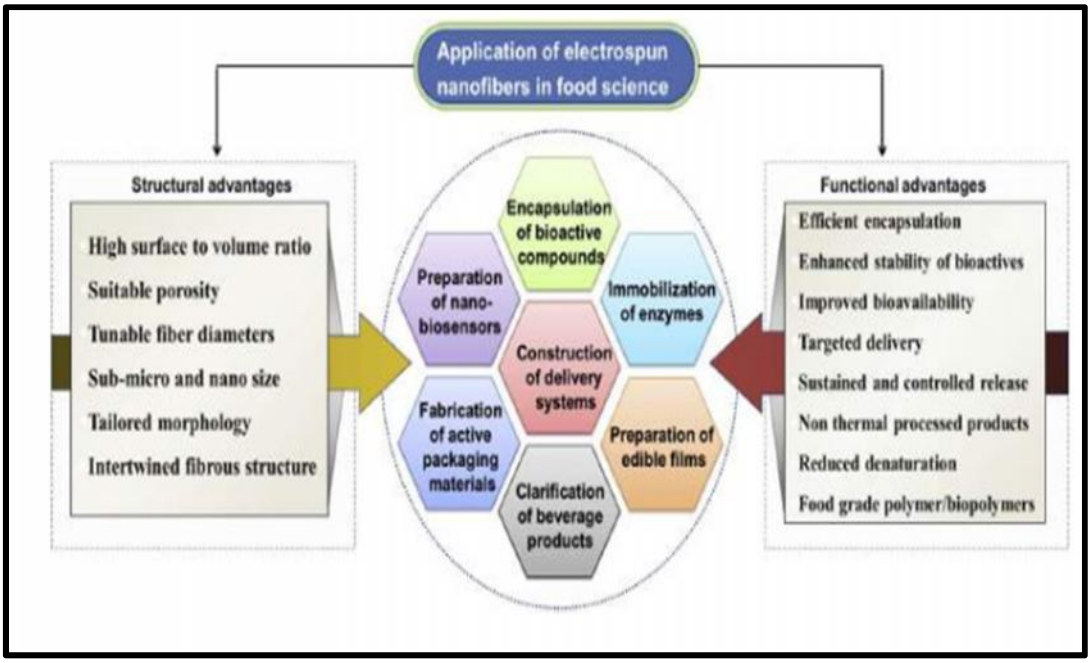

Figure (1.1): A diagram of the advantages and applications of electrospun nanofibers in food science [10].

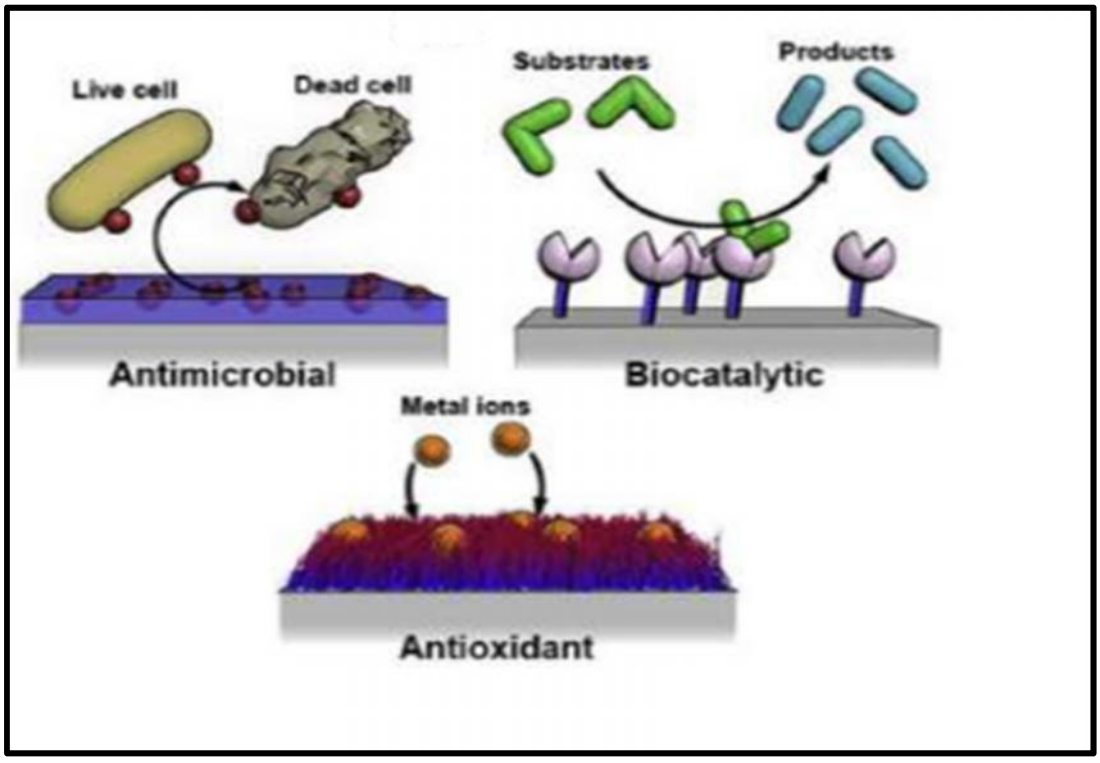

Figure (1.2): Schematics of significant types of active food packaging [10, 11].

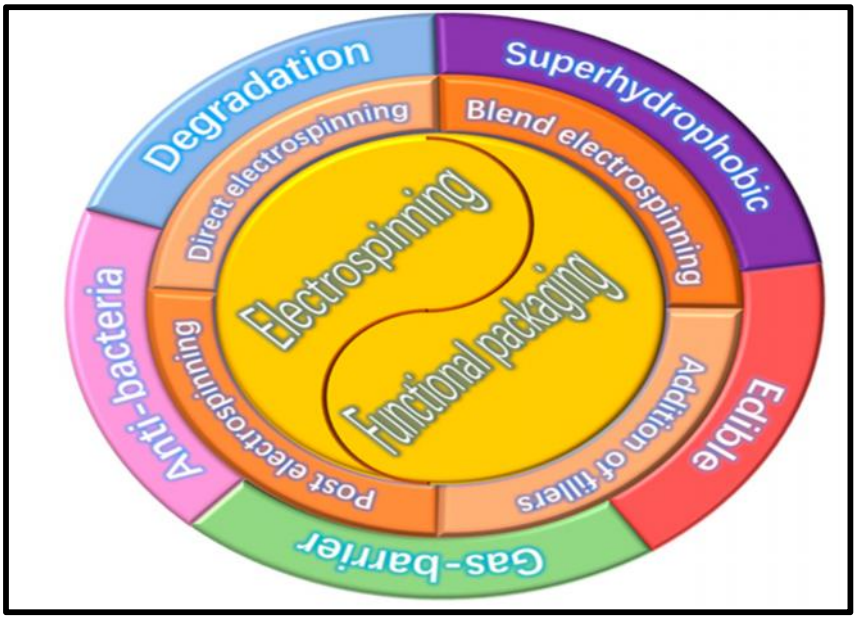

Figure (1.3): Overview of functional electrospun and food packaging materials diagram [12].

1.2 Aims of The Thesis

1-Create nanofiber mats for food packaging from natural and synthetic biopolymeric blend by electrospinning technique and selecting the best blending bio-nanofiber.

2-Explore newer aspects of natural, environmentally friendly materials for sustainability and minimize the consumption of synthetic materials, such as essential oils and walnut tree bark powder to improve the antibacterial, antioxidant, and hydrophobic properties suitable for active food packaging.

1.3 Thesis Layout

This thesis consists of the following chapters:

Chapter One: Is an introduction about food packaging and nanofibers used in this packaging, as well as, the aim of this thesis.

Chapter Two: Focus on the nanotechnology in food packaging, nanofibers production methods, especially electrospinning process, electrospinning methods, the used materials and literature review.

Chapter Three: Introduces the experimental work, which involves the used materials, procedure of sample processing according to ASTM standards and test equipment selected.

Chapter Four: Covers the results and discussion of the experimental work.

Chapter Five: Summarizes the work conclusions and gives some suggestions for future work.

Additionally, references as well as Arabic abstract are included.

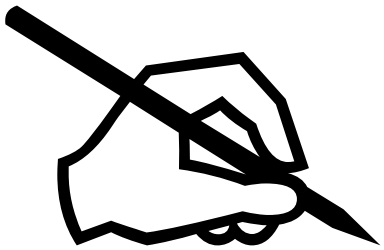

CHAPTER TWO

THEORETICAL PART AND LITERUTURE REVIEW

2.1 Introduction

Nanotechnology is the emerging revolution having great potential in every sectors from mechanics to medicine including food industry [13]. In the food industry, nanotechnology is playing a crucial role as a promising technology for solving problems via innovative solutions that relate to food safety, food processing, food packaging Fig. (2.1) as well as functional foods. Among these, the application of nanotechnology to food packaging has taken more attention due to the enhancement of food product quality and safety. In this regard, nanotechnology can improve food packaging that provides safer, healthier, high-quality foods with increased shelf life without affecting the sensory and physical characteristics of the food products [14].

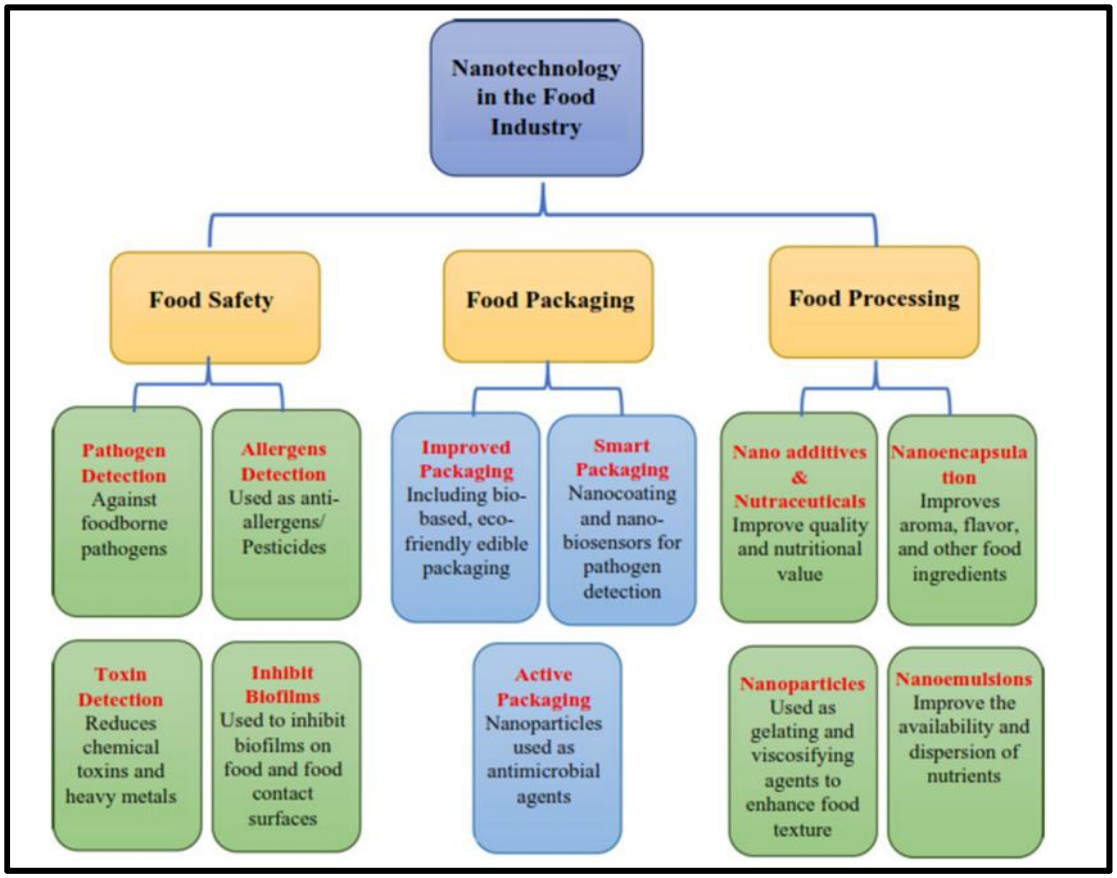

Figure (2.1): The application of nanotechnology in food safety, food packaging and food processing [14].

Nanomaterials are materials that can be in the form of powder or liquid solution that present significantly different physical and chemical properties at nanoscales compared to their micro size that contains the same chemical composition. Nanomaterials are assorted into different types based on their particle size, structure, and characteristics. Accordingly, nanomaterials classifications include nanoparticles, nanocapsules, nanoclays, nanoemulsions, nanotubes, nanofibers, and nanolaminates. Each of these nanomaterials has potential applications in the food industry and can be made via several methods [14,15].

Electrospinning is a technique used to develop fibers of metals, ceramic, composites and polymers of few microns to nanoscale range by aligning the fibers [16].

Currently, the electrospun polymer nanofibers have become important in a wide range of applications due to the unique properties of nanofibers which have high surface area, high porosity, and superior mechanical, electrical, and chemical properties. Electrospinning is a direct extension of electrospraying, which is also termed electrohydrodynamic (EHD) spray, which was first patented in 1902 by Morton and Cooley who both invented methods which were able to disperse fluids by using electrostatic forces [17].

The main difference between electrospinning and electrospraying is that continuous fibers are formed in electrospinning, whereas small droplets are produced in electrospraying. To simplify this process and understand its basic principle, let’s imagine a spherical droplet of a liquid with low molecular weight held in a vacuum [18].

Two opposite forces appeared in Fig.(2.2) will effect on this droplet: the electrostatic force and the surface tension. The first one considered as a repulsive force tries to deform the droplet shape, while the other struggles to keep the spherical shape of the droplet. The charge

increases, by increasing the strength of the electric field, to a critical point where the electrostatic force overcomes the surface tension; then the droplet breaks up to smaller droplet in a process named as electrospraying. When higher molecular weight solution is used, ultrafine fibers will form due to the sufficient chain entanglements of the polymer solution which lead to a steady get formation rather than droplets, and the process is then called electrospinning [19,20].

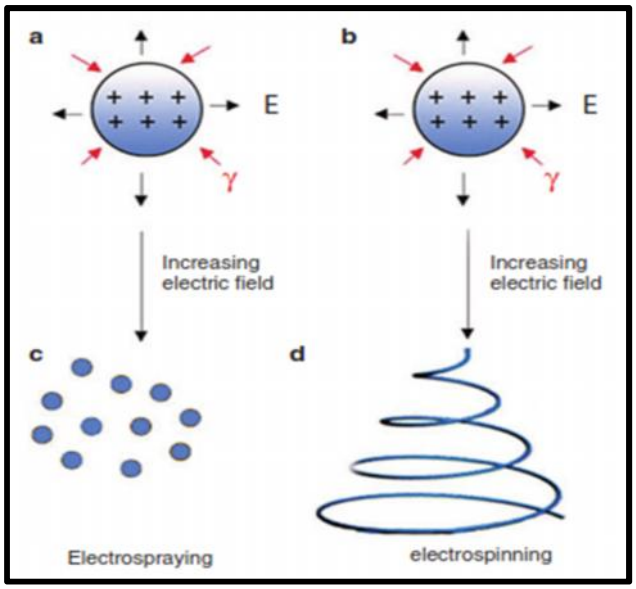

Figure (2.2): Phenomena of electrospraying and electrospinning: when the electrostatic repulsive forces overcome the surface tension of the liquid, the droplet (a) disintegrates into smaller droplets and fiber (b, c), respectively [19].

2.2 Electrospinning Process

There are a number of different processing techniques that can be used for fabrication of nanofibers, like drawing, template synthesis, phase separation, self-assembly and electrospinning. Table (2.1) shows the comparison of these techniques for the production of nanofibers [21].

An additional unique synthetic method, electrostatic spinning (electrospinning), has received much attention lately. This process was patented by Antonin Formhals in 1934 and has recently become an

attractive method for the preparation of polymeric and composite nanofibers [22].

Electrospinning, the simple and flexible fiber forming technique that utilizes electrical instead of mechanical forces to draw fibers out of a polymer solution or melt. Unlike conventional methods of spinning fibers that rely on mechanical forces, electrospinning yields these fibers by electrostatic forces. This enables formation of nonwoven fiber mats having high surface to volume ratio due to the small fiber sizes and therefore favors the increased nano effects, which include increased surface reactivity, high strength to weight ratio, higher thermal conductivity and improved mechanical properties [23].

Fiber formation during electrospinning occurs in three stages: (1) polymer jet initiation and extension; (2) whipping instability; and (3) polymer jet solidification and collection. A Taylor cone is usually observed in the first stage as electrostatic force overcomes surface tension forces. When the applied voltage overcomes the polymer solution's opposing surface charge, the polymer jets out of the solution, elongates and whips due to charge instabilities and ultimately gets collected on the plate. As the polymer jet bends randomly, it forms a conical shape and is directed towards the oppositely-charged collecting plate [24].

In electrospinning, one can use polymers, polymer blends, sol-gels and ceramic precursors to obtain nanofibers and different structures such as core-shell, hollow, ribbon-like, porous and aligned nanofibers can be produced. Electrospinning is superior to other methods with its relatively low cost, high production rate and simplicity. In addition to unique properties of nanofibers, electrospun nanofibers are easily functionalized with nanoparticles, additives, bioactive agents; therefore, multifunctional electrospun nanofibers can be produced [25].

Table (2.1):- Comparison between methods for nanofibers production [21].

Methods	Advantages	Disadvantages
Drawing	• Simple process • Wide selection of materials	• Difficult to form fibers with constant diameter • Limitation of dimensions of the fibers and arrangement
Template synthesis	• The diameters of the resulting fibers are monodisperse • Easy to change the diameter using different models	• Complex process • Limitation of dimensions of the fibers and arrangement
Phase separation	• Simple equipment is required • Three-dimensional arrangement of pores	• Long production time • Only for selective polymers • Lack of control of fiber arrangement
Self-assembly	• Easy to obtain smaller nanofibers • Three-dimensional arrangement of Pores	• Long preparation time • Lack of control of fiber orientation and arrangement
Electrospinning	• Simple and cost effective • Can be applied to various materials • Produces long fibers, continuous and randomly distributed • Applicable to industrial production	• Instability of the jet

2.3 The Basic Setup for Electrospinning

The primary electrospinning apparatus consists of three major components: a high-voltage power supply which creates an electrical field between a positively-charged syringe needle and a grounded collector, a syringe pump, and a grounded target to deposit the resultant fibers. Figure (2.3) shown a schematic illustration of the typical electrospinning set-up [26].

The basic principle of electrospinning relies on formation of nanofibers through electric field. The solution in a syringe is pumped through the outlet of the spinneret at a controlled rate by means of syringe

pump. At the same time, high voltage in 10-30 kV range is applied from high voltage power supply; molecules within the solution are charged and create a repulsive force; this results in deformation of drop in cone-shaped named as Taylor cone. When threshold voltage value is surpassed, the repulsive force overcomes the surface tension of the solution and polymer jet is formed in the tip of spinneret. While aforementioned jet going towards the grounded collector, the solvent evaporates and nanofibers are collected on the collector [27,28].

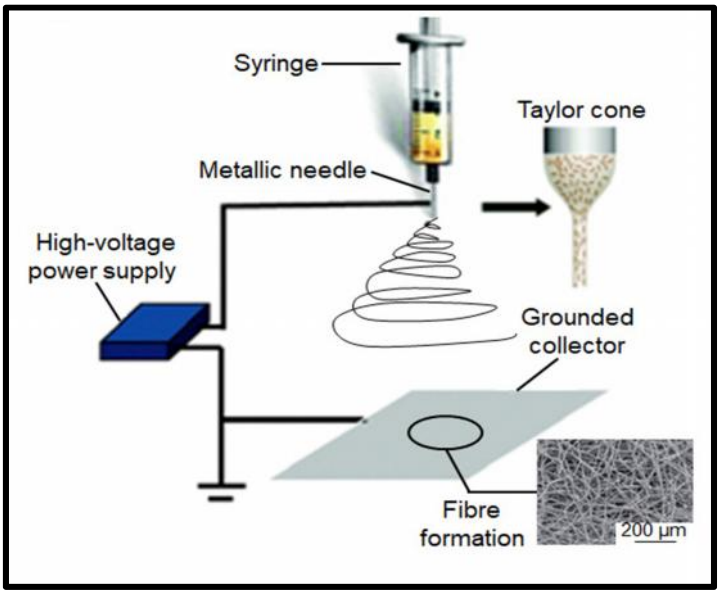

Figure (2.3): Schematic illustration of the typical electrospinning set-up [26].

2.4 Factors Influencing on Electrospinning Process

Electrospinning process strongly depends on several parameters as shown in figure (2.4), which can be divided into three main groups: solution parameters (concentration, molecular weight, viscosity, surface tension, and conductivity), processing parameters (applied voltage, feed flow rate, types of collectors, tip to collector distance) and ambient parameters (humidity, temperature). All of these parameters directly affect the generation of smooth and bead-free electrospun fibers. Therefore must be controlled on these parameters [29].

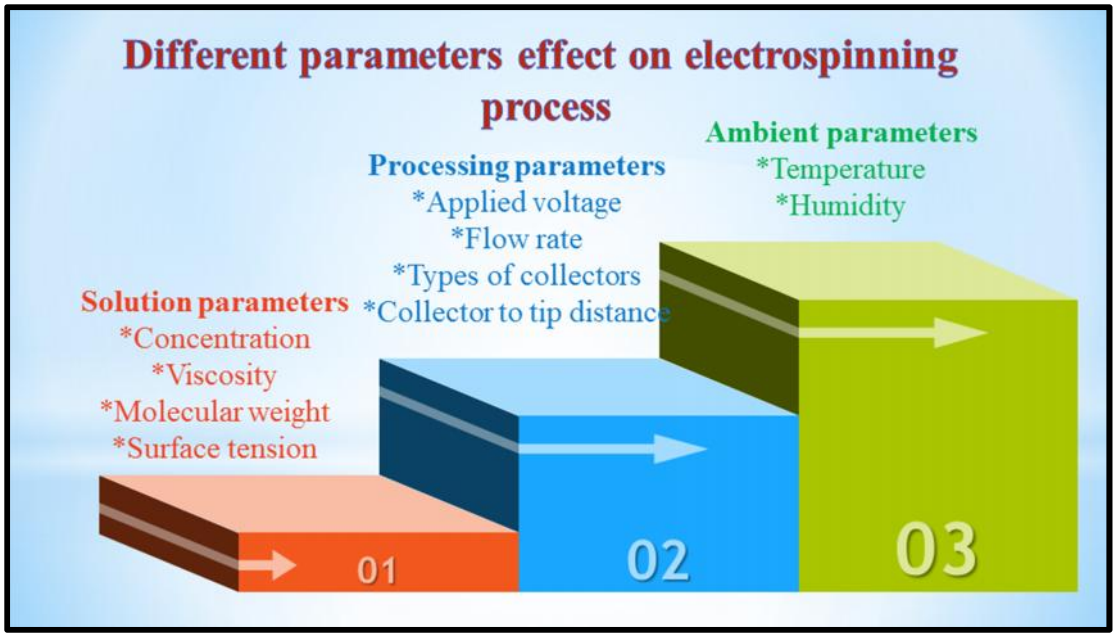

Figure (2.4): The different parameters effect on electrospinning process [44].

2.4.1 Solution Parameters

2.4.1.1 Concentration

The concentration of the polymer impacts the electrospinning process in different ways and these are discussed as follows:

a) When the concentration of the polymer is low, electrospraying takes place instead of electro spinning because the solution becomes less viscous and thus increases the surface tension.

b) When the concentration of the polymer is slightly high, the solution becomes sufficiently viscous leading to fibers and beads formation.

c) When the concentration is suitable, very smooth nature of nanofibers is achieved.

d) If the concentration of the polymer is very high in solution, micro-sized ribbons are formed. Figure (2.5) gives the Scanning Electron Microscope images of nanofibers according to concentration differences [30].

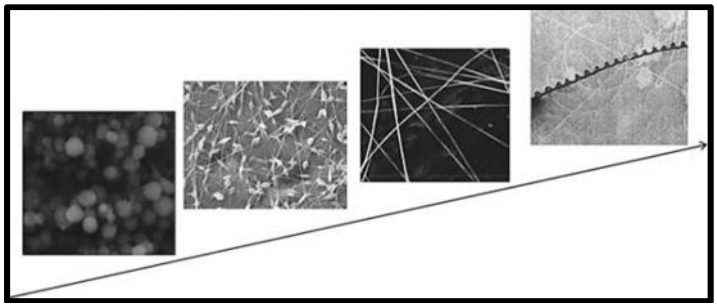

Figure (2.5): SEM of different concentrations of polymer solution [30].

2.4.1.2 Molecular Weight

The molecular weight of polymer influences the solution viscosity and thus has an important effect on fiber morphology. For example, decreasing the molecular weight of polymers while maintaining other parameters constant resulted in the formation of bead-like structures. On the other hand, higher molecular weight resulted in smooth fibers initially followed by ribbon-like fibers upon further increase in molecular weight. High molecular weight polymers show the highest degree of entanglement and pose difficulties for the electric field to pull on individual polymer chains to obtain a thin fiber [31].

2.4.1.3 Viscosity

Solution viscosity plays an important role in fiber morphology and size during the electrospinning process. In general, the viscosity of the solution is associated to the extent of polymer molecule chain entanglement within the solution. The entanglement of polymers is crucial to the fiber formation. The polymer solution should show high polymer entanglement without prevention of jet movement. In other words, below a critical viscosity value, applied voltage results in bead formation due to Rayleigh instability [32].

The solution viscosity has been strongly related to the concentration of the solution and molecular weight of polymer. the relationship between concentration and fiber formation was explored and

polymer droplets and beaded structure was observed when dilute solutions were used due to insufficient overlap between molecular chains. Viscosity of solutions affects not only the fiber formation but also the diameter of produced fibers, as the higher viscosity discourages bending, and the jet path reduces. Reduced jet path resulted in less stretching of the solution so fiber diameter increases [33].

The morphology of the beads on the fibers changes shape as the solution viscosity changes from a rounded droplet-like shape with low viscosity solutions to stretched droplet or ellipse to smooth fibers when sufficient viscosity is achieved, as shown in figure (2.6) [34].

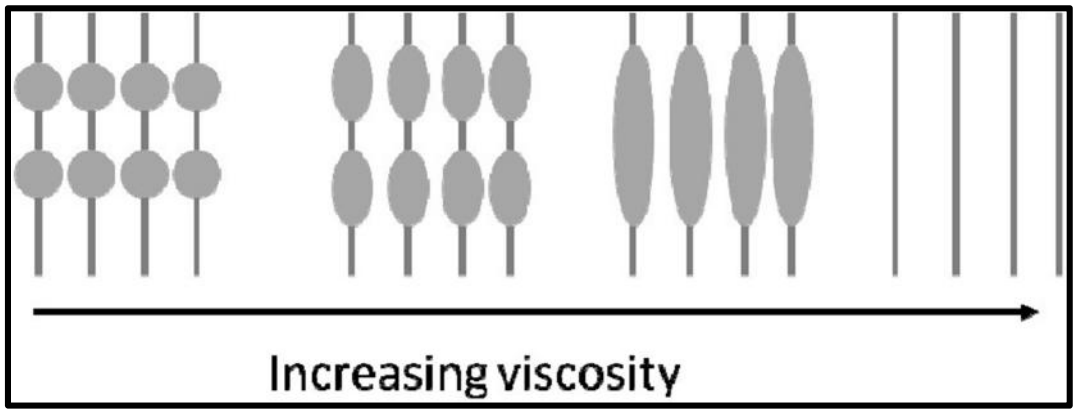

Figure (2.6): Schematic showing the effect of increasing the polymer solution viscosity on the morphology of the resulting electrospun fibers.

2.4.1.4 Surface Tension

Surface tension is a function of composition and plays a critical role in electrospinning process. It is the primary force opposing applied voltage during electrospinning process and determines electrospinnability. The feed solutions with low surface tension produce fibers without beads. However, it does not mean all solutions with low surface tension can be electrospun. Surface tensions of polymer solutions change with concentration, chemical composition and temperature [35].

2.4.1.5 Conductivity

Solution conductivity is mainly determined by the polymer type and solvent sort. Usually, natural polymers are generally polyelectrolytic in nature, in which the ions increase the charge carrying ability of the polymer jet, subjecting to higher tension under the electric field, resulting in the poor fiber formation. Additionally, the electrical conductivity of the solution can be tuned by adding the ionic salts. This also helps in controlling the fiber diameter [36].

2.4.2 Processing Parameters

2.4.2.1 Voltage

The applied voltage plays an important role in the electrospinning process. At low voltages, nonuniform fibers with beads may be formed, but at high voltages, there is tends to slightly decrease the length of the single jet, increase the apex angle of the Taylor cone, and produce thicker and nonuniform fibers, and also greater amounts of charge in high voltage will lead to drawn faster and a greater volume of solution from the tip of the needle, resulting in a smaller and less stable Taylor cone [37].

2.4.2.2 Flow Rate

The flow rate of the polymer from the syringe influences the jet velocity and the material transfer rate. The lower feed rate is more desirables as the solvent will get enough time for evaporation. Thus, there should always be a minimum flow rate of the spinning solution. It has been demonstrated that the fiber diameter and the pore diameter increases with an increase in the polymer flow rate and the morphological structure can be slightly changed by changing the flow rate. High flow rates result in beaded fibers because of unavailability of proper drying time prior to reaching the collector [38].

2.4.2.3 Collectors

Collectors usually act as the conductive substrate to collect the charged fibers during the electrospinning process. Aluminum foil is used as a collector in most cases but it is difficult to transfer the collected nanofibers to other substrates for various applications. Different kinds of collectors have been developed including wire mesh, pin, grids, parallel or gridded bar, rotating rods or wheel, liquid bath , etc., depending on the type of application. As shown in figure (2.7) [39].

It was also found that the packing density was influenced by the conductivity of the collectors. When this charge was not dissipated when collected on nonconducting collectors, the fibers repelled one another, yielding a more porous structure [22].

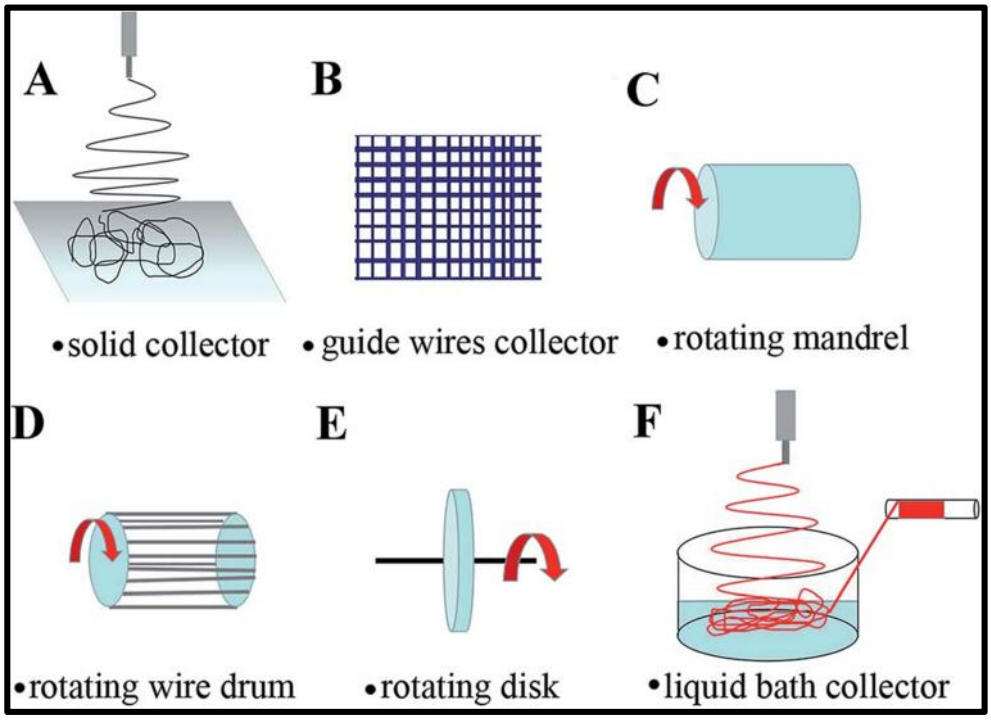

Figure (2.7): Type of collectors used in the electrospinning set-up: (A) solid collector, (B) guide wire collector, (C) rotating mandrel, (D) rotating wire drum, (E) rotating disk, (F) liquid bath collector [39].

2.4.2.4 Distance Between the Tip of Syringe and Collector

The distance between the syringe nozzle and the collector affects the degree of volatilization of the solvent, which controls the size and the morphology of the electrospun fibers. The solvent can be sufficiently volatilized when the receiving distance is increased to a certain extent, while electrospun fibers with smaller diameters can be obtained [40].

On the other hand, the electric field strength will be reduced with an increasing receiving distance, which will lead to a decrease of the jet velocity, a weaker tensile action, leading to an increase in the diameter of the fibers. An appropriate distance is required for the drying of the fibers before reaching the collector. If the distance is too close or too far, fibers with beads are obtained [41].

2.4.3 Ambient Parameters

2.4.3.1 Humidity

Relative humidity and temperature have a significant influence on the morphology of nanofibers. The solidification of the charged jet during electrospinning is affected by humidity which ultimately affects the diameter of nanofibers. humidity controls the diameter of electrospun nanofibers. The thickness of nanofibers increases with the increase in relative humidity and vice versa. The relative humidity dependent increase or decrease of the diameter of nanofibers is based on the rate of solvent evaporation. The solvent evaporation rate is high at low relative humidity [42].

2.4.3.2 Temperature

Temperature also affect the diameter and morphology of the nanofibers. The morphology of the fibers were found to be “beaded” for the low temperature ($T<40°C$) solutions, but at higher ($T>60°C$) temperatures of polymer solution, the fibers became flat. The bead

formation was eliminated at low temperature polymer solutions by changing the other electrospinning process parameters. The results obtained at low temperature of polymer solutions were more predictable due to the controllable vapor pressure of solution [43].

2.5 Electrospinning Methods

Electrospinning methods can be divided into many types. Based on the properties of electrospinning solution, it can be divided into blend electrospinning, emulsion electrospinning, suspension electrospinning. According to the structure of spinneret, it can be divided into single-fluid electrospinning, coaxial electrospinning, Janus electrospinning, and multi- fluid electrospinning as shown in Figure (2.8) [45].

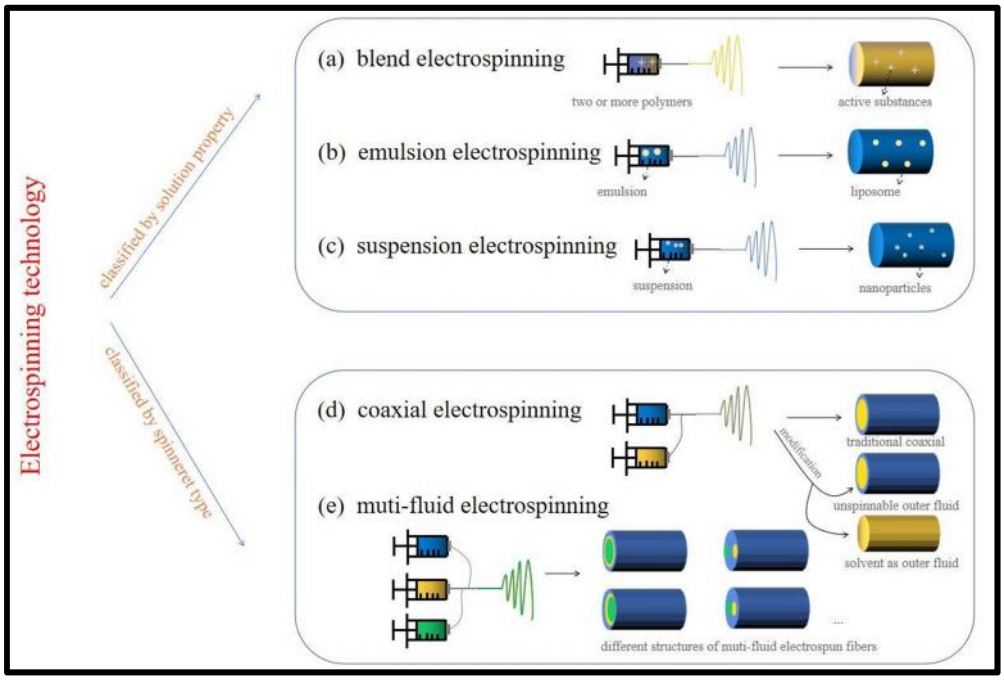

Figure (2.8): Classification of electrospinning technology [45].

2.5.1 Blend Electrospinning

Blend electrospinning is a method in which more than two polymers and additional active substances are dissolved in a solvent system simultaneously as the working electrospinning solution. The combination of the two polymers can enable them to achieve the

advantage property compensation from each other, and results in preparing a new nanofiber with target properties, including the improvement of hydrophobicity, hydrophilicity, spinnability, mechanical properties, stability, biological activity and so on [45,46].

2.5.2 Emulsion Electrospinning

The emulsion electrospinning is based on two or multiple phases, which are not mixed during the electrospinning process. The phases are immiscible and typically stabilized by proper surfactants. Generally, two types of emulsions are used for electrospinning process. Water in-oil emulsions are based on lipophilic continuous phase and hydrophilic droplet phase. This type of emulsion is used for encapsulation of polar and hydrophilic molecules, such as proteins. The second type is oil-in-water (O/W) emulsions. The continuous phase is formed by hydrophilic solution and droplet phase by lipophilic solution [47].

2.5.3 Suspension Electrospinning

Solid-in-liquid dispersions, termed either “suspension” or “sol” depending on particle size and visual appearance, can be electrospun similarly to emulsions in a wide range of compositions. In most cases, water-soluble matrix polymers and surfactants are dissolved in an aqueous continuous phase, to which the powdered solid particles or pre-made dispersions are added. This technique is compatible with a range of different particle types from biology to catalysis. In fact, unstable dispersions can often lead to clogging in needle-based setups [48].

2.5.4 Coaxial Electrospinning

Coaxial electrospinning is a type of electrospinning method in which the structure of the spinneret is changed, the spinneret consists of two nozzles that are concentrically aligned, and the core and sheath precursor solutions are fed at a controlled rate through the inner and outer

nozzle, respectively. At the orifice of the spinneret, a compound droplet is generated, and upon applying voltage, charges are induced in the droplet. The distribution of these charges depends on the electrical conductivity of both the core and sheath solutions [49].

However, here in coaxial electrospinning, solid core−sheath fibers are formed on the collector. The relative alignment of the inner and outer nozzle affects the entrainment and, consequently, the resulting fiber morphology [50].

2.5.5 Multi-Fluid Electrospinning

In multifluid electrospinning, in addition to the widely used core–shell structure and Janus structure, other multifluid electrospinning has also been carried out to study nanofibers with more complex structures have been developed through combining three or more fluid channels. According to the structural characteristics of different spinnerets, nanofibers with specific structures can be prepared on the basis of the application needs [51].

2.6 Applications of Electrospinning

Since electrospun nanofibers have large surface to volume ratio, high porosity and superior mechanical properties, electrospinning has received increased attention to produce nanofibers. Although electrospinning is an old method to produce fibers, in recent years, it has been widely used in tissue engineering scaffolds, wound healing, drug delivery, filtration, biosensors, immobilization of enzymes, food packaging and in the textile industry as shown in figure (2.9) [52].

The application of electrospun fiber membrane in actual food packaging have been widely studied in recent 10 years. The literature search statistics of food packaging from “Web of Science” as shown in Figure (2.10) [45].

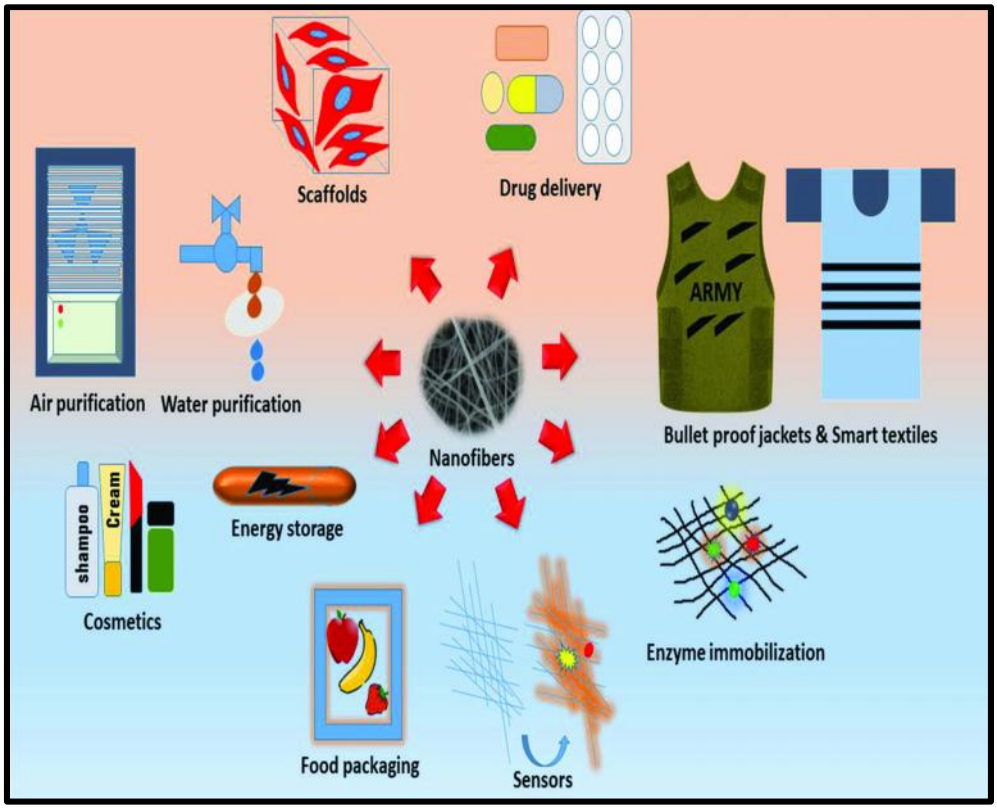

Figure (2.9): Various applications of electrospun nanofibers [52].

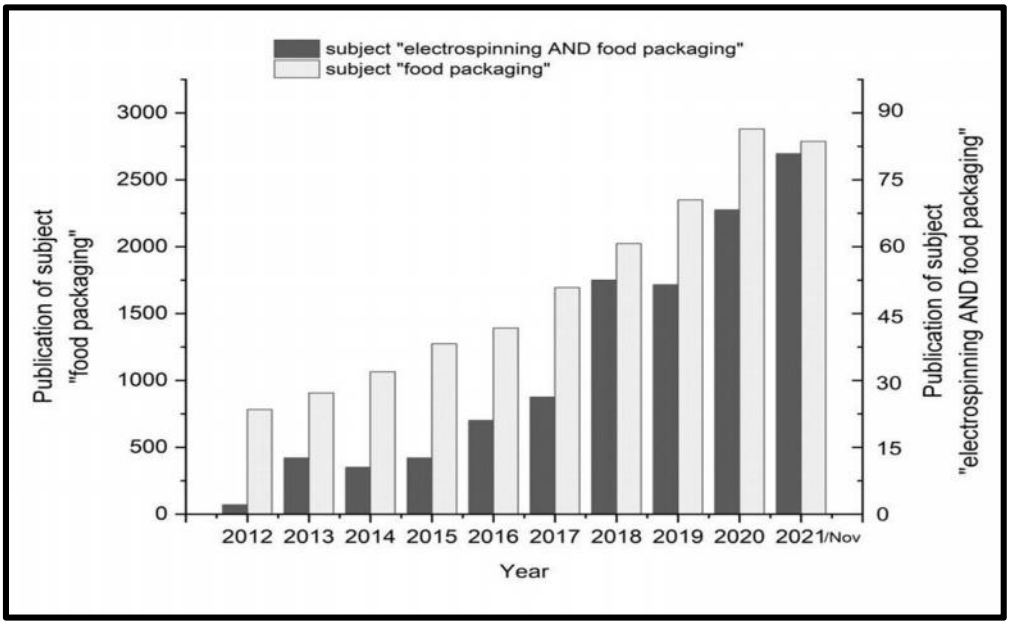

Figure (2.10): Literature retrieval statistics on the "Web of Science" platform with the subject of food packaging and electrospinning AND food packaging from 2012 to November 2021 [45].

2.7 Food Packaging

Food packaging can protect food from processing, distribution handling and storage. It not only can provide protection but also can be named active. Active packaging could act as an oxygen scavenger or antimicrobial agent. Nanofibers were produced to be biocompatible and with functional active compounds. Those compounds could be immobilized on the surface of fibers or encapsulated inside of fibers. The advantages of this nanofiber structured package are large surface and high encapsulation ability. Apart from active packaging, electrospun nanofibers can also been used as a smart packaging. Smart packaging refers to the material used for packages to that could monitor the quality changing during storage. It shows great significance in the food industry [53].

In addition to these active and smart packaging, electrospun fibers can be used as multilayered structures. Nanofibers can provide mechanical reinforcement as a better protection for fragile textured foods and add other functional properties [54].

2.8 Requirement for Food Packaging

Food packages are active if they contain an ingredient that can release/absorb substances into or from the food/headspace thereby preserving food quality and providing a reasonable extension of shelf life [55].

Generally, active packaging systems can be classified under two major categories depending upon its functioning mode: compounds that absorb (scavengers) or discharge (emitters) gasses to transform the package’s internal atmosphere actively. Therefore, scavengers can be defined as compounds employed to eliminate undesirable substances from the internal packaging environment, such as oxygen, moisture, ethylene,

carbon dioxide, and odors/flavors. In contrast, emitter systems are designed to discharge certain substances possessing desirable properties to produce a suitable positive impact in the food packaging headspace [56].

However, Food packaging plays a critical role in preventing food from external environmental adverse factors, such as light, moisture, microorganisms, and oxygen to sustain the food quality. The functional packaging materials applied in the food field, some additional features must be considered, such as degradable, superhydrophobic, edible, antibacterial and high barrier [12]. Figure (2.11) illustrate the different types of active food packaging.

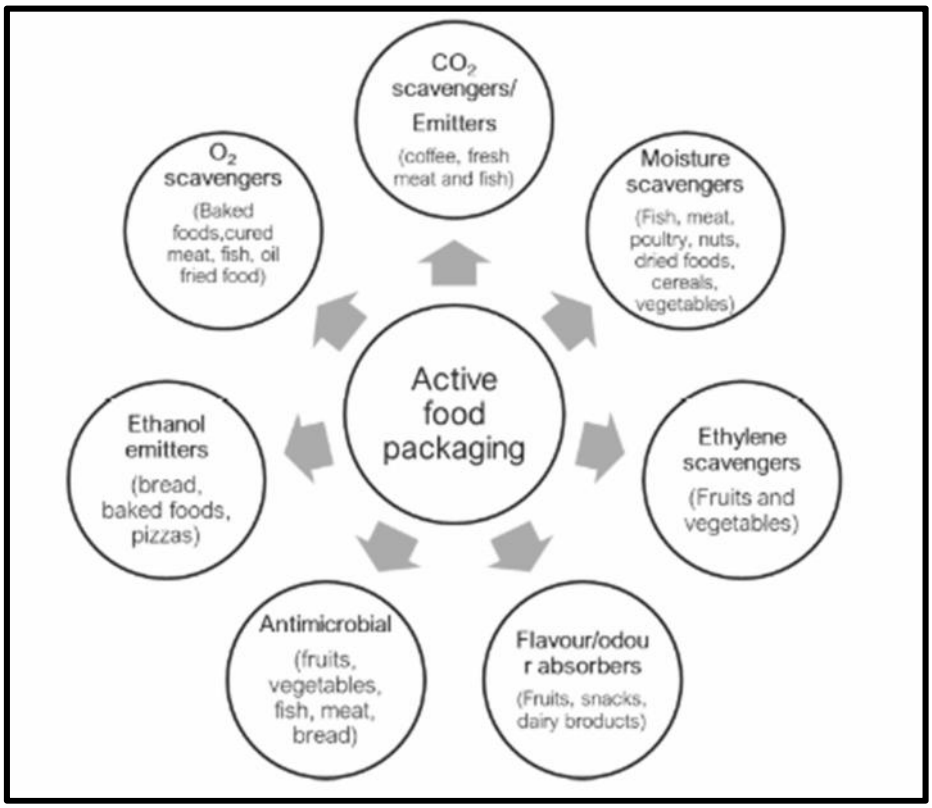

Figure (2.11): Different types of active food packaging indicating their need in packing different foods.

2.9 Hydrophobic/Hydrophilic Behavior of Food Packaging

The terms “hydrophilic surface” and “hydrophobic surface” have been used extensively in literature for many years, which describe opposite effects of the behavior of water on a solid surface. A hydrophilic surface has strong affinity to water molecules, whereas hydrophobic surfaces repel water [109].

The surface hydrophobhicity and hydrophilicity was determined by measuring water contact angle. This measurement is an important parameter for food packaging applications. Generally, hydrophobhic property of films is desirable for food packaging applications in order to maintain the quality and prolong shelf life [110].

Hydrophobicity and hydrophilicity is another property of different polymers. Due to this property such, polymers can be used for different applications. If the contact angle between surface and droplet is greater than 90°, then such a surface is known as the hydrophobic surface. For a super-hydrophobic surface, the contact angle should be greater than 150°, in such a case water droplet attains spherical shape and roll of the surface [111].

The contact angle can be increased with the roughness of the surface and air trapped between the water and the surface. In a super-hydrophobic surface, the grip between the surface and the dirt particle is smaller than the grip between the particle and droplet; as a result, the particle is captured by the droplet of water, results in the cleaning of the surface as mentioned in the Figure (2.12) [112].

The contact angle range for each wetting and non-wetting scenario is shown in Figure (2.13) [109].

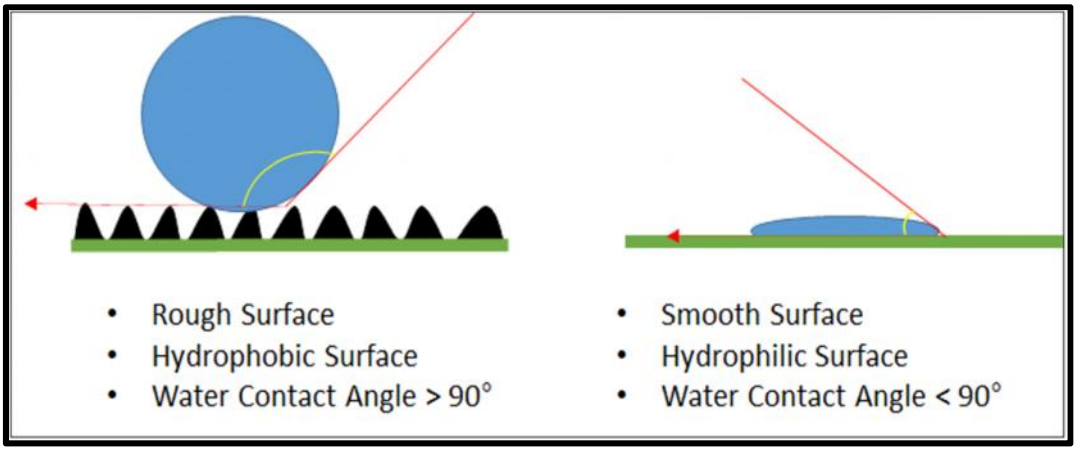

Figure (2.12): Surface mechanism of the hydrophobic and hydrophilic behavior [112].

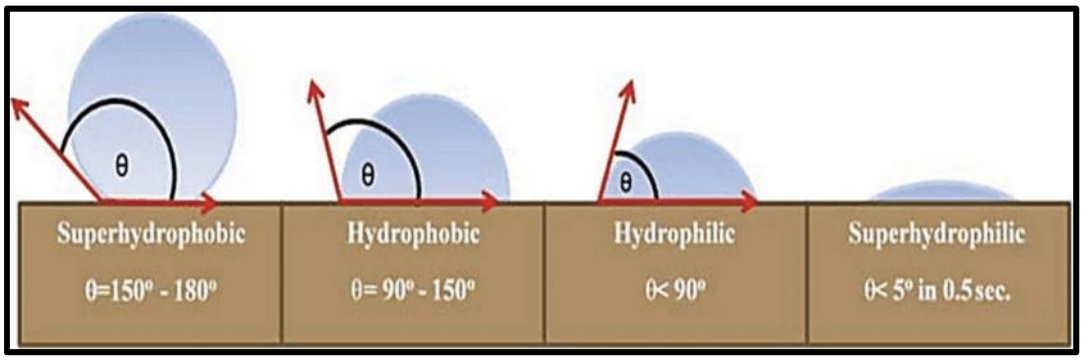

Figure (2.13): Schematic of water droplet's contact angle with different surface wettability [109]**.**

2.10 Types of Polymers Used in Electrospinning of Food Packaging

Food packaging materials are based on petrochemical synthetic polymers such as (PVC, PET, PE, PP, etc.) because of historic factors, low-cost, and good barrier performances. These polymers are nonbiodegradable and worldwide they have already raised a lot of environmental concerns regarding short- and long-term pollution [57,58].

These two factors are putting an increasing pressure on food industry to develop new types of antimicrobial packaging materials, mainly based on natural, renewable sources, or biopolymers that are environmentally safe. While the simplest way to achieve antimicrobial

activity is to modify the currently used packaging materials, the environmental pressure is slowly phasing out the nonbiodegradable polymers [59].

More, recently, interest has increased significantly in the use of biodegradable biopolymers for sustainable food packaging applications. Such materials include polymeric films made of natural polymers, such as starch, zein, and gelatin; polymers synthesized from nature-derived monomers such as polylactic acid (PLA). Different types of polymers ranging from natural to synthetic are rapidly becoming the most interesting subject of research in the sector of the food packaging [60].

Synthetic polymers, such as polycaprolactone (PCL), poly (propylene carbon) (PPC), Polylactic acid (PLA), Polyvinyl alcohol (PVA), Poly(ethylene oxide) (PEO), poly(ethylene glycol) (PEG) and Poly (ethylene terephthalate) (PET) . Natural polymer, such as Cellulose, Chitosan (CS), Zein, Soy and whey protein, Gelatin, Starch, Collagen and Pullulan.

2.11 Essential Oils Used in Food Packaging

Essential oils (EOs) are volatile liquids extracted from various organs of plants. EOs are biosynthesised in aromatic plants as secondary metabolites, and are mainly composed of terpenes, but also contain other chemical compounds [61].

The chemical components of essential oils are volatile and susceptible to easy degradation due to temperature, light, oxygen, and moisture. Hence, encapsulating systems, such as micro and nano-particles, capsules, droplets, and fibers, are required to deliver still-functional EOs to a specific target and in a controlled fashion [62].

In this vein, essential oils encapsulation into polymeric fibers has opened new ways for wound dressings, scaffolds for tissue engineering, and active food-packaging structures with progressed antimicrobial

activities. Moreover, the nanofibers can supply naturally derived chemical compounds in a controlled manner and prevent their degradation. Essential oils, because of their antioxidant, antiparasitic, insecticidal, antidepressant, food preservative, analgesic, and anti-inflammatory properties, are recently gaining popularity [63].

Therefore, the latest research paid enormous attention to nanofibers application with antimicrobial agents that will be used in tissue engineering, drug delivery, active food packaging, cosmetics, and wound healing. The natural distillate of essential oils is classified as generally recognized as safe (GRAS) by the US Food and Drug Administration (US-FDA); therefore, it received approval for safety and effectiveness [64].

However, the use of EOs in food preservation is limited in some extent due to their insolubility in water and special flavor which would alter the original sensory property of food. Encapsulation is helpful in improving the solubility and stability of EOs and masking their undesirable flavor as well. These encapsulation nanofibers with essential oil also exhibit improved mechanical properties and are harmless to the human body. Therefore, we can expect these multifunctional nanofibers, which have antimicrobial properties, CO_2 reduction effect and moisture prevention effect, to be applied in a variety of other fields [65,66].

These EOs such as oregano oil, peppermint oil, clove oil, thyme oil, lavender oil, eucalyptus oil, ginger oil, tea tree oil, cinnamon oil, chamomile oil, angelica oil and rosemary oil.

2.12 Plant-Derived Mucilage Used in Food Perseveration

Nowadays, due to the hazardous effect of synthetic polymers on human health, people showed major interest in plant-based naturally

derived biopolymers (gums, mucilage, cellulose, and glucans) as an effective ingredient for the formulation of eco-friendly, sustainable, cost-effective products [67].

Mucilages are generally extracted from certain plants and microorganisms. They are hydrophilic polymers, mainly composed of water-soluble polysaccharides and proteins, which interact with water to form a viscous mass. They have been used in foods as thickeners, gelling agents, texture enhancers, and emulsifiers [68,69].

Recently, mucilages obtained from various plants and plants parts (i.e. seeds, fruits, leaf) have been used to develop novel edible packages. The use of mucilages in edible packages and in food preservation applications is increasingly preferred to synthetic materials due to their intrinsic properties, such as nontoxicity, biocompatibility, biodegradability, antimicrobial properties, good antioxidant properties and can enhance the shelf life, storage capacity with reduce the loss of moisture. The mucilage has high tensile strength and barrier properties against different gases which reduce the firmness and weight loss of coated products [69,70].

Extracted mucilages from various seeds such as basil, cress, flax seed, chia and fenugreek are the most commonly applied hydrocolloids for biodegradable films. The sources, family and molecular structure of these seed mucilages are summarized in Table (2.2) [71].

Table (2.2): A summary of sources, family and main monosaccharide compositions of different seed mucilages [71].

Seed mucilages	Source	Family	Main monosaccharide compositions
Basil seed	*Ocimum basilicum L.*	*Lamiaceae*	Glucan (2.31%), xylan (24.29%) and glucomannan (43%)
Cress	*Lepidium sativum*	*Cruciferae*	D-Glucuronic acid (6.7%), D-galacturonic acid (8%),galactose (4.7%), mannose (38.9%), rhamnose (1.9%), arabinose (19.4%), fructose (6.8%) and glucose (1%)
Flaxseed	*Linum usitatissimum L.*	*Linaceae*	Rhamnose (21.2-27.2%), fructose (5-7.1%)arabinose (9.2-13.5%), xylose (21.1-37.4% galactose (20-28.4%), glucose (2.1-8.2%)
Chia	*Salvia hispanica L.*	Lamiaceae	Xylose (38.5%), glucose (19.6%), arabinose (9.6%), galactose (6.1%), glucuronic acid (18.7%), galacturonic acid (5.3%)
Fenugreek	*Trigonella foenum graecum*	*Legume*	Galactose/mannose ratio (1.00:1.02 to 1.00:1.14)

2.13 Polymer Blends

A polymer blend is a mixture of two or more polymers/ copolymers with or without compatibilizers to obtain the benefit of all components. Polymer blends provide the best properties of each polymer,

reduce cost, improve functionality for the desired end use. Polymer blends may be homogenous or heterogenous [55].

Generally, polymer blends are classified into either homogeneous (miscible on a molecular level) or heterogeneous (immiscible) blends. Miscible (singlephase) blends are usually optically transparent and are homogeneous to the polymer segmental level. Single-phase blends also undergo phase separation that is usually brought about by variations in temperature, pressure, or in the composition of the mixture. Since, ultimately, the properties of a polymer blend will depend on the final morphology. Generally, polymer blends can be completely miscible, partially miscible or immiscible, depending on the value of ΔG_m.

The free energy of mixing is given by

$$\Delta Gm = \Delta Hm - T\Delta Sm \quad \text{.....(2-1)}$$

Where ΔG_m is the Gibbs energy of mixing, ΔS_m is the entropy factor and is a measure of disorder or randomness, is always positive. ΔH_m is the heat that is either consumed (endothermic) or generated (exothermic) during mixing [72,73].

2.14 Compatible Blends

An immiscible polymer blend that exhibits macroscopically uniform physical properties is called compatible. Compatibility means the capability of individual component substances in either an immiscible polymer blend or a polymer composite to show interfacial adhesion in which interfaces between phases or components are maintained by intermolecular forces, chain entanglements, or both, across the interfaces. Compatibility of polymer blends is often achieved through favorable specific interaction such as hydrogen bonding [74].

2.15 Materials Used in This Thesis

2.15.1 Poly(vinyl alcohol) (PVA)

PVA is a synthetic polymer with excellent properties for biocomposite film. It has a strong oxygen barrier, which allows small amounts of gas because the hydrogen bonding between the hydrogen groups is too strong. PVA also has excellent properties in film formation and chemical resistance. PVA is a polymer with a unique planar zig-zag structure with a carbon backbone. On top of being biodegradable, PVA is also cost-effective, fully renewable, non-toxic, nonflammable and water-soluble synthetic polymer [75,76].

PVA is synthesized from vinyl acetate via a radical polymerization process that yielded polyvinyl acetate (PVAc) as an intermediate product, which was then followed by a hydrolysis process on the acetate group of PVAc to allow the changes to the hydroxyl group to produce PVA. There are two types of PVA hydrolysis based on the degree of hydrolysis; fully hydrolyzed and partially hydrolyzed PVA. The temperatures involved in the fully and partially hydrolyzed processes are 230°C and 180 to 190°C,respectively [76,77].

PVA is an eco-friendly, being biocompatible and biodegradable, resulting in comparably high fiber forming. Considering its high mechanical strength, PVA is very fit to act as the matrix of composite electrospun nanofibers. Features of PVA include nonionic properties, semi-crystalline structure, processability, and fantastic spinnability [78,79]. The molecular structure of PVA is shown in Figure (2.14) [80].

It is generally recognized as safe (GRAS) according to Food and Drug Administration (FDA), it has a hydrophilic nature, and it contains a high density of reactive functional groups. Polyvinyl alcohol (PVA) film is a kind of antistatic film with good performance, which is widely used

in the sales and packaging of textiles and clothing. Compared with polyethylene, polypropylene and other general-purpose films, polyvinyl alcohol film exhibits the advantages of high transparency, good antistatic property, which can significantly reduce the dust absorption effect [81]. Table (2.3) shows physical properties of polyvinyl alcohol (PVA) [82].

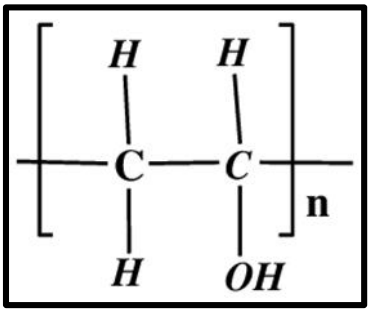

Figure (2.14): Chemical structure of polyvinyl alcohol (PVA) [80].

Table (2.3): Physical Characteristics of Poly (vinyl alcohol) (PVA) [82].

S.NO.	Property	Result
1	Appearance	Cream colored granular powder
2	Odour	Odourless
3	Taste	Tasteless
4	Solubility in water	Soluble
5	Solubility in Alcohol	Slightly Soluble
6	Solubility in organic solvents	Insoluble
7	Melting Point	180 to 190°C
8	Degree of hydrolysis	86.5 to 89%.

2.15.2 Corn Starch (ST):-

Starch is a natural polymeric carbohydrate and found in plant tissues, such as leaves, stems, seeds, roots and tubers. It is also found in certain algae and bacteria. Starch exists in semi-crystalline granules of different size, shape and morphology depending on its botanical source

[83]. Nevertheless, most starches are composed of two structurally distinct molecules: amylose, a linear or lightly branched α-1–4 linked d-glucopyranose, and amylopectin, a highly branched molecule of α-1–4 linked d-glucopyranose with α-1–6 branch linkages. The amylose/amylopectin ratio in starches varies with botanical origin. Figure shown (2.15) amylose and amylopectin structure [84].

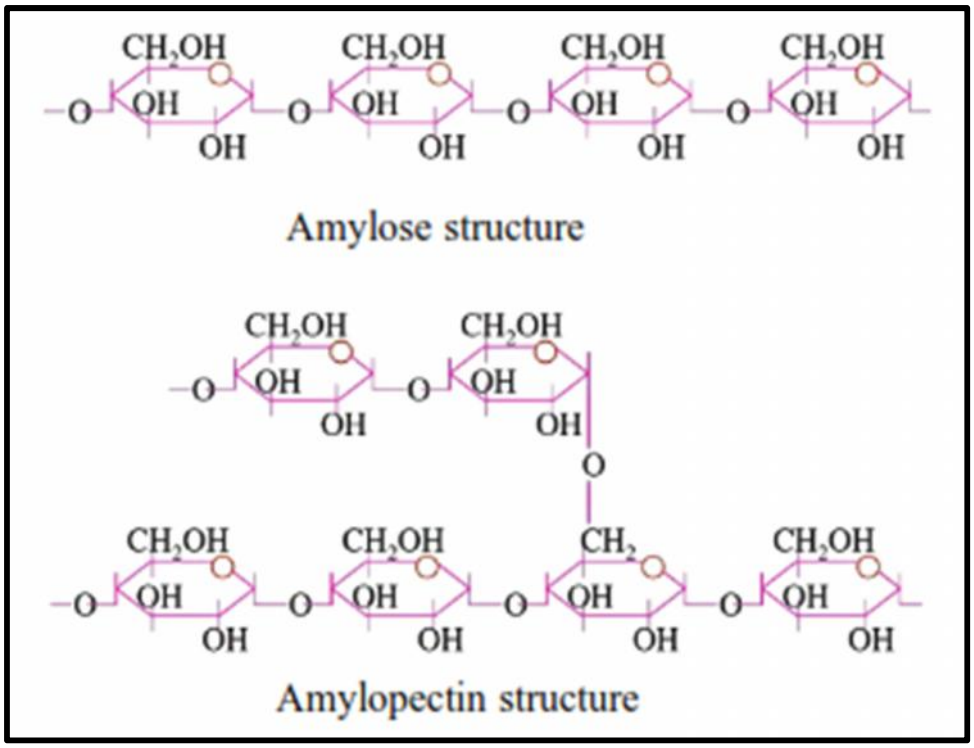

Figure (2.15): Amylose and amylopectin structures [85].

Amylose and amylopectin structure differences, leading to its performance, are significantly different. Amylose can be dissolved in 70°C~80°C hot water. Branched-chain starch is insoluble. Amylose and amylopectin content in the natural starch depends upon the source of starch. The contents of amylose and amylopectin in different starch sources were different. Amylose accounts for 23% in common corn. The most important property of starch is that the granule expands under the

excess water heating. And then amylose and amylopectin dissolve. That is the gelatinization of starch [85].

Starch is considered as one of the most common natural polymers available abundantly. It finds applications in various fields like pharmaceutical, medical and food. It is extensively used for film formation in food packaging, and its properties are enhanced when it is used or blended with other materials. However, the mechanical properties of pure starch fibers are very good and provide great properties to the film [86].

Starch contains three hydroxyl groups naturally in each repeating unit, which is the reason that it easily forms inter- and intra-molecular hydrogen bonds. In addition, starch in fibrous form is problematic due to its poor strength, water resistance, thermal stability, and process ability. It can be enhanced when blended with other biopolymers, and thus, it is extensively used in the formation of composite films [87].

2.15.3 Cress Seed Mucilage (CSM)

Cress seed gum exists in the envelope alongside the outer layer of the seeds of garden cress (Lepidium sativum L.) plant as a member of *Cruciferae* family. The seeds consist of 6.5–15% of the mucilage, which contains cellulose (18.3%) and uronic acid containing polysaccharides. Water can thus penetrate between the polyuronide chains, allowing them to hydrate and swell, so dispersing the cellulose micelles. The gel is a network of hydrated cellulose micelles, scattered with more heavily hydrated uronide chains. The associated carbohydrate polymer has a weight-average molecular weight of about 540 kDa [88].

Plant mucilages are also used for thickening, binding, disintegrating, emulsifying, suspending, stabilizing, and as gelling agents. These characteristics are related to their structural properties and

metabolic functions in food, pharmaceutical, cosmetic, textile and biomedical products [89].

Cress seeds as a good source of hydrocolloids, contain large amount of mucilaginous substances with anionic nature, which make them a good candidate for electrospinning. The cress seed mucilage possesses a high mannose to galactose ratio (8.2) and D-glucuronic acid (6.7%), D-galacturonic acid (8%), rhamnose (1.9%), arabinose (19.4%), fructose (6.8%) and glucose (1%) as shown in figure (2.16) [90].

However, due to different chain conformations and repulsive forces exist among the polyanions in the solution, application of mucilage for electrospinning is limited. Therefore, blending these bio-polyelectrolytes with a non-toxic, water soluble, synthetic polymers such as poly vinyl alcohol (PVA) or polyethylene oxide (PEO), reduces repulsive forces within the charged biopolymer solutions and allows spinning of the fibers [91].

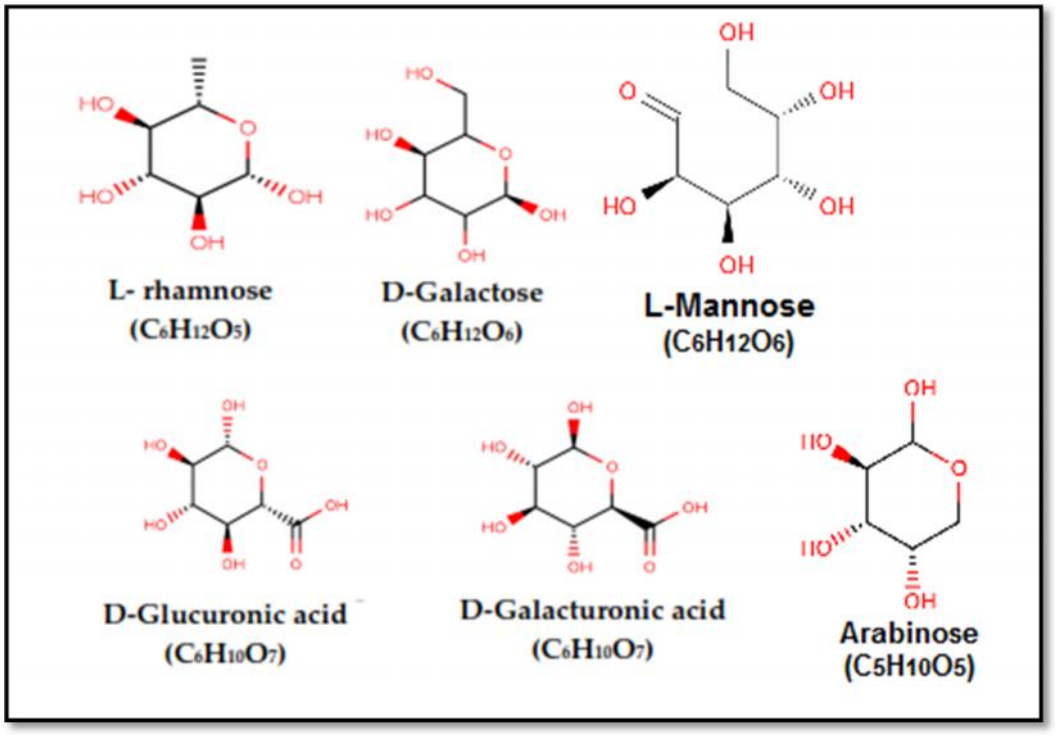

Figure (2.16): Chemical structure of cress seed mucilage components [67].

2.15.4 Moringa Essential Oil (MO)

Moringa oil is extracted from Moringa oleifera (Moringaceae). Recent studies displayed that moringa oil became popular because of its healthful properties, excellent oxidative stability and high antimicrobial activity [92].

All parts of the Moringa tree (leaves, seeds, roots and flowers) are suitable for human and animal consumption. The seeds, instead, have attracted scientific interest as Moringa oleifera seed kernels contain a significant amount of oil (up to 40%) with a high-quality fatty acid composition (oleic acid > 70%) and, after refining, a notable resistance to oxidative degradation [93].

Oil is the main component of the seed and represents 36.7% of the seed weight. The oil can be extracted almost entirely by solvent extraction, generally n-hexane, whereas less yield is obtained by cold press extraction. In fact, only 69% (on average) of the total oil contained in seeds can be extracted by cold press. Among rural dwellers, the edible oil is extracted by boiling de-husked seeds with water, and collecting the oil from the surface of the water [93,94].

Apart from the oil, the seed has a high protein content, on average 31.4%, whereas carbohydrate, fiber and ash contents are 18.4%, 7.3% and 6.2%, respectively [95]. While the structure of fatty acids in this oil shown in figure (2.17) [93,96] .

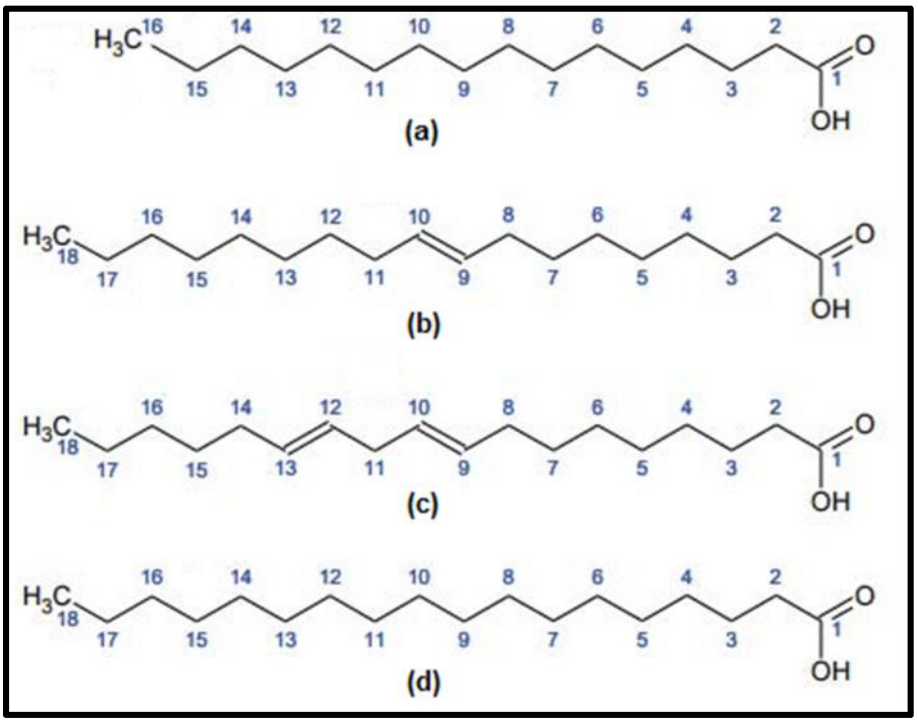

Figure (2.17): Fatty acid structure (a) Palmatic acid, (b) Oleic acid, (c) Linoleic acid, (d) Stearic acid [96].

2.15.5 Cardamom Essential Oil (CO)

Green cardamom (Elettaria cardamomum). Researches about the essential oils of green cardamom, one of the most performance spices in food, have shown antioxidant and antibacterial properties [97].

Cardamom oil is obtained by distillation of powdered seeds of cardamom. Steam distillation is the common method employed for the production of oil. The quality of the oil depends on the variety, rate and time of distillation. The major chemical constituents of cardamom oil are 1,8 cineole (25–45%), α-terpinyl acetate (20–53%), limonene (5.6%), linalyl acetate (8.2%), and linalool (5.4%). The structure of chemical constituents for this oil shown in figure (2.18), additionally to fatty acids which display in figure (2.18) [98].

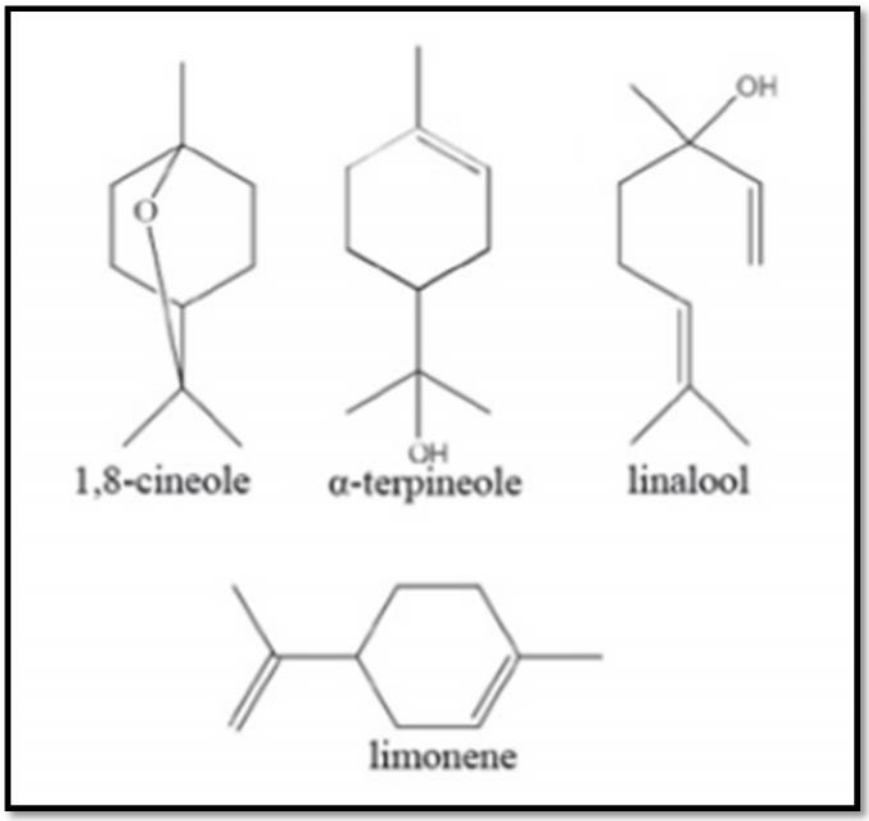

Figure (2.18): Chemical structures of some components of cardamom oil [98].

2.15.6 Clove Bud Essential Oil (CBO)

Clove (Syzygium aromaticum). Clove oil commonly obtained by hydro distillation, steam distillation, or solvent extraction method. Clove oil is a mixture of different constituents, with three main active ingredients being eugenol, caryophyllene, and aceteugenol. It is contributed to the antimicrobial and antioxidant properties of the oil. Clove oil from plants and other products of secondary metabolites have enormous benefits in medicine, food industry, fragrance, cosmetics and pharmaceutical industry [99].

Clove oil can be obtained from distillation of buds, leaf or stem, each resulting in an oil having different characteristics of oil. Clove bud oil, a colourless or yellow liquid, is obtained from distillation of buds. Clove buds contain 15 to 20 % of oil by weight. The main oil constituents are eugenol (70–95 %), eugenol acetate (up to 20 %) and β-caryophyllene

(12–17 %). The chemical structures of eugenol, eugenol acetate and β-caryophyllene are illustrated in Figure (2.19), additionally to fatty acids which display in figure (2.17) [100].

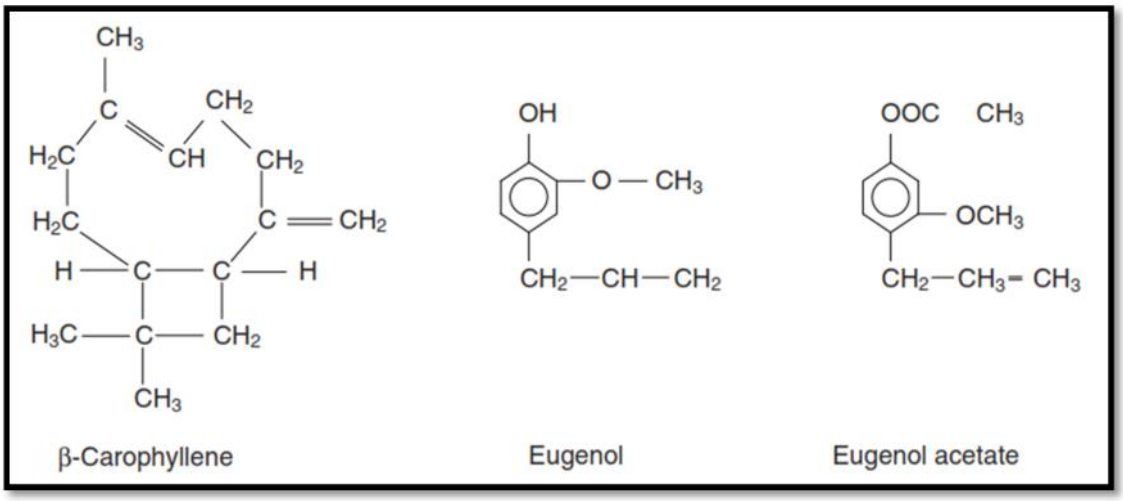

Figure (2.19): Chemical structures of eugenol, eugenol acetate and β-carophyllene [100].

2.15.7 Thyme Essensial Oil (TO)

Thyme oil is a plant secondary metabolite with natural, safe and non-toxic properties, is refined from thymus vulgaris. It has been registered in European flavoring list, and classified as generally recognized as safe (GRAS) by FDA. Application of thyme oil is considered as an efficient treatment for food preservation and control of postharvest decay of fresh produce [101].

TO is rich in phenolic compounds, such as thymol and carvacrol, rendering great antioxidant and antimicrobial activity, among other biological activities. In contrast, the essential oil compounds are sensitive to external deleterious elements such as oxygen, moisture, light, and high temperatures. Therefore, they are prone to degradation, which can be an obstacle for their effectiveness as bioactive agents. Thus, the application of essential oils in food and/or food packaging requires protection and

stabilization, which can be achieved through encapsulation by electrospinnng method [86].

The main components of thyme oil are the isomeric phenolic monoterpenes thymol (2-isopropyl-5-methylphenol) and carvacrol (2-methyl-5-(propan-2-yl)phenol). Both these monoterpenes are biosynthesized by the hydroxylation of p-cymene after the aromatization of γ-terpinene to p-cymene. Thymol is a colorless, crystalline compound with characteristics including strong odor and solubility in alcohol and other organic solvents, but it is only slightly soluble in water. Carvacrol, on the other hand, is a colorless to pale yellow liquid, insoluble in water but highly soluble in ethanol, acetone, and diethyl ether and with a thymol odor. Structures of thymol, carvacrol, and other thyme components (p-cymene, γ-terpinene, linalool, β-myrcene, terpinen-4-ol) are shown in Figure (2.20), additionally to fatty acids which display in figure (2.17) [102].

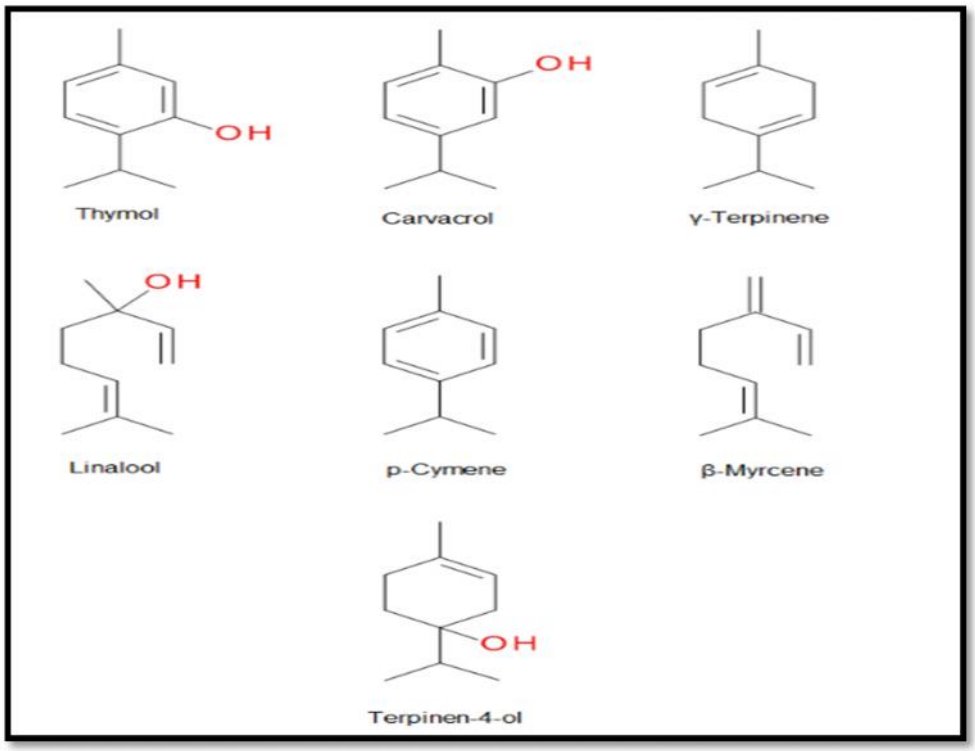

Figure (2.20): The structure of the main components of thyme essential oil [102].

2.15.8 Fenugreek Essential Oil (FO)

Fenugreek, scientifically known as *Trigonella Foenum Graecum*. Fenugreek seed is a good source of essential amino acids, especially leucine, lysine, and total aromatic amino acids. Recently, researchers have found that the seed contains 20%–25% protein, 6%–8% oil, 45%–50% dietary fiber, and 2%–5% steroidal saponin [103].

The seeds and leaves of this plant are extensively employed as an anti-microbial, anti-inflammation, anti-cancer and antioxidant agent. Moreover, the seeds of fenugreek have also been reported to have strong free radical scavenging activity [104].

Fenugreek oil consist of phenolics, alkaloids, anthracene glycosides, flavonoids, saponins, tannin, volatile oils, and phenolics make it an astonishing antimicrobial agent. Fenugreek oil has potential preservation effects against various microbe strains that cause food-borne illness, and therefore, can be substituted for chemical preservatives [105].

Fenugreek seed oil mostly comprising 54.13% linoleic acid, 16.21% palmitic acid, 4.56% pinene, 3.87% 4-pentyl-1-(4-propyl cyclohexyl)-1-cyclohexene and 3.19% linoleic acid methyl ester along with 18 more chemical compounds those are comprising 99% of total fenugreek oil. The structure of this component shown in figure (2.21), additionally to fatty acids which display in figure (2.17) [106].

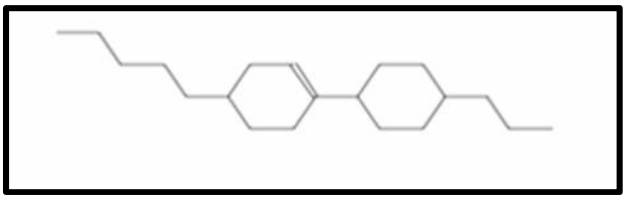

Figure (2.21): Chemical structure of (4-pentyl-1-(4-propyl cyclohexyl)-1-cyclohexene).

However, the use of these essential oils faces some limitations that one of them is its high volatility, thereby decreasing its effectiveness. One way

to address this problem is by Nanoencapsulation such as electrospinning method [97].

2.15.9 Walnut Tree Bark Powder (WB)

Walnut (Juglans regia L.) is the most widespread tree nut in the world. The tree is commonly called as the Persian walnut, white walnut, English walnut or common walnut. It belongs to juglandaceae and has the scientific name Juglans regia [107].

Walnut bark is known as a resinous and scented material. The dried stem bark can be used as a tooth cleaner. It is also employed as a dyeing agent for staining the lips in some countries. It has been claimed that it possesses anti-inflammatory, blood purifying, and anticancer properties. It has contain several therapeutically active constituents, especially polyphenols. the dried walnut bark has significant amounts of totat phenol content compared to its prepared extracts (34.83–311 and 9.8 mg/g) respectively. Juglans regia L. stem bark contains chemical constituents, namely β-sitosterol, ascorbic acid, juglone, folic acid, gallic acid, regiolone, and quercetin-3-α-L-arabinoside as shown in figure (2.22) [108].

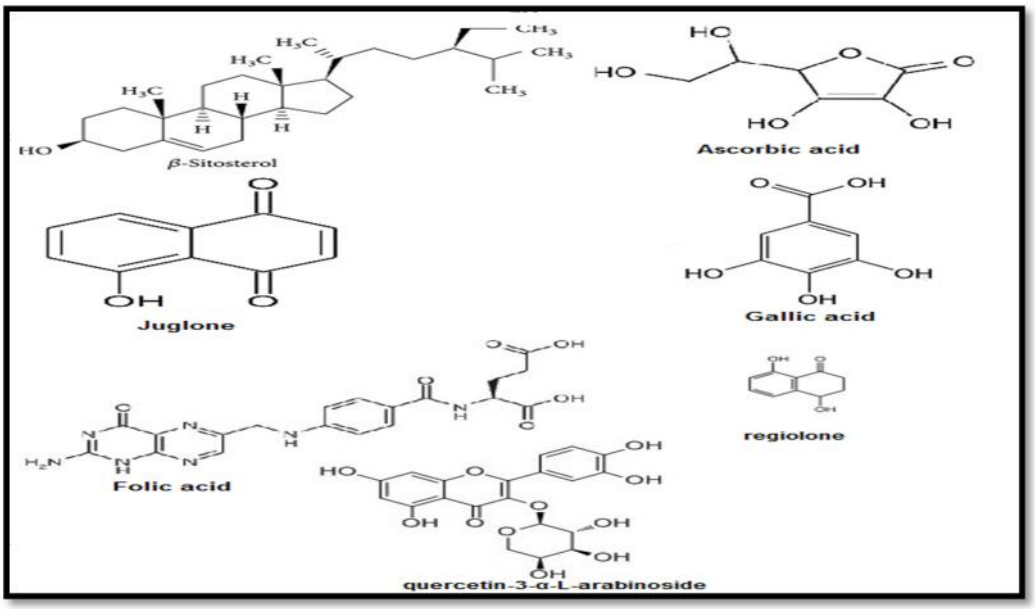

Figure (2.22): Chemical constituents of walnut tree bark [108].

2.16 Chemical Degradation

Degradation is generally defined as a loss of relevant properties of a material which develops gradually as a result of an exposure to external conditions. Degradation of polymers may be induced by thermal activation, oxidation, photolysis, radiolysis, or hydrolysis as shown in figure (2.23). If the degradation is affected by the biological environment, it may also be referred to as biodegradation [113].

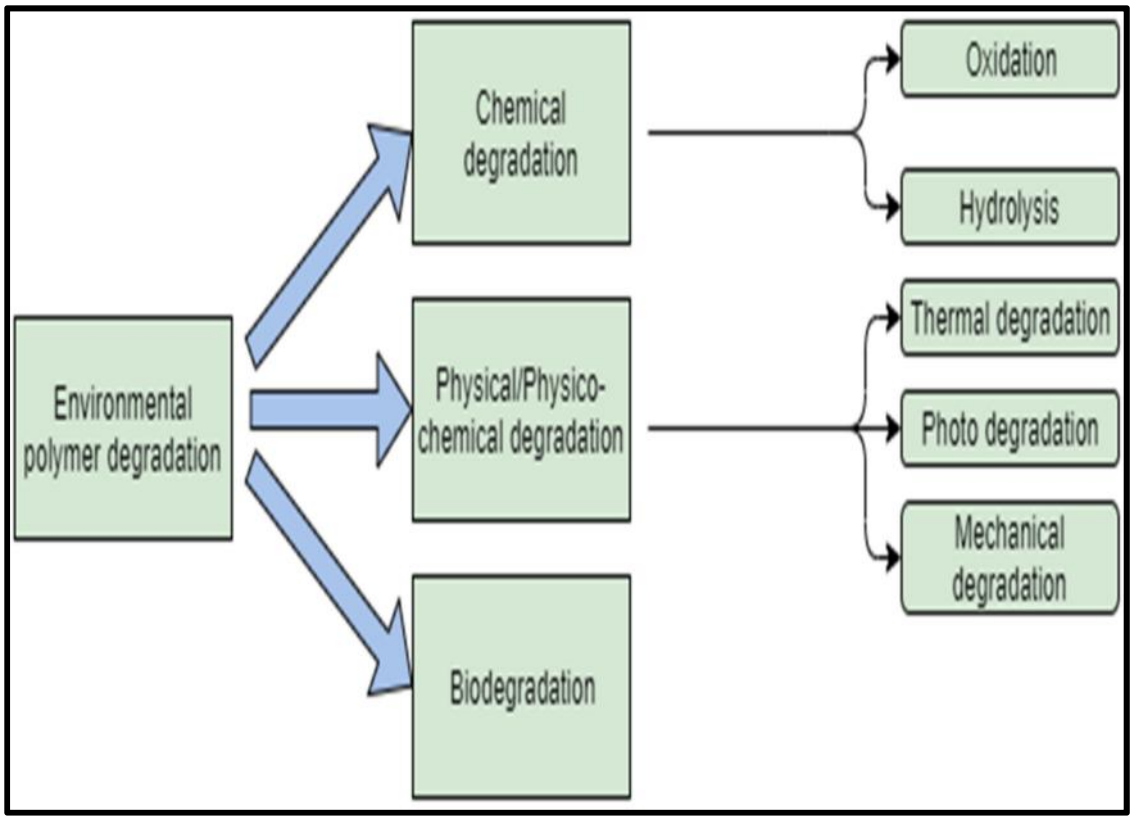

Figure (2.23): Schematic presentation of polymer degradation [113].

Chemical degradation causes the main deterioration of polymeric chains by a random cleavage of covalent bounds, depolymerization as shown in figure (2.24), or cross linking of linear polymers, interfering with regularly order chain and with crystallinity, finally resulting in a decrease of mechanical properties [114].

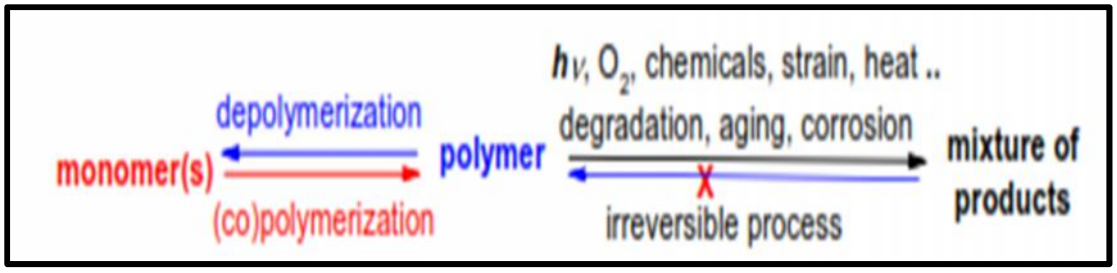

Figure (2.24): Relation among polymerization, depolymerization and degradation [115].

Oxidation is the primary driver for degradation of polymers when exposed to oxygen-containing environments, either under thermal, photo-oxidative, radiative or combined conditions. The exact oxidation level of the material more easily accessible through NMR, or IR based methods. NMR can provide exact oxidation levels, but is more limited when solid samples need to be analyzed or when oxidation levels are low. Therefore, the most widely applied analytical method to assess oxidation levels is to analyze and quantify carbonyl formation in polymers via IR spectroscopy due to the strong absorbance features of the C=O stretch vibration usually in the 1800 to 1650 cm^{-1} range [116].

FTIR analysis is capable of monitoring other chemical changes that take place throughout the lifetime of a material, by detecting the functional groups present at distinct bands. The CI is used to specifically monitor the absorption band of the carbonyl species formed during photo or thermo-oxidation processes, by measuring a ratio of the carbonyl peak relative to a reference peak. Not only is the CI used to measure oxidation occurring throughout the lifetime of polymers, but it is also employed to predict their service life and to develop stabilisation additives for materials [117].

2.17 Antioxidant Activity Assays

Dried polymeric solutions or their nanofibers (0.1g) were mixed with distilled water (10mL) on a magnetic stirrer at 500 rpm at room

temperature until finely dissolved solutions were obtained. These solutions were used in the antioxidant activity assay [118].

2.17.1 DPPH Assay

DPPH (2,2-diphenyl-1-picryl-hydrazyl-hydrate) free radical method is an antioxidant assay based on electron-transfer that produces a violet solution in ethanol. This free radical, stable at room temperature, is reduced in the presence of an antioxidant molecule, giving rise to colorless ethanol solution. The use of the DPPH assay provides an easy and rapid way to evaluate antioxidants by spectrophotometry, so it can be useful to assess various products at a time [118].

2.18 Antibacterial Assay

The antibacterial activity of the samples was determined by growth inhibition study method using Escherichia coli (E. coli) and Staphylococcus aureus (S. aureus). Three types of bacterial colonies were thawed in lysogeny broth (LB) and were incubated separately for overnight in a shaking incubator at 37ºC. Using the spread plate method, after mixing 1 mL of thawed bacterial suspension containing around 10^5colony forming units for each bacteria with 9 mL of LB solution. The bacterial solution was suspended on the nutritive agar plate, and the samples were carefully placed on the inoculated plates. The agar plates with samples were incubated at 37ºC for 24 h. The inhibition area measurement was measured [66].

2.19 Literature Review

Bogdanel Silvestru, et al. (2014) investigated the antibacterial property and antioxidant activity of two active components within polylactic acid (PLA) nanofibers via electrospinning (PLA/Ag-NP/VitaminE nanofibers). The characterization of PLA/Ag-NP/VitaminE nanofibers was performed by SEM, TEM and XRD. Ag-NP has average

diameter of 2.7 ± 1.5 nm within the PLA nanofiber matrix with a few aggregates. PLA/Ag-NP/VitaminE nanofibers inhibited growth of Escherichia coli, Listeria monocytogenes, and Salmonella typhymurium up to 100 % whereas the antioxidant activity of PLA/AgNP/VitaminE nanofibers was determined as 94 %.

The results of the tests on fresh apple and apple juice indicated that, the PLA/Ag/VitaminE nanofiber membrane actively reduced the polyphenol oxidase activity. These materials could find application in food industry as a potential preservative packaging for fruits and juices [119].

Touseef Amna, et al. (2015) illustrated the new class of antimicrobial hybrid packaging mat composed of biodegradable polyurethane supplemented with virgin olive oil and zinc oxide via electrospinning. Instead of mixing antimicrobial compounds directly with food, incorporation in packaging materials allows the functional effect at food surfaces where microbial activity is localized.

The nanofibers were characterized by SEM, EDX, XRD and TEM. The antibacterial activity was tested against two common foodborne pathogens viz., Staphylococcus aureus and Salmonella typhimurium. The results indicated that incorporation of olive oil in the polymer affected morphology of PU nanofibers and nanocomposite packaging were able to inhibit growth of pathogens. This mat can be used as packaging for meat products to reduce contamination and could serve to replace PVC films [120].

Lin Lin, et al. (2017) showed a novel antibacterial packaging material was engineered by incorporating cinnamon essential oil/β-cyclodextrin (CEO/β-CD) proteoliposomes into poly(ethylene oxide) (PEO) nanofibers by electrospinning technique. Herein, PEO was a stabilizing polymer and used as electrospinning polymeric matrix for the

fabrication of CEO/β-CD proteoliposomes nanofibers. The CEO/β-CD inclusion complex was prepared by the aqueous solution method and characterized by Raman and FTIR spectroscopy. The antibacterial efficiency of CEO/β-CD proteoliposomes against *B. cereus* was enhanced without any impact on sensory quality of beef.

The results demonstrated that the CEO/β-CD proteoliposomes nanofiber scan significantly extend the shelf life of beef and have potential application in active food packaging [121].

Ping Shao, et al. (2018) reported the effects of different concentrations (0.5%, 1%, 1.5%, w/v) of tea polyphenols (TP) incorporated into pullulan Carboxymethylcellulose sodium (Pul-CMC) solutions on electrospun nanofiber films. The morphological features of nanofibers were modulated through adjusting process parameters (e.g. concentration of polymer solution, applied voltage and feeding rate). It was observed that polymers under lower concentration of TP produced nanofibers with smaller diameters.

When the TP concentration of solution is 1%, its diameter distribution is more uniform, with the average diameter of 127 nm. Increasing the applied voltage from 19 to 21 kV and the feed rate from 0.36 to 0.6 mL/h leads to a reduction in mean fiber diameter. An increase of the feeding rate decreased the nanofibers diameter. FTIR and DSC analysis indicated the successful and stable incorporation of TP into pullulan-CMC nanofibers. For the application, fibrous Pul-CMC-TP films showed a significant effect on prolonging the shelf-life and improved the quality of the fruit during storage [122].

Aylin Altan, et al. (2018) were produced the composite fibrous films from zein and poly(lactic acid) (PLA) by incorporating carvacrol at three different concentrations (5, 10 and 20%) using electrospinning. Results demonstrated that highly volatile carvacrol was successfully

encapsulated in electrospun zein and PLA fibers. The morphology and size of fibers by SEM images showed that bead free fibers. Thermogravimetric analysis (TGA) for the incorporation of carvacrol in PLA fibers showed increased thermal stability, while in the case of zein, the addition of carvacrol did not influence the thermal stability of zein fibers.

The antioxidant activity of carvacrol loaded zein fibers ranged from 62 to 75%, while antioxidant capacity of PLA fibers varied from 53 to 65% for (5-20) % carvacrol content. As a result carvacrol loaded electrospun fibers with its antioxidant and antimicrobial properties can be used to extend shelf life of fresh foods as a new approach of electrospun fibers in food applications [123].

Yaowen Liu , et al. (2018) were reported the fabrication of four polylactic acid/tea polyphenol (PLA/TP) composite nanofibers, with PLA/TP ratios of 5:1, 4:1, 3:1, and 2:1, that were successfully prepared by electrospinning. The fibers of resulting composite materials were morphologically uniform, with fiber diameters that decreased with increasing TP content.

The mechanical properties of the PLA/TP-3:1 nanofibers were slightly compromised compared to those of the PLA fibers, with a tensile strength and elongation at break of (9.28 ± 3.6) MPa and (50.36% ± 10.88%), respectively, which meet the requirements for food packaging applications. The PLA/TP-3:1 composite fiber also exhibited the strongest DPPH RSA (95.07%±10.55%) and good antimicrobial activities against *E. coli* and *S. aureus* (92.26% ± 5.93% and 94.58% ±6.53%, respectively). Therefore, PLA/TP composite nanofibers have the potential to be alternative bioactive materials for food packaging applications [124].

Yuyu Liu, et al. (2018) illustrated the ethylcellulose/gelatin solutions containing various concentrations of zinc oxide (ZnO) nanoparticles were electrospun, and the resultant nanofibers were characterized by SEM, FTIR, mechanical testing, water contact angle, and water stability. Results indicated that ZnO nanoparticles acting as fillers interacted with polymers, resulting in the enhanced surface hydrophobicity and water stability of nanofibers.

The antibacterial assay showed a concentration-dependent effect of ZnO on the viabilities of *Escherichia coli* and *Staphylococcus aureus*. Notably, the antimicrobial efficiency of the 1.5 wt% ZnO-containing fibers against *S.aureus* was 43.7%, but increased to 62.5% after UV irradiation at 364 nm, possibly due to the significantly increased amounts of intracellular reactive oxygen species. These results suggested that the ZnO-containing nanofibers with excellent surface hydrophobicity, water stability and antimicrobial activity exhibited potential uses in food packaging [125].

Suelen Goettems Kuntzler, et al. (2018) were developed electrospinning method produced long and continuous nanofibers containing 3% chitosan/2% PEO/1% phenolic compounds were 214 ± 37 nm in diameter. These nanofibers presented degradation temperature higher in relation of the phenolic compounds, an important parameter for food packaging. The chitosan/PEO nanofibers exhibited antibacterial activity against *S. aureus* (6.0 ± 0.7 mm) and, chitosan/PEO/phenolic compounds nanofiber presented 6.4 ± 1.1 mm and 5.5 ± 0.4 mm for *S. aureus* and *E. coli* respectively. This polymeric nanofibers produced from chitosan and containing phenolic compounds have properties that therefore allow their application as active packaging [126].

Tian-Tian Yue, et al. (2018) showed the potential application of electrospun CMCS/PEO nanofiber membrane in fruit fresh-keeping. The

microstructure, antibacterial activity, and air permeability of the nanofiber membrane have been tested. For comparison, the fresh-keeping effects of commercial cling wrap and CMCS/PEO nanofiber membranes on strawberries' rotting rate and weight loss rate have been studied.

The results indicate that the electrospun CMCS/PEO membrane could effectively avoid water loss in strawberries and has a remarkable effect to prolong strawberries' shelf life due to its breathability and antibacterial activity. In addition, the composite CMCS/PEO, nanofiber membrane is non-poisonous and edible, which can be suitable as packing materials for fruit. Compared with typical conventional coatings. This environmentally friendly technology may provide an alternative approach to the fruit in growing, transporting, and selling [127].

Kelly Johana Figueroa-Lopez, et al. (2018) evaluated the effect of using electrospun polycaprolactone (PCL) as a barrier coating and black pepper oleoresin (OR) as a natural extract on the morphology, thermal, mechanical, antimicrobial, oxygen, and water vapor barrier properties of solvent cast gelatin (GEL). The antimicrobial activity of the multilayer system measured for (GEL) cast films were coated by the so-called electrospinning coating technique was also evaluated against Staphylococcus aureus strains for 10 days.

The results showed that the multilayer system containing PCL and OR increased the thermal resistance, elongated the GEL film, and significantly diminished its permeance to water vapor. Active multilayer systems stored in hermetically closed bottles increased their antimicrobial activity after 10 days by inhibiting the growth of Staphylococcus aureus. This study demonstrates that addition of electrospun PCL ultrathin fibers and OR improved the properties of GEL films, which promoted its potential use in active food packaging applications [6].

Li He, et al. (2019) showed an active polyvinyl alcohol (PVA) composite film incorporating pomegranate peel extract (PPE) and sodium dehydroacetate (SD) by electrospinning process. The effects of the ratio of PPE to SD (1:0, 1:0.5, 1:1, 0.5:1,0:1) on physical properties, appearance, oxidation resistance, and antibacterial performance of the resulting films were investigated and showed that the ideal PPE to SD ratio is 1:1

The results show that the addition of PPE and SD to PVA film can improve its elongation at break, but has no significant effect on its light transmission or water vapor permeability. The FTIR results indicate that the PVA/PPE/SD electrospun film is not a simple physical mixture, but instead involves multiple chemical reactions.

The antibacterial effect against S. aureus show results better than that against E. coli. When combined between PPE and SD at ratio (1:1). The results of this study can use in food packaging applications [128].

Kowsalya E, et al. (2019) exhibited that the peel extract of Vitis vinifera (black grapes) possesses the capacity to synthesize silver nanoparticles (AgNPs) of significant bactericidal activity. Additionally, were incorporated the synthesized AgNPs in poly(vinyl alcohol) matrix through the electrospinning method.

The AgNPs and Ag/PVA nanofiber showed good antibacterial activity against tested food pathogenic bacterial strains. The Ag/PVA nanofiber demonstrated an increased shelf life when surface-coated over the fruits, Citrus limon (lemon) and Fragaria ananassa (strawberry). These results indicated that Ag/PVA nanofiber can potentially be used as antimicrobial packaging for food preservative applications. [129].

Maryam Nazari, et al. (2019) showed that the cinnamon essential oil (CEO) nanophytosomes (N/CEO) successfully incorporated in cross-linked PVA nanofiber (PVAc-N/CEO) via the electrospinning method to

improve the antibacterial activity and reduced the toxicity of CEO during storage period.

The antibacterial effect results against both Gram-positive and Gram-negative bacteria showed improved during 12 days and reduced the toxicity of CEO on human colon cancer cells compare with CEO loaded PVAc nanofiber (PVAc-CEO). Also, results show the microbial assays on raw shrimps showed that the (PVAc-N/CEO) sample increased significantly the shelf-life more than other samples.

This results exhibited that this novel hybrid nanostructure (PVAc-N/CEO) can be used as a new approach to improving application of various essential oils in food packaging [131].

Lin Lin, et al. (2019) studied the moringa oil-loaded chitosan nanoparticles (MO/CNPs) and fabricate MO/CNPs embedded gelatin nanofibers for biocontrol of Listeria monocytogenes and Staphylococcus aureus on cheese. The optimal MO/CNPs were prepared by the ionic crosslinking method with the concentration of moringa oil at 20 mg/mL and chitosan at 3.0 mg/mL. The optimal concentration of MO/CNPs embedded in gelatin nanofibers was found to be 9.0 mg/mL after the determination of nanofiber physical properties.

The results of SEM and AFM confirmed that the nanofibers were prepared successfully and achieved uniform diameter at 142.5 nm. For the application on cheese, MO/CNPs nanofibers possessed high antibacterial activity against L. monocytogenes and S. aureus at 4 °C and 25 °C for 10 days, without any effect on the sensory quality of cheese. As a result, MO/CNPs nanofibers could be a promising active food packaging material for food preservation [92].

Yadong Tang, et al. (2019) showed the gelatin nanofibers incorporated with two kinds of essential oils (EOs); peppermint (PO) and chamomile (CO), were fabricated by electrospinning for potential edible

packaging application. Electron microscopy showed that smooth and uniform morphology of the gelatin/EOs was obtained. (^{1}H-NMR) spectrum confirmed the existence of PO and CO in nanofibers after electrospinning. The addition of EOs led to an enhancement of the water contact angle of nanofibers. The antioxidant activity was significantly improved for the nanofibers loaded with CO, while the anti-bacteria activity against *Escherichia coli* (*E. coli*) and *Staphylococcus aureus* (*S. aureus*) was better for the fibers with PO addition.

Finally, the MTT assay with NIH-3T3 fibroblasts demonstrated the absence of cytotoxicity of the gelatin/EOs nanofibers. Thus, this study suggest that the developed gelatin/PO/CO nanofiber could be a promising candidate for edible packaging [132].

S.K.V. Bharathi, et al. (2020) illustrated the Zein nanofibre/chitosan (Z-NF/CH) bilayer film manufactured by using direct electrospinning of zein on solution cast chitosan film. Zein nanofibres, with an average fibre diameter of ~286 nm, exhibit a slight increase in antioxidant activity than those of solution cast zein film. Nanofibre coating on chitosan film showed a significant improvement in antioxidant activity, without significantly affecting mechanical properties and moisture permeability characteristics.

The bilayer film has proved to possess anti-browning ability on fresh-cut fruits. Thus, zein nanofibre coated chitosan bilayer films can be used as an efficient packaging material for fresh-cut fruits and vegetables because of their edible, biodegradable and unique surface characteristics that support their antioxidant potential [133].

Samira Dehghani, et al. (2020) studied the potential of chia seed mucilage (CSM) as a new source of carbohydrate for encapsulation of green cardamonmum essential oils (GCEOs). ^{1}H NMR spectrum, FTIR

spectrum, and SEM imaghas confirmed the existence of the GCEOs in the nanofibers. The nanofibers of CSM and polyvinyl alcohol have not antibacterial property, while nanofibers containing GCEOs show antibacterial activity against E. coli and S. aureus. Incorporating GCEOs in CSM nanofibers improved the antioxidant of the generated nanofibers. The amount of radical scavenging for the nanofibers containing 16 (mg/ml) of GCEOs was 18% and increasing the GCEOs concentration up to 64 (mg/ml) leads to grow the activity up to 41%. Thus, this study indicates that nanofiber can be used as a novel antioxidant and antibacterial agent in the food and pharmaceutical industry [97].

Laura M Fonseca, et al. (2020) showed that the thyme essential oil (TEO) is an excellent natural substitute for synthetic compounds to maintain the quality and safety of food products acting as an antioxidant agent. The nanoencapsulation of TEO at concentrations of (1%, 3%, and 5% v/w) in electrospun nanofibers made of starch (50% w/v) and formic acid (75% v/v). Rheological parameters of the fiber-forming solutions were measured, and various physical and chemical properties of the nanofibers were analyzed.

The results showed the starch/TEO nanofibers homogeneous morphology and high encapsulation efficiency (EE, 99.1% to 99.8%), which, along with (FTIR) spectrum and (TGA) analysis, indicate strong protection of the phenolic compounds of TEO. The antioxidant activity against 2,2-diphenyl-1-picrylhydrazyl (DPPH) radicals of the starch/TEO nanofibers varied from 11.1% to 14.2% and the inhibition values (29.8%) against hydroxyl radicals were the same for free TEO and the nanofibers.

Finally, owing to these properties, electrospun starch/TEO nanofibers can be applied in food products or food packaging [86].

Sen Li, et al. (2020) studied a novel degradable antioxidant nanomaterial with hordein, quercetin and chitosan via electrospinning.

Heat treatment was applied to increase the water resistance of the blended nanofibre film. Results showed that heat treatment significantly improved the water resistance of the blended nanofiber film without affecting its antioxidant activity. In addition, the heat-treated NF film also delayed the rate of enzymatic browning of the incised apple and potato surfaces. Physiochemical analysis indicated that heat treatment could result in the crosslinking of the electrospun blended NFs and alter their physiochemical properties. Thus, heat treatment could be an effective method to improve the mechanical characteristics of protein-based NFs, and the heat-treated hordein-quercetin-chitosan electrospun nanofibre film was a novel biodegradable material with excellent antioxidant activity and water resistance for food packaging [134].

Ying Zhou, et al. (2020) fabricated gelatin/ angelica essential oil (AEO) nanofibers with a certain percentage of AEO (0%,3%, 6%, 9% v/v) via electrospinning technique. SEM images revealed all the electrospun membranes possessed homogeneous nanofibrous morphology.^{1}H-NMR analysis confirmed the existence of AEO in the gelatin/AEO nanofibers. The addition of AEO reduced the wettability and enhanced the water barrier function of gelatin nanofibers.

The radical scavenging assay and antibacterial activity indicated that the gelatin/AEO nanofibers have excellent antioxidant activity and good antibacterial function against both Gram-positive and Gram-negative bacteria. Moreover, MTT assay revealed the non-cytotoxicity of gelatin/AEO nanofibers. These results indicate that the developed gelatin/AEO nanofibers show great potential as a food packaging material [135].

Vivek Kumar Pandey, et al. (2020) showed the stable silver nanoparticles (AgNPs) of size 80 ± 11 nm produced by chitosan (CH) mediated green synthesis were blended with polyvinyl alcohol (PVA) to

form electrospun fibrous composite nano-layers (FCNLs). The crystallinity and chemical nature of the electrospun composite was characterised by using X-ray diffraction (XRD) and FTIR spectroscopy, respectively, and its hydrophobicity was characterised by measuring the water contact angle.

The electrospun composite showed effective antimicrobial activity against Listeria monocytogenes (gram +ve) and Escherichia coli (gram –ve) bacterial species. The electrospun composite, when tested as packaging material for meat, showed bioactivity and extended the meat shelf-life by one week. The electrospun nanocomposite is able to inhibit microbial degradation of packaged food and extend its keeping quality in an eco-friendly manner [136].

Motahira Hashmi, et al. (2021) studied the fabrication and characterization of CMC nanofibers using polyvinyl alcohol (PVA) and polyvinylpyrrolidone (PVP) as capping agents and carriers for sustainable food packaging applications. From the results of morphological characterization, it was concluded that CMC could be electrospun along with PVA and PVP, and possess uniform morphology. The water contact angle was also measured to confirm the stability of nanofibrous mats in outdoor use. It was concluded that all nanofibers were found to be hydrophobic due to crosslinking.

Tensile properties were also found to be conformed to the target application as all nanofibers of the tricomponent blend had tensile strengths well above 10 MPa. Air permeability was concluded that all nanofibrous mats possess excellent air permeability, From the results of performed tests, it was observed that nanofiber mats possess enough mechanical, structural, and morphological properties to be used as food packaging [137].

Die Zhang, et al. (2021) illustrated the functional starch composite nanofibrous films were successfully fabricated by combining electrospinning technique and vapor cross-linking reaction. The hydrogen bonding interaction between starch and tea polyphenol (TP) was demonstrated by FTIR and XRD analysis.

The incorporation of TP/SNF provided antioxidant activity. Static tensile testing revealed that the mechanical property of starch composite fibrous films could be improved with the incorporation content of 10%TP and the cross-linking reaction exhibited little effect on its antioxidant activity.

In addition, the wettability experiments showed that the cross-linked time improve the hydrophobicity of the composited films with the water contact angle up to 87.2 after 2.5 h reaction time. In conclusion, the fabricated starch-based fibrous films with multiple functionalities of good mechanical property, antioxidant activity and hydrophobicity showed promising potential for food packaging [138].

Elham Ansarifar, et al. (2022) investigated the effect of thyme essential oil (TEO) encapsulated into zein electrospun fiber film on extending the shelf life and preserving the quality of strawberry fruit during storage. Results indicated that TEO presented potent antibacterial activity against Bacillus cereus, Escherichia coli and Aspergillus fumigatus.

The scanning electron microscopy images of zein fiber had a linear shape, absence of beads, and smooth surface. The encapsulation efficiency (EE) of TEO in the zein fiber was about 75.23%. Encapsulated TEO released at a slower rate than free TEO. The zein/TEO fibers (zein fiber film loaded with TEO) decreased weight loss and maintained the anthocyanin content, frmness and color of the strawberries during storage. After 15 days of storage, weight loss reduced about 15% and

firmness was higher about 20% in packed fruit with zein/TEO fibers compared to control [139].

2.20 Summary of Literature Review

The literature review cover many researchers who studied the food packaging nanofibers and study its antibacterial, antioxidant, and antifungal behavior, the effect the natural fillers and its types on these behavior.

Most researchers focused on using polymers that hydrophobic in nature and which dissolve in toxic organic solvents for producing hydrophobic nanofibers or using polymers which dissolve in water for prepare edible nanofibers.

While in current study, it is interested to prepare nanfibers with hydrophobic features based on highest contact angle in wettability test despite using polymers dissolve in water.

Additionally, utilize natural filler from walunt tree bark as powder and not as solution to obtain antibacterial, antioxidant, and antifungal nanofibers.

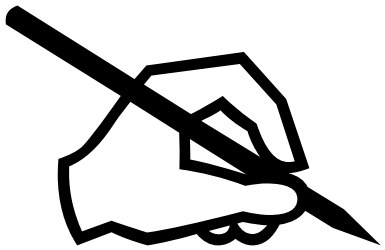

CHAPTER THREE

EXPERIMENTAL WORK

3.1 Introduction

This chapter covers the most important details about the methodology used in this thesis, starting with materials selection and specification, preparation of blend, and the devices of inspection.

3.2 Materials Used

3.2.1 Poly (vinyl alcohol) (PVA)

Poly (vinyl alcohol) was used as a powder from central drug house (P) Ltd. Its specification is listed in the table (3.1).

Table (3.1): Specification of the used PVA.

Property	Specification
Physical Form	A white to off-white crystalline powder/ flakes / granular
Molecular Weight	13000-23000 g/mol
Solubility	Soluble in hot water
Viscosity (4% water)	9.00 to 21.00 cP
Hydrolysis (mole %)	87-89%
pH (4% water)	4.5-6.5

3.2.2 Corn Starch (ST)

Corn starch (ST) was obtained from Alpha Chemika (India) as powder. Its specification and chemical composition are shown in table (3.2).

Table (3.2): Specification and chemical composition of the used (ST).

Property	Specification
Physical Form	A white /almost white powder
Composition	25% amylose and 75% amylopectin
Ash Content %	0.13 %

3.2.3 Cress Seed Mucilage (CSM)

Cress seed was acquired from the Iraqi market. Mucilage was extracted by washing the seed in distilled water for 1 min. to remove any contaminants. Then, the cress seed (5 to 100 (w/w)) was added to deionized water, which was mixed using a magnetic stirrer at 100ºC for 15 minutes. Afterward, a cloth filter was used to separate the seed from the mucilage in the solution. The mucilage solution is then allowed to cool before being utilized in the experiment.

3.2.4 Essential Oils (EOs)

The essential oils used in this study, such as moringa oil (MO), cardamom oil (CO), clove bud oil (CBO), thyme oil (TO), and fenugreek oil (FO) were purchased from Iraqi market.

3.2.5 Walnut Tree Bark Powder (WB)

The walnut tree bark (Juglandacea) was purchased from the Iraqi market and was washed and dried the bark in the oven at 40º C for 1 hour to remove any contaminants. After that was grinded by stainless steel grinder, which has the following specifications (230 V~50Hz, 650W), and dried in the oven at 40º C for one hour. Then was examined by particle size analyze (D50= 1.235 µm).

3.3 Preparation of Samples

3.3.1 First Part

The first blend in this part consist from dissolve (8g) PVA in (100 ml) of hot distilled water at 80^{o}C for 90 minutes under a magnetic stirrer.

Then, prepare the starch gelatinization solution by dissolving (2.5 wt.%) of starch in (100 ml) of hot distilled water at 90 ^{o}C for 15 minutes and selected (2.5 wt.%) because the maximum concentration of starch used to form nanofibres along with PVA

is limited to 3%. On increasing the starch concentration to 3.5 % weight, the viscosity of the solution increased, and it was not suitable for electrospinning [87].

PVA-STA solutions were created by incorporating PVA and STA in various volume ratios (60:40, 50:50, and 40:60) using a magnetic stirrer for one hour at room temperature. The second blend consist of mixing the cress seed mucilage and PVA for 1 hour using a magnetic stirrer to obtain homogeneous solutions with varying volume ratios (60:40, 50:50, and 40:60).

Finally, using a magnetic stirrer, the two blends from PVA-STA-CSM were combined for 1 hour in various volume ratios (40:35:25, 40:30:30, and 40:25:35). All these blends were prepared for producing nanofiber by the electrospinning method.

The ideal volume ratio was selected on based the highest contact angle for (PVA-STA), (PVA-CSM), and (PVA-STA-CSM) nanofibers. This part of the research plan is shown in a diagram (3.1).

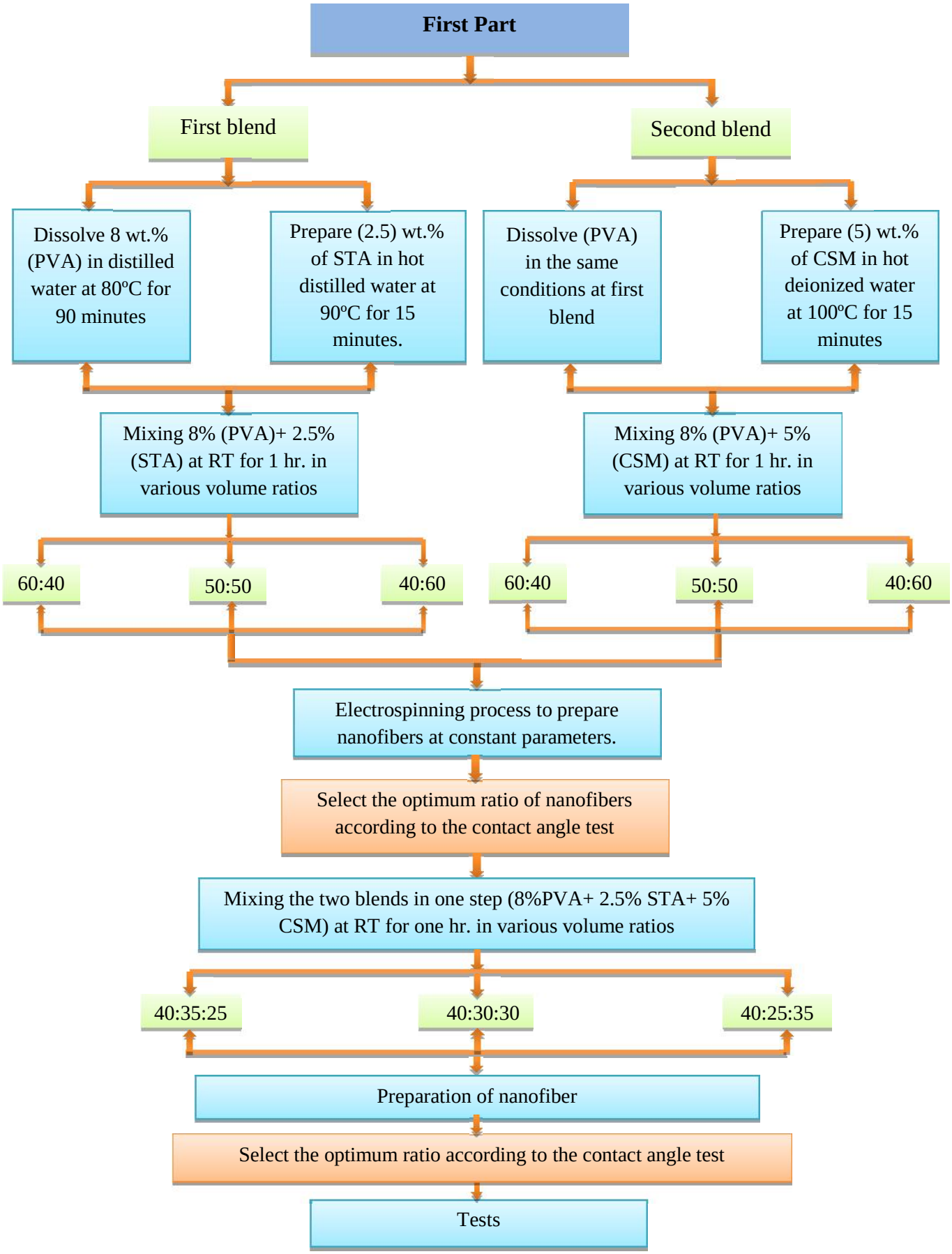

Figure (3.1): Diagram of the first part of the work plan.

3.3.2 Second Part

Filler addition from essential oils such as (Moringa oil, Cardamom oil, Clove bud oil, Thyme oil, and fenugreek oil) in various concentrations (1, 5, 10 wt.%). Each oil mix with optimum ratio (40:30:30) of (PVA-STA-CSM) separately for 24hr. by a magnetic stirrer at room temperature. The other addition from walnut tree bark (WB) powder in different percentages (0.3, 0.5, 0.7 wt.%), which blend with (40PVA:30STA:30CSM) for 3hr. using a magnetic stirrer at room temperature as shown in a diagram (3.2).

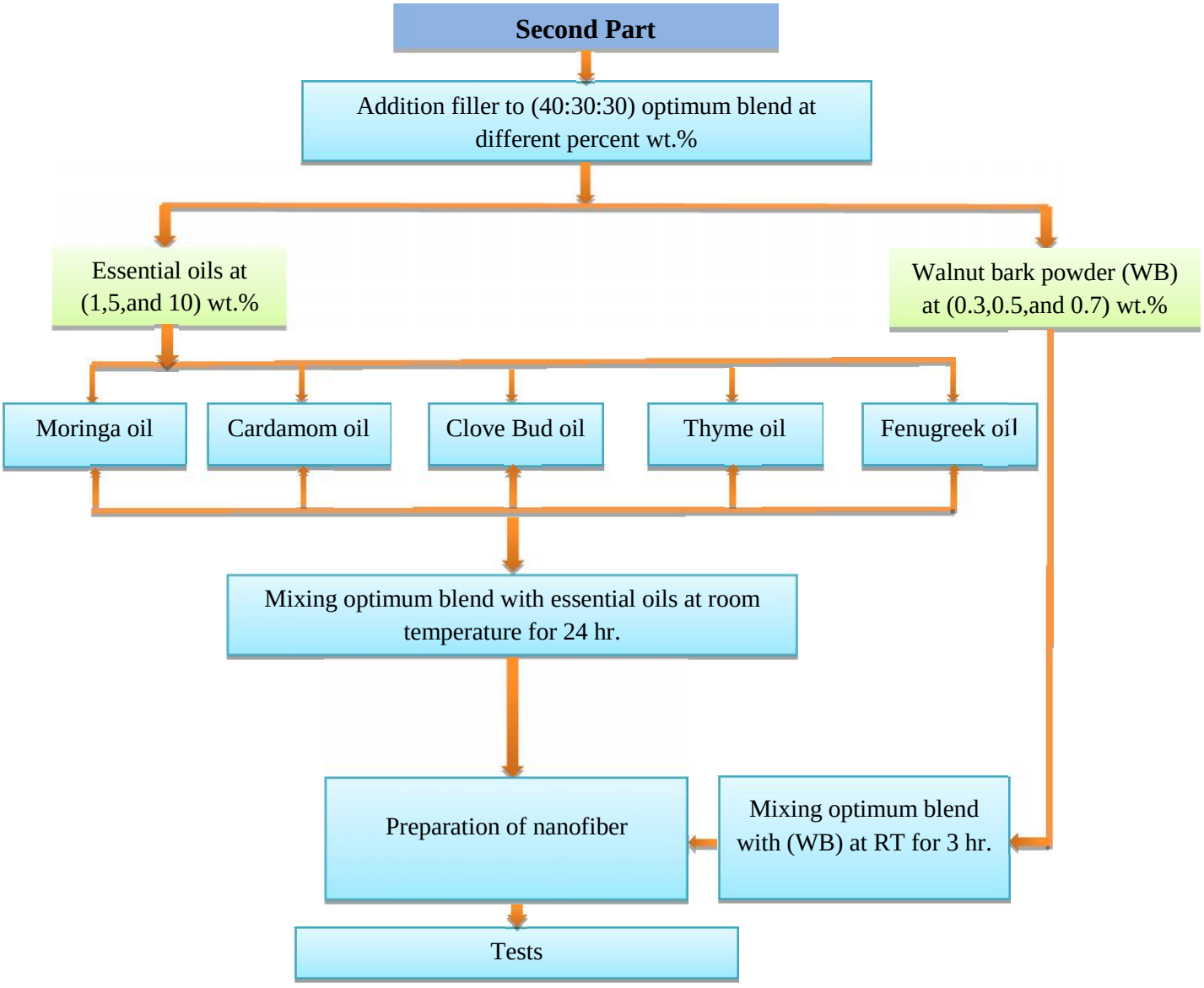

Figure (3.2): Diagram of the second part of the work plan.

3.3.3 Third Part

The final blend consists of (10%) from each essential oils blended with (0.5%) of (WB) by using a magnetic stirrer for 24hr. at room temperature for preparation of nanofiber as illustrated in a diagram (3.3). These percentages were chosen according to antibacterial activity and antioxidant activity. Table (3.3) displayed the symbols of all samples in every part of research plan.

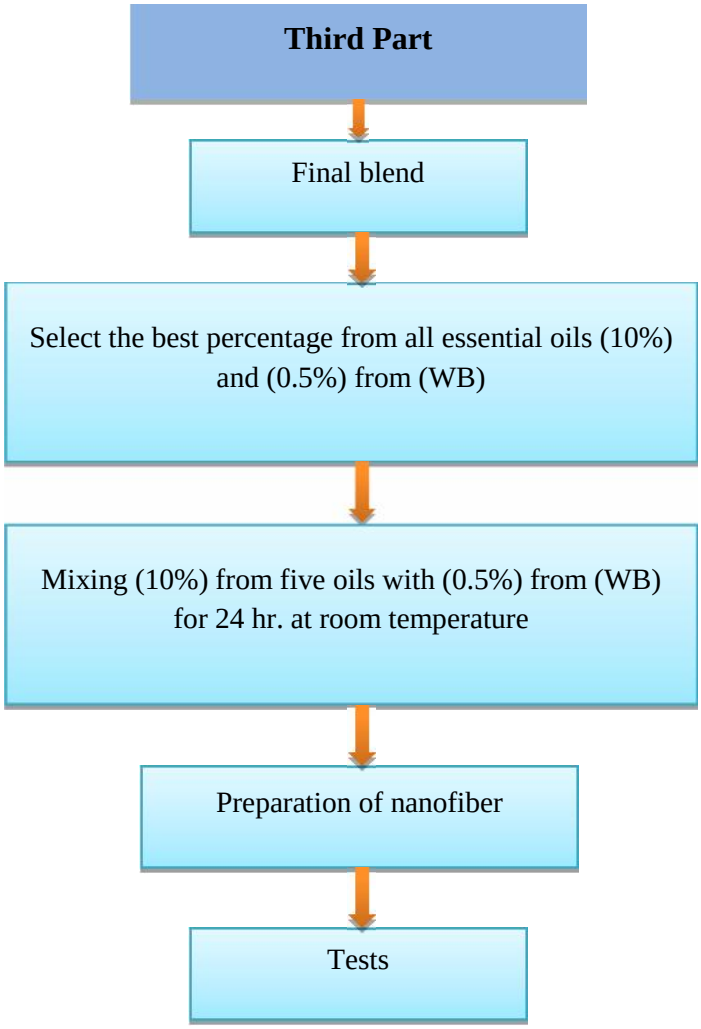

Figure (3.3): Diagram of the third part of the work plan.

Table (3.3): Component and Symbols of samples in all parts.

No. of Part	Name of Sample	Symbol
The first	PVA 100%	S_1
	PVA:STA (60:40)	S_2
	PVA:STA (50:50)	S_3
	PVA:STA (40:60)	S_4
	PVA:CSM (60:40)	S_5
	PVA:CSM (50:50)	S_6
	PVA:CSM (40:60)	S_7
	PVA:CSM:STA (40:30:30)	S_8
	PVA:CSM:STA (40:35:25)	S_9
	PVA:CSM:STA (40:25:35)	S_{10}
The second	PVA:CSM:STA (40:30:30) [Basic]	S_8
	Basic+1%MO	S_8+MO_1
	Basic+5%MO	S_8+MO_2
	Basic+10%MO	S_8+MO_3
	Basic+1%CO	S_8+CO_1
	Basic+5%CO	S_8+CO_2
	Basic+10%CO	S_8+CO_3
	Basic+1%CBO	S_8+CBO_1
	Basic+5% CBO	S_8+CBO_2
	Basic+10% CBO	S_8+CBO_3
	Basic+1%TO	S_8+TO_1
	Basic+5%TO	S_8+TO_2
	Basic+10%TO	S_8+TO_3
	Basic+1%FO	S_8+FO_1
	Basic+5%FO	S_8+FO_2
	Basic+10%FO	S_8+FO_3
	Basic+0.3%WB	S_8+WB_1
	Basic+0.5%WB	S_8+WB_2
	Basic+0.7%WB	S_8+WB_3
The third	Basic+10%MO+10%CO+10%CBO+10%TO+ 10%FO+0.5%WB	S_f

3.4 Electrospinning Process

All parts of the research plan were carried by electrospinning device to produce nanofibers as shown in figure (3.4) at constant parameters applied voltage (20 kV), flow rate (1ml/hr.), distance between collector and needle (20 cm), and speed collector (600 r.p.m)). After that, the parameters of electrospinning vary for the final blend in part three, as displayed in the table (3.4). Table (3.5) illustrate the symbol of final blend at these parameters.

Table (3.4): Parameters of the electrospinning process.

No. of Part	Electrospinning Conditions					Ambient Parameter
	Applied voltage (kV)	Distance (cm)	Flow rate (ml/hr.)	Speed of collector (r.p.m)	Needle diameter (mm)	
First	20	20	1	600	0.4	Temperature (20-40) ºC Humidity % (25-40)
Second	20	20	1	600	0.4	
Third	20	20	1	600	0.4	
	26	20	1	600	0.4	
	20	20	1	600	0.2	
	26	20	1	600	0.2	
	20	20	0.5	600	0.4	
	26	20	0.5	600	0.4	

Table (3.5): Symbols of final blend at different parameters.

No. of Part	Name Sample	Symbol	
		Voltage (20kV)	Voltage (26kV)
Third part at different electrospinning conditions	**Basic+10%MO+10%CO+ 10%CBO+10%TO+10% FO+0.5%WB**	S_f	S_{f1}
		Needle Diameter (0.2mm)	
		Voltage (20 kV)	Voltage (26 kV)
		S_{f2}	S_{f3}
		Flow Rate (0.5ml/hr.)	
		Voltage (20 kV)	Voltage (26 kV)
		S_{f4}	S_{f5}

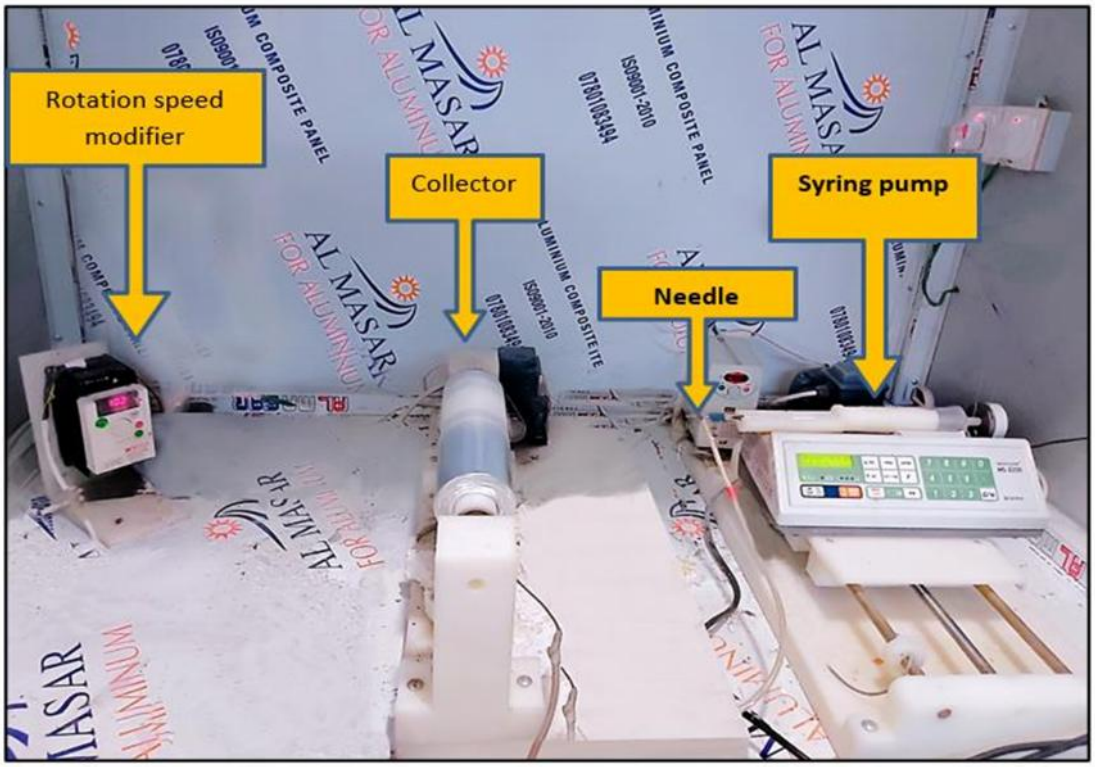

Figure (3.4): The electrospinning device.

3.5 Sampling

The shape of samples before and after the electrospinning method is illustrated in figure (3.5).

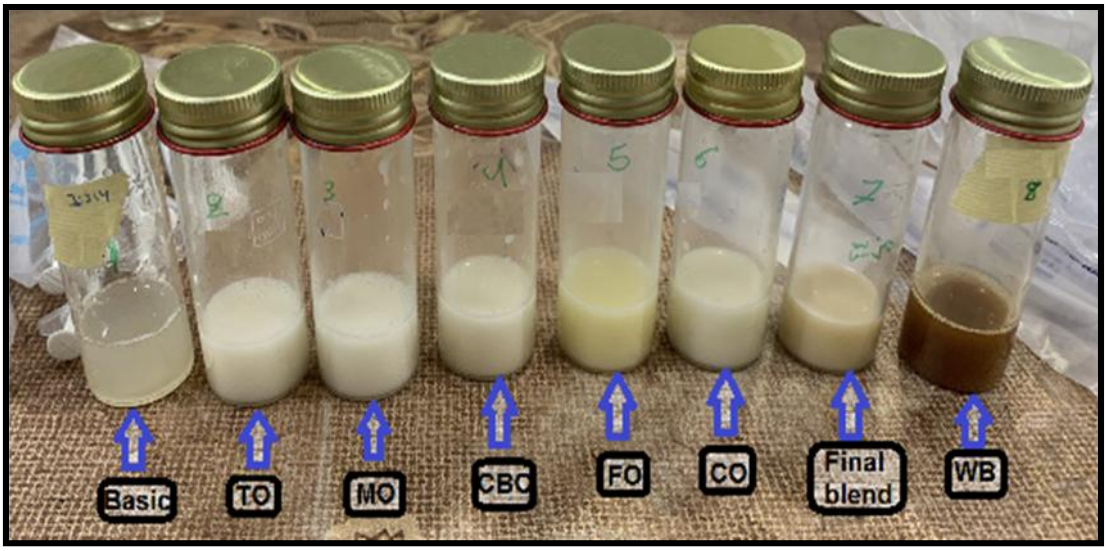

(a)

(b)

Figure (3.5): Samples (a) liquid before electrospun , (b) nanofibers of samples after electrospun.

3.6 Tests

The following tests were carried out for all parts of the research plan, as illustrated in figure (3.6).

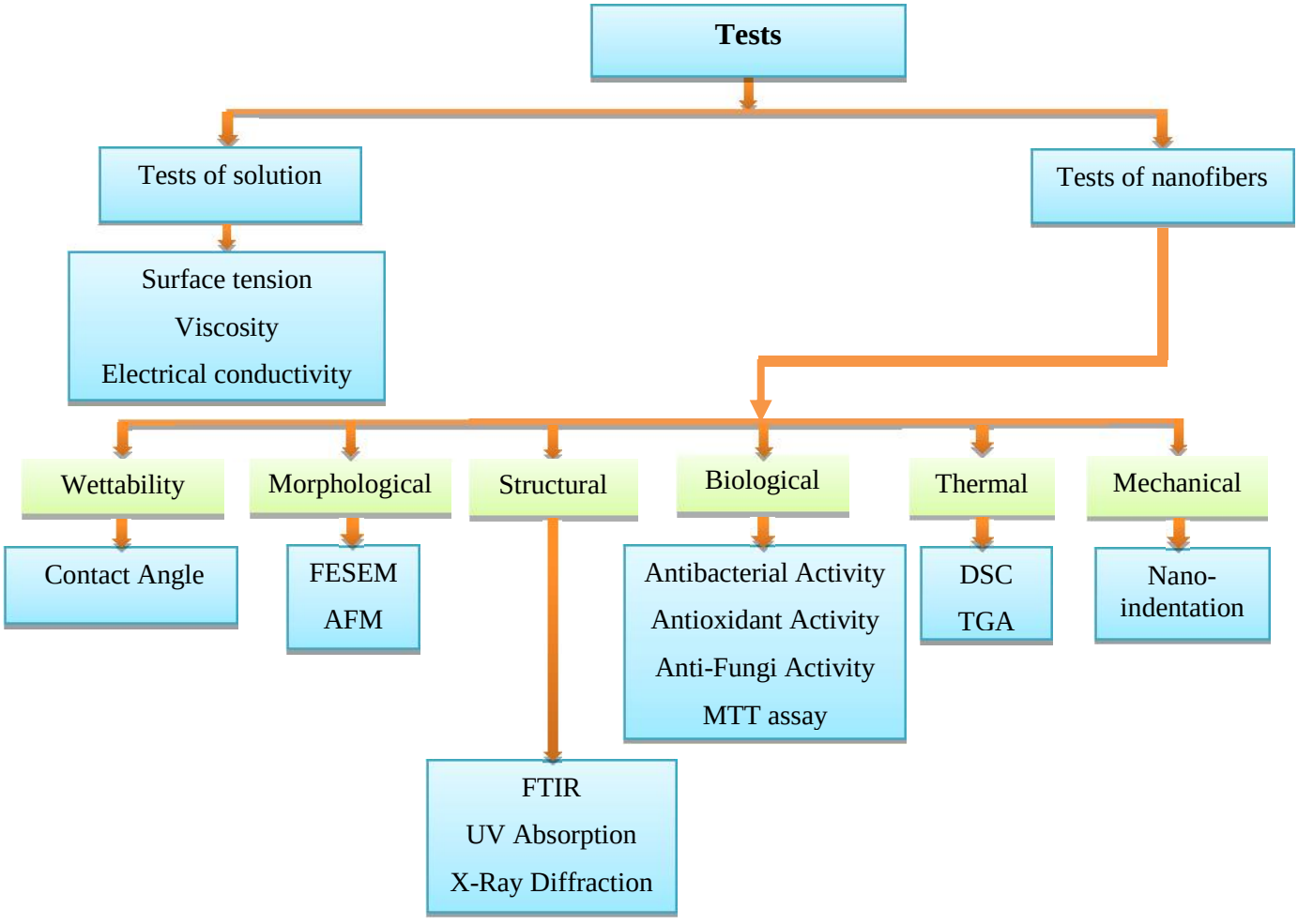

Figure (3.6): Tests diagram of all samples.

3.6.1 Solution Tests

3.6.1.1 Surface Tension

The surface tension of solutions was calculated by TEN202 Surface Interfacial Tensiometer in mN/m and consisted of a platinum ring immersed in a solution which was put in a cylindrical petri dish.

3.6.1.2 Viscosity

The viscosity of solutions was measured by (Brookfield DV-III Ultra Rheometer) at torque (19), RPM (20), and shear rate (40 1/sec) in cP units.

3.6.1.3 Electrical Conductivity

The electrical conductivity of solutions was calculated by (model HANNA instruments - EC 214 conductivity Meter).

3.6.2 Nanofibers Tests

3.6.2.1 Contact Angle

The wettability of the nanofiber samples was measured by calculating the contact angle (SL200B Optical Dynamic / Static Interfacial Tensiometer & Contact Angle Meter which manufactured in KINO Industry Co., Ltd., USA with contact angle range from 0^{o} to 180^{o}. This device makes calculation and comparison of left and right contact angle as well as calculate their average value giving a Real-time data graph monitoring changes of contact angle with video recording.

3.6.2.2 Fourier Transformation Infrared Spectroscopy (FTIR)

FTIR test was achieved by Fourier transform infrared spectrometer and according to ASTM (E1252). FTIR device type IR Affinity-1 (made in Japan). It is equipped with a room temperature DTGS detector, a mid-IR source (4000 to 400) cm^{-1} and a KBr beam splitter.

3.6.2.3 Differential Scanning Calorimetry (DSC)

DSC measurements were carried out according to ASTM (D3418-03) under a nitrogen gas atmosphere. The prepared samples with the weight of (8-10)± 0.5 mg were mounted in aluminum pans and heated up from 0 to 350 °C with a heating rate of 10 °C/min.

3.6.2.4 Ultraviolet-visible spectrophotometer (UV-Visible)

UV-Visible spectrophotometer, type UV-1800, (Shimadzu-Japan) was used as shown in figure (3.7). The liquid sample was put in the quartz cell of the device (1 cm). The aim of this test was to measure optical absorbance spectra for solutions.

Figure (3.7): Ultraviolet-Visible spectrophotometer device.

3.6.2.5 X-Ray Diffraction (XRD)

It is a rapid analytical technique primarily used for phase identification of crystalline materials and also can provide information on unit cell dimensions. It is generated in a cathode ray tube by heating a filament to produce accelerated electrons toward the target by applying high voltage. The crystal structure of the samples was investigated by the X-Ray Diffraction (Philips PAN alytical –X'Pert High Score Plus) at room temperature using CuK α (λ=1.54060 °A) as shown in figure (3.8).

The diffractograms were measured in the 2θ for 0-80°with X-ray voltage equal to 40 kV and Xray current equal to 30 mA.

Figure (3.8): Philips / PAN alytical X'Pert Pro-MPD (XRD) device.

3.6.2.6 Field Emission Scanning Electron Microscopy (FESEM)

Field emission scanning electron microscopy and "energy dispersive x-ray (EDX) tests were carried to the prepared nanofibers to check the fibers diameter distribution and the, smoothness and also the chemical components of them using the "FESEM (Zeiss Sigma 300- HV) GERMANY" instrument as shown in figure (3.9).

Figure (3.9): FESEM with EDX instrument.

3.6.2.7 Atomic Force Microscopy (AFM)

Film surfaces were also analyzed by an NT-DMT Atomic Force Microscope (NTEGRA Prima model, Moscow, Russia) operating in tapping mode as shown in figure (3.10). The images were processed using the software Nova Px (NT-MDT Co., Moscow, Russia, 2013) and three-dimensional images of the film surfaces (0μm - 16μm) were obtained.

Figure (3.10): Atomic Force Microscopy (AFM) device.

3.6.2.8 Thermogravimetric Analysis (TGA)

This test aims to study the thermal stability property of nanofibers samples. TGA manufactured by (Perkin-Elmer, Waltham, MA, USA) as shown in figure (3.11). TGA measurements were carried out under a heating rate of 20°C/min at a temperature range 40 to 900 °C. This device consists of a furnace with a recording balance which holds the sample holder, a temperature programmer, an enclosed space for building up the required atmosphere, and hardware (computer) that records and displays the data.

Figure (3.11): Thermogravimetric Analysis (TGA) device.

3.6.2.9 Antibacterial Activity (Zone Inhibition Method)

By using the Agar Well, the Diffusion Method was used to determine the antibacterial activity of the samples. The Muller Hinton agar plates were prepared and were inoculated with Escherichia coli (E. coli) and staphylococcus aureus (*S. aureus*) as test organisms that spread on the surface of the media with the help of a sterile swab. Finally, these plates, after put the samples, were incubated at 37°C, and after 24 hours of incubation; zones of inhibition were visualized and measured the diameter of the inhibition zone and recorded in mm [140].

3.6.2.10 Antioxidant Activity (DPPH Method)

The electron-donating ability of samples and standards - gallic acid and Vit-C were determined from bleaching of purple-colored ethanol solution of DPPH. This spectrophotometric assay by free radical scavenging activity uses the stable radical 2, 2-diphenyl-1-picrylhydrazyl as a reagent. DPPH was prepared at a concentration of 0.002%. Different concentrations of samples were taken in separate test tubes, and volumes were made up to 2 mL using ethanol. Then 2 mL of DPPH solution (2.0 to 0.001 mg/mL) was added to each test tube, and these solutions were kept in the dark for thirty minutes. The same procedure was followed for

Vit-C and gallic acid as well. All the samples were tested in triplicate. Later optical density was recorded at 517 nm using a spectrophotometer. Ethanol with DPPH was used as a control. The formula used for calculation is as below [141]:

% Inhibition of DPPH activity = (A-B/A) * 100 ……..……(3-1)

Where A = Optical density of control.

B = Optical density of a sample.

3.6.2.11 Antifungi Activity

The antifungal potential of the prepared samples was investigated against candida fungal using agar well diffusion assay [142, 143]. About 20mL of on Muller–Hinton (MH) agar was aseptically poured into sterile Petri dishes. The fungal species were collected from their stock cultures using a sterile wire loop [144]. After culturing the organisms, (6 mm) diameter wells were bored on the agar plates using of a sterile tip. Into the bored wells, different concentrations of the samples were used. The cultured plates containing the samples and the test organisms were incubated overnight at 37°C before measuring and recording the average the zones of inhibition diameter [141,145]. Data were statically analysis using Graphpad prism program [146]. Data are represented as mean ± SD of three experiments. Indicate statistically significant difference at $p<0.05$ [147,148].

3.6.2.12 MTT Assay

Samples were placed in a UV light chamber for 2 h. Samples were cut into 1 cm^2 squares and placed in a 48-well polystyrene cell culture plate. Then, 250 μL cell culture media containing 12,500 Human gastric fibroblast (HGF) cells was added to each well and incubated at 37 ºC, 95% relative humidity, and 5% CO_2 for 1, 3, and 7 days. After

completion of the time needed for cell culture, old media was discarded and 250 μL fresh media was added, followed by addition of (12 mM) MTT dye. Samples were incubated for 3 h to let the dye react with cells and produce formazan precipitates. Finally, precipitated dye was dissolved in 200μL DMSO and absorbance was measured at 540 nm using ELISA reader.

3.6.2.13 Nano-indentation

Nanoindentation testing is a method to measure the mechanical properties of a material such as hardness and Young's modulus on the microscopic scale using Ultra Nano Hardness Tester (UNHT), manufactured by CSM Instruments (Switzerland), with capacity of 30 µN to 100 mN having a load resolution of 5 µN (figure 3.12).

Figure (3.12): Nano-indentation device.

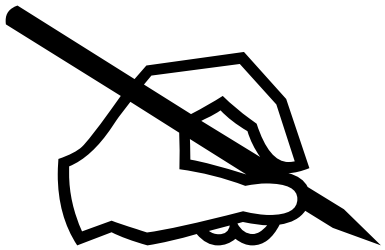

CHAPTER FOUR

RESULTS AND DISCUSSTION

4.1 Introduction

This chapter includes the characterization of the used plant-derived mucilage, essential oils (EOs), and powder. Additionally, the analysis of the results and the required calculations related to the solution tests, such as (viscosity, electrical conductivity and surface tension) and nanofibers tests, such as (contact angle, FTIR, DSC, FESEM, AFM, UV-Vis spectroscopy, TGA, Anti-bacterial activity, Anti-oxidant activity, Anti-fungi activity, MTT assay and Nano-indentation) and their discussion as well as studying the effect of each addition on all properties of nanofibers used to food packaging applications.

4.2 Characterization of the used mucilage and EOs

4.2.1 Cress Seed Mucilage (CSM)

The constituents detected in this mucilage were analyzed in the Babylon agriculture directorate/central laboratory, as shown in the table (4.1).

Table(4.1): Characteristic of the cress seed mucilage.

Characteristic	Value
Ca (ppm)	250
Mg (ppm)	25
K (ppm)	236.5
Na (ppm)	4.1
pH	6.1
Electrical conductivity (µS/cm)	885

4.2.2 Moringa Oil (MO)

High Performance Liquid Chromatography (HPLC) was used to know the compounds in this oil as shown in figure (4.1) and table (4.2)

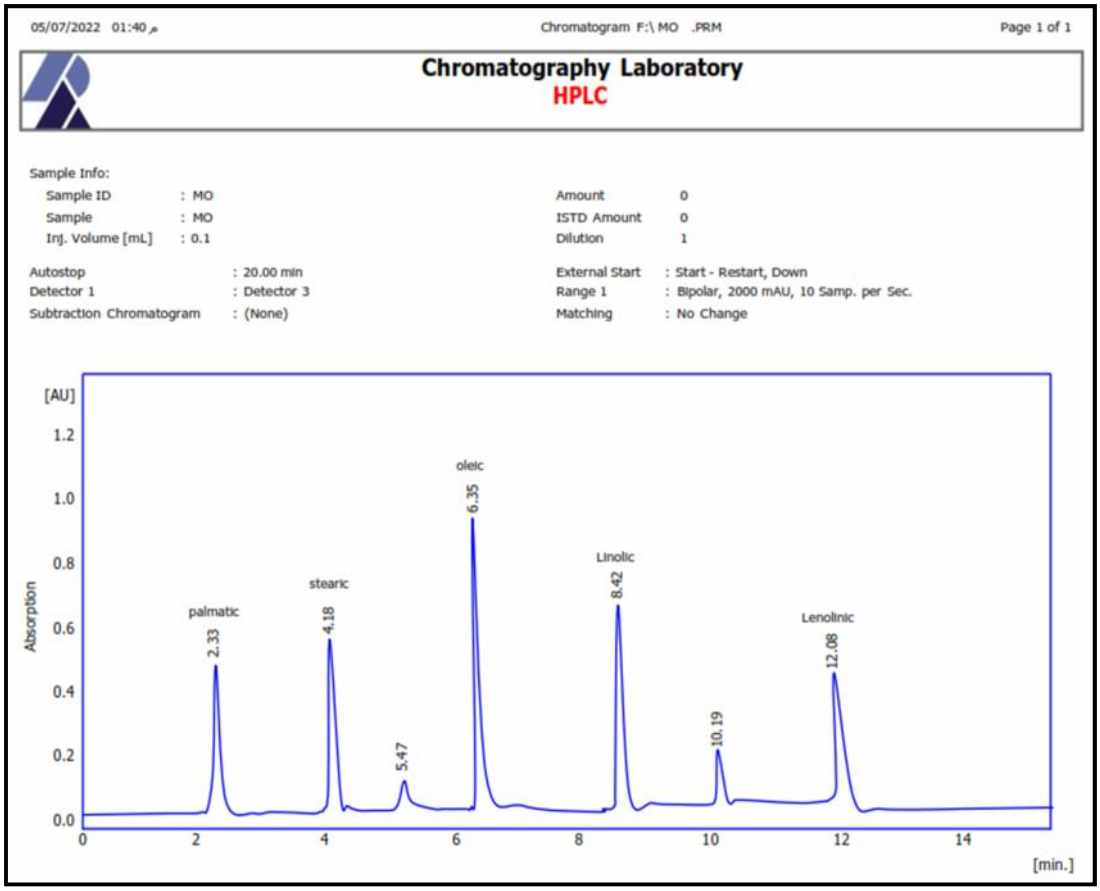

Figure (4.1): HPLC diagram of MO.

Table (4.2): Characteristic of MO used.

Characteristic	Data
Palmatic Acid	6.5 %
Stearic Acid	2.8 %
Oleic Acid	62.5 %
Linolic Acid	17.5 %
Lenolinic Acid	0.25 %
pH	5

4.2.3 Cardamom Oil (CO)

Performance Liquid Chromatography (HPLC) was used to know the compounds in this oil as shown in figure (4.2) and table (4.3).

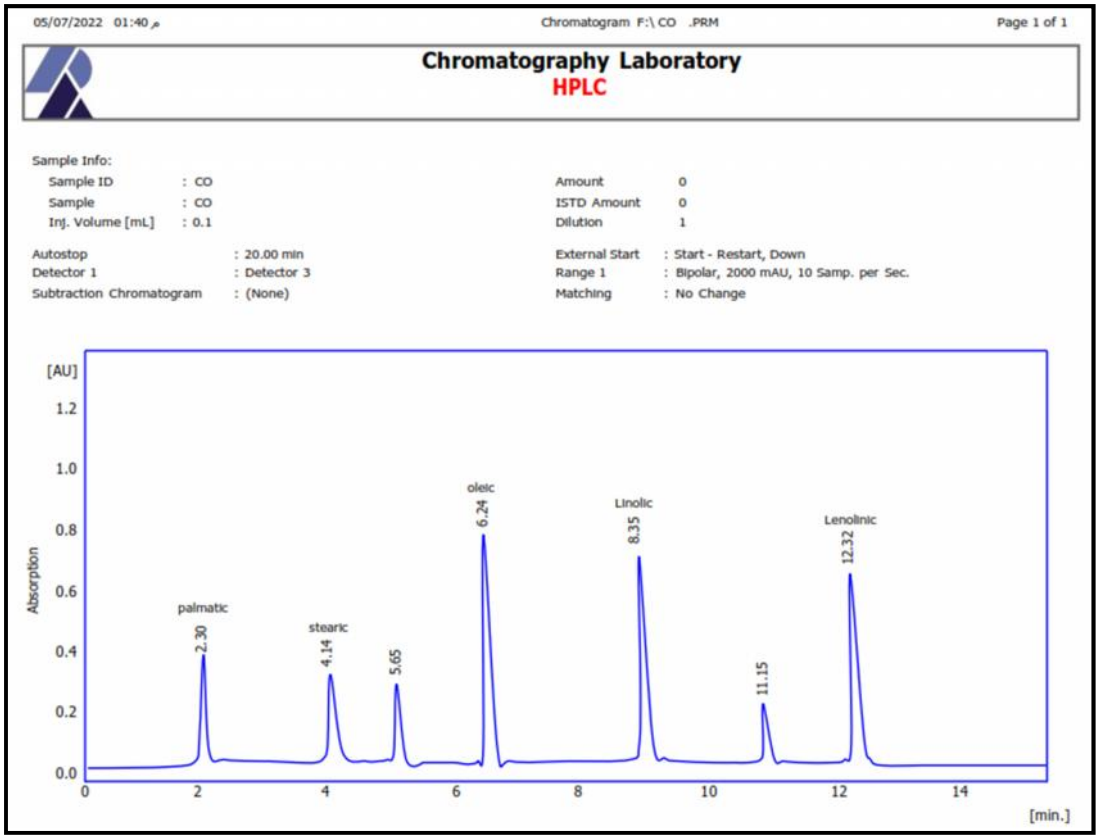

Figure (4.2): HPLC diagram of CO.

Table (4.3): Characteristic of CO used.

Characteristic	Data
Palmatic Acid	7.0 %
Stearic Acid	5.4 %
Oleic Acid	30.5 %
Linolic Acid	22.9 %
Lenolinic Acid	0.8 %
pH	5

4.2.4 Clove Bud Oil (CBO)

High Performance Liquid Chromatography (HPLC) was used to know the compounds in this oil as shown in figure (4.3) and table (4.4).

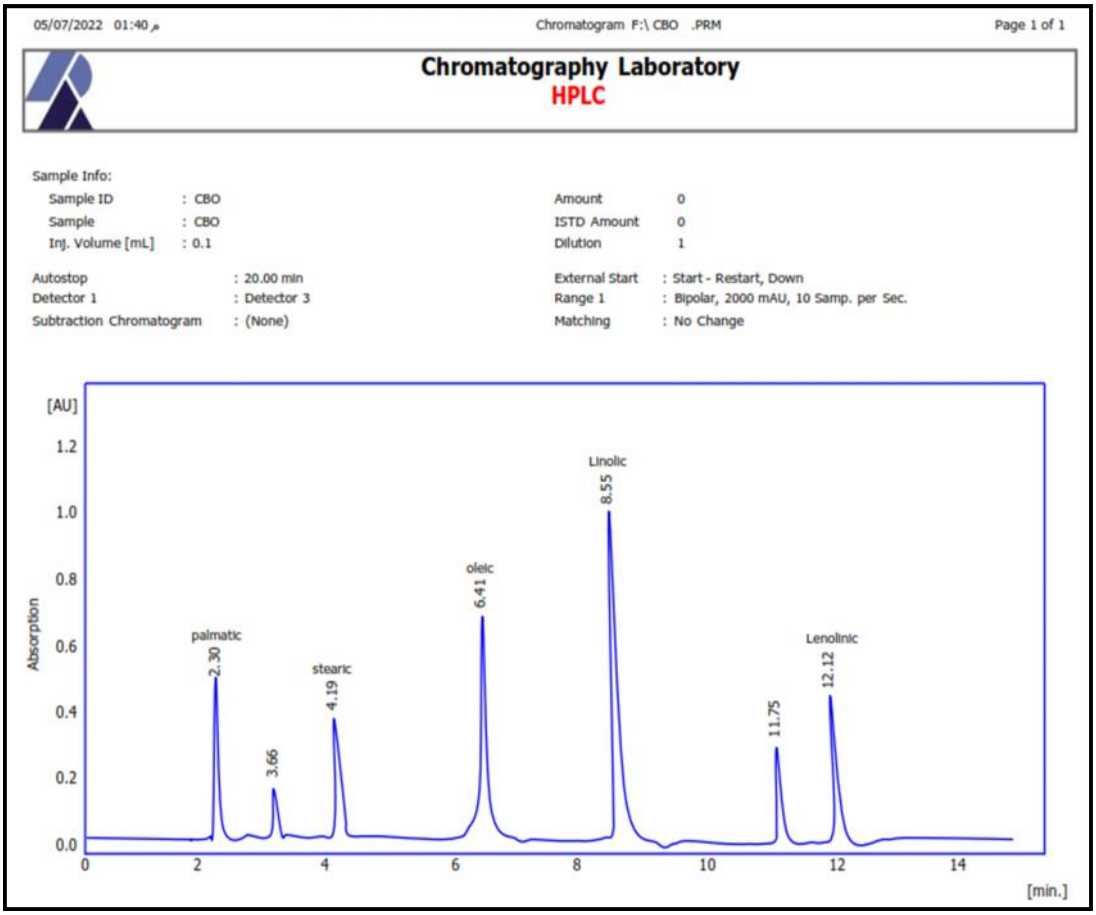

Figure (4.3): HPLC diagram of CBO.

Table (4.4): Characteristic of CBO used.

Characteristic	Data
Palmatic Acid	8.1 %
Stearic Acid	6.5 %
Oleic Acid	32.5 %
Linolic Acid	40.5 %
Lenolinic Acid	1.1 %
pH	5

4.2.5 Thyme Oil (TO)

High Performance Liquid Chromatography (HPLC) was used to know the compounds in this oil as shown in figure (4.4) and table (4.5).

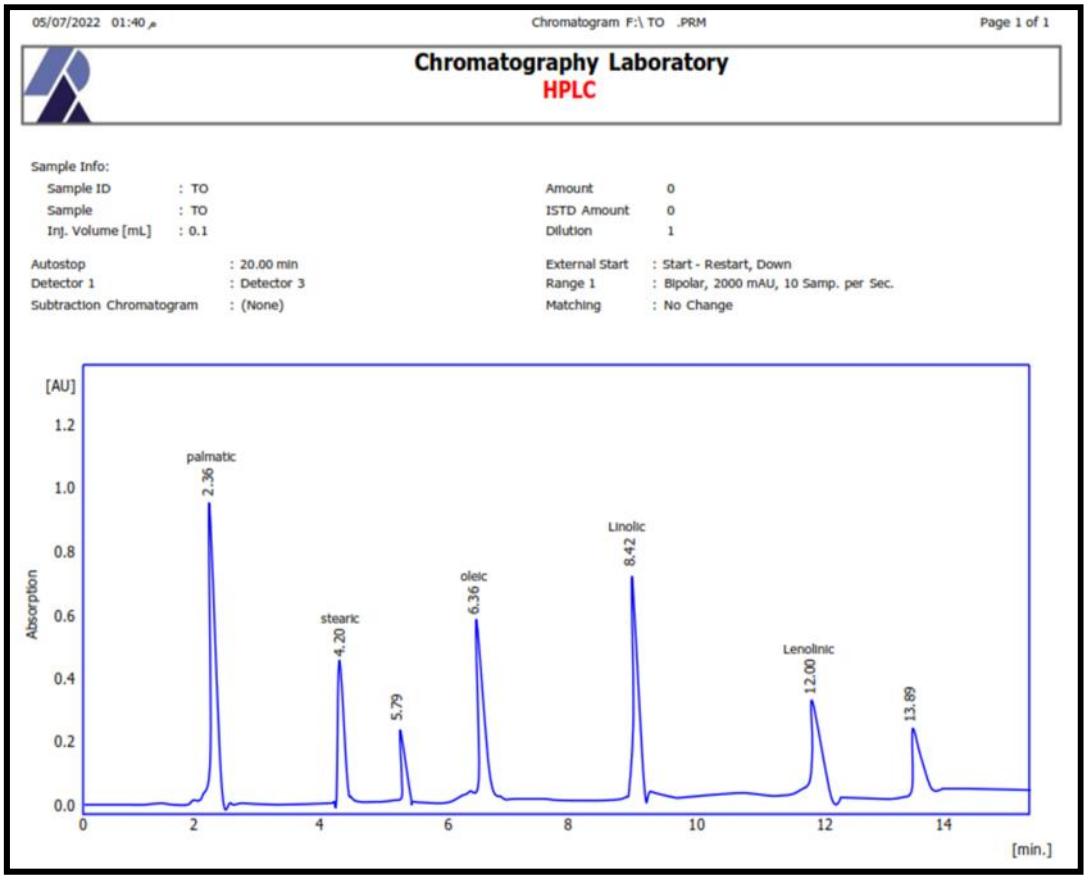

Figure (4.4): HPLC diagram of TO.

Table (4.5): Characteristics of TO used.

Characteristics	Data
Palmatic Acid	50.5 %
Stearic Acid	8.5 %
Oleic Acid	9.4 %
Linolic Acid	11.5 %
Lenolinic Acid	1.5 %
pH	4.5

4.2.6 Fenugreek Oil (FO)

High Performance Liquid Chromatography (HPLC) was used to know the compounds in this oil as shown in figure (4.5) and table (4.6).

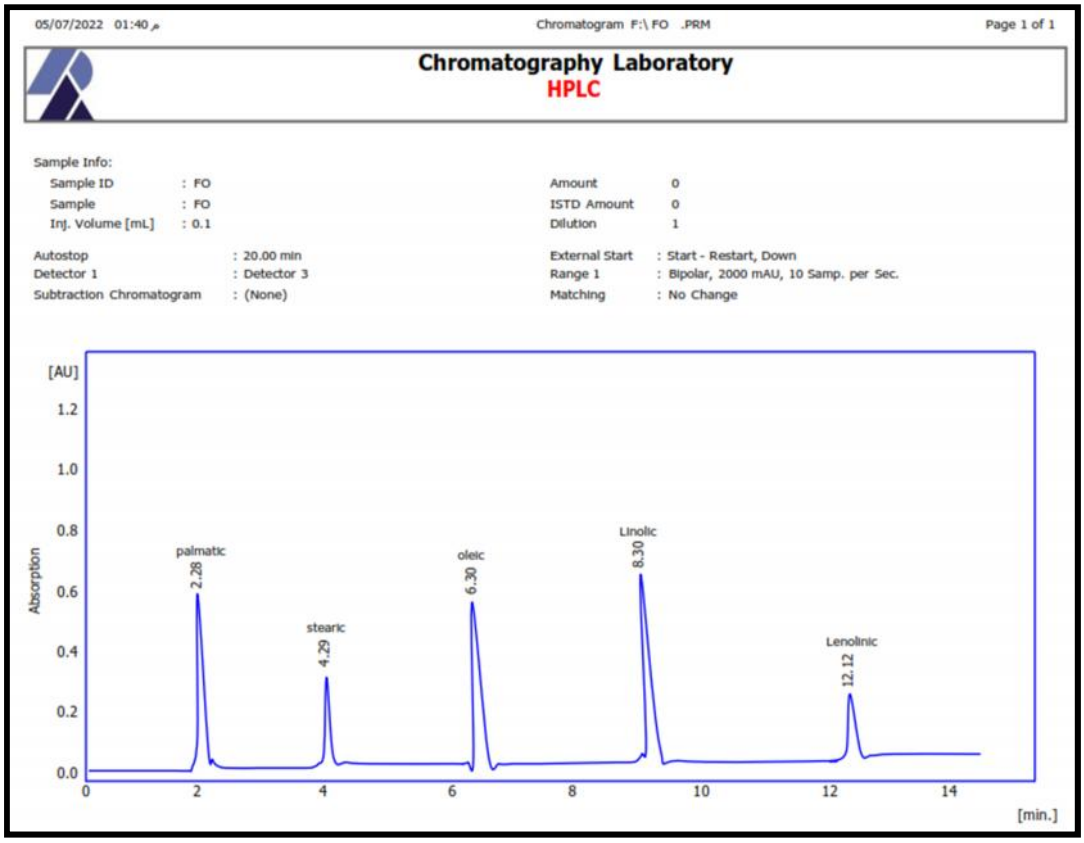

Figure (4.5): HPLC diagram of FO.

Table (4.6): Characteristics of FO used.

Characteristics	Data
Palmatic Acid	5.4 %
Stearic Acid	4.1 %
Oleic Acid	30.5 %
Linolic Acid	49.2 %
Lenolinic Acid	0.7 %
pH	4.5

4.2.7 Walnut Tree Bark Powder (WB)

the chemical components of this powder were detected by gas chromatography-mass (GC-MS). As shown in figure (4.6)

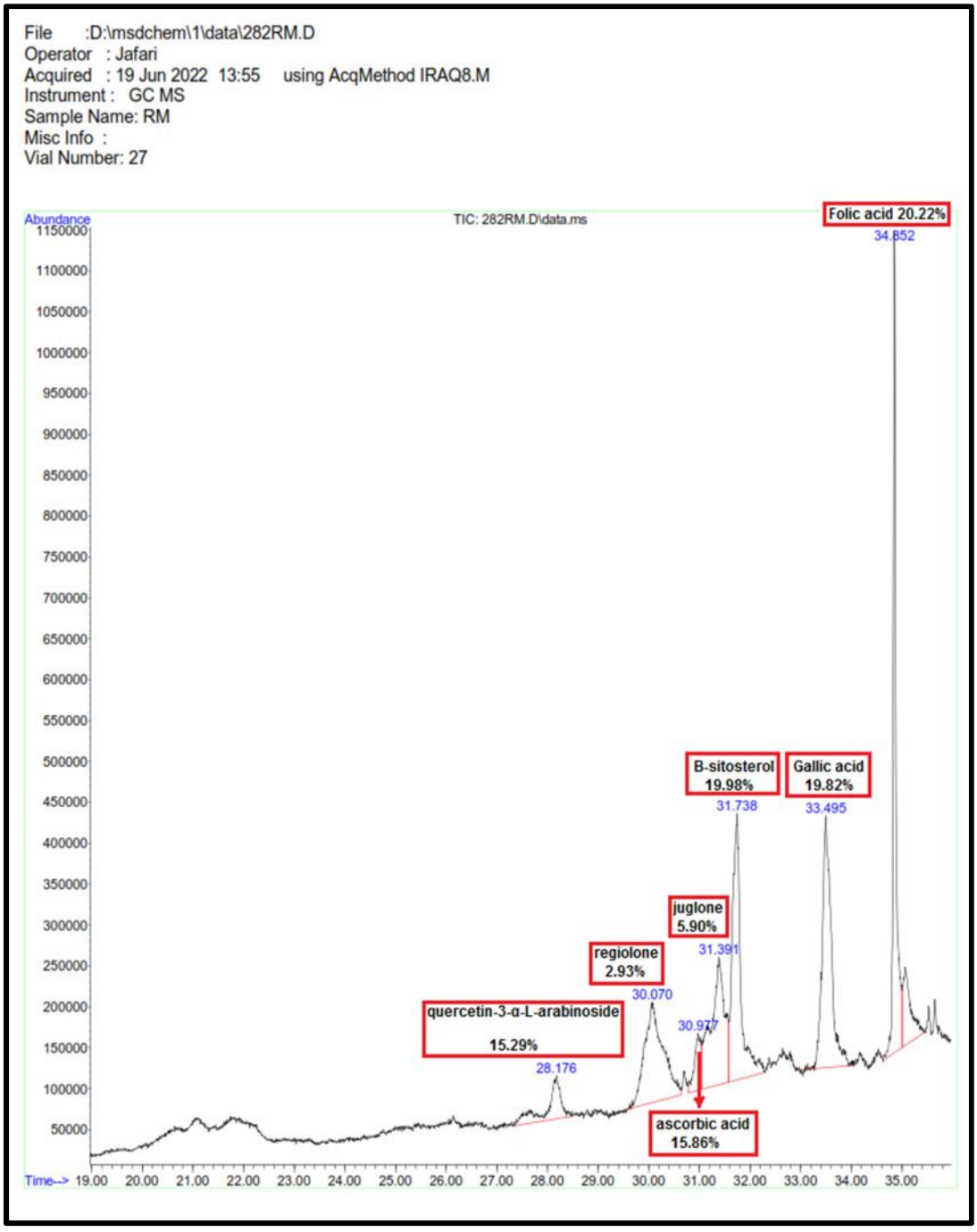

Figure(4.6): GC-MS result of (WB) powder.

4.3 Solution Characterizations Results

4.3.1 Surface Tension

Surface tension is one of the most important factors that influence the spinnability of the polymer solution. Notice from figure (4.7) increase

the surface tension from (35.58 to 38.46) after adding STA of (S_4) which consistent with reported by [149].

Meanwhile, the results revealed that by adding the CSM to PVA, the surface tension of (S_7) significantly increased from (35.58 to 40.51). It is probably due to the high surface tension of the pure CSM solution. these results agreement with [150].

The surface tension value of basic sample (S_8) about (38.6 mN/m) and decreased after addition the essential oils due to the surface tension lower of these oils and this result is in consistence with [151].

While the surface tension increased after incorporation WB in basic blend (S_8) which agreement with other studies by [152, 153].

Finally, the final blend (S_f) appear moderate surface tension due to the convergence between the particles of basic blend and additives and additionally to moderate cohesive forces between them.

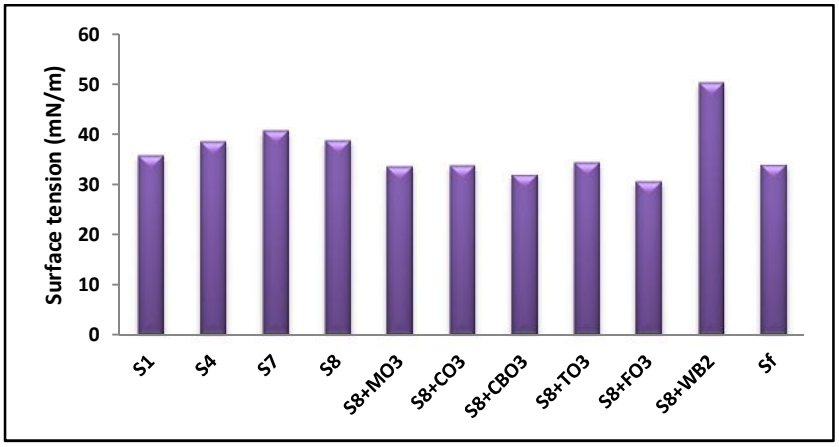

Figure (4.7): Surface tension of samples in all parts.

4.3.2 Viscosity

Viscosity of polymer solutions for electrospinning are important physical parameters which can deeply affect their spinnability and the morphology of the resulting fibers. From the figure (4.8) observed the viscosity of samples decreased after addition STA and this may be attributed to the structural organization of amylose and amylopectin in the starch granule or due to the amount and interaction of its component, it

can capture or release water after the gelatinization process. This is in concur with reported by [154].

Whereas notice the addition of CSM increased the viscosity of sample (S_7) which is in agreement with the previous report by [97, 155].

The viscosity of basic blend (S_8) about (390 cP) and increased when the essential oils was added which is in consistence with other researches by [156, 157].

Meanwhile, the viscosity of samples decreased after addition WB to the basic blend (S_8) and this is agreement with previous studies by [158].

The viscosity of final blend (S_f) increased as a result to the incorporation all additives in (S_8).

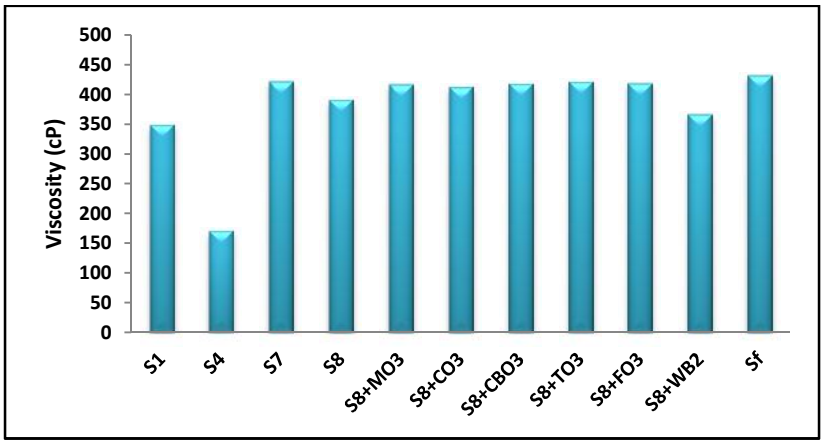

Figure (4.8): Viscosity of samples in all parts.

4.3.3 Electrical Conductivity

Electrical conductivity are important parameter affecting the electrospinning behaviors of polymer solutions and measured in Babylon agriculture directorate/central laboratory. The electrical conductivity values of all samples were observed in figure (4.9), which show decrement in conductivity after incorporation STA in (S_1) because STA reduces the amount of free ions in the solution due to the presence of

polar covalent connections between PVA and STA. Which are accordance with the previous reports by [159].

Furthermore, the electrical conductivity increased with adding CSM to (S_1) due to the ionic nature of CSM which agrees with the results published by [160].

The electrical conductivity of basic blend (S_8) was (695 µS/cm) and decreased after additives incorporation from essential oils because these oils can be related to non-ionic structure. The results agreed with the results reported by [97, 157].

Whereas the conductivity of samples with adding WB increased because the ionic nature of WB, this is in line with other research reported by [161].

The electrical conductivity of final blend (S_f) was moderate about (674 µS/cm).

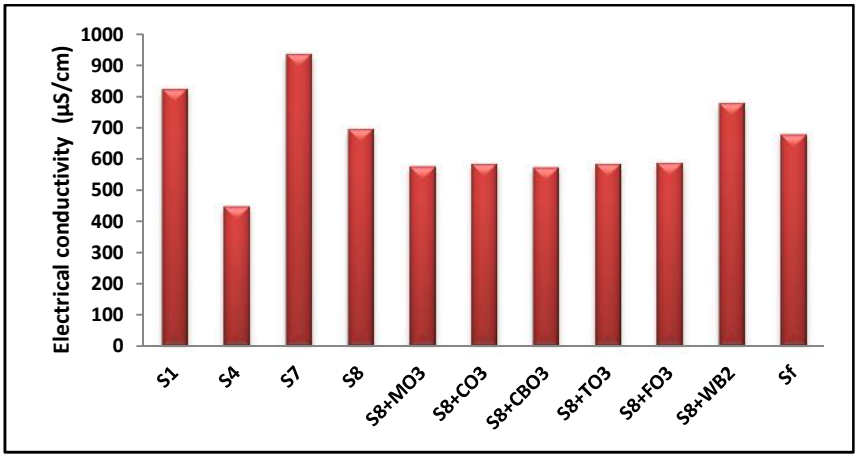

Figure (4.9): Electrical conductivity of samples in all parts.

4.4 Nanofiber Characterizations Results

4.4.1 Wettability (Contact Angle)

The hydrophilic or hydrophobic nature of polymeric nanofibers plays an important role while targeting final applications. Food packaging should be hydrophobic to sustain in the wet environment. Hydrophilicity

of substance may be analyzed by calculating the water contact angle (WCA).

Table (4.7) appear increment in contact angle after adding STA and CSM but still in the range of hydrophilic character due to the OH groups that were presented through mixing of solution samples that lead to the hydrophilic nature of its structure for these additions, which is in agreement with [162, 163].

The (WCA) value of (S_8) reached to (74.049 ºC) and this value decreased with an increasing essential oils concentration (1 and 5 wt.%) for (MO, CO, TO, and FO). This is likely due to the presence of greater (-OH) groups within the nanofibers membrane and these results are consistence with other studies by [65, 164].

Furthermore, the (WCA) value increased with addition (10 wt.%) of (MO, CO, TO, and FO), but still below 90°. The possible reason could be to high concentration of these oils improved the viscosity of the spinning solution, thus the spinning nanofiber became thicker and may be related to the surface roughness which is in line with previous reported by [157, 164].

Whereas (WCA) reduced for all concentrations (1, 5, and 10 wt.%) of (CBO). The reason for this decrease might be that the amount of added essential oil reduces the solid-liquid interface voltage by adsorbing on the solid surface and this result is agreement with [151].

Meanwhile, the (WCA) value increased after adding WB with concentration (0.3 and 0.5 wt.%) for (WB_1 and WB_2), but still below 90°. this is attributed to the increased number of polar groups within the electrospun nanofibers by the presence of (O-H) groups of WB. Afterward the (WCA) value for (WB_3) decreased and this lead to more OH bonds consist in this sample which is agreement with [152].

The WCA value increased for final blend (S_f) to (105.358º). This increment may be come back to larger fiber diameters. In addition to surface roughness increases.

Whilst, the (WCA) value decreased in (S_{f1}, S_{f2}, S_{f3}, S_{f4}, and S_{f5}) after changing the electrospun parameters for sample (S_f) as shown in table (4.7) which is in concur with results reported by [152].

Finally, the (WCA) value increased after crosslinking of sample (S_f) by UV radiation for 24 hr. as shown in table (4.7) for (cS_f) from (105.358º to 112.546 º). An increase in the contact angle may be because of interchain and intrachain bonding for (S_8) and additives in the result of crosslinking, which agree with [137].

As results the samples (S_f and cS_f) nanofibers possess enough hydrophobicity character to be used in food packaging applications.

Table (4.7): Contact angles of samples in all parts.

Sample No.	Contact angle (º)
S_1	40.707
S_2	59.625
S_3	64.788
S_4	66.622
S_5	55.800
S_6	60.266
S_7	69.045
S_8	74.049
S_9	72.748
S_{10}	71.167
S_8+MO_1	72.564
S_8+MO_2	71.079
S_8+MO_3	76.442
S_8+CO_1	72.958
S_8+CO_2	70.064
S_8+CO_3	78.612
S_8+CBO_1	69.131
S_8+CBO_2	68.726
S_8+CBO_3	71.496
S_8+TO_1	71.852
S_8+TO_2	74.868

S_8+TO_3	75.595
S_8+FO_1	65.903
S_8+FO_2	69.336
S_8+FO_3	80.832
S_8+WB_1	76.306
S_8+WB_2	78.902
S_8+WB_3	75.903
S_f	105.358
S_{f1}	91.534
S_{f2}	91.418
S_{f3}	87.904
S_{f4}	96.082
S_{f5}	94.182
cS_f	112.546

4.4.2 Field Emission Scanning Electron Microscopy (FESEM)

FESEM was used to observed morphological properties of nanofibers. Nanofibers diameter ranges were calculated using the Digimizer Image Analysis Software program, as shown in figure (4.10). For part one figure (4.10) show the average fiber diameter decreases from (229.192 nm to 148.130 nm for S_1 and S_4 respectively), as well as, the min and max diameter ranges from ((151.320 nm, 313.991 nm) to (70.011 nm, 337.216 nm) for S_1 and S_4 respectively). This decrement in the average diameter of nanofibers occurred after adding STA with bead formation on the surface of nanofibers, due to a drop in solution viscosity and high surface tension that lead to instability of the electrospinning process [165].

S_7 shows that increasing the electrical conductivity of CSM causes nanofiber diameters to shrink significantly, this result agreement with [160]. On the other hand, S_8 demonstrate the average diameter of nanofibers decrease to (86.873 nm) as the min and max diameter ranges from (58.537 to 127.204 nm).

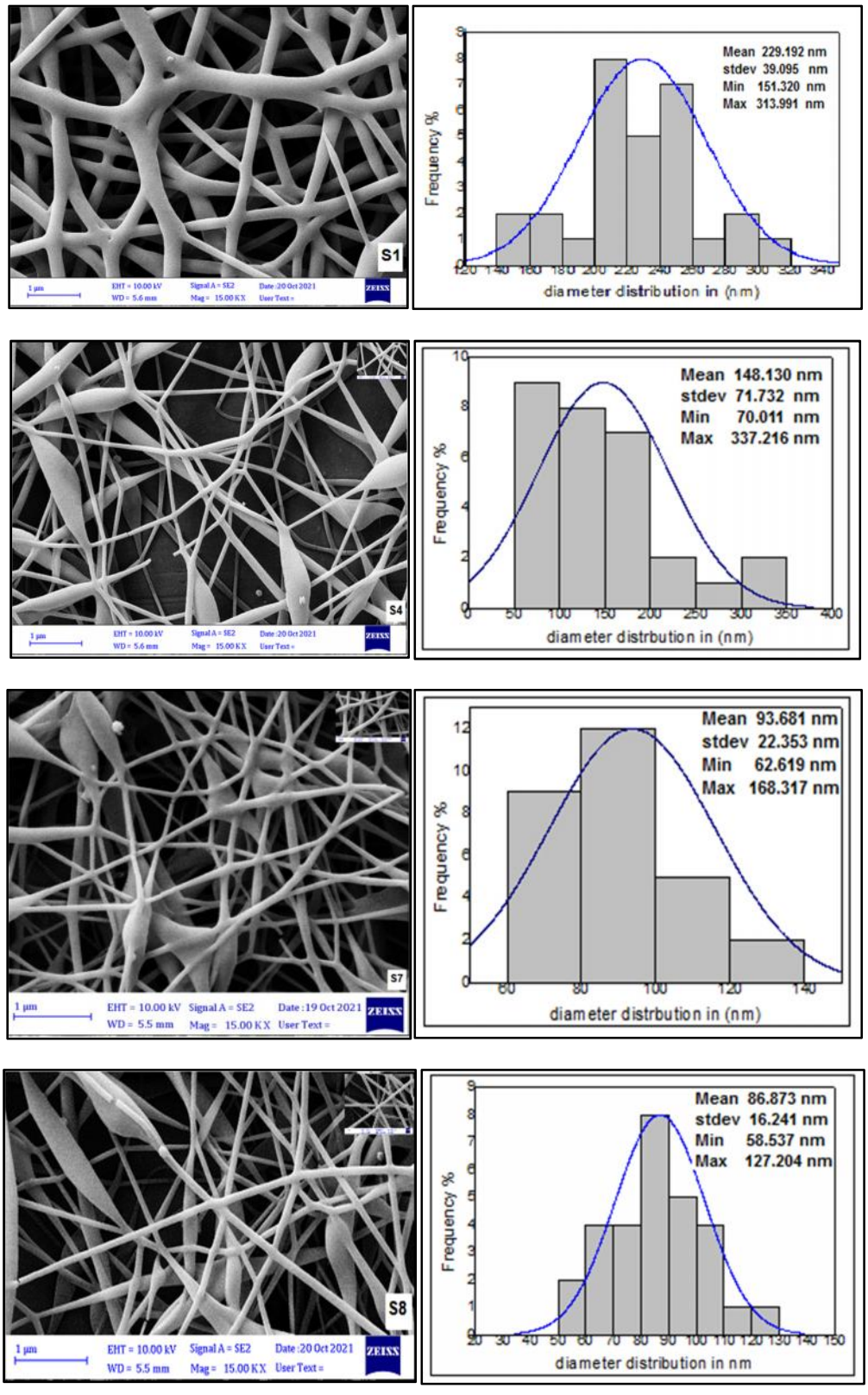

FE-SEM micrographs **Nanofibers diameter distribution histograms**

Figure (4.10): FESEM Micrographs and Nano-fibers diameter distribution histograms for samples in part one.

For the part two. Figure (4.11) in appendix (A) illustrate the effect addition different concentration of essential oils such as moringa oil (1%, 5% and 10% MO) on nanofibers morphology. A significant increase in diameter was observed with the addition of MO. When the MO concentration was increased from (1 to 10 wt.%), the average fiber diameter of (S_8+MO) gradually increased (108.326 nm, 120.385 nm, 125.814 nm for S_8+MO_1, S_8+MO_2, and S_8+MO_3, respectively). Meanwhile the min and max diameter of S_8+MO ranges from ((63.246 nm, 241.868 nm), (60.825 nm, 240.820 nm), (50.282 nm, 219.851 nm) for S_8+MO_1, S_8+MO_2, and S_8+MO_3, respectively).

The reason for this increasing may be the encapsulation of the oil droplets in the fibers and means a generally high viscosity, low surface tension, and conductivity; therefore, it leads to an insufficient stretching of the electrified jet during electrospinning, and more thicker fibers with rather unbounded heterogeneous beads formed. As well as, at (S_8+MO_3) the multi-layer fiber strand of dissociated globules was formed because of the load concentration of the polymer solution. The increase in the average fiber diameter with the amount of essential oil is in line with the previous studies [151, 166, 167].

Also figure (4.12) in appendix (A) demonstrate the effect incorporation different concentration of cardamom oil (1%, 5% and 10% CO) on the surface of resultant electrospun nanofibers. This incorporation of CO caused an increase in the average diameters of the corresponding electrospun nanofibers gradually from (103.355 nm, 127.269 nm, 136.806 nm for S_8+CO_1, S_8+CO_2, and S_8+CO_3, respectively). As well as, the min and max diameter of S_8+CO ranges from ((56.569 nm, 197.231 nm), (79.208 nm, 270.426 nm), (60.241 nm, 270.749 nm) for S_8+CO_1, S_8+CO_2, and S_8+CO_3, respectively) and formation of beads on this nanofibers while at (S_8+CO_3) the multi-layer fiber strand of dissociated

beads was formed because of the load concentration of the polymer solution.

This increment in the average diameter of nanofibers may be a result of entrapment of CO within the fibers, interference in the solution's properties induced by the inclusion of CO, and the oil interacting with the polymer chains that influence the chain entanglements. Additionally designated nanofibers containing CO had lower value of electrical conductivity compared to the basic sample (S_8), which caused in insufficient elongation of polymer jet and fibers with larger diameters. This results agreed with the results reported by [97, 168].

While according to the FESEM images in figure (4.13) which existed in appendix (A), the average fiber diameters of electrospun S_8 loaded with essential oils, such as (CBO, TO and FO) at concentration (10%) for all oils are (148.033 nm, 184.700 nm and 117.416 nm, respectively). Additionally the min and max diameter ranges from ((67.344, 332.055 nm), (103.479, 408.855 nm), (71.109, 268.293 nm) for S_8+CBO_3, S_8+TO_3, and S_8+FO_3, respectively).

The reason for higher the average diameter of nanofibers than S_8 come back to the same reason mentioned in figure (4.10) and (4.11). As well as, the (S_8+TO_3) possess the highest diameter (184.700 nm), due to the thyme oil (TO) is rich in phenolic compounds, such as thymol and carvacrol than another essential oils used as mentioned in chapter two. Which means that the nanofiber thickness is influenced by the essential oil. This result in agreement with [169].

The FESEM images of the samples nanofibers are shown in Figure (4.14) in appendix (A). The drop in average diameters of the nanofibers (S_8) after adding WB with different concentration (0.3, 0.5 and 0.7 wt.%) from (83.573 nm, 76.380 nm for S_8+WB_1 and S_8+WB_2), due to the electrical conductivity of the electrospinning solution increases with

increasing in the amount of WB, resulting in increased extension strength of the electric field during the spinning process.

So, the nanofibers appear with smaller diameters and this consistence with [161]. While the average diameters of nanofibers increment after adding (0.7% WB) in (S_8+WB_3) to (85.233 nm), due to high viscosity which caused resistance to jet stretching with unstable Taylor cone and discontinuous jet during the electrospinning process which agrees with [170].

For part three figure (4.15) in appendix (A) illustrate the final blend (S_f) and the effect different electrospinning conditions on nanofibers morphology. FESEM image of S_f demonstrate the average diameter of nanofibers increase to (277.302 nm), as well as, the min and max diameter ranges from (106.066 nm to 570.088 nm respectively). The increment in average diameter due to the greater resistance for the high concentration (high viscosity) of the final solution to be stretched toward the collector. Another reason may be attributable to the electrical conductivity and surface tension of the solution decreasing.

While the average diameter of nanofibers in S_{f1} reduced from (277.302 to 226.946 nm) due to the voltage increases from (20 to 26 Kv), columbic repulsion of charges within the jet will be increased. As a consequence, the jet will stretch and become thinner to form nanofibers. If the voltage is higher than the optimum range, leads to two types of structural transformations, either completely beads or beaded nanofibers or from cylindrical nanofibers to flat thin nanofibers will be formed.

These kinds of structural transformations can be attributed to the decrease of size of a Taylor cone with the increase of jet speed at higher voltages. The results are consistent with [171].

The FESEM images of nanofibers in S_{f2} and S_{f3} at needle diameter (0.2mm) but with applied voltage ranges from (20 to 26 Kv respectively).

Notice the mean diameter reduced from (277.302 to 224.974 nm for S_f and S_{f2} respectively), meanwhile, the mean diameter of nanofibers in S_{f3} more decreased from S_{f2} and ranges from (224.974 to 214.425 nm).

This decrement in the mean diameter of nanofibers using small needle diameter come back to the travel time of jet will be smaller and this will lead to higher stretching action, and at the end smaller fiber diameters will be collected. As well as, observe more decrement in mean diameter of nanofibers at applied voltage (26 Kv) due to used high potential difference increase a force called electrostatic force which is responsible about stretching the polymer jet and divide it into many smaller jets, so thinner and smoother nanofibers will be collected. These results are in line with [172,173].

Whilst notice the average diameter of nanofibers in S_{f4} and S_{f5} at flow rate (0.5 ml/hr) decrease from (277.302, 252.752 nm for S_f and S_{f4} respectively), meanwhile, the mean diameter of naofibers in S_{f5} reduced to (243.981 nm) at applied voltage (26 Kv). These decrement because at low flow rates, a small droplet size was formed at the capillary tip which made various types of charged jet. The charged jet reduced immediately due to the capability of electric field strength in drawing it during the electrospinning process.

It was observed that at (0.5 mL/hr), the Taylor cone was more stable which resulted in the narrowest fiber diameter distribution. while at the higher applied voltage the time to stretch the fibers is bigger, resulting in thinner nanofibers with multi-layer fiber strand was formed. These results are consistence with [174, 175].

Finally, the crosslinking of sample (S_f) by UV rays for 24 hr. as shown in figure (4.15) for (cS_f).

Figure (4.16) show directionality histogram, and 2D-FFT for samples in all the parts which existed in appendix (B). Orientation of the prepared nano fibers was measured by using the Fiji software (Gaussian method) based on the FESEM images.

This technique is used to infer the preferred orientation of structures present in the input image. It computes a histogram indicating the amount of structures in a given direction.

Table (4.8) demonstrate the directionality analysis of samples in all parts. The direction (°) column reports the center of the gaussian, while the dispersion (°) column reports the standard deviation of the gaussian.

The goodness column reports the goodness of the fit; 1 is good, 0 is bad. The amount value as calculated here under estimates the real proportion of structures with the preferred orientation.

Essential oils addition increased the directionality of the nanofibers from 0.36 of basic sample (S_8) up to (0.57, 0.64, 0.48, 0.58, and 0.40) of (MO_3, CO3, CBO_3, TO_3, and FO_3 respectively) as shown in table 4.8, which means that the properties are anisotropic.

Whereas the directionality of the nanofibers increased from (0.36 up to 0.68) for basic sample (S_8) and final sample (S_f) respectively

EDX test was used to determine the composition of the charged particles as shown in the figure (4.17) for samples in all the parts. Table (4.9) illustrate the amount of all element as (C, O, and Al) in samples. The presence of the aluminum peak is not alarming because the meshes are mounted on an aluminum surface.

The chemical compositions changed from sample to another due to the variations in the compositions of these samples themselves

Table (4.8): The directionality analysis for samples in all the part by utilize Fourier components.

Sample No.	Direction (˚)	Dispersion (°)	Amount	Goodness
S_1	-5.80	8.92	0.34	0.45
S_4	-54.69	3.60	0.20	0.48
S_7	3.75	4.90	0.30	0.56
S_8	22.17	4.54	0.36	0.74
S_8+MO_1	41.07	21.61	0.65	0.81
S_8+MO_2	37.79	11.85	0.37	0.62
S_8+MO_3	4.27	17.93	0.57	0.71
S_8+CO_1	26.67	8.56	0.33	0.71
S_8+CO_2	-12.37	2.90	0.35	0.36
S_8+CO_3	29.63	24.70	0.64	0.62
S_8+CBO_3	-49.44	2.91	0.48	0.49
S_8+TO_3	15.76	47.39	0.58	0.57
S_8+FO_3	-2.71	8.96	0.40	0.68
S_8+WB_1	37.75	13.47	0.37	0.48
S_8+WB_2	23.04	37.49	0.67	0.56
S_8+WB_3	-27.00	8.55	0.25	0.33
S_f	23.81	24.20	0.68	0.47
S_{f1}	-51.93	54.08	0.86	0.24
S_{f2}	-10.05	8.31	0.29	0.54
S_{f3}	35.27	44.80	0.90	0.55
S_{f4}	-39.79	2.26	0.11	0.56
S_{f5}	50.33	26.95	0.81	0.72

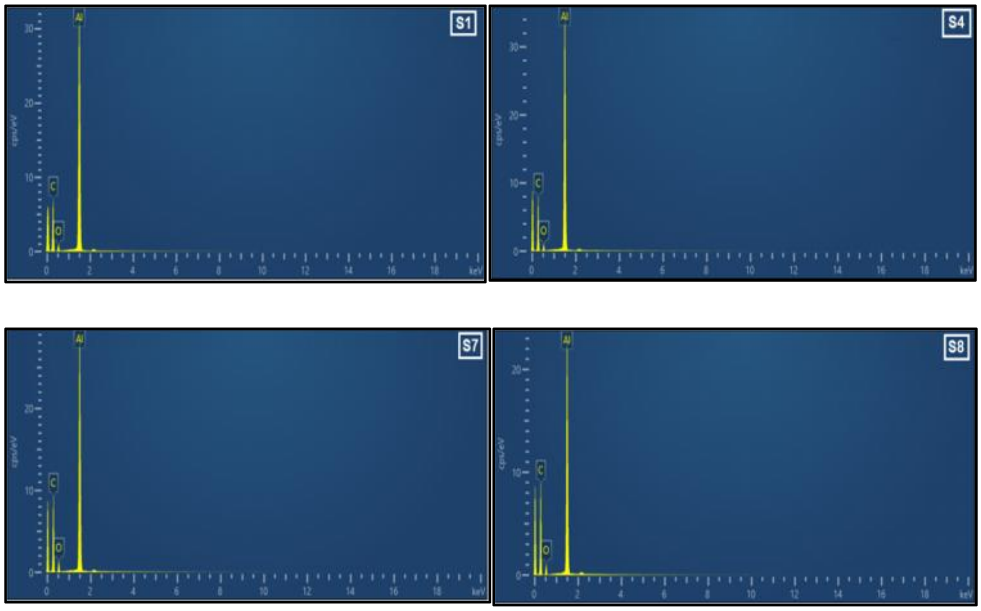

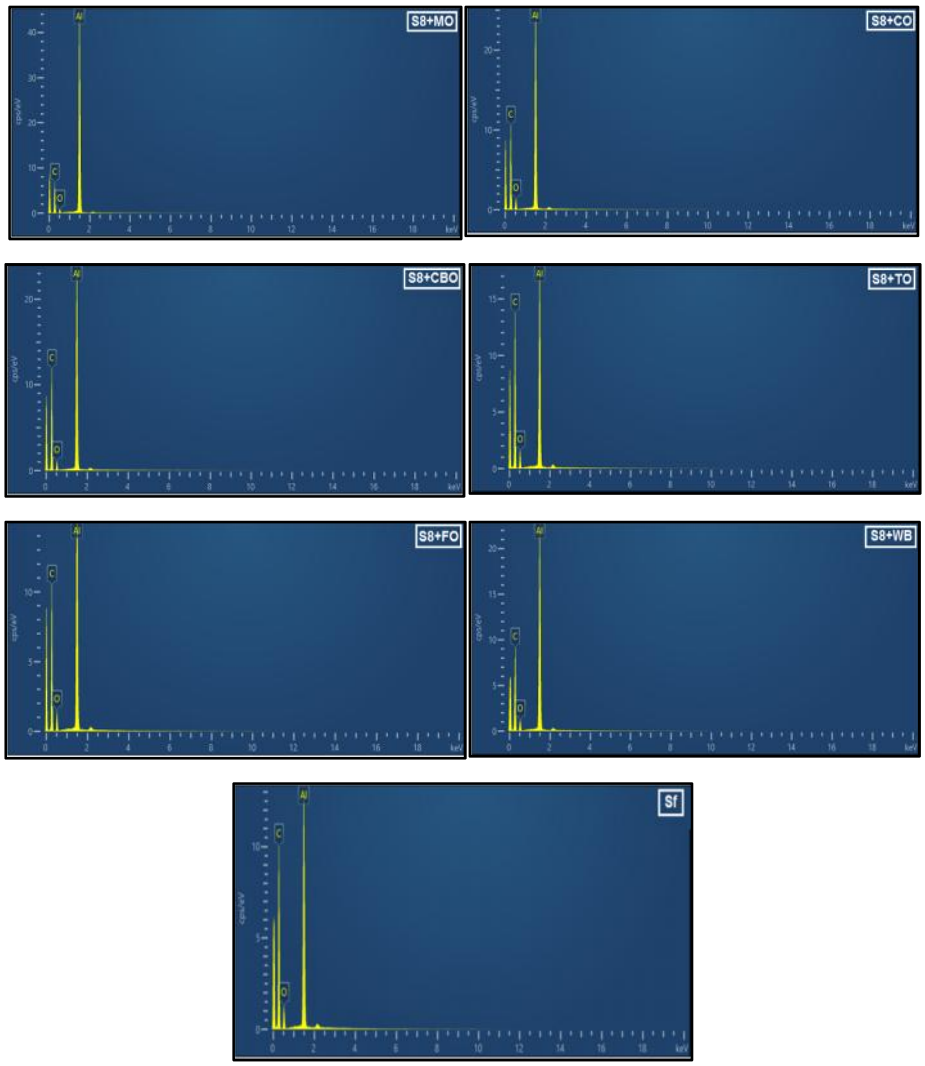

Figure (4.17): EDX test for samples.

Table (4.9): Amount of element for samples in all the part.

Sample No.	Weight%		
	C	O	Al
S1	62.44	6.88	30.68
S4	62.21	6.76	31.04
S7	64.67	9.29	26.04
S8	67.61	8.27	24.11
S_8+MO_3	58.00	5.33	36.66
S_8+CO_3	67.51	9.85	22.64
S_8+CBO_3	70.75	7.99	21.26
S_8+TO_3	71.68	11.89	16.43
S_8+FO_3	68.32	11.27	20.41
S_8+WB_2	67.74	9.89	22.38
S_f	71.22	12.75	16.03

4.4.3 Atomic Force Microscopy (AFM)

AFM is a very useful technique to study the topography and the surface roughness of the nanofibers. The 2D and 3D AFM images of obtained electrospun nanofibrous mats are shown in figure (4.18) which existed in appendix (C). The AFM images have been analyzed by ANOVA software to assess the surface roughness of the electrospun nanofibrous mats of all samples.

The surface roughness of developed nanofibrous mats are stated in table (4.10) and from this table notice lower surface average roughness (Sa), root mean square (Sq), and surface bearing index (S_{bi}) with incorporation of (STA) and (CSM) at (S_4, S_7, and S_8) compared to pure PVA, which could be attributed to the lower average nanofibers diameter of these samples as up mentioned in nanofibers diameter distribution histograms. The results of these samples are in good agreement with the findings of other researchers [150, 176].

The surface average roughness (Sa), root mean square (Sq), and surface bearing index (S_{bi}) for all addition from essential oils increase compared to basic sample (S_8). In addition, the nanofibers with different ratio of (MO and CO) essential oils demonstrated increment in surface roughness as mentioned in table (4.10) that attributed to increase in average nanofibers diameter.

Also notice the surface bearing index (S_{bi}) increment of all essential oils due to these oils enhance mechanical properties of electrospun membranes and addition to increase in nanofibers diameter. These results are in a good accordance with reported by [177-179].

Furthermore, surface roughness after adding different concentrations of WB to the basic sample (S_8) decreased which is

accordance to decreasing nanofibers diameter of these samples. The results are comparable and in agreement with other studies [180, 181].

While noticed increment in the surface roughness and surface bearing index of the final blend (S_f) and this attributed to that they increased of average nanofibers diameter for this sample as shown in FESEM. These properties suitable in food packaging application.

Table (4.10): Surface roughness analysis for the samples in all parts.

Sample No.	Average Roughness (Sa) (nm)	Root Mean Square (Sq) (nm)	Surface Bearing Index (S_{bi})	Surface skewness (Ssk)	Peak-to-peak, Sy (nm)	Ten point height, Sz (nm)
S_1	198.538	246.809	0.617	0.133	1649.83	827.385
S_4	188.821	235.804	0.589	0.013	1710.42	850.352
S_7	180.555	226.331	0.565	-0.030	1670.29	808.578
S_8	159.012	204.591	0.511	-0.034	1985.4	965.12
S_8+MO_1	163.025	206.678	0.516	0.077	1428.8	723.59
S_8+MO_2	166.013	209.78	0.524	0.509	1398.38	701.553
S_8+MO_3	167.487	210.902	0.527	-0.157	1561.06	800.535
S_8+CO_1	162.624	215.618	0.539	0.078	1392.03	696.76
S_8+CO_2	168.383	218.734	0.546	0.182	1794.34	902.272
S_8+CO_3	173.226	225.825	0.564	0.508	1777.03	876.596
S_8+CBO_3	176.606	224.749	0.561	0.044	1662.32	835.727
S_8+TO_3	190.836	243.042	0.607	-0.048	1639.37	827.684
S_8+FO_3	170.715	215.791	0.540	-0.021	1659.29	827.879
S_8+WB_1	152.047	203.684	0.509	-0.028	1688.63	855.61
S_8+WB_2	146.217	198.96	0.497	0.437	1519.94	763.031
S_8+WB_3	156.674	205.248	0.513	-0.276	1640.91	829.564
S_f	210.046	312.154	0.780	0.234	2114.34	1080.75

4.4.3.1 Analysis Pore Volume by ANOVA Software

Nanofiber based food packaging have an advantage over paper based or film based food packaging because of the unique porous structure of nanofiber mats. Pore size is an important criterion for the selectivity and the permeability of the membrane. Pore size and porosity are parameters that directly influence the air permeability of the nanofiber woven.

Air permeability allows food items especially fruits and vegetables to breathe (proper inhale/exhale of oxygen and carbon dioxide), which keeps them fresh for a longer period of time.

Figure (4.19) notice the pore size which analyzed by ANOVA software decreased for (S_4, S_7, and S_8) that attributed to the average nanofibers diameter lower. Whilst the pore size increased after addition essential oils and decreased after incorporation WB in basic material (S_8) because directly related to average nanofibers diameter. These results are concur with reported by [183].

Furthermore, the pore size of final blend (S_f) decrement although the average nanofiber diameter increased and this may be back to form multi-layer fiber strand structure that can fill pores of the membranes which might cause a reduction in pore size and porosity of the membranes. Thus, affect on the air permeability for the nanofiber web which can be considered as feasible for food packaging applications.

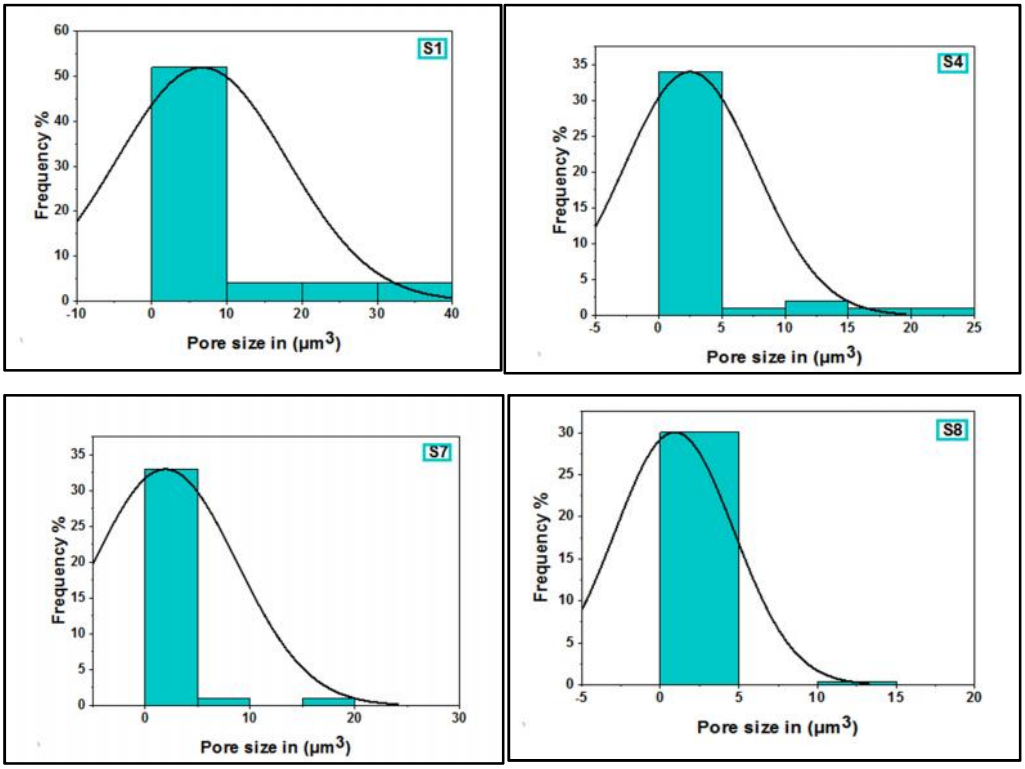

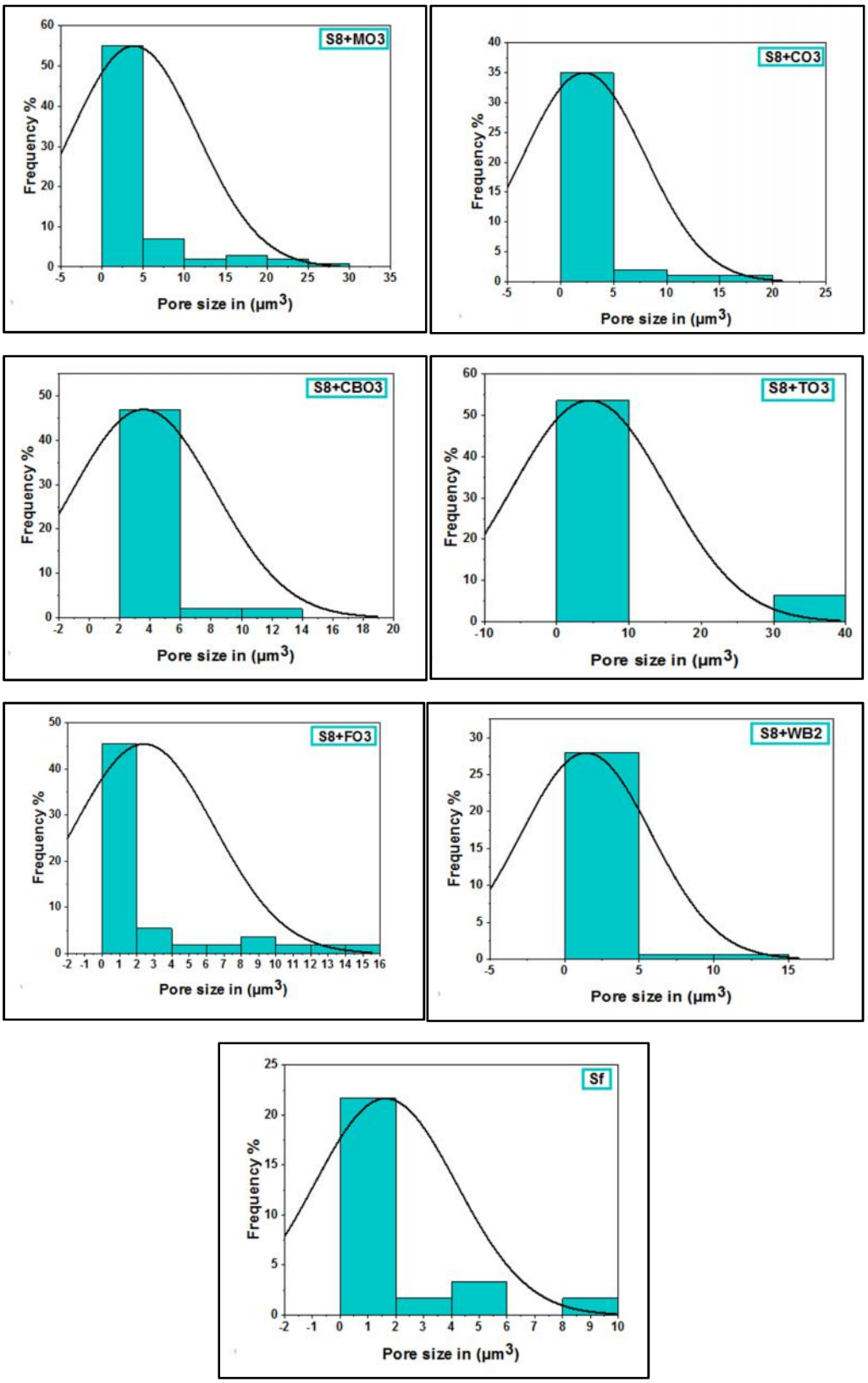

Figure (4.19): The pore size for samples in all parts.

4.4.4 Fourier Transformation Spectroscopy (FTIR)

FTIR analysis was used to investigate the functional groups and molecular interaction and intermolecular interactions among the components within the nanofibers. The FTIR spectrum in figure (4.20) of pure PVA sample shows a strong band at **(**3425 cm^{-1}) as the stretching vibration of hydroxyl group with strong hydrogen bonding, while small bands at (2916 cm^{-1}) is assigned to the characteristic bands of CH stretching vibration.

The stretching vibrational band of C=O at (1651 cm^{-1}) is attributed to the carbonyl functional groups because the residual acetate groups remain after the preparation of PVA from hydrolysis of polyvinyl acetate or oxidation during preparation and processing. The band at (1404 cm^{-1}) corresponds to C-H bending, while the bands observed at (1087 cm^{-1}) is recognized as crystallization sensitive bands which refer to C-O stretching vibration. The peaks at (871 cm^{-1}) corresponds to C-C stretch. Similar results were obtained by [160,184,185].

The FTIR spectra of STA in figure (4-14) shows a strong band at (3441cm^{-1}) was assigned to the characteristic absorption peak of the stretching vibration of -OH. The band at (2939 cm^{-1}) was attributed to the asymmetric stretching of C-H, while the band at (1643 cm^{-1}) was ascribed to the C-O bending associated with the OH group of water molecules adsorbed in the amorphous region of starch granules. The absorbance peak at (1411 cm^{-1}) implied the presence of C-H symmetrical scissoring of CH_2OH moiety.

The band at (1103 cm^{-1}) was attributed to the stretching vibration of C-O. In addition, the characteristic C-O-C ring vibration on starch leads to an absorbance peak at around (700-900 cm^{-1}). The results of FTIR for corn starch showed the similar results with [186,187].

Additionally, the CSM spectrum showed major absorption band at (3402 cm^{-1}) indicates stretching of O-H. Also a sharp peak at (2924 cm^{-1}) refers to stretching symmetric–asymmetric of C-H and symmetric–asymmetric carboxylate group at (1442 and 1651 cm^{-1}) respectively. The band at (1095 cm^{-1}) related to C-O stretching. Band at (617 cm^{-1}) correspond to C-O-H. This spectrum of CSM is consistence with [160, 188].

While the spectrum FTIR of WB pure in figure (4-14) which presented by the broad peak in (3410 cm^{-1}) corresponding to the stretching vibrations of O–H in hydroxyl groups of phenols and the stretching of N–H in amine groups. The peak (2931 cm^{-1}) refer to the stretching of C–H in alkane.

Furthermore, the peak at (1635 cm^{-1}, 1334 cm^{-1}, 1072 cm^{-1} and 779 cm^{-1}) is attributed to the (carbonyl) stretching vibrations of C=O in polyphenols, C-N stretching vibration, C-O stretching vibration in amino acids and C-H aromatic groups, respectively. Therefore the WB rich in polyphenols and amino acids and this consistent with [161].

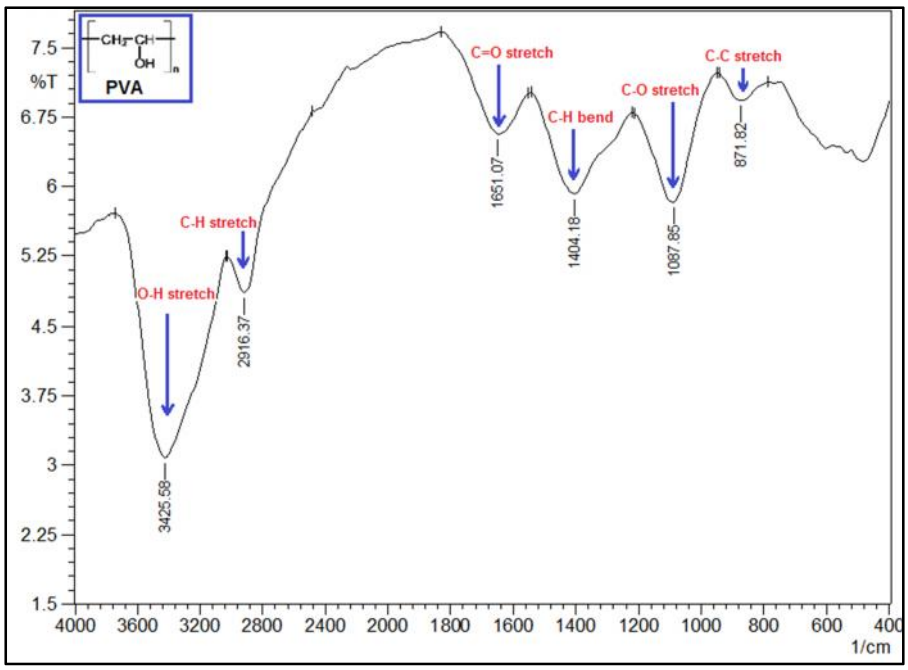

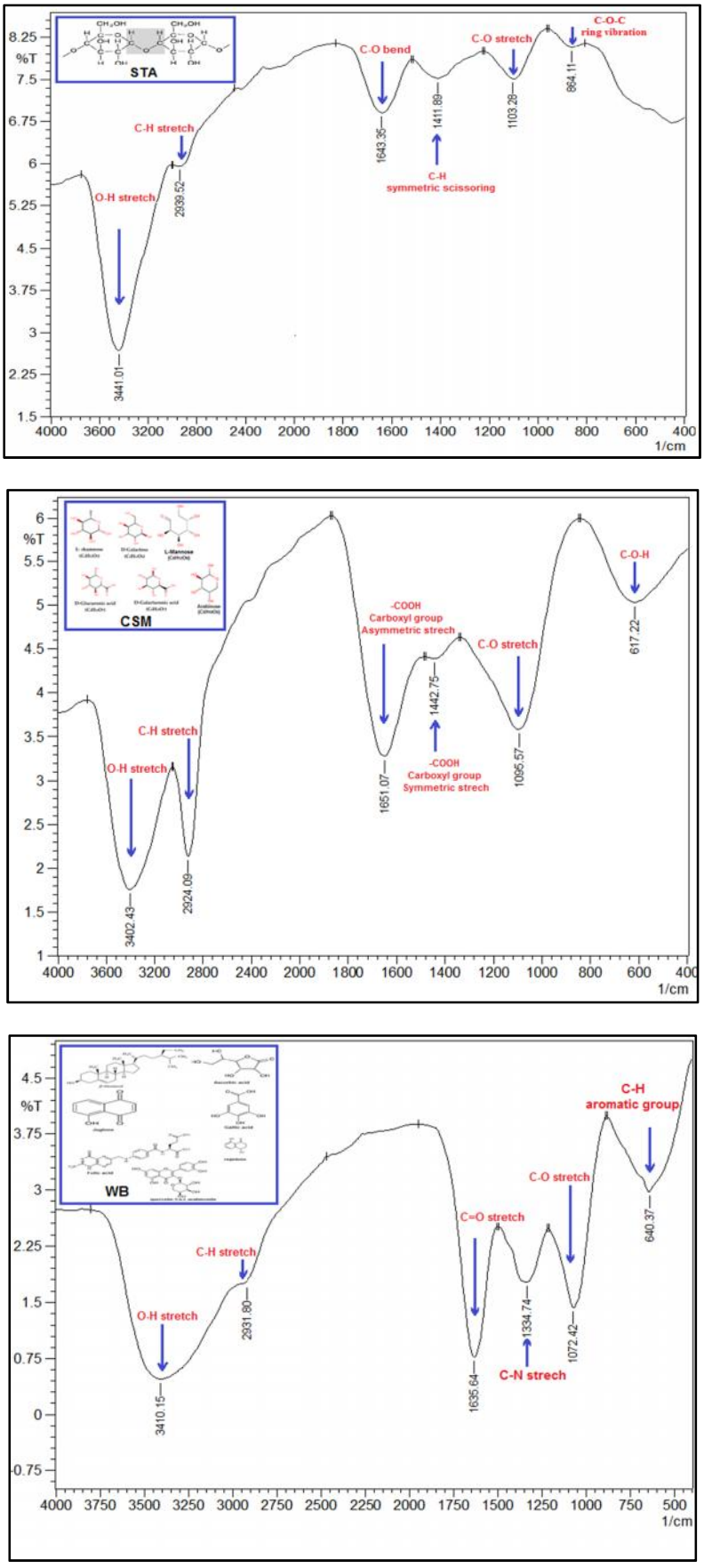

Figure (4.20): FTIR spectra of pure materials PVA, STA, CSM and WB.

In figure (4.21) the FTIR spectra of PVA/STA blends demonstrate the sharp absorption band (3441 cm^{-1}) is the cause of the stretching vibration of (-OH) present in starch. The absorption band at (1620 cm^{-1}) is because of the stretching vibration of (C=O). The vibration of the CH_2 group produces an absorption band at (1442 cm^{-1}). Due to the cause of C-O stretching an absorption band at (1103 cm^{-1}) was produced.

The absorption peak at (879 cm^{-1}) is assumed to the C-C stretching. These absorption peaks in FTIR spectrum of PVA/STA nanofibers proved that no chemical interactions exist between PVA and STA. Similar findings were obtained by [186].

The FTIR spectrum for PVA/CSM nanofibers as shown in figure (4-15), notice a decrement in an intensity and wavenumber at (1627 cm^{-1}) which indicate to the C=O carbonyl group. The PVA spectra existence can be justify by two peaks at (1419 cm^{-1}) and (879 cm^{-1}) while a band at (1103 cm^{-1}) indicating that CSM was present in nanofibers, which proved the existence of both polymers in nanofibers and confirmed that no chemical interactions occurred between CSM and PVA. Similar results are reported by [160].

While the FTIR spectrum of PVA/CSM/STA was obvious a decrement in an intensity and wavenumber at (1635 cm^{-1}) that indicate to the C=O carbonyl group. furthermore, notice the band peak at about (2916- 2939 cm^{-1}) not appear and this maybe comeback to broken in C-H stretch bond and broad band region at (1473 cm^{-1}) and (1134 cm^{-1}) which referred to increasing C-H bend and C-O stretch bonds.

Additionally,the width of the O-H band at (3448 cm^{-1}) was broaden in PVA/CSM/STA nanofibers spectrum, indicated the enhancement of hydrogen bonding between (PVA, CSM and STA) nanofibers.The results showed that just physical interaction existed among the components and no chemical interactions occurred.

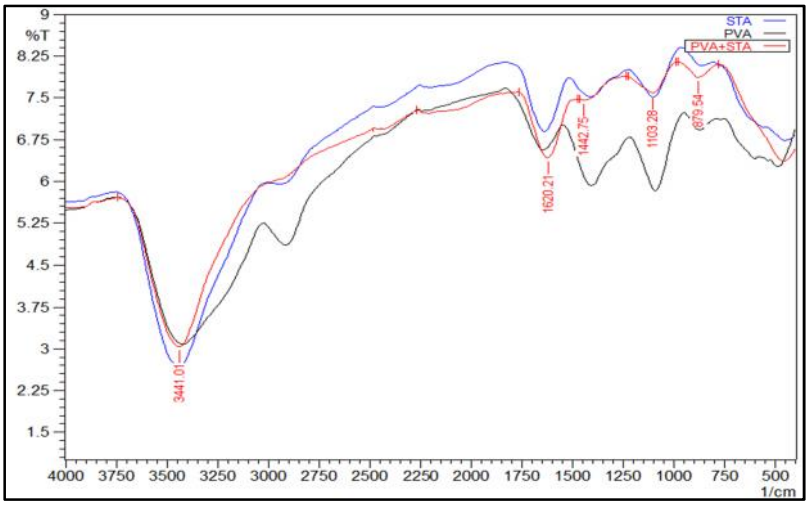

(a)

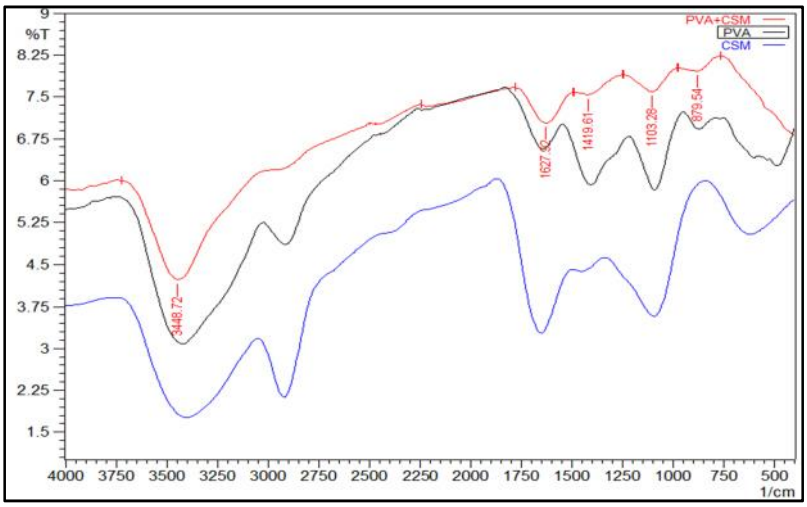

(b)

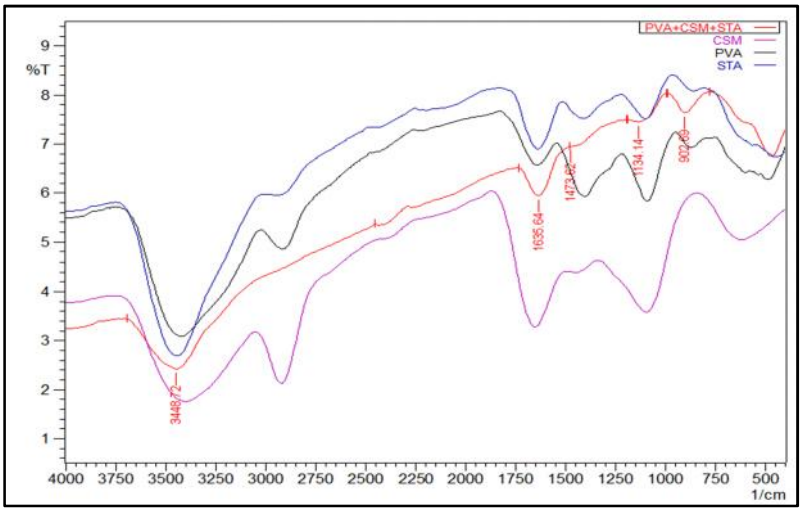

(c)

Figure (4.21): FTIR spectra of (a) PVA/STA, (b) PVA/CSM, and (c) PVA/STA/CSM samples.

The FTIR spectrum of (PVA/CSM/STA/MO) nanofibers in figure (4.22) similar to that of (PVA/CSM/STA) in figure (4.21), but the peaks at (879, 1095 and 1404 cm^{-1}) broadened and shifted to lower frequencies which means the increment in these bonds (C-C stretch, C-O stretch and C-H bend) respectively. Furthermore, the intensity of absorption peak at (1643 cm^{-1}) reduced which indicate to the C=O carbonyl group.

In addition, the absorption peak at (2924 cm^{-1}) appear due to existence this peak in MO. Notice increment in the intensity of the obsorption peak at (3410 cm-1) that reffered to increasing O-H bonds. The results revealed that (PVA/CSM/STA/MO) nanofibers were prepared precisely and entrapped MO successfully and these results agreed with [189].

For FTIR spectrum (PVA/CSM/STA/CO) nanofibers, the peaks at (3402 cm^{-1}, 1404 cm^{-1} and 1080 cm^{-1}) widened and increased in the intensity which denotated of increment in bonds (O-H stretch, C-H bend and C-O stretch) respectively. While the intensity decrement of C=O carbonyl group at (1651 cm^{-1}). The results showed the CO was placed in (PVA/CSM/STA) successfully and consistence with reported by [97].

While FTIR spectrum of (PVA/CSM/STA/CBO), (PVA/CSM/STA/TO) and (PVA/CSM/STA/FO) nanofibers as shown in figure (4.22) were similar to that of (PVA/CSM/STA) but with increased in the intensity of some absorption peaks and shifted to lower fequencies which reffered to increment in bonds (O-H stretch, C-H bend and C-O stretch) respectively. Meanwhile, notice the intensity of C=O carbonyl group at about (1643-1651 cm^{-1}) decreased.

Additionally, the absorption peak at about (2916-2924 cm^{-1}) appear which comeback to (CBO, TO and FO respectively). These results

confirmed that all these essential oils was successfully incorporated in electrospun fibers and line with reported by [101, 171, 190].

The FTIR spectra of (PVA/CSM/STA/WB) has the same spectra of (PVA/CSM/STA) that indicates to good embedding ability and stable structure. But notice the peak at (3433 cm^{-1}) broadened and shifted towards the lower wavenumbers and this referred to intermolecular interactions between (PVA/CSM/STA) and WB which represent by hydrogen bonds between the carbonyl groups of (PVA/CSM/STA) and the hydroxyl groups of WB. This agrees with reported by [161].

As well as the carbonyl index which refer to the thermo oxidative degradation for nanofiber that was noticed from the intensity of carbonyl band at (1643 cm^{-1}). This the intensity decrease after adding WB due to its nature antioxidant which reduced from thermo oxidative degradation of nanofiber. These results agreement with research by [191].

Whilst the FTIR spectrum of final blend (S_f) similar to spectra of (PVA/CSM/STA) with decreased in the intensity of carbonyl group and widened in the absorption peaks which denoted of increment in bonds (O-H stretch, C-H bend and C-O stretch) as shown in table (4.11). These results confirmed that all these additions was successfully incorporated in electrospun fibers.

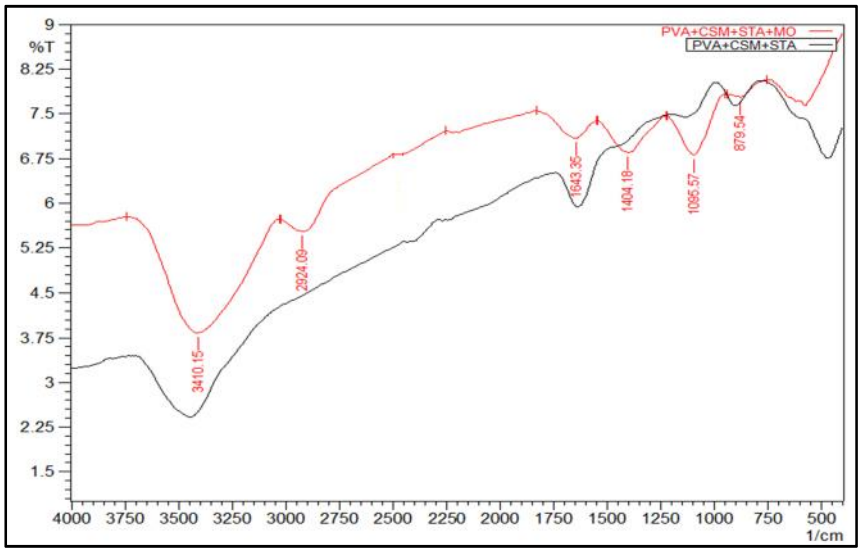

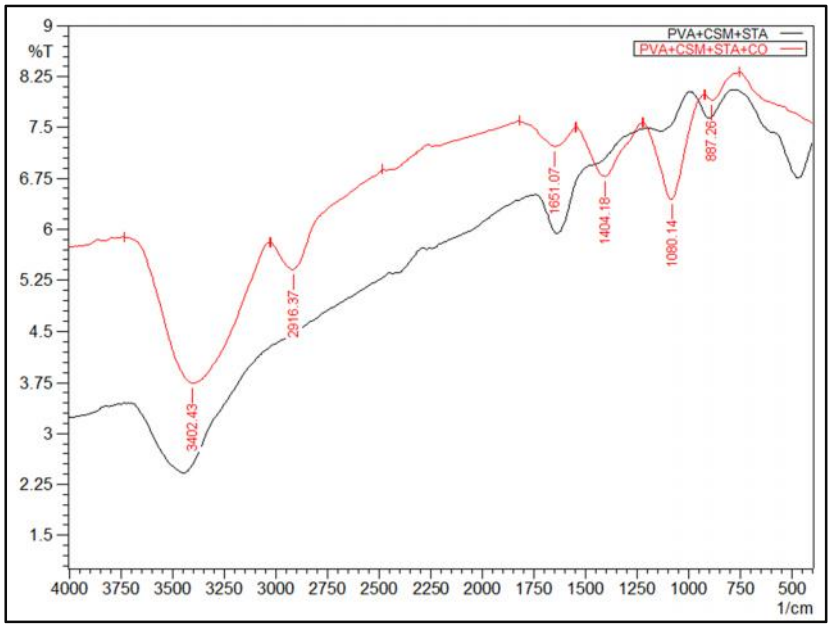
PVA+CSM+STA
PVA+CSM+STA+CO
%T
3402.43
2916.37
1651.07
1404.18
1080.14
887.26
1/cm

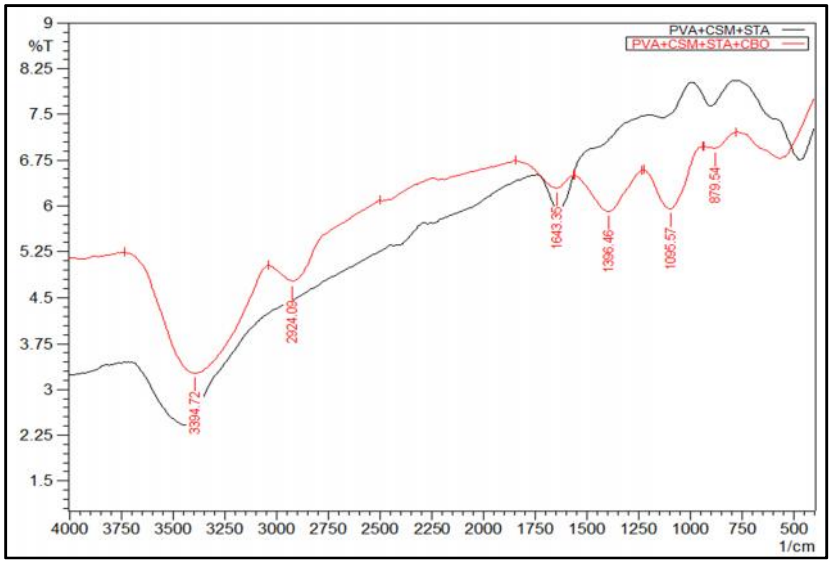
PVA+CSM+STA
PVA+CSM+STA+CBO
%T
3394.72
2924.09
1643.35
1396.46
1095.57
879.54
1/cm

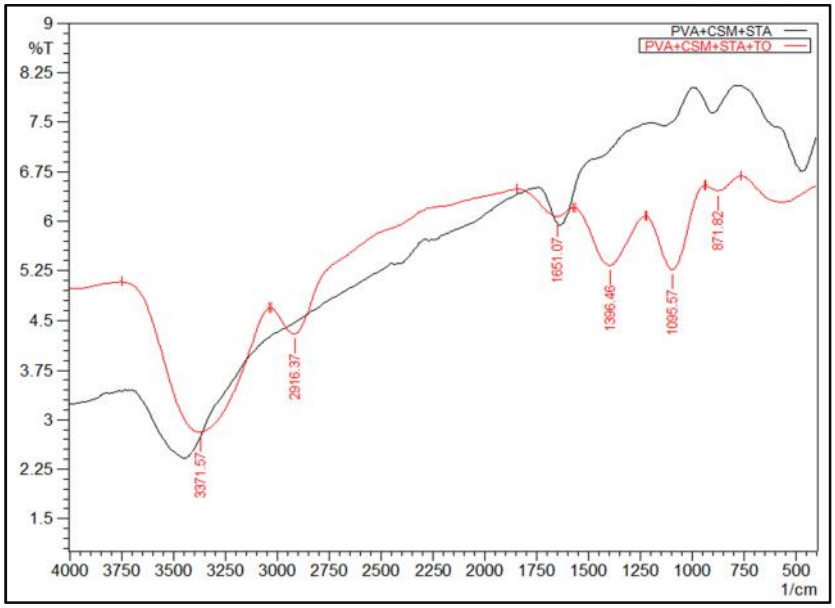
PVA+CSM+STA
PVA+CSM+STA+TQ
%T
3371.57
2916.37
1651.07
1396.46
1095.57
871.82
1/cm

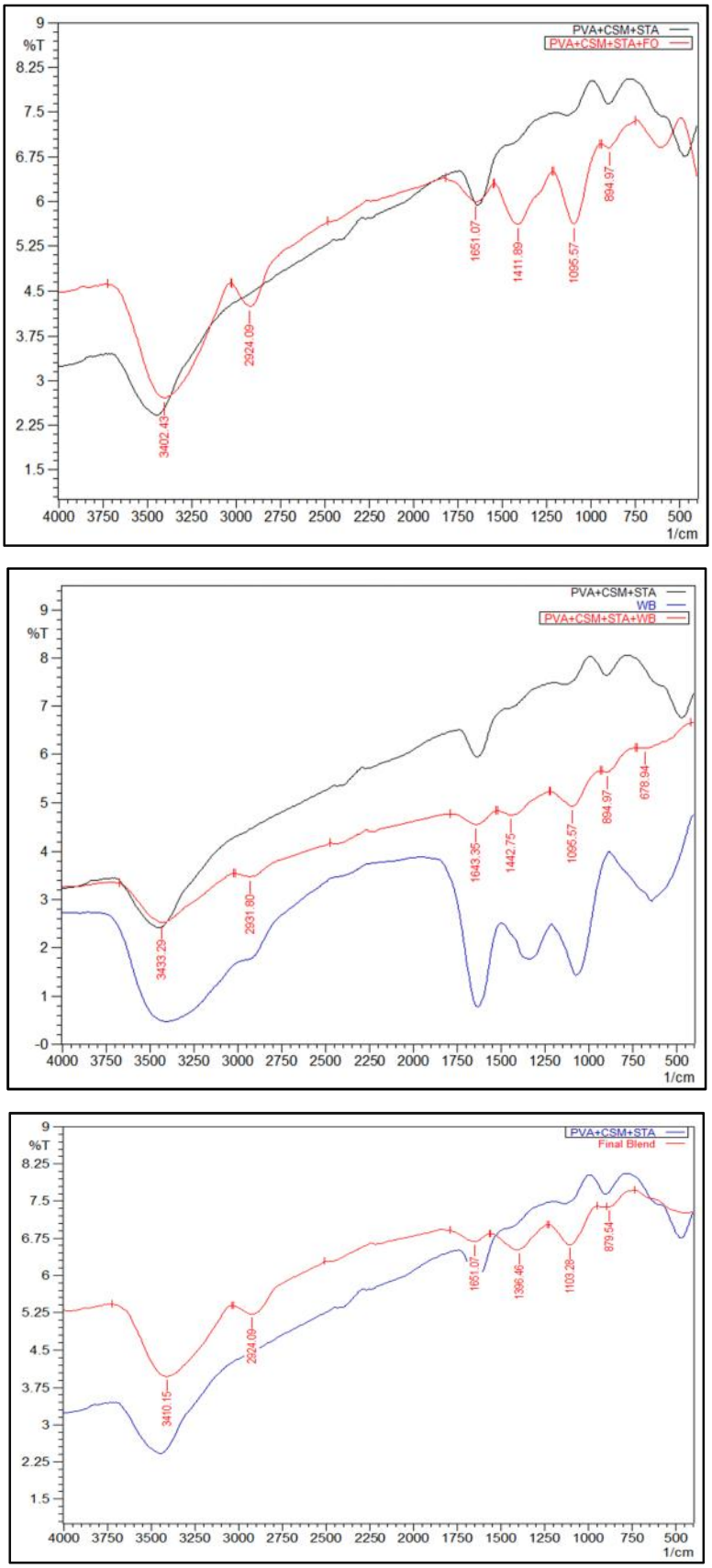

Figure (4.22): FTIR spectra of MO, CO, CBO, TO, FO, WB and final sample.

Table (4.11): Band wavenumber variation for samples in all parts.

Experimental transmission peak/cm^{-1}	Type of bond
3370-3450	O–H stretching in hydroxyl groups and N–H stretching in amine groups
2916-2940	C-H stretching in alkane
1620-1651	C=O stretch carbonyl group, C-O bending and -COOH carboxyl group asymmetric stretch
1334-1473	C-N stretch, C-H bend and -COOH carboxyl group symmetric stretch
1072-1134	C-O stretch
864-902	C-O-C ring vibration and C-C stretch
617-678	C-O-H and C-H aromatic group

4.4.5 Differential Scanning Calorimetry (DSC)

In order to investigate the thermal behavior, such as melting, crystallization and formation of crystalline structure, the DSC measurements was performed. The results from DSC curve of samples in all parts are presented in figure (4.23) which existed in appendix (D) and table (4.12). The melting temperature was (226.17 ºC) of (S_1) nanofibers and this value agreement with that reported by [192, 193].

When STA was added, the T_m decreased. The reduction in T_m was attributed to the reduction in the cohesive forces of attraction between the polymer chains. The change in enthalpy of melting (ΔH_m J/g) used to determine the reactive interactions of polymer blends. It was clearly shown that the enthalpy of (S_4) blend decreased from (15.73 J/g for PVA to 13.87 J/g for blend) due to the fact that the intermolecular interaction in the compound was decreased. These results consistence with [186, 194].

The DSC curve of (S_7) nanofibers show the melting temperature (T_m) decrement to 223.79ºC and this indicated that CSM slightly disturbed the arrangement of the PVA chain thus the crystalline region was probably reduced slightly. Therefore, this finding shows sufficient effect on the amorphous region in the blends. In addition, notice minor decrease in the ΔH_m from (15.73 to 15.62 J/g) which agrees with reported data by [163].

The melting temperature (T_m) of (S_8) nanfibers slightly increased to (227.62 ºC). Meanwhile, the enthalpy of fusion increment to (18.62 J/g). This is due to the CSM consists of galacturonic acid, L-rhamnose, D-galactose, and L-arabinose. These carbohydrate molecules of mucilage have excellent potential to interact with other molecules such as starch (Amylose and Amylopectin) by hydrogen bonds which confirmed by FTIR analysis. These results line with reported by [195].

The melting temperature (T_m) of the nanofibers slight increase with addition essential oils from (227.62 ºC) to (228.04 ºC, 228.63 ºC, 227.74 ºC, 229.04 ºC, and 227.82 ºC for MO, CO, CBO, TO, and FO respectively), mainly due to the essential oil had the ability to increase chains mobility of the basic blend which opportunity to interact with the carbonyl groups on (PVA/CSM/STA) blend chains via hydrogen bonding which confirmed by FTIR analysis.

Furthermore, notice increment in the enthalpy (ΔH_m) from (18.62 J/g) to (20.62, 20.73, 19.32, 21.10, and 19.14 J/g for MO, CO, CBO, TO, and FO respectively). This results similar to observed by [167,196].

Whereas DSC curve of (S_8+WB_2) nanofibers appear increment in the melting temperature (T_m) from (227.62 ºC) to (229.74 ºC) and increase in the enthalpy of fusion (21.73 J/g). This is due to increment the intermolecular interactions between the carbonyl group of basic blend

and amine group of WB by hydrogen bonds as mentioned in FTIR analysis. This concur with [158].

Lastly, the DSC curve of final blend (S_f) indicate to increase Tm to (233.00 ºC) and enthalpy of fusion (23.22 J/g). This refer to a greater interaction between basic blend and all additives which lead to miscible blend.

Table (4.12): The melting temperature and enthalpy of the samples.

Sample No.	T_m (ºC)	ΔH_m (J/g)
S_1	226.17	15.73
S_4	219.47	13.87
S_7	223.79	15.62
S_8	227.62	18.62
S_8+MO_3	228.04	20.62
S_8+CO_3	228.63	20.73
S_8+CBO_3	227.74	19.32
S_8+TO_3	229.04	21.10
S_8+FO_3	227.82	19.14
S_8+WB_2	229.74	21.73
S_f	233.00	23.22

4.4.6 Thermogravimetric Analysis (TGA)

Thermalgravitmetry Analysis (TGA) is a common and helpful technique which is used for determination material thermal stability by monitoring the weight loss of the nanofibers when heated. TGA curve from figure (4.24) of pure PVA (S_1) nanofibers showed three-step degradation behaviors.

The first step below 150˚C was due to the removal of moisture and adsorbed water. The second step show sharp degradation referred to the degradation of PVA backbone. The third step around 840˚C was depicted to the degradation of vinyl acetate group of PVA. Majority weight loss of pure PVA nanofibers was occurred around 300˚C. The weight loss (W_{loss}%) of (S_1) nanofibers at 740 ºC was (42%)

which represent the thermal stability for this sample. This similar to results reported by [197].

The TGA curve of (S_8) nanofibers illustrated three steps. For the first step moisture loss occurred in the range of (40-120 ºC). The second step indicated decomposition of saccharide rings and disintegration of macromolecular chains of CSM as well as beginning of degradation of the side chains of PVA and STA that started from 160ºC and terminated at 380ºC and this may be due to the bonds existed in CSM need to energy about (340- 760 kJ/mol) while PVA bonds required energy about (340- 470 kJ/mol) to its broken. The third step was from (390 to 660 ºC) which was related to the decomposition of the main chain of PVA, STA, and the saccharide rings and disintegration of macromolecular chains of CSM.

The weight loss (W_{loss}%) of (S_8) nanofibers at the same temperature as mention up (740 ºC) was (77 %). Thermal stability of this sample higher than for PVA due to the presence of carbohydrates and proteins in the mucilages (CSM) which enhances the stability and uniformity of the sample [89].

Incorporation of essential oils in the nanofibers matrix (S_8) led to a three-step degradation process, where the first degradation step, between (40-150 ºC) for all essential oils might be due to gradual evaporation of essential oil moisture and adsorbed water. The second degradation step between (200-360 ºC) for (MO, CBO, and FO), but for CO and TO between (160-260 ºC) and (160-360 ºC) respectively, resulting from partial vaporization of highly volatile organic compounds in essential oils during the electrospinning process. The third step between (360-520 ºC), (350-740 ºC), and (350-770 ºC) for (MO, CBO, and FO) respectively, but for CO and TO between (270-410 ºC) and (360-510 ºC) respectively which corresponding to the degradation of

matrix and residual compounds in these oils because the essential oils need to greater energy to broken bonds inside.

The weight loss at the end of heating from matrix loaded essential oils (W_{loss}%) was about (97-98 %) at (740 ºC) attributed to the interaction between matrix and essential oils, thus leading to a higher heat resistance of the resulting nanofibers, compared with the matrix. This results concur with [198, 199].

Whereas the (S_8+WB_2) nanofibers were degraded in three steps. The first step which occurred in the range of (40-120 ºC) is probably due to the evaporation of the moisture absorbed by the WB and volatile compounds (low molecular weight esters and fatty acids) which are inherent to the WB. The second step represents gradual weight loss that started from 160 ºC and terminated at 365 ºC which may be due to the degradation of matrix and WB. The third step between (375-620 ºC) which attributed to the degradation of matrix and residual compounds in WB that need to higher energy to broken bonds inside it.

The weight loss (W_{loss}%) from this nanofibers was (79.6 %) at 740 ºC. Based on the obtained results, it can be concluded that the incorporation of WB improves the thermal stability of the matrix and may act as a radical scavenger during the thermal degradation process, leading to higher (W_{loss}%) as a consequence. This results similar with reported by [200].

The final blend (S_f) appear three-step degradation behaviors. the first step between (40-160 ºC) due to removal of moisture absorbed by the WB and volatile compounds and adsorbed water. The second step is between (240-460 ºC) shows gradual degradation resulting from degradation of matrix and additives. The third step about (470-810 ºC) was depicted to the degradation main chains of matrix and residual

compounds in final blend. The weight loss (W_{loss}%) of final blend nanofibers at 740 ºC was (98.59%).

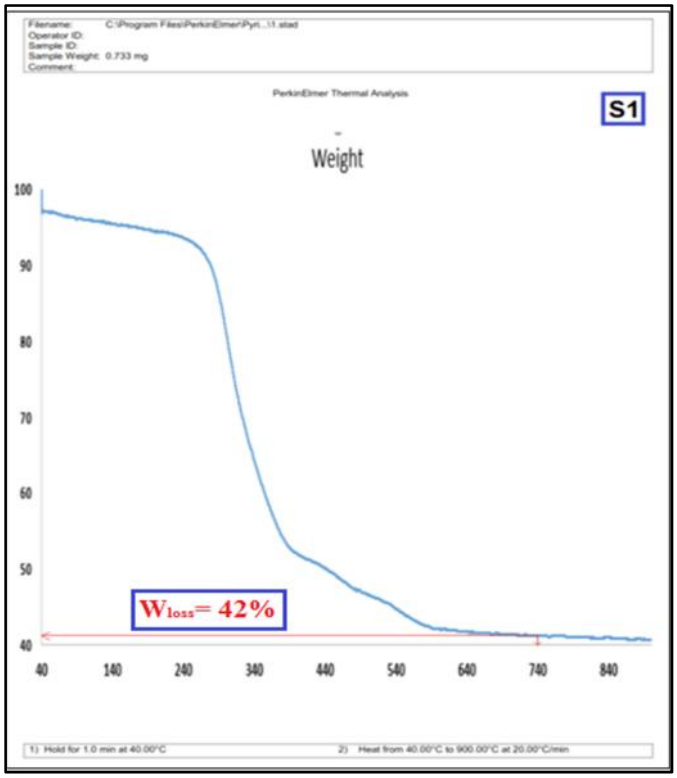

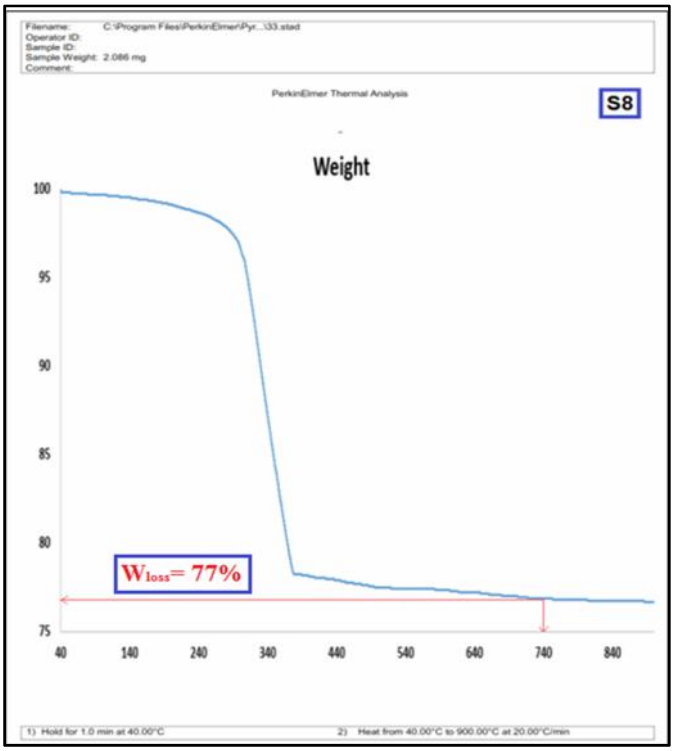

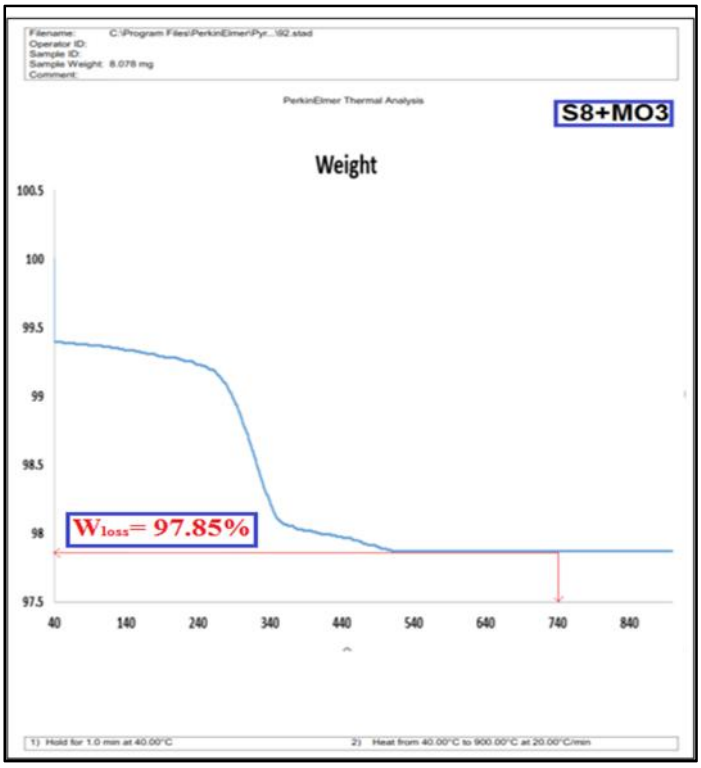
Filename: C:\Program Files\PerkinElmer\Pyr...\62.stad
Operator ID:
Sample ID:
Sample Weight: 8.078 mg
Comment:
PerkinElmer Thermal Analysis
S8+MO3
Weight
100.5
100
99.5
99
98.5
98
97.5
Wloss= 97.85%
40
140
240
340
440
540
640
740
840
1) Hold for 1.0 min at 40.00°C
2) Heat from 40.00°C to 900.00°C at 20.00°C/min

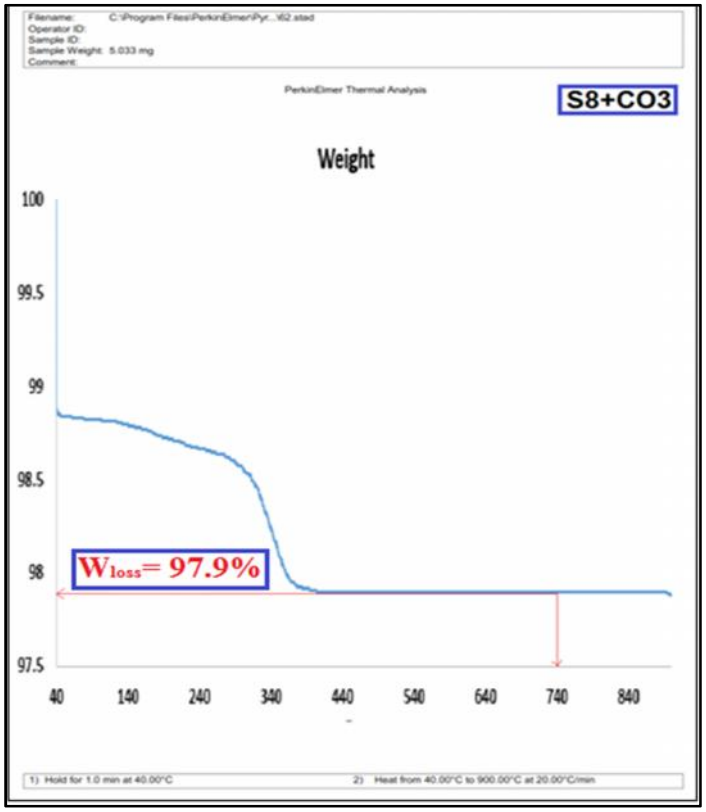
Filename: C:\Program Files\PerkinElmer\Pyr...\62.stad
Operator ID:
Sample ID:
Sample Weight: 5.033 mg
Comment:
PerkinElmer Thermal Analysis
S8+CO3
Weight
100
99.5
99
98.5
98
97.5
Wloss= 97.9%
40
140
240
340
440
540
640
740
840
1) Hold for 1.0 min at 40.00°C
2) Heat from 40.00°C to 900.00°C at 20.00°C/min

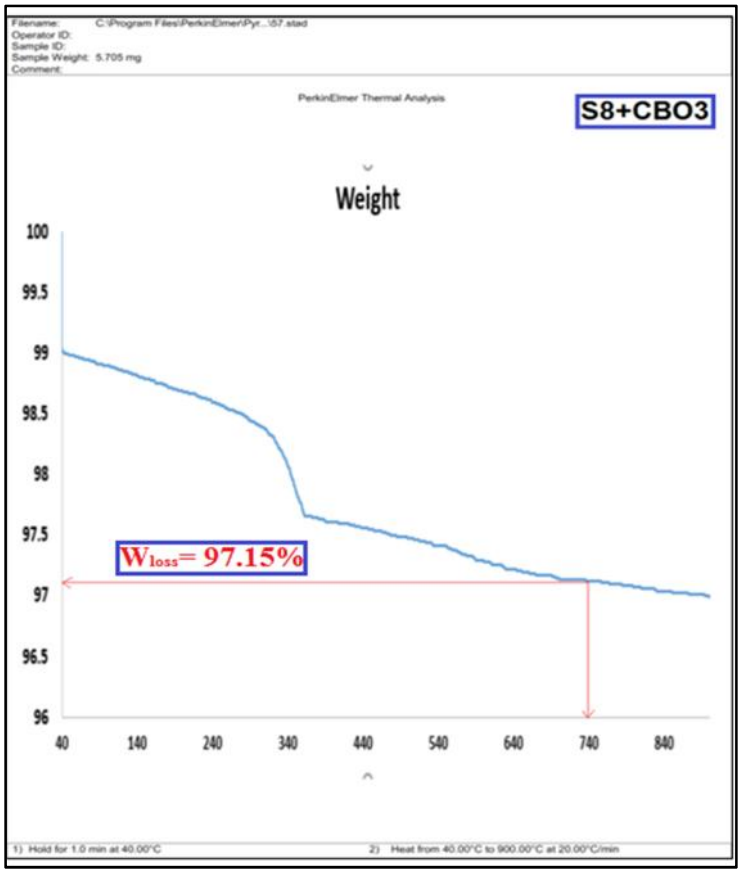
Filename: C:\Program Files\PerkinElmer\Pyr...\57.stad
Operator ID:
Sample ID:
Sample Weight: 5.705 mg
Comment:
PerkinElmer Thermal Analysis
S8+CBO3
Weight
100
99.5
99
98.5
98
97.5
97
96.5
96
40
140
240
340
440
540
640
740
840
Wloss= 97.15%
1) Hold for 1.0 min at 40.00°C
2) Heat from 40.00°C to 900.00°C at 20.00°C/min

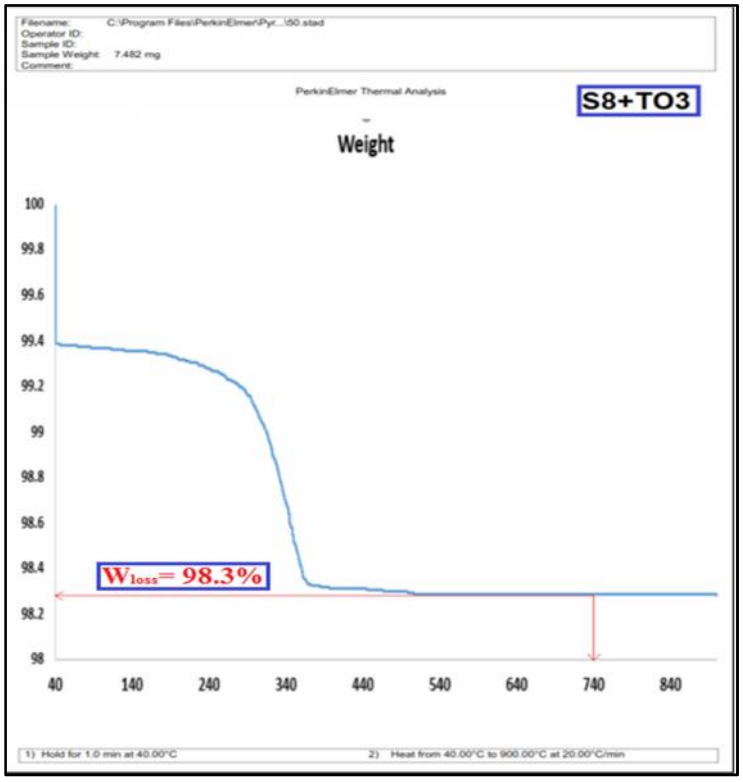
Filename: C:\Program Files\PerkinElmer\Pyr...\50.stad
Operator ID:
Sample ID:
Sample Weight: 7.482 mg
Comment:
PerkinElmer Thermal Analysis
S8+TO3
Weight
100
99.8
99.6
99.4
99.2
99
98.8
98.6
98.4
98.2
98
40
140
240
340
440
540
640
740
840
Wloss= 98.3%
1) Hold for 1.0 min at 40.00°C
2) Heat from 40.00°C to 900.00°C at 20.00°C/min

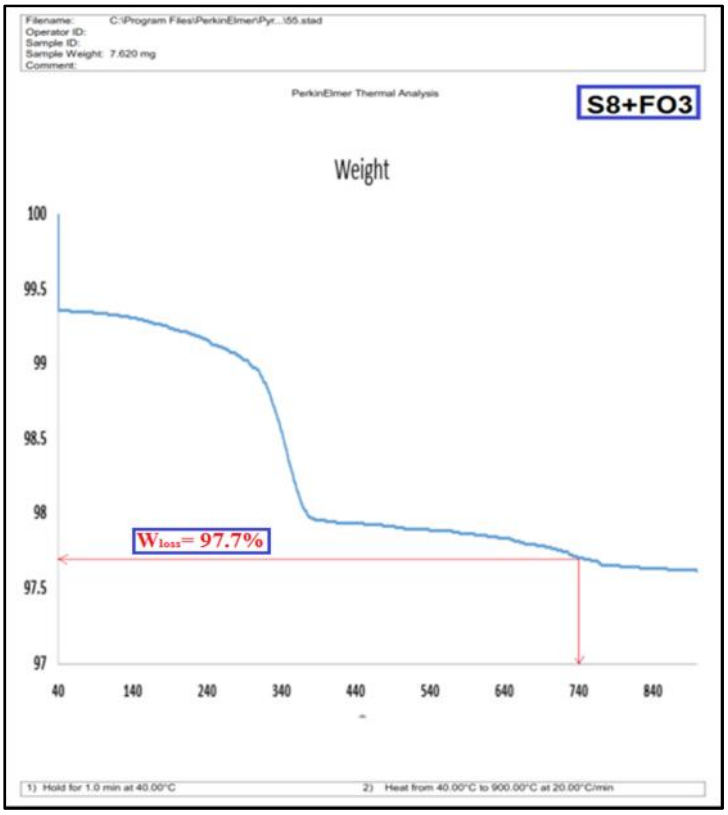
Filename: C:\Program Files\PerkinElmer\Pyr...\55.stad
Operator ID:
Sample ID:
Sample Weight: 7.620 mg
Comment:
PerkinElmer Thermal Analysis
S8+FO3
Weight
100
99.5
99
98.5
98
97.5
97
40
140
240
340
440
540
640
740
840
Wloss= 97.7%
1) Hold for 1.0 min at 40.00°C
2) Heat from 40.00°C to 900.00°C at 20.00°C/min

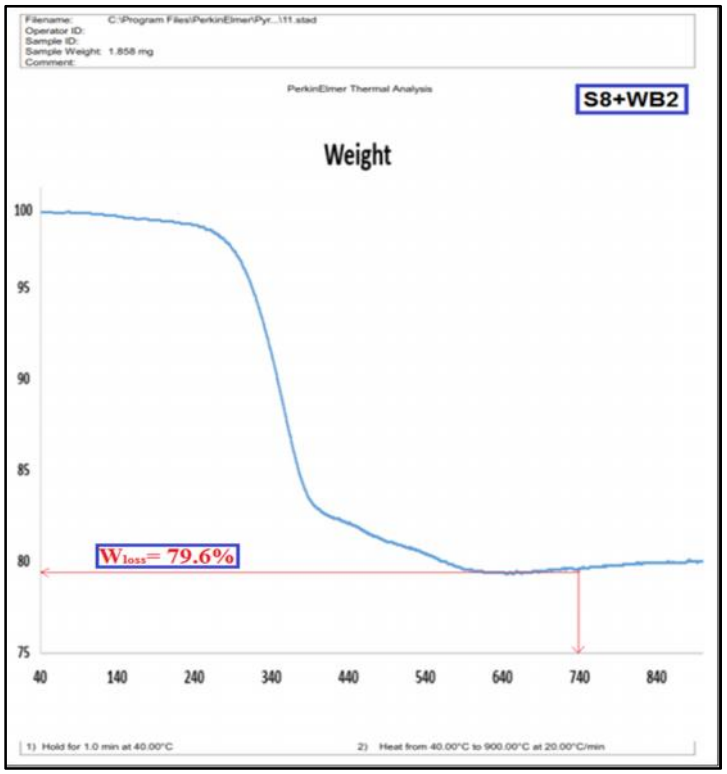
Filename: C:\Program Files\PerkinElmer\Pyr...\11.stad
Operator ID:
Sample ID:
Sample Weight: 1.858 mg
Comment:
PerkinElmer Thermal Analysis
S8+WB2
Weight
100
95
90
85
80
75
40
140
240
340
440
540
640
740
840
Wloss= 79.6%
1) Hold for 1.0 min at 40.00°C
2) Heat from 40.00°C to 900.00°C at 20.00°C/min

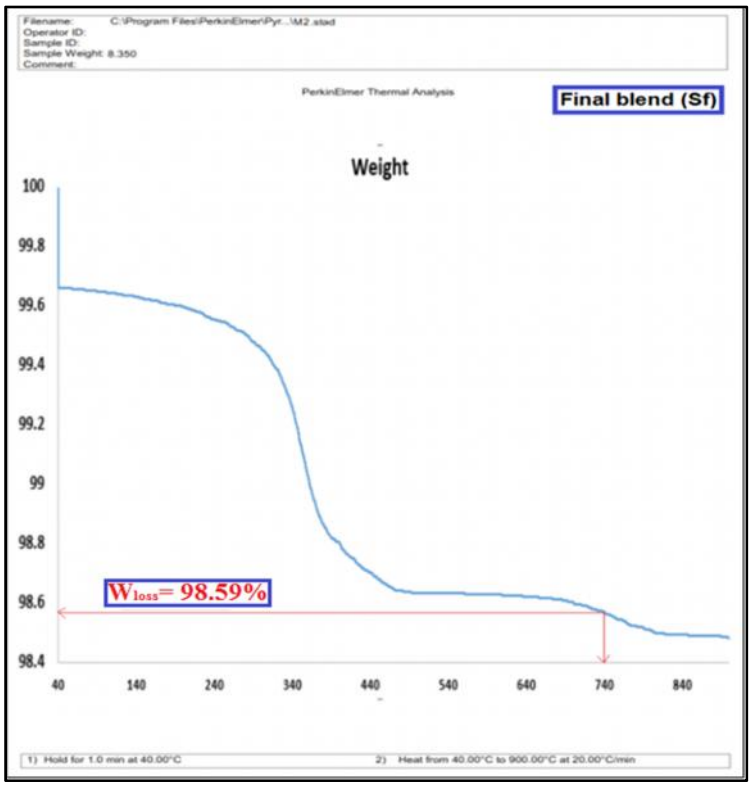

Figure (4.24): TGA curves of samples.

4.4.7 UV–Visible Spectroscopy

UV light forms free radicals in food leading to the destruction of food components i.e. antioxidants, lipids, nutrients, color pigments, and formation of off-flavors. It is necessary to protect food against the effects of light, especially UV radiation. The UV-Vis spectra of basic sample (S_8) in figure (4.25 A) exhibited a single peak at about (230 nm) band corresponding to $\pi \rightarrow \pi^*$ transition of (C=O) and related to absorption band of this sample in UV region.

While figure (4.25 B) display UV-Vis spectra of essential oils that consisted of three characteristic peaks at 330 nm, 730 nm and 990 nm wavelength bands and this represent to absorbance spectra within the ultra violet (UV), visible (Vis), and infrared (IR) spectrum. So display $n \rightarrow \pi^*$ and $\pi \rightarrow \pi^*$ transitions. The (n) electrons (or the nonbonding electrons) are the ones located on the oxygen of the carbonyl group. Thus,

the (n → π*) transition corresponds to the excitation of an electron from one of the unshared pair to the (π*) orbital as shown in figure (4.26).

Meanwhile, the UV-Vis spectra of WB appear single beak at (330 nm) which represent absorbance spectra within ultra violet (UV). These result in line with reported by [201, 202]. Thus, all additives show π→π* and n → π* transitions.

The UV-Vis spectra of final sample (S_f) show two characteristic peaks at 330 nm and 990 nm wavelength bands and this referred to absorbance spectra within the ultra violet (UV) and infrared (IR) spectrum. Which is considered necessary to protect food from these radiations.

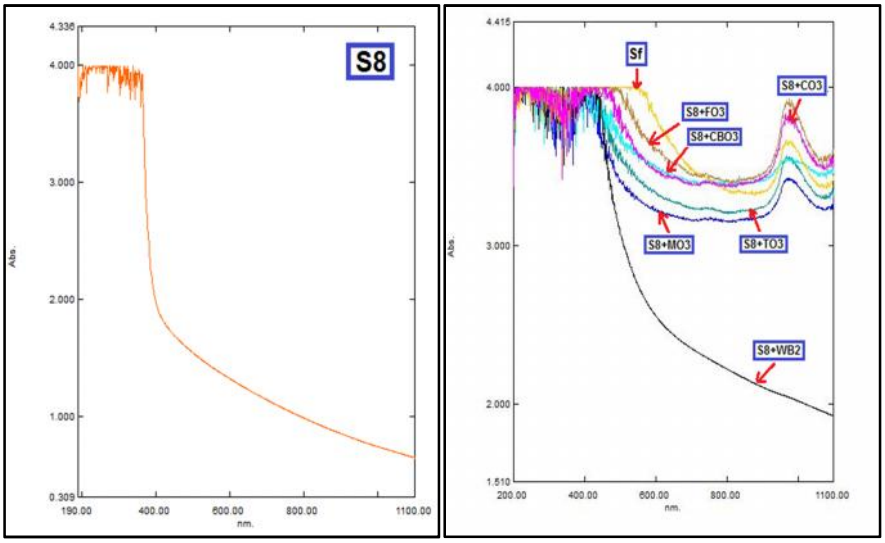

(A) **(B)**

Figure (4.25): The UV-Vis spectrum of samples A) basic sample (S_8), B) all additives and final sample (S_f).

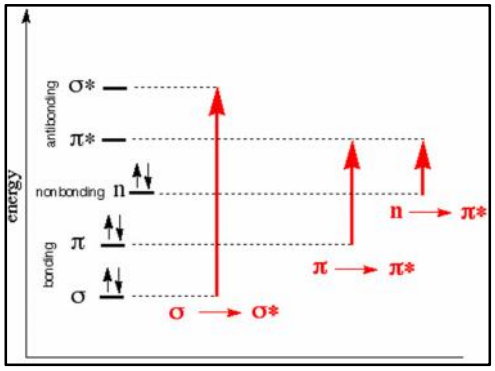

Figure (4.26): Hypothetical energy diagram.

4.4.8 X- Ray Diffraction (XRD)

The XRD used to measure crystalline properties such as crystallite size. The crystalline structure depends on characteristics of the polymer (molecular weight), process parameters of electrospun. Figure (4.27) represents the (XRD) patterns of basic (S_8) and final blend (S_f) nanofiber while table (4.13) show results of crystalline properties for S_8 and S_f nanofibers.

The main peak in 2θ=25º for (S_8) but observe (2θ=23º) for (S_f), The final blend had a crystallite size more than of basic and the peak width slight greater which referred to occurrence of more interaction between molecules by hydrogen bonding. The crystallite size was calculated from the Debye–Scherrer equation:

$$\textbf{Crystallite Size} = \frac{K * \lambda}{\beta * cos\theta} \qquad \text{.....(4.1)}$$

Where β ($2\theta_2$-$2\theta_1$) is the full width at half of the maximum (FWHM), (K) and (λ) is a constant with a value of 0.89, 1.54 Aº respectively, and θ is the Bragg angle.

Table (4.13): The results of crystallite size for (S_8) and (S_f) nanofibers.

Sample No.	Crystallite Size (nm)	2Ɵ (°)	d-spacing (Aº)
S_8	3.150	25.20	3.530
S_f	3.587	23.09	3.747

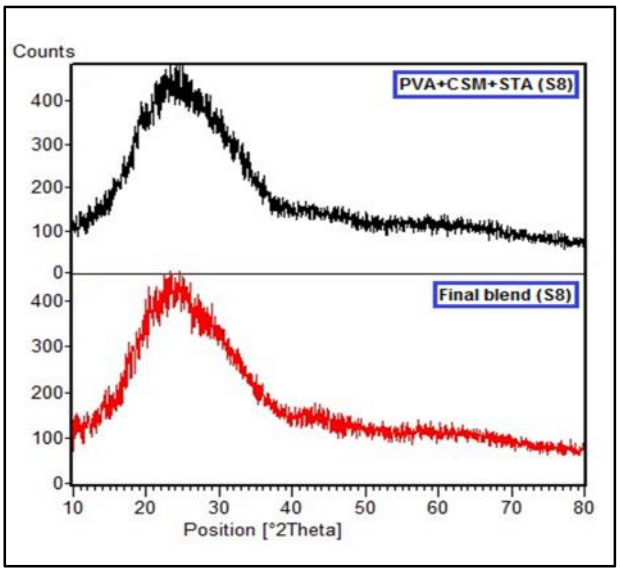

Figure (4.27): XRD curves of matrix (S_8) and final blend (S_f).

4.5 Biological Tests Results

4.5.1 Antibacterial Activity

One of the important requirements for the advanced fiber based packaging materials is to prevent and/or inhibition of the bacterial growth and colonization at the food surfaces.

The essential oils with potent antimicrobial activity has been recognized as a natural antimicrobial agent for food preservation. Thus, the antibacterial activity of all sample nanofibrous mats was tested against Gram-positive (S. aureus) and Gram-negative (E. coli) bacteria. The inhibition zone of all percentage used in additives against S. aureus and E. coli is shown in table (4.14) and figure (4.28).

The basic blend (S_8) does not exhibit any antimicrobial properties, while apparent inhibition rings are detected around percentage additives. From this table can be observed that inhibition increased with increasing additives concentration in the basic (S_8), The inhibition zone diameter of MO_2 and MO_3 was ((15 -19 mm) and (17-20 mm)) against (E. coli) and (S. aureus) respectively and this concur with reported by [189].

While nanofibers containing CO show antibacterial activity against both bacteria. The enhancement of the antibacterial activity of nanofibers due to increasing the concentration of CO in nanofibers can be related to the existence of antibacterial compounds α-terpinyl acetate and linalool in CO as mentioned in chapter two.

The results showed in table (4.14) of CO_2 and CO_3 was ((11 -19 mm) and (17-20 mm)) against (E. coli) and (S. aureus) respectively. The inhibition zone diameter against S. aureus is higher than E. coli that can be attributed to the impenetrable property of phospholipid outer membrane of Gram- negative bacteria in comparison with the lipophilic outer membrane of Gram-positive bacteria. This current finding was consistent with the results demonstrated by [97].

The nanofibers containing CBO showed the inhibition zone diameter of CBO_2 and CBO_3 was ((12 -16 mm) and (18-20 mm)) against (E. coli) and (S. aureus) respectively. The results revealed that eugenol compound existed in CBO as illustrative in chapter two is the main antimicrobial substance and this result agreement with [190].

The inhibition zone diameter of TO_2 and TO_3 was ((14 -15 mm) and (19-18 mm)) against (E. coli) and (S. aureus) respectively and this due to the phenolic compounds in Thyme structure is responsible for antibacterial activities. These compounds are Thymol, carvacrol, and terpinene. This similarly to study by [139].

The inhibition zone showed by FO_2 and FO_3 was ((17 -17 mm) and (20-18 mm)) against (E. coli) and (S. aureus) respectively. The results proved that even at a minimum concentration, fenugreek oil (FO) would be an effective antimicrobial agent. Also other research reported a good inhibitory effect of FO [105].

While the diameter of inhibition zone increased after adding WB to the basic with different percentage WB_1, WB_2, and WB_3 was

((17 -13 mm), (20-17 mm), and (15-16 mm)) against (E. coli) and (S. aureus) respectively as an antibacterial agent due to the main antibacterial active substance (juglone) existed in the composition of WB and this results agreement with [161].

Finally, the final blend (S_f) nanofibers dissolve in distilled water at different percentage (62.5, 125, 250, and 500%) and its symbols (S_f2, S_f3, S_f4, and S_f5 respectively). The inhibition zone diameter for these samples against (E. coli) and (S. aureus) was ((30 -25 mm), (34-10 mm), (36-15 mm), and (37-20 mm) to (S_f2, S_f3, S_f4, and S_f5) respectively.

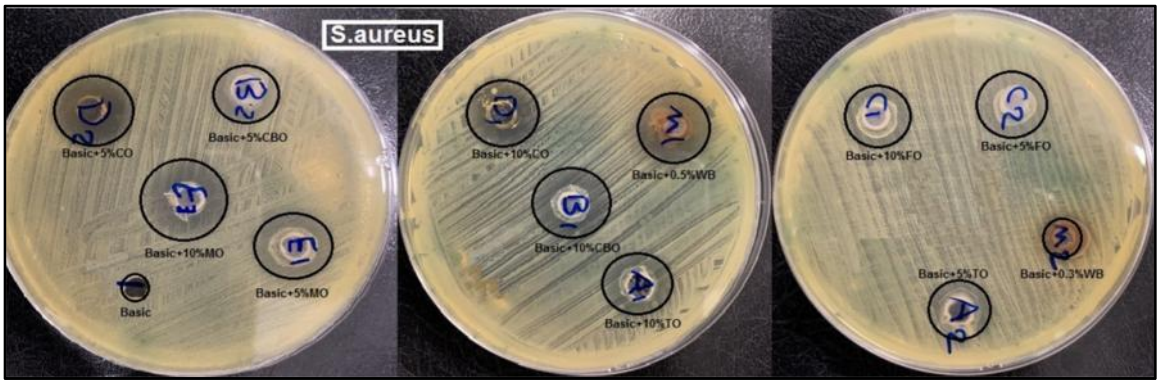

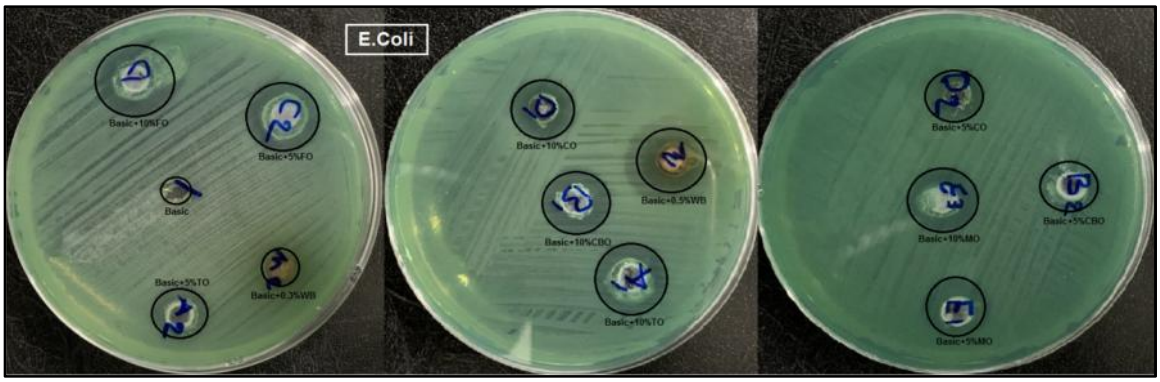

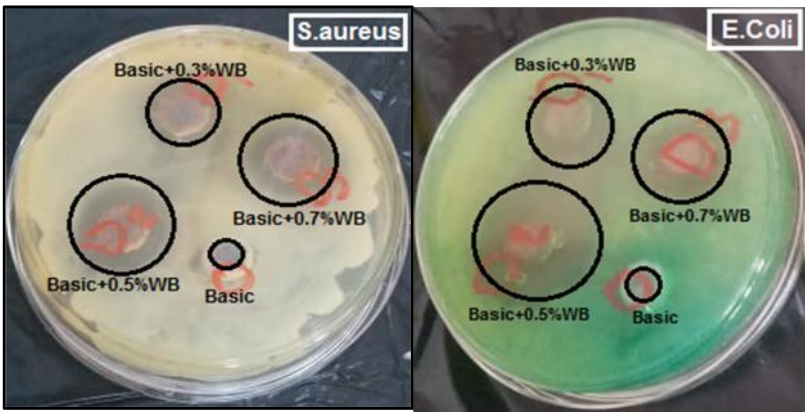

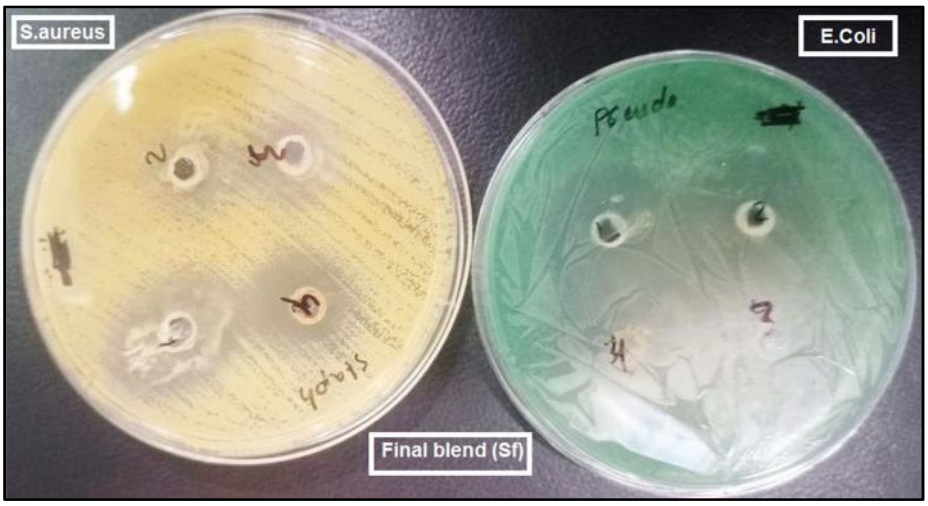

Figure (4.28): The inhibition area of basic, all additives, and final blend against E. coli and S. aureus.

Table (4.14): Inhibition zone diameter of all samples.

Sample No.	E. coli Inhibition Zone Diameter (mm)	S. aureus Inhibition Zone Diameter (mm)
S_8	0	0
S_8+MO_2	15	19
S_8+ MO_3	17	20
S_8+CO_2	11	19
S_8+ CO_3	17	20
S_8+CBO_2	12	16
S_8+ CBO_3	18	20
S_8+TO_2	14	15
S_8+ TO_3	19	18
S_8+FO_2	17	17
S_8+ FO_3	20	18
S_8+WB_1	17	13
S_8+WB_2	20	17
S_8+WB_3	15	16
S_f2	30	25
S_f3	34	10
S_f4	36	15
S_f5	37	20

4.5.2 Antioxidant Activity

The antioxidant activity was examined by using (2, 2-diphenyl-1-picrylhydrazyl) (DPPH) assay to statement the presence antioxidant compounds of all additives such as (MO, CO, CBO, TO, FO, and WB) in the nanofibers samples. Antioxidants delay the oxidation of fats, thereby extending the shelf-life of food products. DPPH used as the free radical is stabilized by accepting electrons from the additives which represent antioxidant or hydrogen radicals which then turn into a stable molecule.

The initial color of DPPH solution was purple and it will turn to mustard (near yellow) in the presence of antioxidant resulting in a reduction in absorbance value. Figure (4.29) and table (4.15) show the inhibition of DPPH activity at different concentration (40, 50, 60, 70, 80, and 90 µg/ml) increased with increment percentage of MO due to phenolic compounds existed in this oil that represent the most important antioxidant. This is similar to the results of [201, 203].

Polyphenols in WB which proven to exist by the FTIR spectrum analysis are famous for their antioxidant properties. Figure (4.30) and table (4.15) displays the antioxidant activity of nanofibers samples increased after adding WB in different percent WB_1, WB_2, and WB_3. These results assured that the WB was successfully inserted into the S_8 nanofibers and this consistent with the research of [204].

The inhibition of DPPH activity at different concentration (40, 50, 60, 70, 80, and 90 µg/ml) increase for additives (CO_3, CBO_3, TO_3, and FO_3) as illustrated in figure (4.31) and table (4.15). This is due to the phenolic and flavonoid compounds of these essential oils especially thymol and carvacrol are the most important antioxidant as mentioned in chapter two. These results are similar with the reported by [205-207].

Whereas the final blend (S_f) from figure (4.31) and table (4.15) showed higher inhibition of DPPH activity at different

concentration (40, 50, 60, 70, 80, and 90 µg/ml) which referred to incorporation all additives inside the basic in an excellent way.

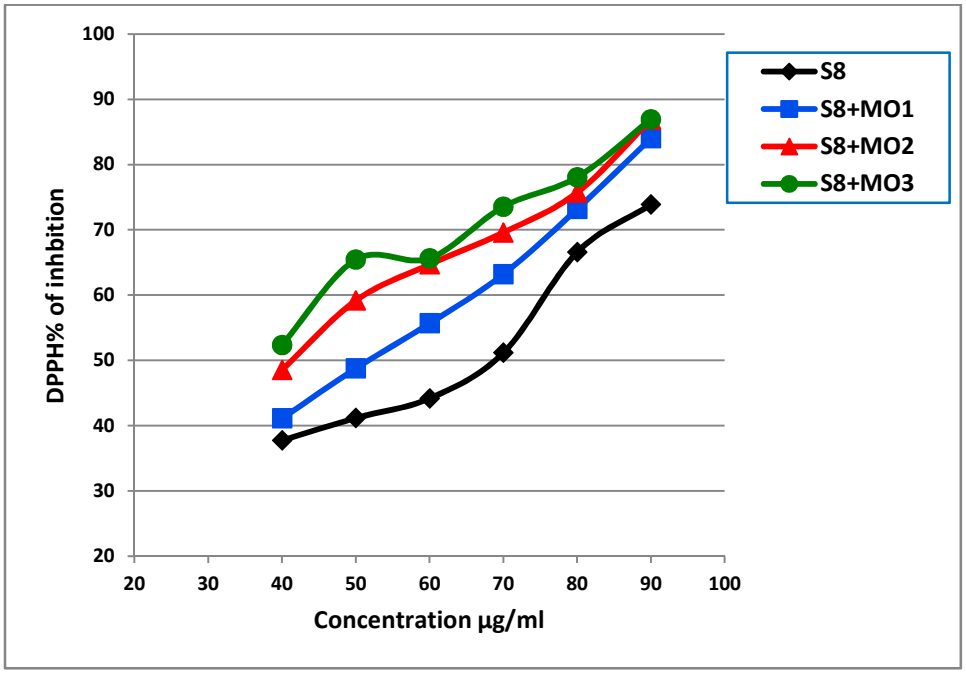

Figure (4.29): The effect of moringa oil in different concentration on DPPH radical scavenging activity.

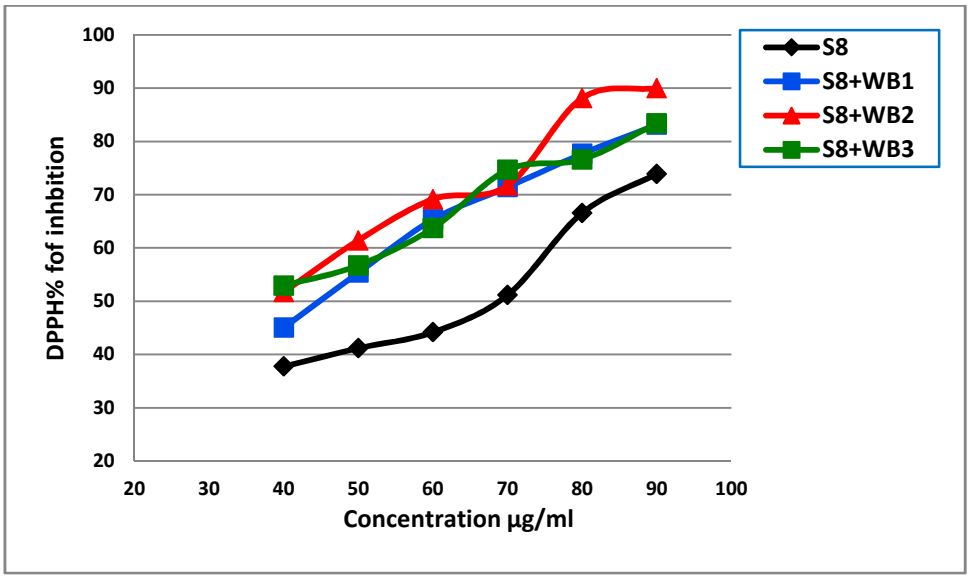

Figure (4.30): The effect of walnut bark powder in different concentration on DPPH radical scavenging activity.

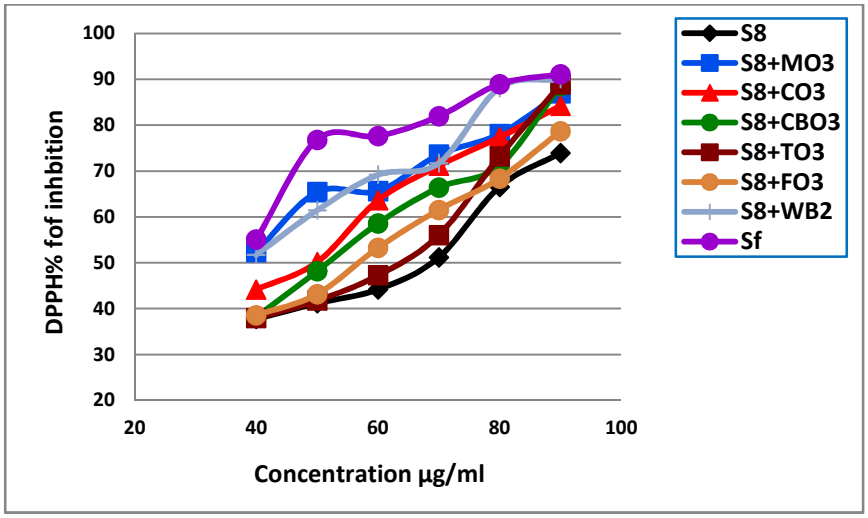

Figure (4.31): DPPH radical scavenging activity of all samples.

Table (4.15): DPPH radical scavenging activity of all samples.

Sample No.	Inhibition of DPPH activity % at different concentration (µg/ml) of samples					
	40	**50**	**60**	**70**	**80**	**90**
S_8	37.733	41.175	44.178	51.144	66.55	73.88
S_8+MO_1	41.11	48.775	55.655	63.188	73.17	84
S_8+MO_2	48.51	59.148	64.68	69.577	75.702	86.872
S_8+MO_3	52.361	65.425	65.622	73.544	78.063	86.934
S_8+CO_3	44.14	50.127	63.577	71.1344	77.333	84.2
S_8+CBO_3	38.177	48.145	58.555	66.368	71.175	88.522
S_8+TO_3	37.922	41.723	47.226	55.98	73.17	88.82
S_8+FO_3	38.544	43.156	53.271	61.52	68.355	78.66
S_8+WB_1	45.025	55.341	65.319	71.419	77.659	83.125
S_8+WB_2	51.702	61.402	69.148	71.688	88.106	90
S_8+WB_3	52.928	56.702	63.725	74.643	76.595	83.389
S_f	55.042	76.8085	77.617	81.9149	88.9362	91.102

4.5.3 Antifungal Activity

The antifungal effects of electrospun mats were determined by using disc diffusion method against candida bacteria. Figure (4.32) and table (4.16) show the basic blend (S_8) does not exhibit any antifungal properties but inhibition zone diameter against candida for (S_8+TO_3) at

different percentages (12.5, 25, 50, and 100 %) was (8, 9,10, and 15 mm) respectively.

This antifungal activity in this sample comeback to essential oils that has phenolic compounds such as thymol and carvacrol proved to have the best antifungal effect. These results agreement with [102, 208].

While figure (4.33) and table (4.16) displayed the inhibition zone diameter against candida for (S_8+WB_2) at different percentages (12.5, 25, 50, and 100 %) was (8, 10, 12, and 16 mm) respectively. This is due to polyphenol in WB has antifungal properties which is similar with the results of [209, 210].

Lastly, the inhibition zone diameter against candida of final blend (S_f) at different percentages (62.5, 125, 250, and 500%) was (10, 11, 13, and 18 mm) respectively as shown in figure (4.34) and table (4.16) .

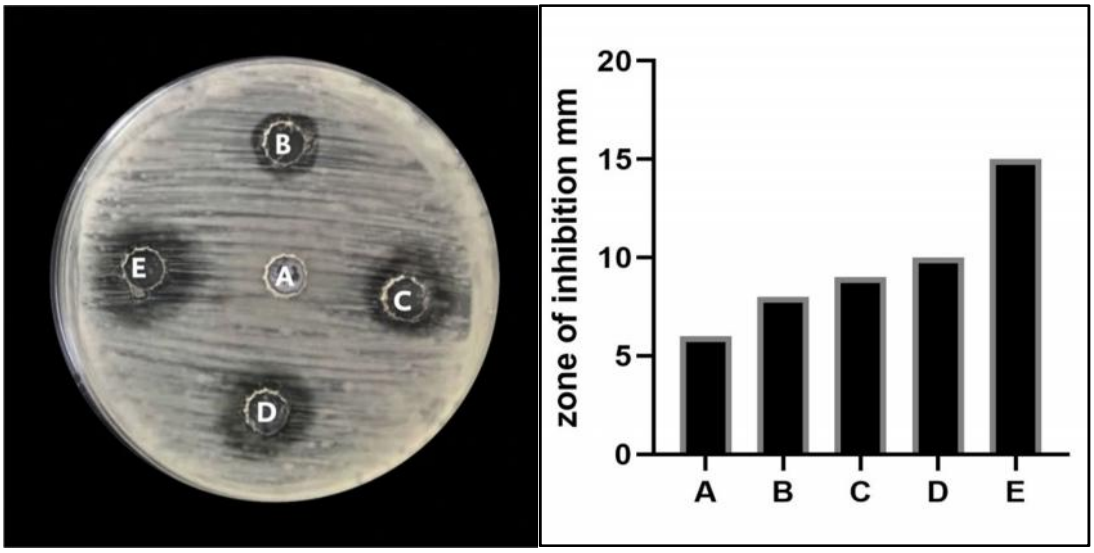

Figure (4.32): Antifungal activity of (S_8+TO_3) against Candida. A,(S_8). B, 12.5 %. C, 25 %. D, 50 %. E, 100 %

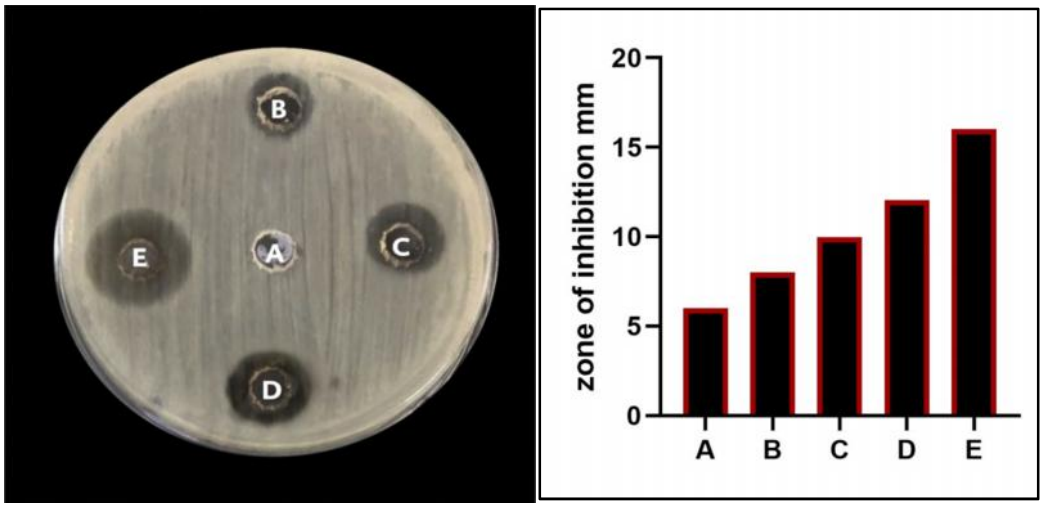

Figure (4.33): Antifungal activity of (S_8+WB_2) against Candida. A, (S_8) B, 12.5 % C, 25 % D, 50 % E, 100 %.

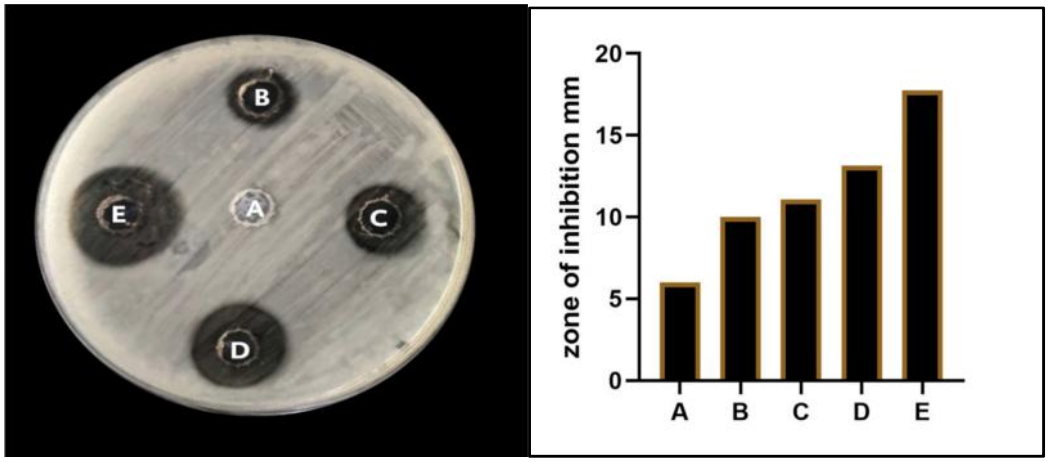

Figure (4.34): Antifungal activity of (S_f) against Candida. A, (S_8) B, 62.5% C, , 125% D, , 250% E, 500 %.

Table (4.16): Inhibition Zone Diameter of (S_8), (S_8+TO_3), (S_8+WB_2), and (S_f).

Sample No.	**Antifungal Activity Inhibition Zone Diameter (mm) at Different Concentration**			
	12.5%	**25%**	**50%**	**100%**
S_8	6			
S_8+TO_3	8	9	10	15
S_8+WB_2	8	10	12	16
S_f	**62.5%**	**125%**	**250%**	**500%**
	10	11	13	18

4.5.4 MTT Assay

The absence of cytotoxicity is an essential requirement of food packaging. To evaluate the cytotoxicity of samples nanofibers, MTT assay was applied. The viability and growth of human gastric fibroblast cells are presented by the absorbance value of samples nanofibers after 7 days incubation, as shown in figure (4.35). It was observed that all additives and final sample exhibited high cell viability by increasing in absorbance value. Thus results indicate no cytotoxic secretion for all samples which is eligible for food packaging applications.

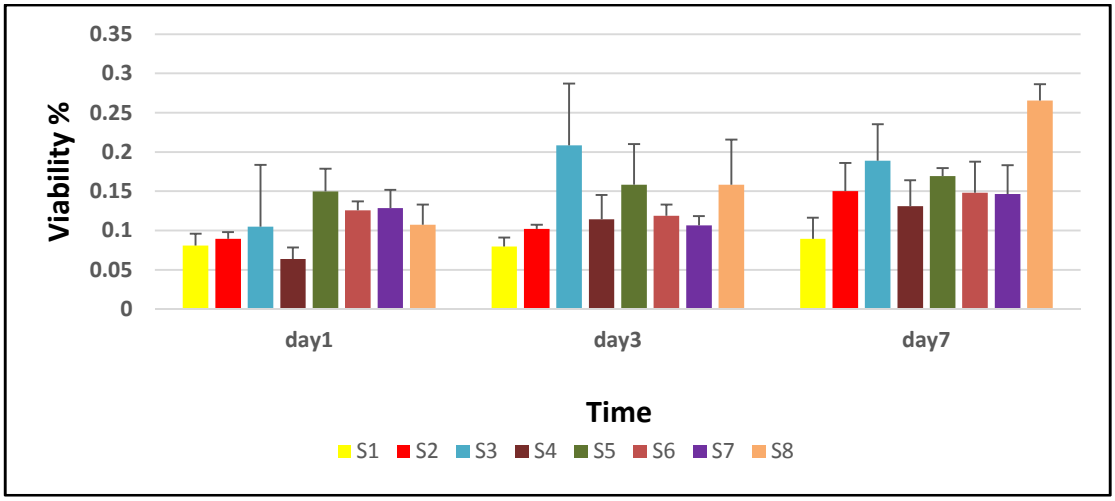

Figure (4.35): The viability of human gastric fibroblast cell seeded on samples nanofibers (S1:basic (S_8), S2: (S_8+MO), S3: (S_8+CO), S4: (S_8+CBO), S5: (S_8+TO), S6: (S_8+FO), S7: (S_8+WB) and S8: final sample (S_f)) After 7 Days.

4.6 Nano-Indentation Results

The nanoindentation method is a novel approach carried out to understand the mechanical properties of nanofibers. Figure (4.36) shows Load–displacement curves of nanofiber samples. Figure (4.37) demonstrate schematic of a section through an indentation using a conical indenter. In addition, notice the young modulus, hardness, and stiffness from table (4.17) increased from ((0.46-1.36 GPa), (0.012-0.048 GPa),

and (0.8-1.26 µN/nm)) for S_8 and S_f respectively. These results are agreement with the previous studies by [211].

The moderate mechanical properties of NFs are an important factor for food packaging application. The effective packaging should retain its shape under food loading and during their storage. It was also concluded that these nanofiber mats have enough mechanical strength to be used for food packaging applications.

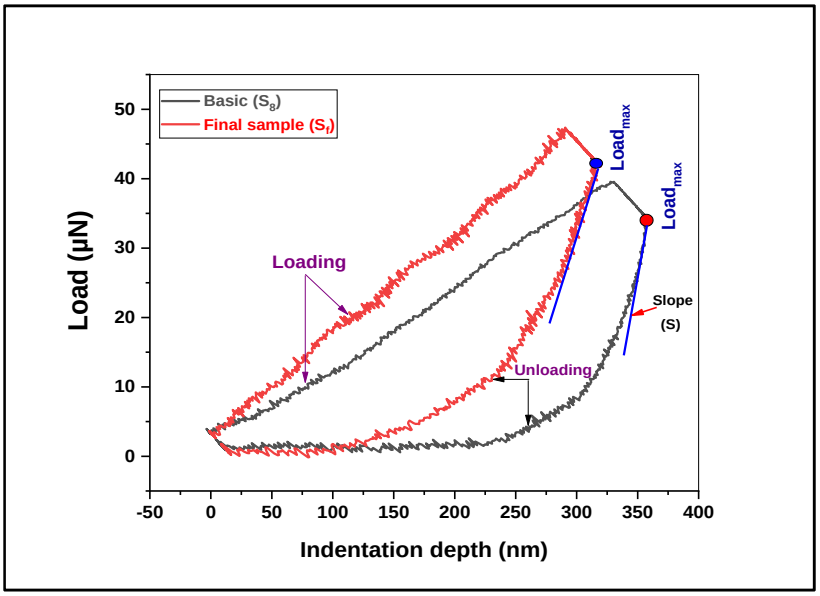

Figure (4.36): Load–indentation depth curves of basic (S_8) and final sample (S_f).

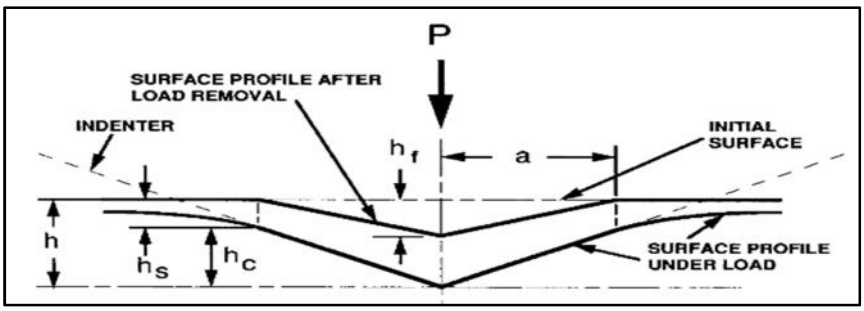

Figure (4.37): Schematic representation of a section through an indentation using a conical indenter [212].

Table (4.17): The parameters which measured from this test of S_8 and S_f.

Parameters	Basic Blend (S_8)	Final Blend (S_f)
Er(GPa)	0.46	1.36
Hardness(GPa)	0.012	0.048
Contact Depth (h_c) (nm)	323.6	251.46
Contact Stiffness (S) (µN/nm)	0.8	1.26
Max Force (µN)	34.26	36.3
Depth Max (nm)	359.04	321.1
h.f	210.378	103.946

4.7 Efficiency Study (Food Packaging)

An experimental study was carried out to investigate suitability potential of nanofibers based food packaging by comparing with plastic based packaging. Fruits and vegetables and freshness were taken and packed in containers. One container without nanofiber and the other was packed by nanofiber mat (S_f) sample were used in this experiment. All samples were placed in room temperature. After that vegetables were examined after 10 days.

Figure (4.38) shows the results obtained by the experiment. It can be observed that fruits and vegetables packed in nanofiber based packaging were having better freshness than that packed by the plastic one. There may be several reasons behind these results related to properties which possess it these nanofiber sample as compared to plastic container. In addition, it can significantly enhance shelf life of fruits and vegetables.

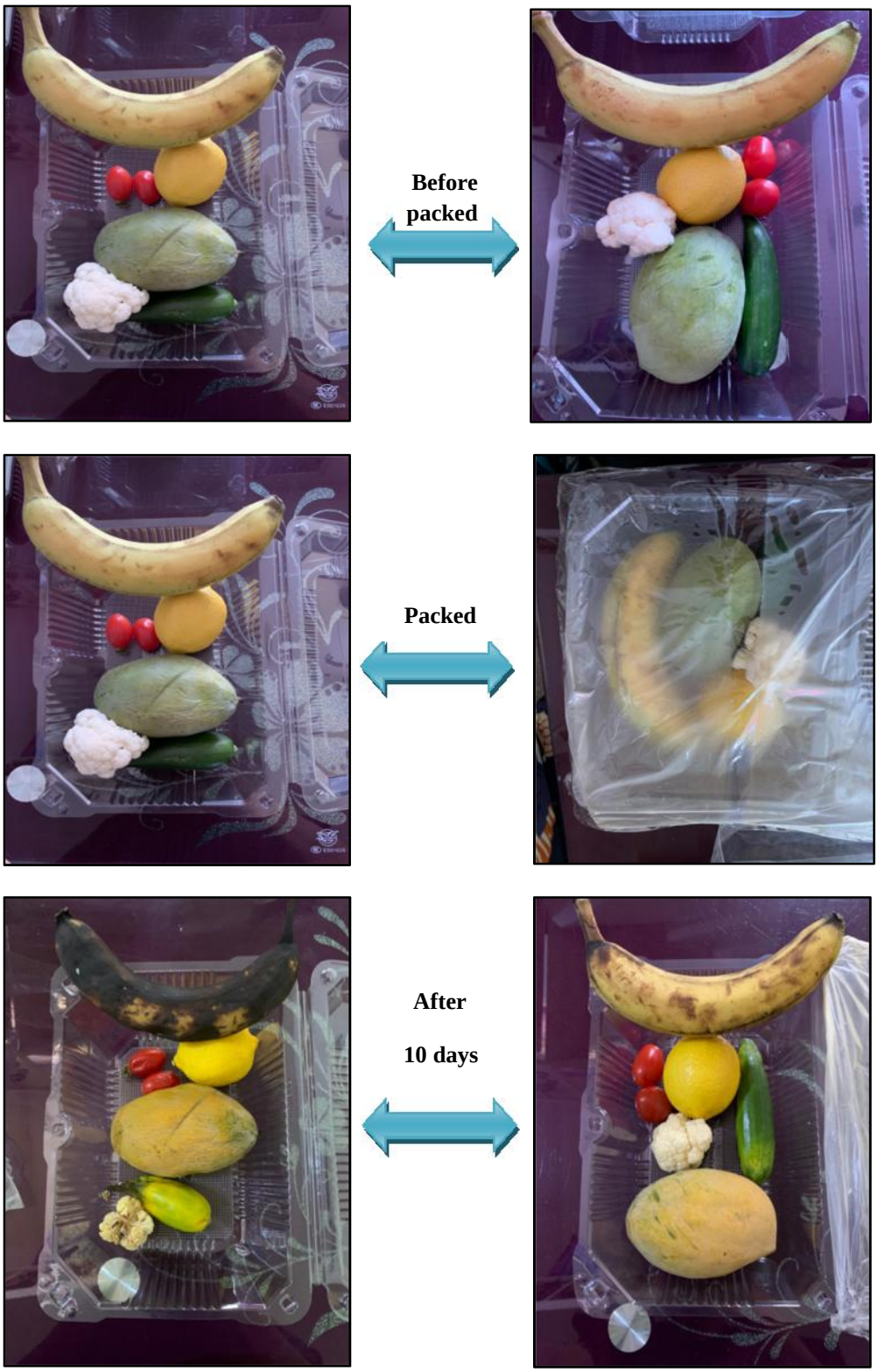

Figure (4.38): Observatory experiments for suitability of nanofibers based food packaging for fruits vegetables up to 10 days at 25 ºC temperature.

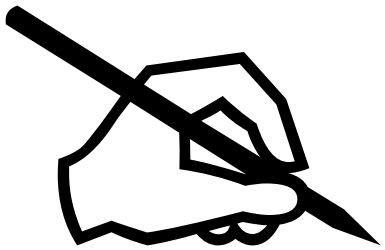

CHAPTER FIVE

CONCLUSIONS AND RECOMENDATIONS

5.1 Conclusions

From this study results that are mentioned in previous chapters which interested for used natural and biomaterials in food packaging applications to study the effect different additives from essential oils and walnut tree bark powder on morphological, structure, biological and physical properties of basic sample nanofiber which can be used in food packaging. It concluded the following:

1. The results of the polymeric solution tests indicate that viscosity, surface tension, and electrical conductivity all have a direct effect on how electrospun fibers behave. When essential oils add to basic sample (S_8) increased viscosity while reducing surface tension and electrical conductivity. The addition of walnut tree bark powder has a lower viscosity and higher electrical conductivity with surface tension. Additionally, the viscosity of final sample (S_f) increase and moderate value for electrical conductivity and surface tension.
2. The select best volume ratio of (PVA-STA-CSM) was (40:30:30) according to the highest contact angle.
3. The water contact angle was also measured to confirm the stability of nanofibrous mats in outdoor use. It was concluded that final sample nanofiber were found to be hydrophobic and increment after crosslinking by UV radiation for 24 hr. from (105.358º to 112.546º). An increase in the contact angle may be because of interchain and intrachain bonding for (S_8) and additives in the result of crosslinking.
4. From morphological results for nanofiber noticed increment the average nanofibers diameter of the final sample (S_f). Thus, lead to

increase the surface roughness and surface bearing index for this sample. These properties suitable in food packaging application.

5. Observed the pore size which analyzed by ANOVA software of final sample (S_f) decreased. Thus, affect on the porosity and air permeability for the nanofiber web which can be considered as feasible for food packaging applications.
6. From the results of FTIR, there are not created chemical bond but only the main bands of final sample (S_f) were shifted which indicated a good incorporation between basic sample (S_8) and all additives.
7. From DSC results, the melting temperature increased from (227.62 to 233.00 ºC) and the enthalpy of fusion increased from (18.62 to 23.22 J/g) for basic and final sample respectively which enhance the mechanical properties of final nanofibers.
8. From TGA results, the thermal stability of final sample improves from (77 % to 98.59%).
9. The UV-Vis spectra results of final sample show absorbance spectra within the ultra violet (UV), visible (Vis), and infrared (IR) spectrum that lead to protect food against the effects of light, especially UV radiation and IR radiation.
10. From biological test results, the antibacterial inhibition increased for final sample (S_f) as a result of incorporation all additives in basic sample (S_8).
11. The antioxidant activity results, noticed the inhibition of DPPH activity increased for final sample which was proven in FTIR curve. In addition the antifungal properties increment by increase the inhibition zone diameter against candida.

12. The modulus of elasticity, hardness, and stiffness of final sample nanofibers improved which is considered necessary for food packaging applications.
13. Considering all results and from compatibility study test it is suggested that final sample nanofibers can be used for food packaging.

5.2 Recommendations

1- The creation of nano-fibrous tissues utilized in package displays using various bio-polymers, such as polyethylene glycol and polyacryl amide, as a biodegradable material.

2- Using additional natural oils to enhance viscosity, such as turmeric and sunflower oils.

3- Altering the pumping settings to achieve the optimal morphology of the resultant fibers, such as altering the solution concentrations, the target being employed, or the needle diameter.

References

[1] X. Niu, Y. Liu, Y. Song, J. Han, and H. Pan, “Rosin modified cellulose nanofiber as a reinforcing and co-antimicrobial agents in polylactic acid /chitosan composite film for food packaging,” *Carbohydr. Polym.*, vol. 183, pp. 102–109, 2018, doi: 10.1016/j.carbpol.11.079.

[2] A. Bahrami, R. Delshadi, E. Assadpour, S. M. Jafari, and L. Williams, “Antimicrobial-loaded nanocarriers for food packaging applications,” *Adv. Colloid Interface Sci.*, vol. 278, p. 102140, 2020, doi: 10.1016/j.cis.2020.102140.

[3] M. Noruzi, “Electrospun nanofibres in agriculture and the food industry: a review,” *J. Sci. Food Agric.*, vol. 96, no. 14, pp. 4663–4678, 2016, doi: 10.1002/jsfa.7737.

[4] V. Siracusa, P. Rocculi, S. Romani, and M. D. Rosa, “Biodegradable polymers for food packaging: a review,” *Trends Food Sci. Technol.*, vol. 19, no. 12, pp. 634–643, 2008, doi: 10.1016/j.tifs.2008.07.003.

[5] R. M. S. Cruz, “Food Packaging; Innovations and Shelf-Life; Edition 1”, 2017.

[6] K. J. Figueroa-Lopez, J. L. Castro-Mayorga, M. M. Andrade-Mahecha, L. Cabedo, and J. M. Lagaron, “Antibacterial and barrier properties of gelatin coated by electrospun polycaprolactone ultrathin fibers containing black pepper oleoresin of interest in active food biopackaging applications,” *Nanomaterials*, vol. 8, no. 4, 2018, doi: 10.3390/nano8040199.

[7] S. C. Shit and P. M. Shah, “Edible Polymers: Challenges and Opportunities,” *J. Polym.*, vol. 2014, pp. 1–13, 2014, doi: 10.1155/2014/427259.

[8] T. Senthil Muthu Kumar, K. Senthil Kumar, N. Rajini, S.

Siengchin, N. Ayrilmis, and A. Varada Rajulu, “A comprehensive review of electrospun nanofibers: Food and packaging perspective,” *Compos. Part B Eng.*, vol. 175, p. 107074, 2019, doi: 10.1016/j.compositesb. 107074.

[9] R. Pérez-Masiá, J. M. Lagaron, and A. López-Rubio, “Development and Optimization of Novel Encapsulation Structures of Interest in Functional Foods Through Electrospraying,” *Food Bioprocess Technol.*, vol. 7, no. 11, pp. 3236–3245, 2014, doi: 10.1007/s11947-014-1304-z.

[10] P. Wen, M. H. Zong, R. J. Linhardt, K. Feng, and H. Wu, “Electrospinning: A novel nano-encapsulation approach for bioactive compounds,” *Trends Food Sci. Technol.*, vol. 70, no. October, pp. 56–68, 2017, doi: 10.1016/j.tifs.2017.10.009.

[11] L. J. Bastarrachea, D. E. Wong, M. J. Roman, Z. Lin, and J. M. Goddard, “Active packaging coatings,” *Coatings*, vol. 5, no. 4, pp. 771–791, 2015, doi: 10.3390/coatings5040771.

[12] L. Zhao, G. Duan, G. Zhang, H. Yang, S. Jiang, and S. He, “Electrospun functional materials toward food packaging applications: A review,” *Nanomaterials*, vol. 10, no. 1, 2020, doi: 10.3390/nano10010150.

[13] M. Sahoo, S. Vishwakarma, C. Panigrahi, and J. Kumar, “Nanotechnology: Current applications and future scope in food,” *Food Front.*, vol. 2, no. 1, pp. 3–22, 2021, doi: 10.1002/fft2.58.

[14] Z. H. Mohammad, F. Ahmad, S. A. Ibrahim, and S. Zaidi, “Application of nanotechnology in different aspects of the food industry,” *Discov. Food*, vol. 2, no. 1, 2022, doi: 10.1007/s44187-022-00013-9.

[15] A. M. Grumezescu and A. M. Holban, “Preface for Volume 12: Impact of Nanoscience in the Food Industry,” *Impact Nanosci.*

Food Ind., vol. 12, pp. xxi–xxiii, 2018, doi: 10.1016/B978-0-12-811441-4.00023-6.

[16] A. Ashfaq, N. Khursheed, S. Fatima, Z. Anjum, and K. Younis, "Application of nanotechnology in food packaging: Pros and Cons," *J. Agric. Food Res.*, vol. 7, no. September 2021, doi: 10.1016/j.jafr.100270.

[17] J. Anu Bhushani and C. Anandharamakrishnan, "Electrospinning and electrospraying techniques: Potential food based applications," *Trends Food Sci. Technol.*, vol. 38, no. 1, pp. 21–33, 2014, doi: 10.1016/j.tifs.2014.03.004.

[18] H. Rodríguez-Tobías, G. Morales, and D. Grande, "Electrospinning and Electrospraying Techniques for Designing Antimicrobial Polymeric Biocomposite Mats," *Nanofiber Res. - Reach. New Height.*, 2016, doi: 10.5772/63470.

[19] I. Alghoraibi and S. Alomari, *Different Methods for Nanofiber Design and Fabrication*. 2018. doi: 10.1007/978-3-319-42789-8_11-2.

[20] W.-J. Li, R. M. Shanti, and R. S. Tuan, *Electrospinning Technology for Nanofibrous Scaffolds in Tissue Engineering*, vol. 9. 2007. doi: 10.1002/9783527610419.ntls0097.

[21] J. B. Moreira, M. G. de Morais, E. G. de Morais, B. da S. Vaz, and J. A. V. Costa, *Electrospun Polymeric Nanofibers in Food Packaging*. Elsevier Inc., 2018. doi: 10.1016/B978-0-12-811441-4.00014-5.

[22] A. R. Unnithan, R. S. Arathyram, and C. S. Kim, *Electrospinning of Polymers for Tissue Engineering*. Elsevier Inc., 2015. doi: 10.1016/B978-0-323-32889-0.00003-0.

[23] A. Barhoum, K. Pal, H. Rahier, H. Uludag, I. S. Kim, and M. Bechelany, "Nanofibers as new-generation materials: From

spinning and nano-spinning fabrication techniques to emerging applications," *Appl. Mater. Today*, vol. 17, pp. 1–35, 2019, doi: 10.1016/j.apmt. 06.015.

[24] H. S. SalehHudin, E. N. Mohamad, W. N. L. Mahadi, and A. Muhammad Afifi, "Multiple-jet electrospinning methods for nanofiber processing: A review," *Mater. Manuf. Process.*, vol. 33, no. 5, pp. 479–498, 2018, doi: 10.1080/10426914. 1388523.

[25] Y. Z. Long, X. Yan, X. X. Wang, J. Zhang, and M. Yu, *Electrospinning*. Elsevier Inc., 2018. doi: 10.1016/B978-0-323-51270-1.00002-9.

[26] C. Wang, "Fabrication of electrospun polymer nanofibers with diverse morphologies," *Molecules*, vol. 24, no. 5, 2019, doi: 10.3390/molecules24050834.

[27] E. Aslan, H. Almeida, S. Al-Deyab, M. El-Newehy, H. Bartolo, and P. J. Bártolo, *The Electrospinning Process*. 2021. doi: 10.1007/978-3-030-35880-8_7.

[28] N. Z. A. Al-Hazeem, "Nanofibers and Electrospinning Method," *Nov. Nanomater. - Synth. Appl.*, 2018, doi: 10.5772/intechopen.72060.

[29] K. Nasouri, A. Haji, A. M. Shoushtari, and A. Kaflou, "A Novel Study of Electrospun Nanofibers Morphology as a Function of Polymer Solution Properties," *Proc. Int. Conf. Nanomater. Appl. Prop.*, vol. 2, no. 3, pp. 3–04, 2013.

[30] P. Ghatmale, P. Garg, S. Kadam, S. Chavan, R. Scholar, and B. Vidyapeeth, "Review: Electro Spinning Technique and Factors Affecting Electro Spun Nano Fibers and Some Applications," *IJSRD-International J. Sci. Res. Dev.*, vol. 4, no. 04, pp. 2321–0613, 2016, [Online]. Available: www.ijsrd.com

[31] R. S. Bhattarai, R. D. Bachu, S. H. S. Boddu, and S. Bhaduri,

"Biomedical applications of electrospun nanofibers: Drug and nanoparticle delivery," *Pharmaceutics*, vol. 11, no. 1, 2019, doi: 10.3390/pharmaceutics11010005.

[32] A. Haider, S. Haider, and I. K. Kang, "A comprehensive review summarizing the effect of electrospinning parameters and potential applications of nanofibers in biomedical and biotechnology," *Arab. J. Chem.*, vol. 11, no. 8, pp. 1165–1188, 2018, doi: 10.1016/j.arabjc. 11.015.

[33] N. Amariei, L. R. Manea, A. P. Bertea, A. Bertea, and A. Popa, "The Influence of Polymer Solution on the Properties of Electrospun 3D Nanostructures," *IOP Conf. Ser. Mater. Sci. Eng.*, vol. 209, no. 1, 2017, doi: 10.1088/1757-899X/209/1/012092.

[34] N. E. Zander, "Hierarchically structured electrospun fibers," *Polymers (Basel).*, vol. 5, no. 1, pp. 19–44, 2013, doi: 10.3390/polym5010019.

[35] N. Okutan, P. Terzi, and F. Altay, "Affecting parameters on electrospinning process and characterization of electrospun gelatin nanofibers," *Food Hydrocoll.*, vol. 39, pp. 19–26, 2014, doi: 10.1016/j.foodhyd. 12.022.

[36] Z. Li and C. Wang, "Effects of Working Parameters on Electrospinning," *SpringerBriefs Mater.*, pp. 15–28, 2013, doi: 10.1007/978-3-642-36427-3_2.

[37] M. Aman Mohammadi, S. M. Hosseini, and M. Yousefi, "Application of electrospinning technique in development of intelligent food packaging: A short review of recent trends," *Food Sci. Nutr.*, vol. 8, no. 9, pp. 4656–4665, 2020, doi: 10.1002/fsn3.1781.

[38] A. Y. Mohammad Anwarul Azim, "Effect of Electrospinning Parameters on Fiber Morphology of Tissue Engineering Scaffolds:

A Review," *J. Fash. Technol. Text. Eng.*, vol. 02, no. 03, 2014, doi: 10.4172/2329-9568.1000114.

[39] Y. Sun, S. Cheng, W. Lu, Y. Wang, P. Zhang, and Q. Yao, "Electrospun fibers and their application in drug controlled release, biological dressings, tissue repair, and enzyme immobilization," *RSC Adv.*, vol. 9, no. 44, pp. 25712–25729, 2019, doi: 10.1039/c9ra05012d.

[40] Y. P. Singh, S. Dasgupta, S. Nayar, and R. Bhaskar, "Optimization of electrospinning process & parameters for producing defect-free chitosan/polyethylene oxide nanofibers for bone tissue engineering," *J. Biomater. Sci. Polym. Ed.*, vol. 31, no. 6, pp. 781–803, 2020, doi: 10.1080/09205063.2020.1718824.

[41] B. Robb and B. Lennox, "The electrospinning process, conditions and control," *Electrospinning Tissue Regen.*, pp. 51–66, 2011, doi: 10.1533/9780857092915.1.51.

[42] A. Garkal, D. Kulkarni, S. Musale, T. Mehta, and P. Giram, "Electrospinning nanofiber technology: A multifaceted paradigm in biomedical applications," *New J. Chem.*, vol. 45, no. 46, pp. 21508–21533, 2021, doi: 10.1039/d1nj04159b.

[43] D. Rodoplu and M. Mutlu, "Effects of electrospinning setup and process parameters on nanofiber morphology intended for the modification of quartz crystal microbalance surfaces," *J. Eng. Fiber. Fabr.*, vol. 7, no. 2, pp. 118–123, 2012, doi: 10.1177/155892501200700217.

[44] G. F. El Fawal, "Polymer Nanofibers Electrospinning: A review," *Egypt. J. Chem.*, vol. 63, no. 4, pp. 1279–1303, 2020, doi: 10.21608/ejchem. 14837.1898.

[45] Y. Wang, H. Xu, M. Wu, and D. Yu, "ES Food and Agroforestry Nanofibers-Based Food Packaging," pp. 1–24, 2022.

[46] J. M. Cornejo Bravo, L. J. Villarreal Gómez, and A. Serrano Medina, “Electrospinning for Drug Delivery Systems: Drug Incorporation Techniques,” *Electrospinning - Mater. Tech. Biomed. Appl.*, no. December, 2016, doi: 10.5772/65939.

[47] M. Buzgo, A. Mickova, M. Rampichova, and M. Doupnik, “Blend electrospinning, coaxial electrospinning, and emulsion electrospinning techniques,” *Core-Shell Nanostructures Drug Deliv. Theranostics Challenges, Strateg. Prospect. Nov. Carr. Syst.*, pp. 325–347, 2018, doi: 10.1016/C2016-0-03458-7.

[48] J. Avossa, G. Herwig, C. Toncelli, F. Itel, and R. M. Rossi, “Electrospinning based on benign solvents: current definitions, implications and strategies,” *Green Chem.*, vol. 24, no. 6, pp. 2347–2375, 2022, doi: 10.1039/d1gc04252a.

[49] P. Rathore and J. D. Schiffman, “Beyond the Single-Nozzle: Coaxial Electrospinning Enables Innovative Nanofiber Chemistries, Geometries, and Applications,” *ACS Appl. Mater. Interfaces*, vol. 13, no. 1, pp. 48–66, 2021, doi: 10.1021/acsami.0c17706.

[50] J. Xue, T. Wu, Y. Dai, Y. Xia, U. States, and U. States, “Electrospinning and Electrospun Nanofibers: Methods, Materials, and Applications,” vol. 119, no. 8, pp. 5298–5415, 2019, doi: 10.1021/acs.chemrev.8b00593.Electrospinning.

[51] X. Liu, H. Xu, M. Zhang, and D. G. Yu, “Electrospun medicated nanofibers for wound healing: Review,” *Membranes (Basel).*, vol. 11, no. 10, 2021, doi: 10.3390/membranes11100770.

[52] T. C. Yadav, “Electrospinning: An Efficient Biopolymer-Based Micro- And Nanofibers Fabrication Technique,” *ACS Symp. Ser.*, vol. 1329, no. January 2020, pp. 209–241, 2019, doi: 10.1021/bk-2019-1329.

[53] M. Dai, “Functionalized Electrospun Nanofibers for Food Science

Applications," no. May 2014, p. 123, 2016, [Online]. Available: http://scholarworks.umass.edu/dissertations_2%0Ahttp://scholarworks.umass.edu/dissertations_2/714

[54] M. Teng, J. Qiao, F. Li, and P. K. Bera, "Electrospun mesoporous carbon nanofibers produced from phenolic resin and their use in the adsorption of large dye molecules," *Carbon N. Y.*, vol. 50, no. 8, pp. 2877–2886, 2012, doi: 10.1016/j.carbon. 02.056.

[55] L. Natarajan, "Studies on electrospun poly (lactic acid) fibers and low density poly (ethylene) / thermoplastic starch blends as food packaging materials. Doctoral thesis, Nanyang Technological University, Singapore.," 2018.

[56] R. Chawla, S. Sivakumar, and H. Kaur, "Antimicrobial edible films in food packaging: Current scenario and recent nanotechnological advancements- a review," *Carbohydr. Polym. Technol. Appl.*, vol. 2, no. December 2020, p. 100024, 2021, doi: 10.1016/j.carpta. 100024.

[57] M. Makaremi, "Safely dissolvable and healable active packaging films based on alginate and pectin," *Polymers (Basel).*, vol. 11, no. 10, pp. 1–18, 2019, doi: 10.3390/polym11101594.

[58] N. Clark, R. Trimingham, and G. T. Wilson, "Incorporating consumer insights into the UK food packaging supply chain in the transition to a circular economy," *Sustain.*, vol. 12, no. 15, 2020, doi: 10.3390/su12156106.

[59] L. F. Zemljič, O. Plohl, A. Vesel, T. Luxbacher, and S. Potrč, "Physicochemical characterization of packaging foils coated by chitosan and polyphenols colloidal formulations," *Int. J. Mol. Sci.*, vol. 21, no. 2, 2020, doi: 10.3390/ijms21020495.

[60] S. Mangaraj, A. Yadav, L. M. Bal, S. K. Dash, and N. K. Mahanti, "Application of Biodegradable Polymers in Food Packaging

Industry: A Comprehensive Review," *J. Packag. Technol. Res.*, vol. 3, no. 1, pp. 77–96, 2019, doi: 10.1007/s41783-018-0049-y.

[61] C. Maes, S. Bouquillon, and M. L. Fauconnier, "Encapsulation of essential oils for the development of biosourced pesticides with controlled release: A review," *Molecules*, vol. 24, no. 14, pp. 1–15, 2019, doi: 10.3390/molecules24142539.

[62] E. Mele, "Electrospinning of Essential Oils: Review," *Polymers (Basel).*, vol. 12,908, pp. 1–16, 2020, [Online]. Available: www.mdpi.com/journal/polymers

[63] S. Ataei, P. Azari, A. Hassan, B. Pingguan-Murphy, R. Yahya, and F. Muhamad, "Essential Oils-Loaded Electrospun Biopolymers: A Future Perspective for Active Food Packaging," *Adv. Polym. Technol.*, vol. 2020, pp. 1–21, 2020, doi: 10.1155/2020/9040535.

[64] A. H. Rather, T. U. Wani, R. S. Khan, B. Pant, M. Park, and F. A. Sheikh, "Prospects of polymeric nanofibers loaded with essential oils for biomedical and food- packaging applications," *Int. J. Mol. Sci.*, vol. 22, no. 8, 2021, doi: 10.3390/ijms22084017.

[65] P. Wen, D. H. Zhu, H. Wu, M. H. Zong, Y. R. Jing, and S. Y. Han, "Encapsulation of cinnamon essential oil in electrospun nanofibrous film for active food packaging," *Food Control*, vol. 59, pp. 366–376, 2016, doi: 10.1016/j.foodcont.2015.06.005.

[66] J. Y. Lee, "Fabrication of antibacterial nanofibrous membrane infused with essential oil extracted from tea tree for packaging applications," *Polymers (Basel).*, vol. 12, no. 1, 2020, doi: 10.3390/polym12010125.

[67] M. M. Tosif, "A comprehensive review on plant-derived mucilage: Characterization, functional properties, applications, and its utilization for nanocarrier fabrication," *Polymers (Basel).*, vol. 13, no. 7, 2021, doi: 10.3390/polym13071066.

[68] R. Kamel, S. M. Afifi, I. A. A. Kassem, N. A. Elkasabgy, and M. A. Farag, “Arabinoxylan and rhamnogalacturonan mucilage: Outgoing and potential trends of pharmaceutical, environmental, and medicinal merits,” *Int. J. Biol. Macromol.*, vol. 165, pp. 2550–2564, 2020, doi: 10.1016/j.ijbiomac.2020.10.175.

[69] I. F. Olawuyi, S. R. Kim, and W. Y. Lee, “Application of plant mucilage polysaccharides and their techno-functional properties’ modification for fresh produce preservation,” *Carbohydr. Polym.*, vol. 272, no. June, p. 118371, 2021, doi: 10.1016/j.carbpol. 118371.

[70] E. Alpizar-Reyes, H. Carrillo-Navas, R. Gallardo-Rivera, V. Varela-Guerrero, J. Alvarez-Ramirez, and C. Pérez-Alonso, “Functional properties and physicochemical characteristics of tamarind (Tamarindus indica L.) seed mucilage powder as a novel hydrocolloid,” *J. Food Eng.*, vol. 209, pp. 68–75, 2017, doi: 10.1016/j.jfoodeng. 04.021.

[71] S. Beikzadeh, A. Khezerlou, S. M. Jafari, Z. Pilevar, and A. M. Mortazavian, “Seed mucilages as the functional ingredients for biodegradable films and edible coatings in the food industry,” *Adv. Colloid Interface Sci.*, vol. 280, p. 102164, 2020, doi: 10.1016/j.cis. 102164.

[72] N. P. Young, “Thermodynamics and Phase Behavior of Miscible Polymer Blends in the Presence of Supercritical Carbon Dioxide,” *J. Chem. Inf. Model.*, vol. 53, no. 9, pp. 1689–1699, 2018.

[73] J. Parameswaranpillai, S. Thomas, and Y. Grohens, “Polymer Blends: State of the Art, New Challenges, and Opportunities,” *Charact. Polym. Blends Miscibility, Morphol. Interfaces*, vol. 9783527331, pp. 1–6, 2015, doi: 10.1002/9783527645602.ch01.

[74] F. Sabzi and A. Boushehri, “Compatibility of polymer blends. I. Copolymers with organic solvents,” *J. Appl. Polym. Sci.*, vol. 101,

no. 1, pp. 492–498, 2006, doi: 10.1002/app.23092.

[75] H. Dai, J. Wang, and N. Liu, “Preparation and properties of poly(vinyl alcohol) films using carbohydrates as plasticizers,” *J. Vinyl Addit. Technol.*, vol. 25, pp. E181–E187, 2019, doi: 10.1002/vnl.21679.

[76] Adriana Yazik and N. A. Tukiran, “Characterization of Polyvinyl Alcohol (PVA) as Antimicrobial Biocomposite Film: A Review,” *Malaysian J. Sci. Heal. Technol.*, vol. 7, no. 2, pp. 79–85, 2021, doi: 10.33102/mjosht.v7i2.215.

[77] R. Nagarkar and J. Patel, “Polyvinyl Alcohol : A Comprehensive Study,” *Acta Sci. Pharm. Sci.*, vol. 3, no. 4, pp. 34–44, 2019.

[78] J. Ding, R. Zhang, S. Ahmed, Y. Liu, and W. Qin, “Effect of sonication duration in the performance of polyvinyl alcohol/chitosan bilayer films and their effect on strawberry preservation,” *Molecules*, vol. 24, no. 7, 2019, doi: 10.3390/molecules24071408.

[79] Y. Jiang, “Long-term antibacterial effect of electrospun polyvinyl alcohol/polyacrylate sodium nanofiber containing nisin-loaded nanoparticles,” *Nanomaterials*, vol. 10, no. 9, pp. 1–27, 2020, doi: 10.3390/nano10091803.

[80] S. A. Salman and N. A. Bakr, “Section C: Physical Sciences DSC and TGA Properties of PVA Films Filled with Na 2 S 2 O 3 .5H 2 O Salt,” *J. Chem. , Biol. Phys. Sci.*, no. March, pp. 0–11, 2018, doi: 10.24214/jcbps.C.8.2.00111.

[81] D. E. Sameen, “Electrospun nanofibers food packaging: trends and applications in food systems,” *Crit. Rev. Food Sci. Nutr.*, vol. 0, no. 0, pp. 1–14, 2021, doi: 10.1080/10408398.2021.1899128.

[82] N. M. Ranjha and S. Khan, “Review Article Chitosan / Poly (vinyl alcohol) Based Hydrogels for Biomedical Applications : A

Review," *J. Pharm. Altern. Med.*, vol. 2, no. 1, pp. 30–42, 2013.

[83] B. Pfister and S. C. Zeeman, "Formation of starch in plant cells," *Cell. Mol. Life Sci.*, vol. 73, no. 14, pp. 2781–2807, 2016, doi: 10.1007/s00018-016-2250-x.

[84] L. Kong and G. R. Ziegler, "Fabrication of pure starch fibers by electrospinning," *Food Hydrocoll.*, vol. 36, pp. 20–25, 2014, doi: 10.1016/j.foodhyd. 08.021.

[85] X. Chen , "Physicochemical properties comparative analysis of corn starch and cassava starch, and comparative analysis as adhesive," *J. Renew. Mater.*, vol. 9, no. 5, pp. 789–992, 2021, doi: 10.32604/jrm. 014751.

[86] L. M. Fonseca, "Electrospun potato starch nanofibers for thyme essential oil encapsulation: antioxidant activity and thermal resistance," *J. Sci. Food Agric.*, vol. 100, no. 11, pp. 4263–4271, 2020, doi: 10.1002/jsfa.10468.

[87] T. Hemamalini and V. R. Giri Dev, "Comprehensive review on electrospinning of starch polymer for biomedical applications," *Int. J. Biol. Macromol.*, vol. 106, pp. 712–718, 2018, doi: 10.1016/j.ijbiomac. 08.079.

[88] F. Behrouzian, S. M. A. Razavi, and G. O. Phillips, "Cress seed (Lepidium sativum) mucilage, an overview," *Bioact. Carbohydrates Diet. Fibre*, vol. 3, no. 1, pp. 17–28, 2014, doi: 10.1016/j.bcdf. 01.001.

[89] R. Waghmare, R. Preethi, J. A. Moses, and C. Anandharamakrishnan, "Mucilages: sources, extraction methods, and characteristics for their use as encapsulation agents," *Crit. Rev. Food Sci. Nutr.*, vol. 62, no. 15, pp. 4186–4207, 2022, doi: 10.1080/10408398. 1873730.

[90] M. A. El-aziz, H. F. Haggag, M. M. Kaluoubi, L. K. Hassan, and A.

F. Sayed, “Characterization of Ethanol Precipitated Cress Seed and Flaxseed Mucilages Compared with Commercial Guar Gum,” *Am. J. Food Technol.*, vol. 11, no. 3, pp. 84–91, 2016, doi: 10.3923/ajft. 84.91.

[91] A. Fahami and M. Fathi, “Development of cress seed mucilage/PVA nanofibers as a novel carrier for vitamin A delivery,” *Food Hydrocoll.*, vol. 81, pp. 31–38, 2018, doi: 10.1016/j.foodhyd. 02.008.

[92] L. Lin, Y. Gu, and H. Cui, “Moringa oil/chitosan nanoparticles embedded gelatin nanofibers for food packaging against Listeria monocytogenes and Staphylococcus aureus on cheese,” *Food Packag. Shelf Life*, vol. 19, pp. 86–93, 2019, doi: 10.1016/j.fpsl. 12.005.

[93] A. Leone, A. Spada, A. Battezzati, A. Schiraldi, J. Aristil, and S. Bertoli, “Moringa oleifera seeds and oil: Characteristics and uses for human health,” *Int. J. Mol. Sci.*, vol. 17, no. 12, pp. 1–14, 2016, doi: 10.3390/ijms17122141.

[94] B. S. Ogunsina and T. N. Indira, “Quality characteristics and stability of Moringa oleifera seed oil of Indian origin,” *J Food Sci Technol*, vol. 51, no. March, pp. 503–510, 2014, doi: 10.1007/s13197-011-0519-5.

[95] M. A. Idris and M. S. Jami, “Moringa Oleifera Seed Extract : A Review on Its Environmental Applications,” *Int. J. Appl. Environ. Sci.*, vol. 11, no. 6, pp. 1469–1486, 2016.

[96] Y. B. Korassa, N. M. Saptarini, R. Mustarichie, and R. Hendriani, “The Potential of Moringa (Moringa oleifera Lamk) Seed Oil as Anti- Alopecia,” *Pharmacogn. J.*, vol. 14, no. 2, pp. 379–387, 2022.

[97] S. Dehghani, M. Noshad, S. Rastegarzadeh, M. Hojjati, and A. Fazlara, “Electrospun chia seed mucilage/PVA encapsulated with

green cardamonmum essential oils: Antioxidant and antibacterial property," *Int. J. Biol. Macromol.*, vol. 161, pp. 1–9, 2020, doi: 10.1016/j.ijbiomac. 06.023.

[98] S. T. Auti and Y. A. Kulkarni, "Neuroprotective effect of cardamom oil against aluminum induced neurotoxicity in rats," *Front. Neurol.*, vol. 10, no. APR, pp. 1–17, 2019, doi: 10.3389/fneur. 00399.

[99] B. Amelia, E. Saepudin, A. H. Cahyana, D. U. Rahayu, A. S. Sulistyoningrum, and J. Haib, "GC-MS analysis of clove (Syzygium aromaticum) bud essential oil from Java and Manado," *AIP Conf. Proc.*, vol. 1862, 2017, doi: 10.1063/1.4991186.

[100] N. Nurdjannah, N. Bermawie, and I. Agency, *chapter 11 Cloves in Handbook of herbs and spices*. Woodhead Publishing Limited, 2012. doi: 10.1533/9780857095671.197.

[101] Y. Zhang, Y. Zhang, Z. Zhu, X. Jiao, Y. Shang, and Y. Wen, "Encapsulation of thymol in biodegradable nanofiber via coaxial eletrospinning and applications in fruit preservation," *J. Agric. Food Chem.*, vol. 67, no. 6, pp. 1736–1741, 2019, doi: 10.1021/acs.jafc.8b06362.

[102] A. Kowalczyk, M. Przychodna, S. Sopata, A. Bodalska, and I. Fecka, "Thymol and thyme essential oil—new insights into selected therapeutic applications," *Molecules*, vol. 25, no. 18, pp. 1–18, 2020, doi: 10.3390/molecules25184125.

[103] L. B. Gu, X. N. Liu, H. M. Liu, H. L. Pang, and G. Y. Qin, "Extraction of fenugreek (Trigonella foenum-graceum L.) seed oil using subcritical butane: Characterization and process optimization," *Molecules*, vol. 22, no. 2, 2017, doi: 10.3390/molecules22020228.

[104] S. Akbari, N. H. Abdurahman, R. M. Yunus, O. R. Alara, and O. O.

Abayomi, “Extraction, characterization and antioxidant activity of fenugreek (Trigonella-Foenum Graecum) seed oil,” *Mater. Sci. Energy Technol.*, vol. 2, no. 2, pp. 349–355, 2019, doi: 10.1016/j.mset. 12.001.

[105] S. B. Dhull, S. P. Bangar, R. Deswal, P. Dhandhi, and M. Kumar, “Development and Characterization of Active Native and Cross-Linked Pearl Millet Starch-Based Film Loaded with Fenugreek Oil,” *Foods*, 2021.

[106] M. Munshi, P. Arya, and P. Kumar, “Physico-chemical analysis and fatty acid profiling of fenugreek (Trigonella foenum-graecum) seed oil using different solvents,” *J. Oleo Sci.*, vol. 69, no. 11, pp. 1349–1358, 2020, doi: 10.5650/jos.ess20137.

[107] Nael Abu Taha, “Utility and importance of walnut, Juglans regia Linn: A review,” *African J. Microbiol. Res.*, vol. 5, no. 32, pp. 5796–5805, 2011, doi: 10.5897/ajmr11.610.

[108] A. Jahanban-Esfahlan, A. Ostadrahimi, M. Tabibiazar, and R. Amarowicz, “A comparative review on the extraction, antioxidant content and antioxidant potential of different parts of walnut (juglans regia l.) fruit and tree,” *Molecules*, vol. 24, no. 11, 2019, doi: 10.3390/molecules24112133.

[109] D. Ahmad, I. van den Boogaert, J. Miller, R. Presswell, and H. Jouhara, “Hydrophilic and hydrophobic materials and their applications,” *Energy Sources, Part A Recover. Util. Environ. Eff.*, vol. 40, no. 22, pp. 2686–2725, 2018, doi: 10.1080/15567036.2018.1511642.

[110] S. S. Narasagoudr, V. G. Hegde, R. B. Chougale, S. P. Masti, S. Vootla, and R. B. Malabadi, “Physico-chemical and functional properties of rutin induced chitosan/poly (vinyl alcohol) bioactive films for food packaging applications,” *Food Hydrocoll.*, vol. 109,

p. 106096, 2020, doi: 10.1016/j.foodhyd. 106096.

[111] B. W. Chieng, N. A. Ibrahim, N. A. Daud, and Z. A. Talib, *Functionalization of Graphene Oxide via Gamma-Ray Irradiation for Hydrophobic Materials*. Elsevier Inc., 2019. doi: 10.1016/B978-0-12-815757-2.00008-5.

[112] A. Salam , "In-vitro assessment of appropriate hydrophilic scaffolds by co-electrospinning of poly(1,4 cyclohexane isosorbide terephthalate)/polyvinyl alcohol," *Sci. Rep.*, vol. 10, no. 1, pp. 1–9, 2020, doi: 10.1038/s41598-020-76471-x.

[113] A. F. Balogová, "In vitro degradation of specimens produced from pla/phb by additive manufacturing in simulated conditions," *Polymers (Basel).*, vol. 13, no. 10, pp. 1–17, 2021, doi: 10.3390/polym13101542.

[114] A. I. Visan, G. Popescu-Pelin, and G. Socol, "Degradation behavior of polymers used as coating materials for drug delivery—a basic review," *Polymers (Basel).*, vol. 13, no. 8, 2021, doi: 10.3390/polym13081272.

[115] J. Vohlidal, "Polymer degradation: A short review," *Chem. Teach. Int.*, vol. 3, no. 2, pp. 213–220, 2021, doi: 10.1515/cti-2020-0015.

[116] M. C. Celina, E. Linde, and E. Martinez, *Carbonyl Identification and Quantification Uncertainties for Oxidative Polymer Degradation*, vol. 188. 2021. doi: 10.1016/j.polymdegradstab.2021.109550.

[117] J. Almond, P. Sugumaar, M. N. Wenzel, G. Hill, and C. Wallis, "Determination of the carbonyl index of polyethylene and polypropylene using specified area under band methodology with ATR-FTIR spectroscopy," *E-Polymers*, vol. 20, no. 1, pp. 369–381, 2020, doi: 10.1515/epoly-2020-0041.

[118] R. Faki, O. Gursoy, and Y. Yilmaz, "Effect of Electrospinning

Process on Total Antioxidant Activity of Electrospun Nanofibers Containing Grape Seed Extract," *Open Chem.*, vol. 17, no. 1, pp. 912–918, 2019, doi: 10.1515/chem-0098.

[119] B. S. Munteanu, Z. Aytac, G. M. Pricope, T. Uyar, and C. Vasile, "Polylactic acid (PLA)/Silver-NP/VitaminE bionanocomposite electrospun nanofibers with antibacterial and antioxidant activity," *J. Nanoparticle Res.*, vol. 16, no. 10, 2014, doi: 10.1007/s11051-014-2643-4.

[120] T. Amna, J. Yang, K. S. Ryu, and I. H. Hwang, "Electrospun antimicrobial hybrid mats: Innovative packaging material for meat and meat-products," *J. Food Sci. Technol.*, vol. 52, no. 7, pp. 4600–4606, 2015, doi: 10.1007/s13197-014-1508-2.

[121] L. Lin, Y. Dai, and H. Cui, "Antibacterial poly(ethylene oxide) electrospun nanofibers containing cinnamon essential oil/beta-cyclodextrin proteoliposomes," *Carbohydr. Polym.*, vol. 178, no. November, pp. 130–140, 2017, [Online]. Available: http://dx.doi.org/10.1016/j.carbpol. 09.043

[122] P. Shao, "Fabrication and characterization of tea polyphenols loaded pullulan-CMC electrospun nanofiber for fruit preservation," *Int. J. Biol. Macromol.*, pp. 1–7, 2017, doi: https://doi.org/10.1016/j.ijbiomac. 10.054.

[123] A. Altan, Z. Aytac, and T. Uyar, "Carvacrol loaded electrospun fibrous films from zein and poly(lactic acid) for active food packaging," *Food Hydrocoll.*, vol. 81, pp. 48–59, 2018, doi: 10.1016/j.foodhyd. 02.028.

[124] Y. Liu, X. Liang, S. Wang, W. Qin, and Q. Zhang, "Electrospun antimicrobial polylactic acid/tea polyphenol nanofibers for food-packaging applications," *Polymers (Basel).*, vol. 10, no. 5, 2018, doi: 10.3390/polym10050561.

[125] Y. Liu, Y. Li, L. Deng, L. Zou, F. Feng, and H. Zhang, *Hydrophobic Ethylcellulose/Gelatin Nanofibers Containing Zinc Oxide Nanoparticles for Antimicrobial Packaging*, vol. 66, no. 36. 2018. doi: 10.1021/acs.jafc.8b03267.

[126] S. G. Kuntzler, J. A. V. Costa, and M. G. de Morais, "Development of electrospun nanofibers containing chitosan/PEO blend and phenolic compounds with antibacterial activity," *Int. J. Biol. Macromol.*, vol. 117, pp. 800–806, 2018, doi: 10.1016/j.ijbiomac. 05.224.

[127] T. T. Yue, "Electrospinning of Carboxymethyl Chitosan/Polyoxyethylene Oxide Nanofibers for Fruit Fresh-Keeping," *Nanoscale Res. Lett.*, vol. 13, 2018, doi: 10.1186/s11671-018-2642-y.

[128] L. He, W. Lan, S. Ahmed, W. Qin, and Y. Liu, "Electrospun polyvinyl alcohol film containing pomegranate peel extract and sodium dehydroacetate for use as food packaging," *Food Packag. Shelf Life*, vol. 22, no. May, 2019, doi: 10.1016/j.fpsl. 100390.

[129] K. E, M. C. K, B. P, T. S. A, and J. C. R. I, "Biocompatible silver nanoparticles/poly(vinyl alcohol) electrospun nanofibers for potential antimicrobial food packaging applications," *Food Packag. Shelf Life*, vol. 21, no. July, 2019, doi: 10.1016/j.fpsl. 100379.

[130] Z. Zhu, Y. Zhang, Y. Zhang, Y. Shang, X. Zhang, and Y. Wen, "Preparation of PANatTiO 2 Nanofibers for fruit packaging materials with efficient photocatalytic degradation of ethylene," *Materials (Basel).*, vol. 16, no. 6, 2019, doi: 10.3390/ma12060896.

[131] M. Nazari, H. Majdi, M. Milani, S. Abbaspour-Ravasjani, H. Hamishehkar, and L. T. Lim, "Cinnamon nanophytosomes embedded electrospun nanofiber: Its effects on microbial quality and shelf-life of shrimp as a novel packaging," *Food Packag. Shelf*

Life, vol. 21, no. June, 2019, doi: 10.1016/j.fpsl. 100349.

[132] Y. Tang, "Electrospun Gelatin Nanofibers Encapsulated with Peppermint and Chamomile Essential Oils as Potential Edible Packaging," *J. Agric. Food Chem.*, vol. 67, no. 8, pp. 2227–2234, 2019, doi: 10.1021/acs.jafc.8b06226.

[133] S. K. V. Bharathi, M. M. Leena, J. A. Moses, and C. Anandharamakrishnan, "Nanofibre-based bilayer biopolymer films: enhancement of antioxidant activity and potential for food packaging application," *Int. J. Food Sci. Technol.*, vol. 55, no. 4, pp. 1477–1484, 2020, doi: 10.1111/ijfs.14492.

[134] S. Li, Y. Yan, X. Guan, and K. Huang, "Preparation of a hordein-quercetin-chitosan antioxidant electrospun nanofibre film for food packaging and improvement of the film hydrophobic properties by heat treatment," *Food Packag. Shelf Life*, vol. 23, no. January, 2020, doi: 10.1016/j.fpsl. 100466.

[135] Y. Zhou, "Angelica essential oil loaded electrospun gelatin nanofibers for active food packaging application," *Polymers (Basel).*, vol. 12, no. 2, 2020, doi: 10.3390/polym12020299.

[136] V. K. Pandey, S. N. Upadhyay, K. Niranjan, and P. K. Mishra, "Antimicrobial biodegradable chitosan-based composite Nano-layers for food packaging," *Int. J. Biol. Macromol.*, vol. 157, pp. 212–219, 2020, doi: 10.1016/j.ijbiomac. 04.149.

[137] M. Hashmi, "Carboxymethyl cellulose (Cmc) based electrospun composite nanofiber mats for food packaging," *Polymers (Basel).*, vol. 13, no. 2, pp. 1–12, 2021, doi: 10.3390/polym13020302.

[138] D. Zhang, "Starch/tea polyphenols nanofibrous films for food packaging application: From facile construction to enhance mechanical, antioxidant and hydrophobic properties," *Food Chem.*, vol. 360, 2021, doi: 10.1016/j.foodchem. 129922.

[139] E. Ansarifar and F. Moradinezhad, “Encapsulation of thyme essential oil using electrospun zein fiber for strawberry preservation,” *Chem. Biol. Technol. Agric.*, vol. 9, no. 1, pp. 1–11, 2022, doi: 10.1186/s40538-021-00267-y.

[140] M. K. A. Mohammed, M. R. Mohammad, M. S. Jabir, and D. S. Ahmed, “Functionalization, characterization, and antibacterial activity of single wall and multi wall carbon nanotubes,” *IOP Conf. Ser. Mater. Sci. Eng.*, vol. 757, no. 1, 2020, doi: 10.1088/1757-899X/757/1/012028.

[141] G. Marinova and V. Batchvarov, “EVALUATION OF THE METHODS FOR DETERMINATION OF THE FREE RADICAL SCAVENGING ACTIVITY BY DPPH,” *Bulg. J. Agric. Sci.*, vol. 17, no. 1, pp. 11–24, 2011.

[142] M. S. Bahjat, H. H., Ismail, R. A., Sulaiman, G. M., and Jabir, “Magnetic Field – Assisted Laser Ablation of Titanium Dioxide Nanoparticles in Water for Anti- Bacterial Applications,” *Inorg. Organomet. Polym. Mater.*, pp. 1–8, 2021, doi: https://doi.org/10.21203/rs.3.rs-176836/v1.

[143] K. S. Khashan, F. A. Abdulameer, M. S. Jabir, A. A. Hadi, and G. M. Sulaiman, “Anticancer activity and toxicity of carbon nanoparticles produced by pulsed laser ablation of graphite in water,” *Adv. Nat. Sci. Nanosci. Nanotechnol.*, vol. 11, no. 3, 2020, doi: 10.1088/2043-6254/aba1de.

[144] K. S. Khashan, B. A. Badr, G. M. Sulaiman, M. S. Jabir, and S. A. Hussain, “Antibacterial activity of Zinc Oxide nanostructured materials synthesis by laser ablation method,” *J. Phys. Conf. Ser.*, vol. 1795, no. 1, 2021, doi: 10.1088/1742-6596/1795/1/012040.

[145] M. A. Jihad, F. T. M. Noori, M. S. Jabir, S. Albukhaty, F. A. Almalki, and A. A. Alyamani, “Polyethylene glycol functionalized

graphene oxide nanoparticles loaded with nigella sativa extract: A smart antibacterial therapeutic drug delivery system," *Molecules*, vol. 26, no. 11, 2021, doi: 10.3390/molecules26113067.

[146] I. H. Ali, M. S. Jabir, H. S. A. Al-Shmgani, G. M. Sulaiman, and A. H. Sadoon, "Pathological and Immunological Study on Infection with Escherichia Coli in ale BALB/c mice," *J. Phys. Conf. Ser.*, vol. 1003, no. 1, 2018, doi: 10.1088/1742-6596/1003/1/012009.

[147] A. Younus, S. Al-Ahmer, and M. Jabir, "Evaluation of some immunological markers in children with bacterial meningitis caused by streptococcus pneumoniae," *Res. J. Biotechnol.*, vol. 14, no. Special Issue I, pp. 131–133, 2019.

[148] M. S. Jabir, "Inhibition of Staphylococcus aureus α-Hemolysin Production Using Nanocurcumin Capped Au@ZnO Nanocomposite," *Bioinorg. Chem. Appl.*, vol. 2022, pp. 1–18, 2022, doi: 10.1155/2663812.

[149] Q. Liang, W. Pan, and Q. Gao, "Preparation of carboxymethyl starch/polyvinyl-alcohol electrospun composite nanofibers from a green approach," *Int. J. Biol. Macromol.*, vol. 190, no. July, pp. 601–606, 2021, doi: 10.1016/j.ijbiomac. 09.015.

[150] H. Rezaeinia, B. Emadzadeh, and B. Ghorani, "Electrospun balangu (Lallemantia royleana) hydrocolloid nanofiber mat as a fast-dissolving carrier for bergamot essential oil," *Food Hydrocoll.*, vol. 100, 2020, doi: 10.1016/j.foodhyd. 105312.

[151] N. Arik, N. Horzum, and Y. B. Truong, "Development and Characterizations of Engineered Electrospun Bio-Based Polyurethane Containing Essential Oils," *Membranes (Basel).*, vol. 12, no. 2, pp. 1–16, 2022, doi: 10.3390/membranes12020209.

[152] W. J. Al-Kaabi, "Development of Inula graveolens (L.) plant extract electrospun/polycaprolactone nanofibers: A novel material for

biomedical application," *Appl. Sci.*, vol. 11, no. 2, pp. 1–10, 2021, doi: 10.3390/app11020828.

[153] E. Altan, "Fabrication of Electrospun Juglans regia (Juglone) Loaded Poly(lactic acid) Scaffolds as a Potential Wound Dressing Material," *Polymers (Basel).*, vol. 14, no. 10, 2022, doi: 10.3390/polym14101971.

[154] J. Porras-Saavedra, L. Ricaurte, N. C. Pérez-Pérez, and M. X. Quintanilla-Carvajal, "Development and characterization of Sechium edule starch and polyvinyl alcohol nanofibers obtained by electrospinning," *Colloids Surfaces A Physicochem. Eng. Asp.*, vol. 649, no. April, 2022, doi: 10.1016/j.colsurfa. 129456.

[155] F. Kurd, M. Fathi, and H. Shekarchizadeh, "Basil seed mucilage as a new source for electrospinning: Production and physicochemical characterization," *Int. J. Biol. Macromol.*, vol. 95, pp. 689–695, 2017, doi: 10.1016/j.ijbiomac. 11.116.

[156] H. Kesici Güler, F. Cengiz Çallıoğlu, and E. Sesli Çetin, "Antibacterial PVP/cinnamon essential oil nanofibers by emulsion electrospinning," *J. Text. Inst.*, vol. 110, no. 2, pp. 302–310, 2019, doi: 10.1080/00405000. 1477237.

[157] J. Pan, F. Ai, P. Shao, H. Chen, and H. Gao, "Development of polyvinyl alcohol/β-cyclodextrin antimicrobial nanofibers for fresh mushroom packaging," *Food Chem.*, vol. 300, 2019, doi: 10.1016/j.foodchem. 125249.

[158] F. K. Mwiiri, J. M. Brandner, and R. Daniels, "Electrospun bioactive wound dressing containing colloidal dispersions of birch bark dry extract," *Pharmaceutics*, vol. 12, no. 10, p. 1, 2020, doi: 10.3390/pharmaceutics12100991.

[159] G. Liu, Z. Gu, Y. Hong, L. Cheng, and C. Li, "Electrospun starch nanofibers: Recent advances, challenges, and strategies for potential

pharmaceutical applications," *J. Control. Release*, vol. 252, pp. 95–107, 2017, doi: 10.1016/j.jconrel. 03.016.

[160] A. Fahami and M. Fathi, "Development of cress seed mucilage/PVA nanofibers as a novel carrier for vitamin A delivery," *Food Hydrocoll.*, vol. 81, pp. 31–38, 2018, doi: 10.1016/j.foodhyd. 02.008.

[161] N. Wang, Z. Liu, J. Yang, Y. Song, and J. Yang, "Investigation of antibacterial activity of one-dimensional electrospun Walnut green husk extract-PVP nanofibers," *Iran. Polym. J. (English Ed.*, vol. 31, no. 6, pp. 779–785, 2022, doi: 10.1007/s13726-022-01037-9.

[162] Z. W. Abdullah and Y. Dong, "Biodegradable and water resistant poly(vinyl) alcohol (PVA)/starch (ST)/glycerol (GL)/halloysite nanotube (HNT) nanocomposite films for sustainable food packaging," *Front. Mater.*, vol. 6, no. April, 2019, doi: 10.3389/fmats. 00058.

[163] M. Soltanzadeh, "Active gelatin/cress seed gum-based films reinforced with chitosan nanoparticles encapsulating pomegranate peel extract: Preparation and characterization," *Food Hydrocoll.*, vol. 129, no. February, 2022, doi: 10.1016/j.foodhyd. 107620.

[164] T. L. Shi, Chong, Zhou, Aying, "Oregano essential oil/β-cyclodextrin inclusion compound polylactic acid/polycaprolactone electrospun nanofibers for active food packaging," *Chem. Eng. Journal*, , vol. 445, no. 136746, pp. 1–33, 2022.

[165] P. Jaiturong, B. Sirithunyalug, S. Eitsayeam, C. Asawahame, P. Tipduangta, and J. Sirithunyalug, "Preparation of glutinous rice starch/polyvinyl alcohol copolymer electrospun fibers for using as a drug delivery carrier," *Asian J. Pharm. Sci.*, vol. 13, no. 3, pp. 239–247, 2018, doi: 10.1016/j.ajps. 08.008.

[166] G. Sahal, B. Nasseri, A. Ebrahimi, and I. S. Bilkay, "Electrospun

essential oil-polycaprolactone nanofibers as antibiofilm surfaces against clinical Candida tropicalis isolates," *Biotechnol. Lett.*, vol. 0123456789, 2019, doi: 10.1007/s10529-019-02660-y.

[167] O. T. Afolabi-owolabi, S. Z. Abidin, and F. Ariffin, "Electrospun Polymer Nanofiber from Moringa Oleifera Kernel Oil with Coaxial Electrospinning Method," *Curr. Nutr. Food Sci.*, vol. 16, no. 1, pp. 90–97, 2018, doi: 10.2174/1573401315666181120113219.

[168] N. Karami, A. Kamkar, Y. Shahbazi, and A. Misaghi, "Electrospinning of double-layer chitosan-flaxseed mucilage nanofibers for sustained release of Ziziphora clinopodioides essential oil and sesame oil," *Lwt*, vol. 140, 2021, doi: 10.1016/j.lwt. 110812.

[169] M. D. Berechet, "Bioactive properties of nanofibres based on concentrated collagen hydrolysate loaded with thyme and oregano essential oils," *Materials (Basel).*, vol. 13, no. 7, 2020, doi: 10.3390/ma13071618.

[170] F. K. Mwiiri, J. M. Brandner, and R. Daniels, "Erratum: Electrospun bioactive wound dressing containing colloidal dispersions of birch bark dry extract (Pharmaceutics, (2020) 12, 770, 10.3390/pharmaceutics12080770)," *Pharmaceutics*, vol. 12, no. 10, p. 1, 2020, doi: 10.3390/pharmaceutics12100991.

[171] P. Koushki, S. H. Bahrami, and M. Ranjbar-Mohammadi, "Coaxial nanofibers from poly(caprolactone)/ poly(vinyl alcohol)/Thyme and their antibacterial properties," *J. Ind. Text.*, vol. 47, no. 5, pp. 834–852, 2018, doi: 10.1177/1528083716674906.

[172] Z. Khan, F. Kafiah, H. Zahid Shafi, F. Nufaiei, S. Ahmed Furquan, and A. Matin, "Morphology, Mechanical Properties and Surface Characteristics of Electrospun Polyacrylonitrile (PAN) Nanofiber Mats," *Int. J. Adv. Eng. Nano Technol.*, no. 3, pp. 2347–6389, 2015.

[173] B. M. Abunahel, N. Z. N. Azman, and M. Jamil, “Effect of Needle Diameter on the Morphological Structure of Electrospun n-Bi2O3/Epoxy-PVA Nanofiber Mats,” *Int. J. Chem. Mater. Eng.*, vol. 12, no. 6, pp. 296–299, 2018.

[174] S. Zargham, S. Bazgir, A. Tavakoli, A. S. Rashidi, and R. Damerchely, “The effect of flow rate on morphology and deposition area of electrospun nylon 6 nanofiber,” *J. Eng. Fiber. Fabr.*, vol. 7, no. 4, pp. 42–49, 2012, doi: 10.1177/155892501200700414.

[175] D. D. Pise, B. B. Ahuja, and S. M. Shendokar, “Study of Process Parameters Affecting the Diameter and Morphology of Electrospun Polyvinylidene Fluoride (PVDF) Nanofibers,” *Int. J. Sci. Res. ISSN (Online Index Copernicus Value Impact Factor*, vol. 14, no. 6, pp. 2319–7064, 2013, [Online]. Available: www.ijsr.net

[176] J. Gomez-Caturla, “Development and evaluation of novel nanofibers based on mango kernel starch obtained by electrospinning,” *Polym. Test.*, vol. 106, 2022, doi: 10.1016/j.polymertesting. 107462.

[177] H. H. Kim, M. J. Kim, S. J. Ryu, C. S. Ki, and Y. H. Park, “Effect of fiber diameter on surface morphology, mechanical property, and cell behavior of electrospun poly(ε-caprolactone) mat,” *Fibers Polym.*, vol. 17, no. 7, pp. 1033–1042, 2016, doi: 10.1007/s12221-016-6350-x.

[178] S. K. Jaganathan, M. P. Mani, and A. Z. M. Khudzari, “Electrospun combination of peppermint oil and copper sulphate with conducive physico-chemical properties for wound dressing applications,” *Polymers (Basel).*, vol. 11, no. 4, pp. 1–15, 2019, doi: 10.3390/polym11040586.

[179] L. Lin, X. Mao, Y. Sun, G. Rajivgandhi, and H. Cui, “Antibacterial properties of nanofibers containing chrysanthemum essential oil and

their application as beef packaging," *Int. J. Food Microbiol.*, vol. 292, pp. 21–30, 2019, doi: 10.1016/j.ijfoodmicro. 12.007.

[180] H. Adeli, M. T. Khorasani, and M. Parvazinia, "Wound dressing based on electrospun PVA/chitosan/starch nanofibrous mats: Fabrication, antibacterial and cytocompatibility evaluation and in vitro healing assay," *Int. J. Biol. Macromol.*, vol. 122, pp. 238–254, 2019, doi: 10.1016/j.ijbiomac. 10.115.

[181] C. La Torre, P. Caputo, P. Plastina, E. Cione, and A. Fazio, "Green husk of walnuts (Juglans regia l.) from southern italy as a valuable source for the recovery of glucans and pectins," *Fermentation*, vol. 7, no. 4, pp. 1–16, 2021, doi: 10.3390/fermentation7040305.

[182] R. Roche and F. Yalcinkaya, "Electrospun Polyacrylonitrile Nanofibrous Membranes for Point-of-Use Water and Air Cleaning," *ChemistryOpen*, vol. 8, no. 1, pp. 97–103, 2019, doi: 10.1002/open.201800267.

[183] L. A. Can-Herrera, A. I. Oliva, M. A. A. Dzul-Cervantes, O. F. Pacheco-Salazar, and J. M. Cervantes-Uc, "Morphological and mechanical properties of electrospun polycaprolactone scaffolds: Effect of applied voltage," *Polymers (Basel).*, vol. 13, no. 4, pp. 1–16, 2021, doi: 10.3390/polym13040662.

[184] I. Korbag and S. Mohamed Saleh, "Studies on the formation of intermolecular interactions and structural characterization of polyvinyl alcohol/lignin film," *Int. J. Environ. Stud.*, vol. 73, no. 2, pp. 226–235, 2016, doi: 10.1080/00207233.2016.1143700.

[185] J. Tahalyani, K. K. Rahangdale, and K. Balasubramanian, "The dielectric properties and charge transport mechanism of π-conjugated segments decorated with intrinsic conducting polymer," *RSC Adv.*, vol. 6, no. 74, pp. 69733–69742, 2016, doi: 10.1039/c6ra09554b.

[186] S. Pokhrel and L. S. Rai, “Fabrication and Characterization of Starch-Based Biodegradable Polymer with Polyvinyl Alcohol,” *J. Nepal Chem. Soc.*, vol. 40, no. 2091–0304, pp. 57–66, 2019, doi: https://doi.org:10.3126/jncs.v40i0.27283.

[187] J. Cai , “Hydrophobic Interface Starch Nanofibrous Film for Food Packaging: From Bioinspired Design to Self-Cleaning Action,” *J. Agric. Food Chem.*, vol. 69, no. 17, pp. 5067–5075, 2021, doi: 10.1021/acs.jafc.1c00230.

[188] H. R. Kavousi, M. Fathi, and S. A. H. Goli, “Stability enhancement of fish oil by its encapsulation using a novel hydrogel of cress seed mucilage/chitosan,” *Int. J. Food Prop.*, vol. 20, no. August, pp. 1890–1900, 2017, doi: 10.1080/10942912. 1357042.

[189] L. Lin, Y. Gu, and H. Cui, “Moringa oil/chitosan nanoparticles embedded gelatin nanofibers for food packaging against Listeria monocytogenes and Staphylococcus aureus on cheese,” *Food Packag. Shelf Life*, vol. 19, pp. 86–93, 2019, doi: 10.1016/j.fpsl. 12.005.

[190] H. Cui, M. Bai, M. M. A. Rashed, and L. Lin, “The antibacterial activity of clove oil/chitosan nanoparticles embedded gelatin nanofibers against Escherichia coli O157:H7 biofilms on cucumber,” *Int. J. Food Microbiol.*, vol. 266, pp. 69–78, 2018, doi: 10.1016/j.ijfoodmicro. 11.019.

[191] N. Rouba, T. Sadoun, N. Boutagrabet, D. Kerrouche, S. Zadi, and N. Mimi, “Thermo-oxidation and biodegradation study of low-density polyethylene /starch films by IR spectroscopy,” *Iran. J. Chem. Chem. Eng.*, vol. 34, no. 4, pp. 69–78, 2015.

[192] X. H. Qin, D. Q. Wu, and C. C. Chu, “Dual functions of polyvinyl alcohol (PVA): Fabricating particles and electrospinning nanofibers applied in controlled drug release,” *J. Nanoparticle Res.*, vol. 15,

no. 1, pp. 1–14, 2013, doi: 10.1007/s11051-012-1395-2.

[193] Y. Liu, H. Wei, Z. Wang, Q. Li, and N. Tian, “Simultaneous enhancement of strength and toughness of PLA induced by miscibility variation with PVA,” *Polymers (Basel).*, vol. 10, no. 10, 2018, doi: 10.3390/POLYM10101178.

[194] E. E. Tănase, M. E. Popa, M. Râpă, and O. Popa, “Preparation and characterization of biopolymer blends based on polyvinyl alcohol and starch,” *Rom. Biotechnol. Lett.*, vol. 20, no. 2, pp. 10306–10315, 2015.

[195] M. M. Tosif, A. Najda, A. Bains, G. Zawiślak, G. Maj, and P. Chawla, “Starch–mucilage composite films: An inclusive on physicochemical and biological perspective,” *Polymers (Basel).*, vol. 13, no. 16, 2021, doi: 10.3390/polym13162588.

[196] S. Amiri and A. Rahimi, “Poly(ε-caprolactone) electrospun nanofibers containing cinnamon essential oil nanocapsules: A promising technique for controlled release and high solubility,” *J. Ind. Text.*, vol. 48, no. 10, pp. 1527–1544, 2019, doi: 10.1177/1528083718764911.

[197] A. Raksa, R. Utke, C. Ruksakulpiwat, P. O. Numpaisal, and Y. Ruksakulpiwat, “Morphological and chemical characterization of electrospun silk fibroin/polyvinyl alcohol nanofibers,” *AIP Conf. Proc.*, vol. 2279, no. October, pp. 4–9, 2020, doi: 10.1063/5.0023319.

[198] Y. Qin, W. Li, D. Liu, M. Yuan, and L. Li, “Development of active packaging film made from poly (lactic acid) incorporated essential oil,” *Prog. Org. Coatings*, vol. 103, pp. 76–82, 2017, doi: 10.1016/j.porgcoat. 10.017.

[199] R. Wongkanya, “Electrospun poly(lactic acid) nanofiber mats for controlled transdermal delivery of essential oil from Zingiber

cassumunar Roxb," *Mater. Res. Express*, vol. 7, no. 5, 2020, doi: 10.1088/2053-1591/ab8fea.

[200] S. Członka, A. Strąkowska, and A. Kairytė, "Effect of walnut shells and silanized walnut shells on the mechanical and thermal properties of rigid polyurethane foams," *Polym. Test.*, vol. 87, p. 106534, 2020, doi: 10.1016/j.polymertesting. 106534.

[201] A. E. T. Norziah M Hani and M. H. Azarian, "Characterization of electrospun gelatine nanofibres encapsulated with Moringa oleifera bioactive extract," *J. Sci. Food Agric.*, vol. 97(10), pp. 3348–3358, 2017.

[202] S. J. Peighambardoust, S. H. Peighambardoust, N. Mohammadzadeh Pournasir, and P. Pakdel, "Properties of active starch-based films incorporating a combination of Ag, ZnO and CuO nanoparticles for potential use in food packaging applications," *Food Packag. Shelf Life*, vol. 22, no. October, p. 100420, 2019, doi: 10.1016/j.fpsl. 100420.

[203] M. Ezz El-Din Ibrahim, R. M. Alqurashi, and F. Y. Alfaraj, "Antioxidant Activity of Moringa oleifera and Olive Olea europaea L. Leaf Powders and Extracts on Quality and Oxidation Stability of Chicken Burgers," *Antioxidants*, vol. 11, no. 3, 2022, doi: 10.3390/antiox11030496.

[204] P. Pusporini, D. Edikresnha, I. Sriyanti, T. Suciati, M. M. Munir, and K. Khairurrijal, "Electrospun polyvinylpyrrolidone (PVP)/green tea extract composite nanofiber mats and their antioxidant activities," *Mater. Res. Express*, vol. 5, no. 5, 2018, doi: 10.1088/2053-1591/aac1e6.

[205] B. S. Munteanu, "Antioxidant/antibacterial electrospun nanocoatings applied onto PLA films," *Materials (Basel).*, vol. 11, no. 10, 2018, doi: 10.3390/ma11101973.

[206] and S. Hasani, Maryam Hasani, “Nano-encapsulation of thyme essential oil in chitosan-Arabic gum system: Evaluation of its antioxidant and antimicrobial properties,” *JTrends Phytochem. Res.*, vol. 2(2), pp. 75–82, 2018.

[207] R. M. Y. Sweeta Akbari, Nour Hamid Abdurahman, “Extraction, characterization and antioxidant activity of fenugreek (TrigonellaFoenum Graecum) seed oil,” *Mater. Sci. Energy Technol.*, vol. 12, pp. 349–355, 2019, doi: https://doi.org/10.1016/j.mset. 12.001.

[208] H. N. Yavuz, F. Karbancioğlu Güler, and F. Altay, “Effects of Electrospinning on Antifungal Properties of Thyme and Cardamom Oils,” *Eurasian J. Food Sci. Technol.*, vol. 5, no. 2, pp. 105–116, 2021.

[209] A. A. Faisal, M. A. Abed, and A. I. Hussein, “The use of walnut tree bark powder as a teeth whitener,” *Indian J. Public Heal. Res. Dev.*, vol. 10, no. 12, pp. 1300–1303, 2019, doi: 10.37506/v10/i12/ijphrd/192227.

[210] Nael Abu Taha, “Utility and importance of walnut, Juglans regia Linn: A review,” *African J. Microbiol. Res.*, vol. 5, no. 32, 2011, doi: 10.5897/ajmr11.610.

[211] J. Rnjak-Kovacina, “Tailoring the porosity and pore size of electrospun synthetic human elastin scaffolds for dermal tissue engineering,” *Biomaterials*, vol. 32, no. 28, pp. 6729–6736, 2011, doi: 10.1016/j.biomaterials.2011.05.065.

[212] W. C. Oliver and G. M. Pharr, “An improved technique for determining hardness and elastic modulus using load and displacement sensing indentation experiments,” 1992.

Appendix A

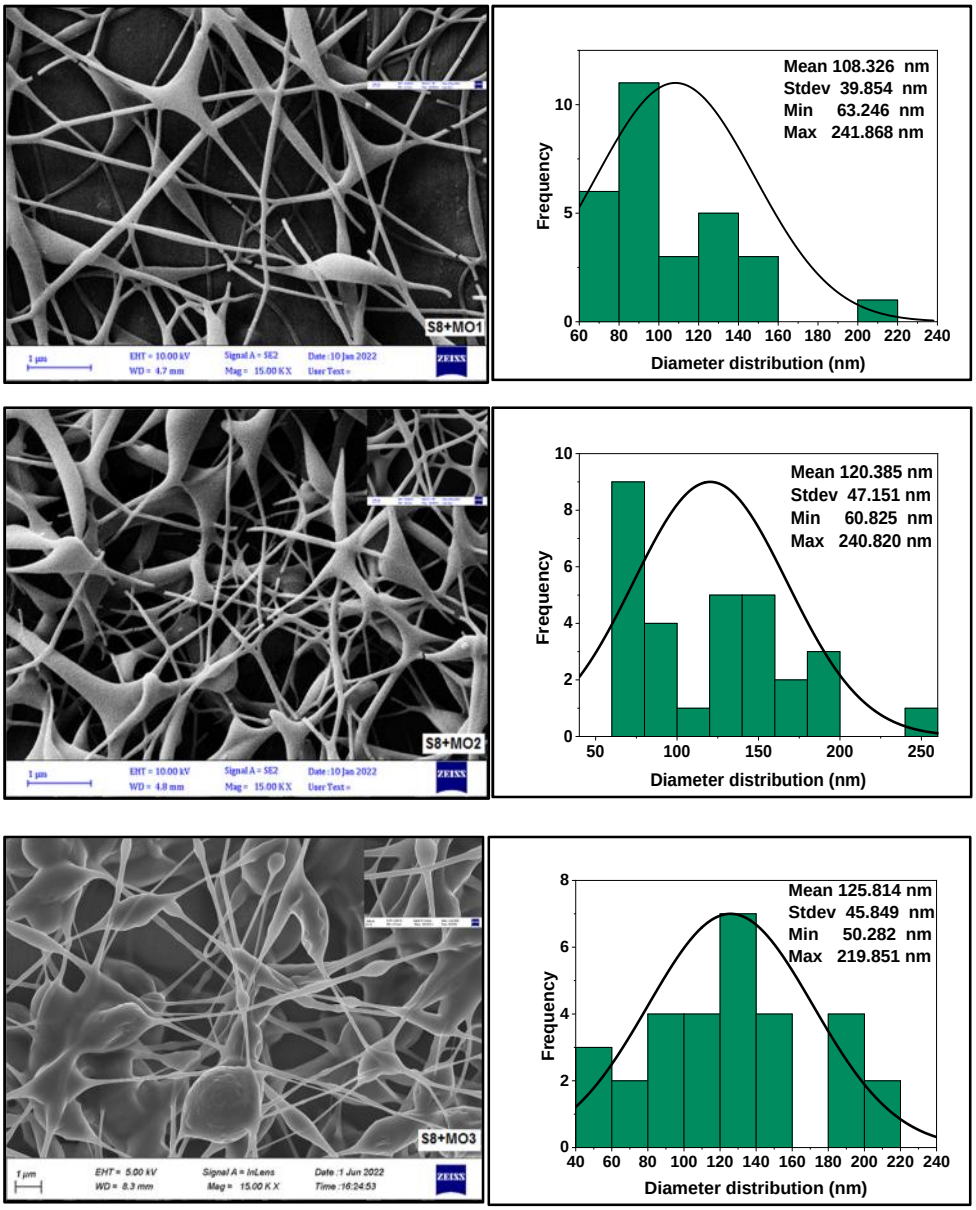

FE-SEM micrographs **Nanofibers diameter distribution histograms**

Figure (4.11): FESEM Micrographs and Nano-fibers diameter distribution histograms for moringa oil (MO) in part two.

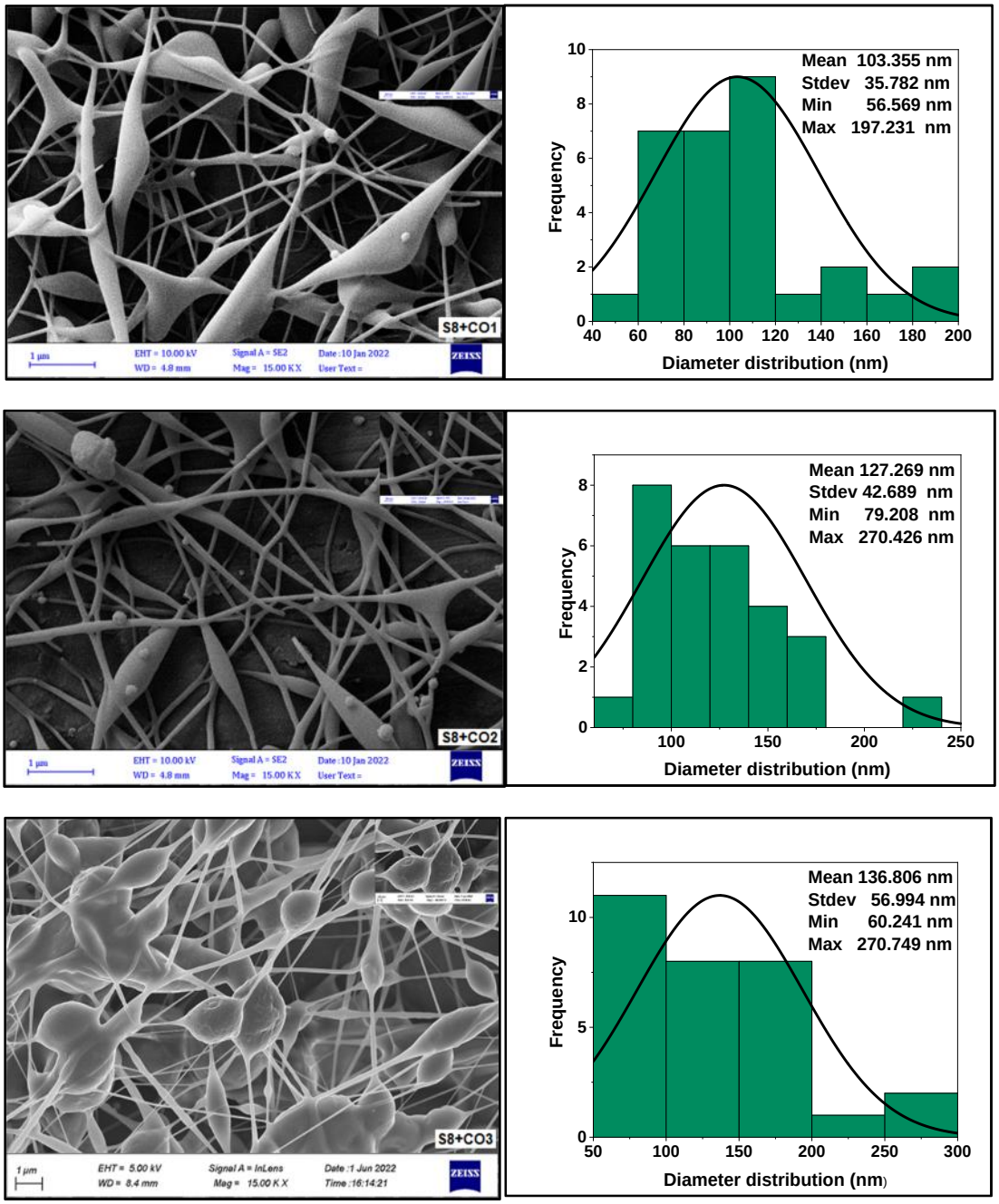

FE-SEM micrographs **Nanofibers diameter distribution histograms**

Figure (4.12): FESEM Micrographs and Nano-fibers diameter distribution histograms for cardamom oil (CO) in part two.

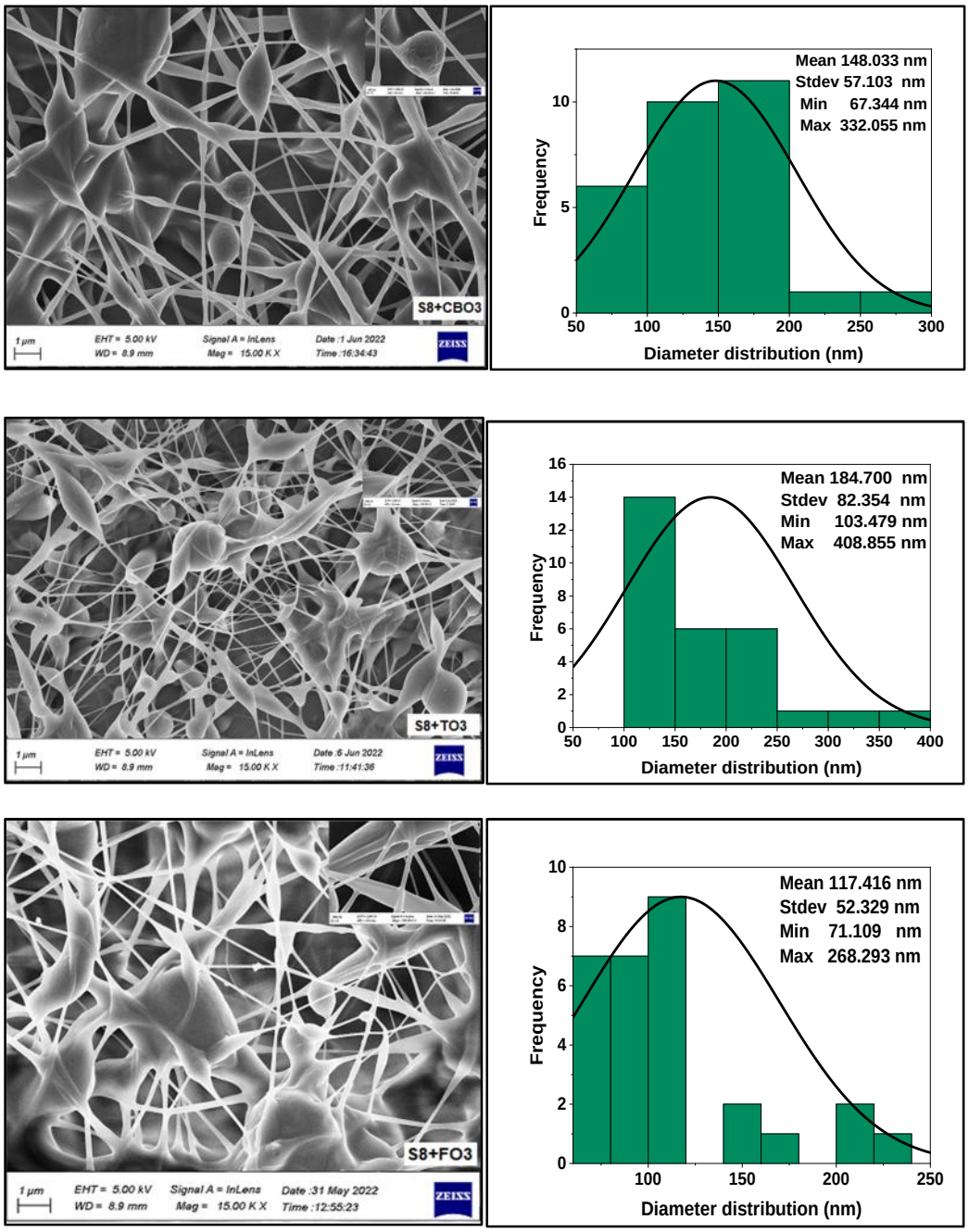

FE-SEM micrographs **Nanofibers diameter distribution histograms**

Figure (4.13): FESEM Micrographs and Nano-fibers diameter distribution histograms for clove bud oil (CBO), thyme oil (TO), and fenugreek oil (FO) in part two.

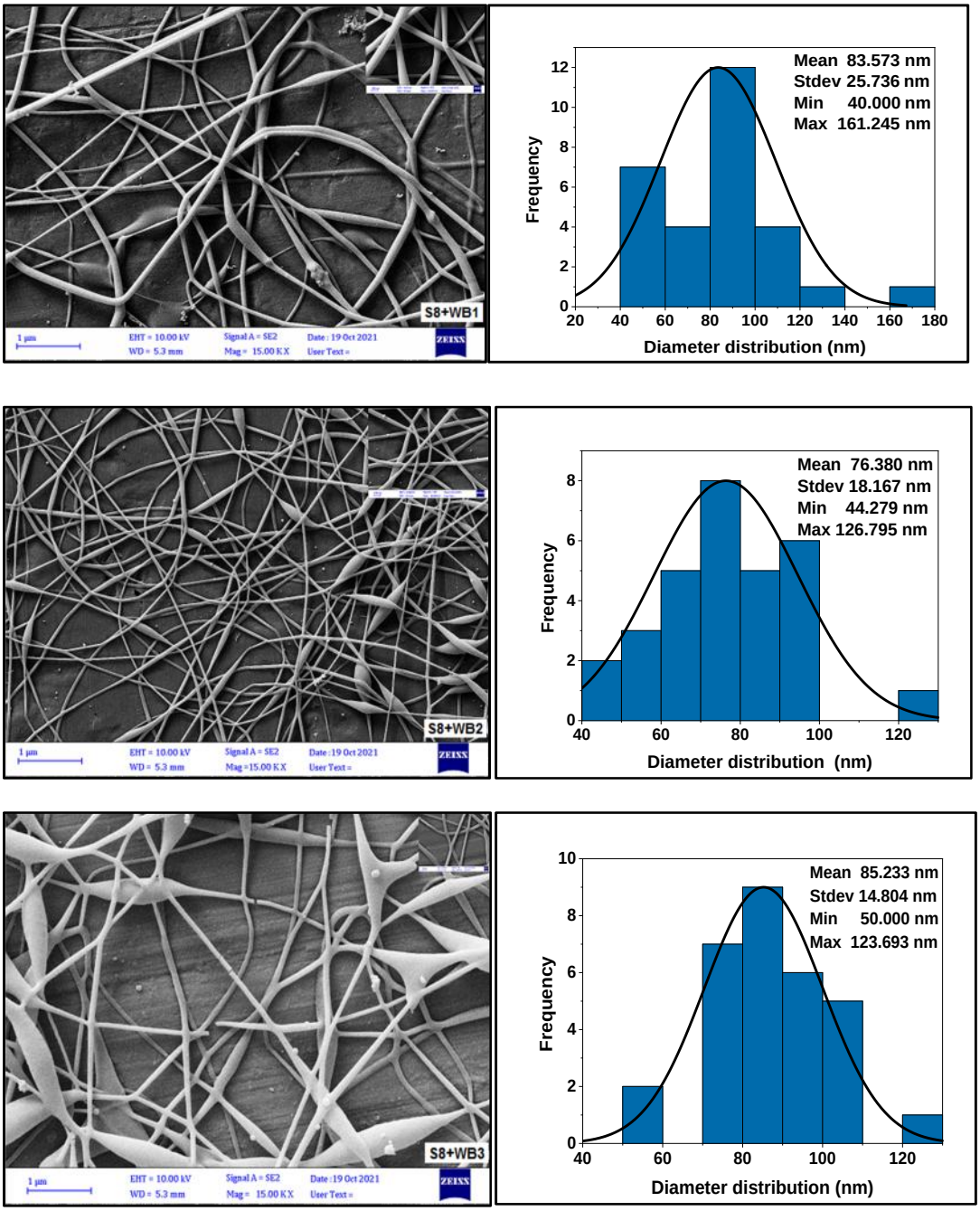

FE-SEM micrographs **Nanofibers diameter distribution histograms**

Figure (4.14): FESEM Micrographs and Nano-fibers diameter distribution histograms for walnut tree bark (WB) in part two.

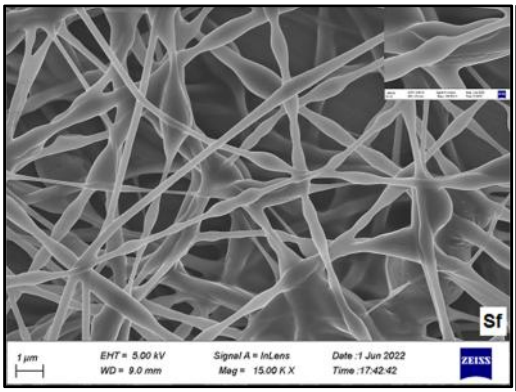
Sf
1 µm
EHT = 5.00 kV
WD = 9.0 mm
Signal A = InLens
Mag = 15.00 K X
Date :1 Jun 2022
Time :17:42:42
ZEISS

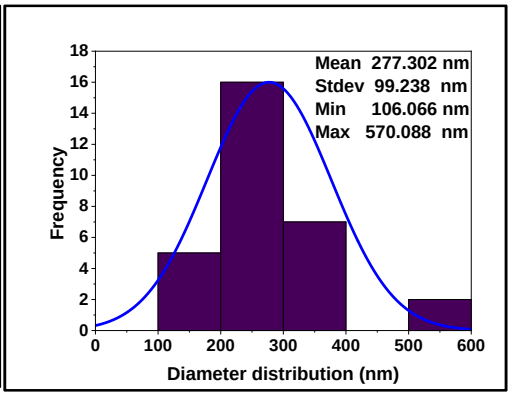
Mean 277.302 nm
Stdev 99.238 nm
Min 106.066 nm
Max 570.088 nm
Frequency
Diameter distribution (nm)

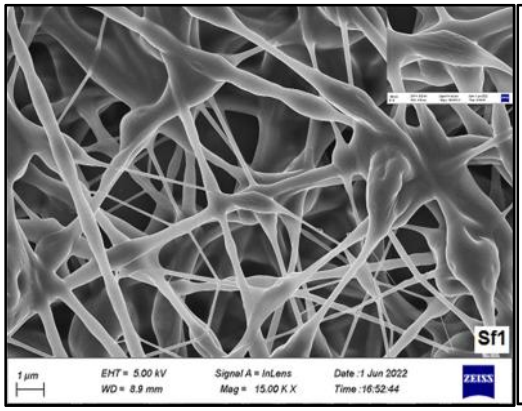
Sf1
1 µm
EHT = 5.00 kV
WD = 8.9 mm
Signal A = InLens
Mag = 15.00 K X
Date :1 Jun 2022
Time :16:52:44
ZEISS

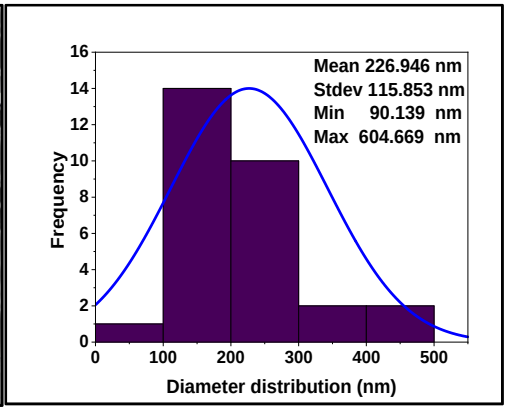
Mean 226.946 nm
Stdev 115.853 nm
Min 90.139 nm
Max 604.669 nm
Frequency
Diameter distribution (nm)

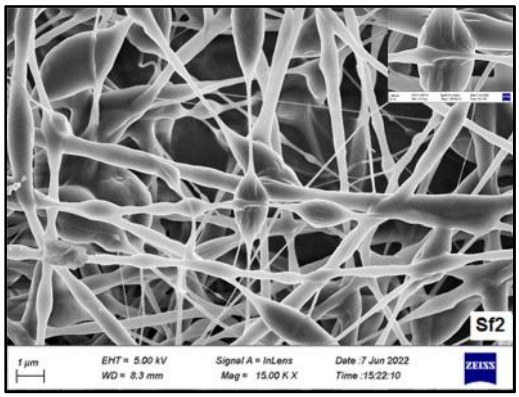
Sf2
1 µm
EHT = 5.00 kV
WD = 8.3 mm
Signal A = InLens
Mag = 15.00 K X
Date :7 Jun 2022
Time :15:22:10
ZEISS

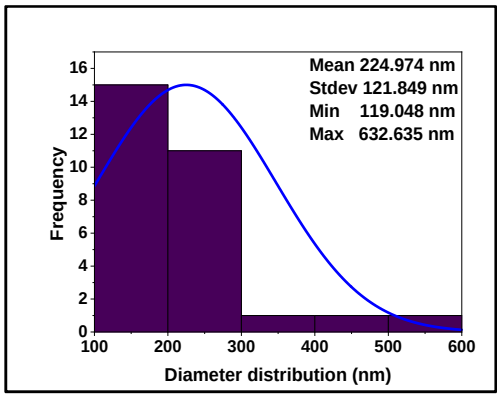
Mean 224.974 nm
Stdev 121.849 nm
Min 119.048 nm
Max 632.635 nm
Frequency
Diameter distribution (nm)

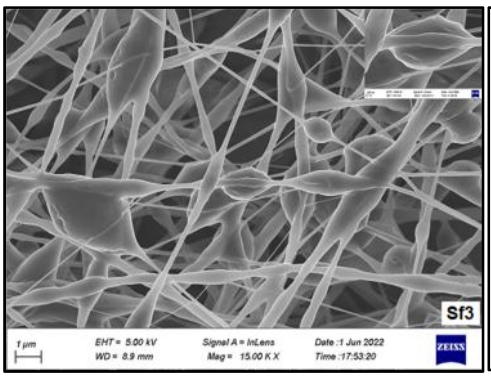
Sf3
1 µm
EHT = 5.00 kV
WD = 8.9 mm
Signal A = InLens
Mag = 15.00 K X
Date :1 Jun 2022
Time :17:53:20
ZEISS

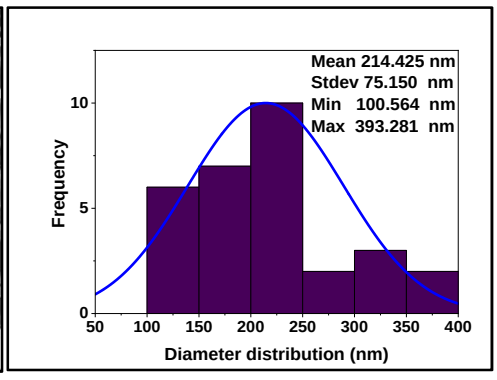
Mean 214.425 nm
Stdev 75.150 nm
Min 100.564 nm
Max 393.281 nm
Frequency
Diameter distribution (nm)

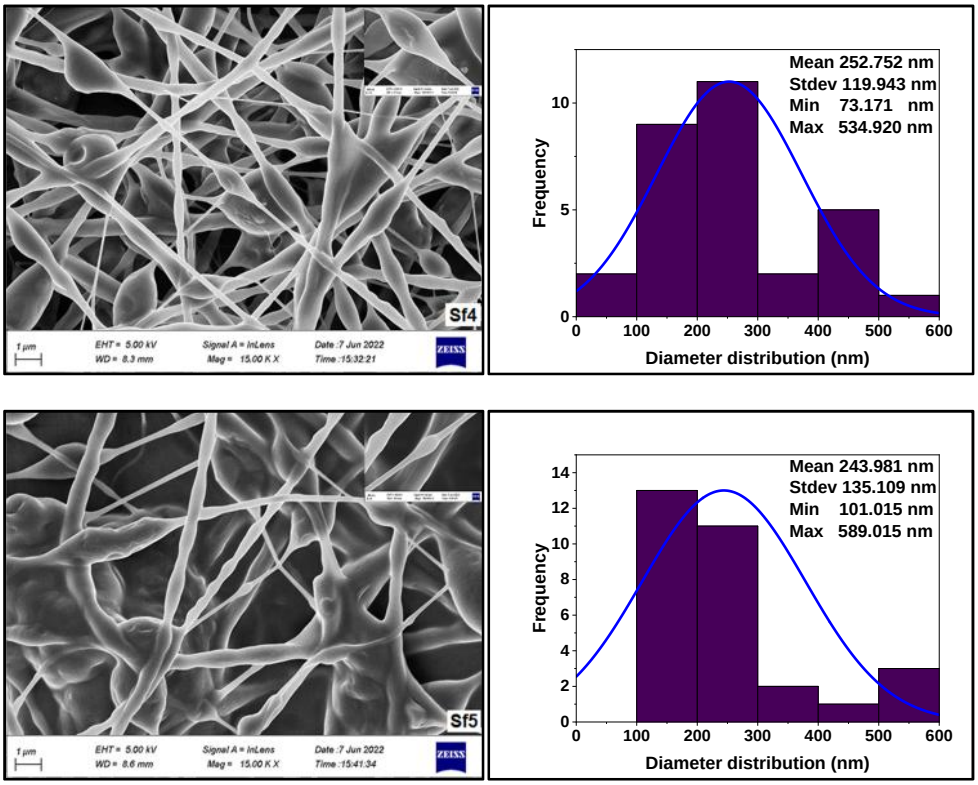

FE-SEM micrographs **Nanofibers diameter distribution histograms**

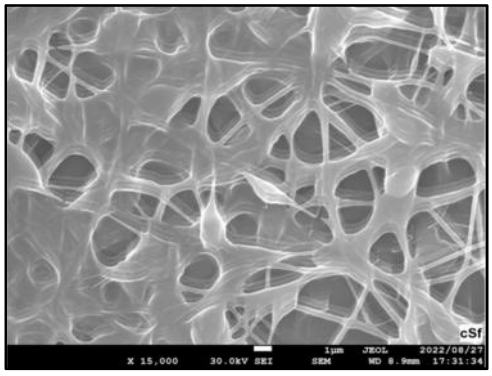

SEM micrographs

Figure (4.15): FESEM Micrographs and Nano-fibers diameter distribution histograms for samples in part three.

Appendix B

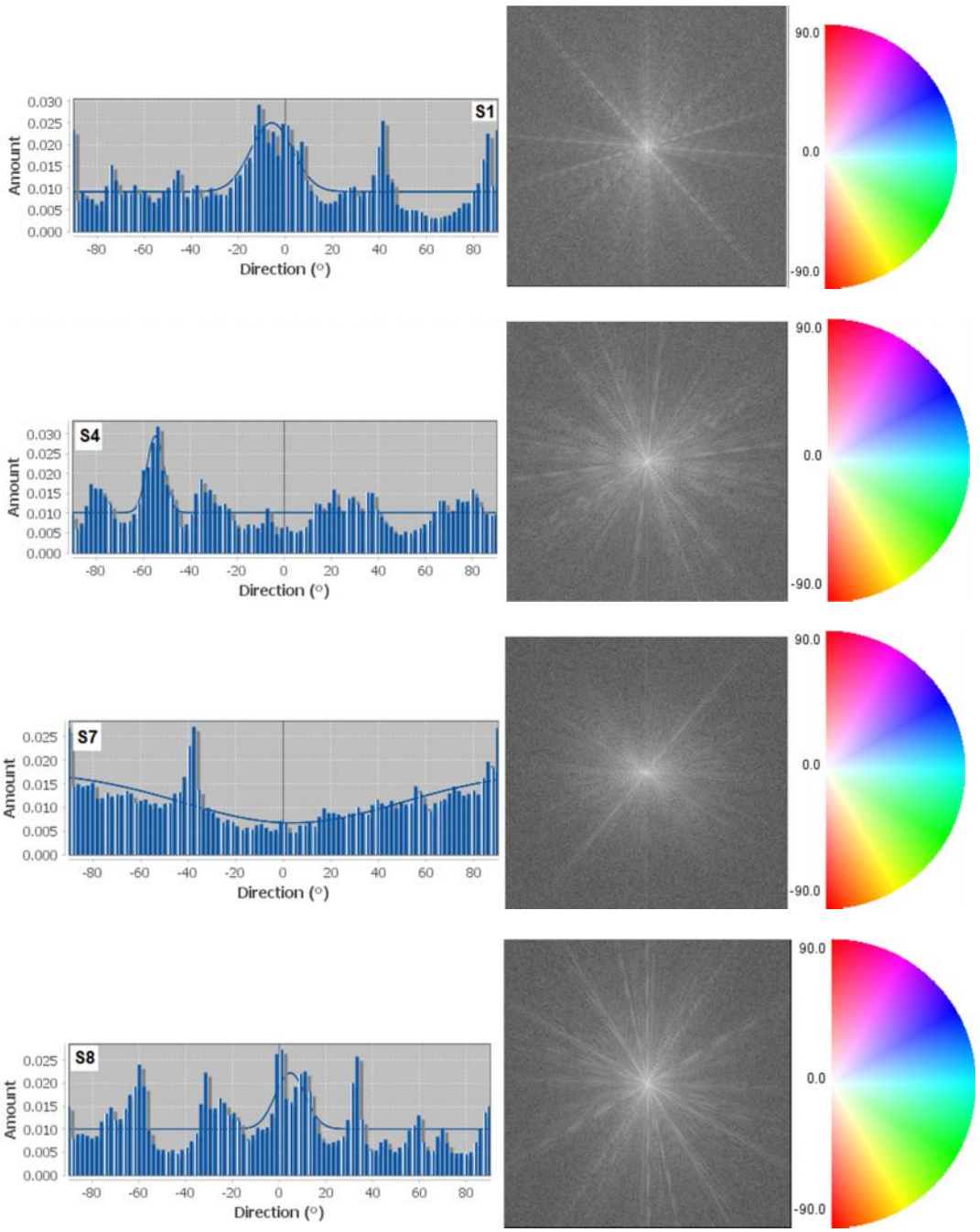

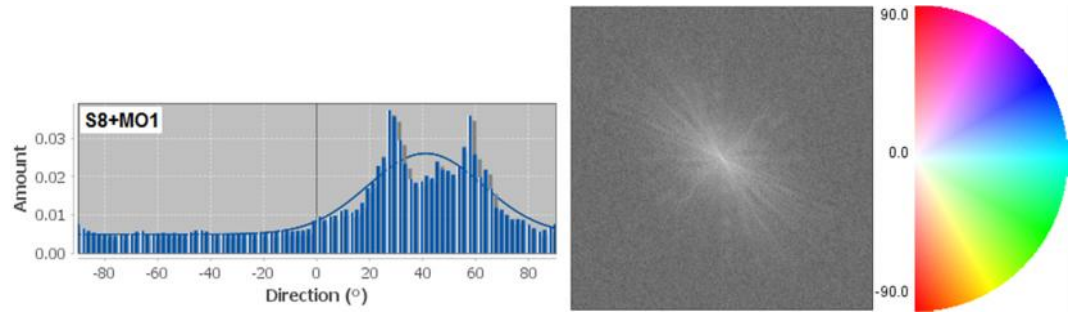
S8+MO1
Amount
0.03
0.02
0.01
0.00
-80 -60 -40 -20 0 20 40 60 80
Direction (°)
90.0
0.0
-90.0

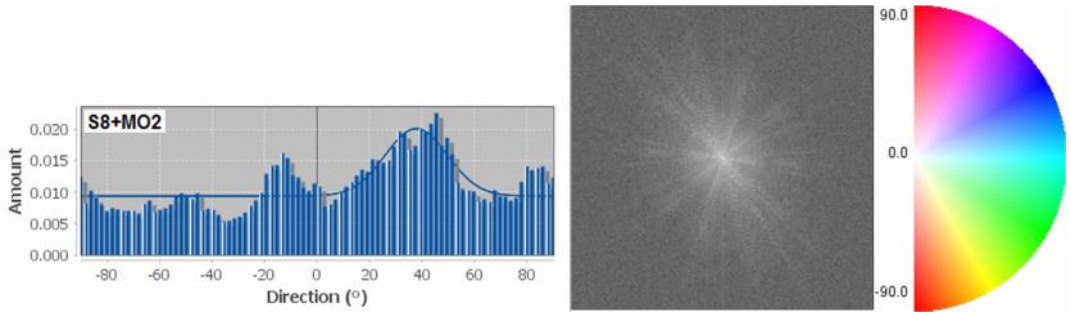
S8+MO2
Amount
0.020
0.015
0.010
0.005
0.000
-80 -60 -40 -20 0 20 40 60 80
Direction (°)
90.0
0.0
-90.0

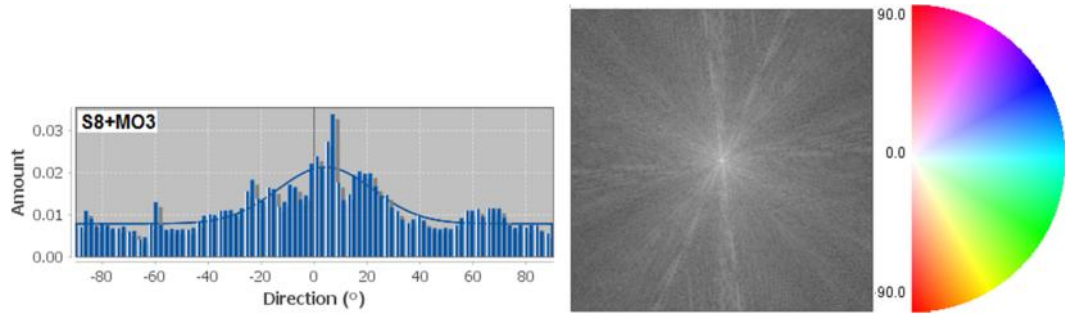
S8+MO3
Amount
0.03
0.02
0.01
0.00
-80 -60 -40 -20 0 20 40 60 80
Direction (°)
90.0
0.0
90.0

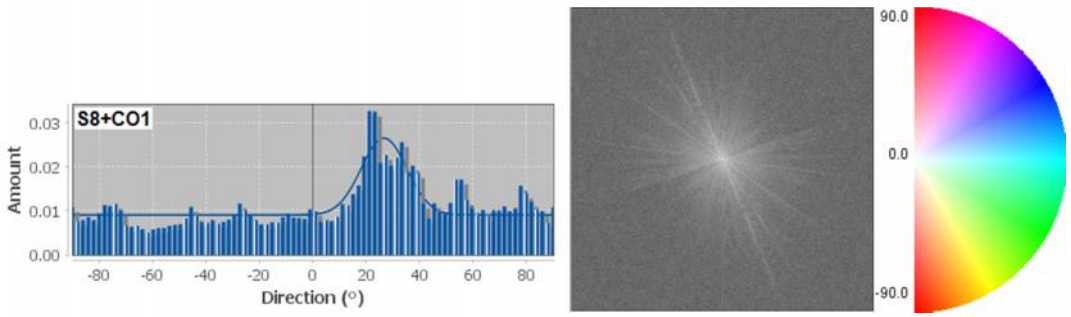
S8+CO1
Amount
0.03
0.02
0.01
0.00
-80 -60 -40 -20 0 20 40 60 80
Direction (°)
90.0
0.0
-90.0

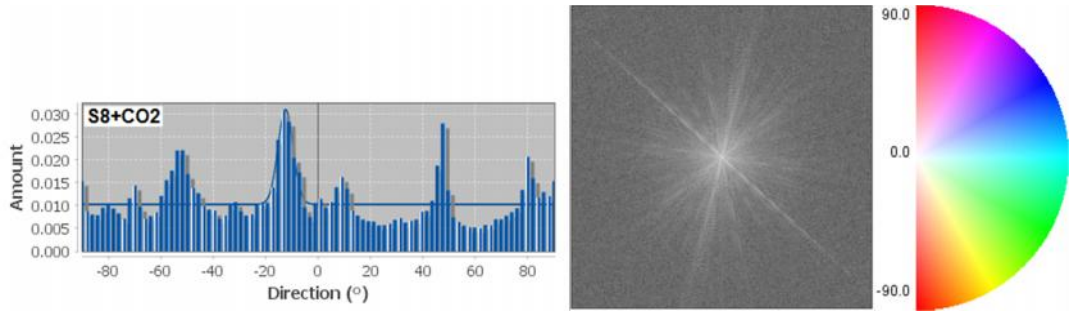
S8+CO2
Amount
0.030
0.025
0.020
0.015
0.010
0.005
0.000
-80 -60 -40 -20 0 20 40 60 80
Direction (°)
90.0
0.0
-90.0

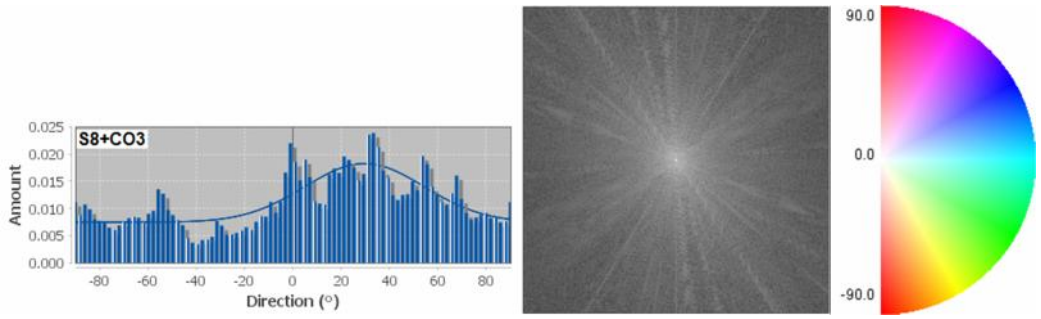
S8+CO3
Amount
0.025
0.020
0.015
0.010
0.005
0.000
-80 -60 -40 -20 0 20 40 60 80
Direction (°)
90.0
0.0
-90.0

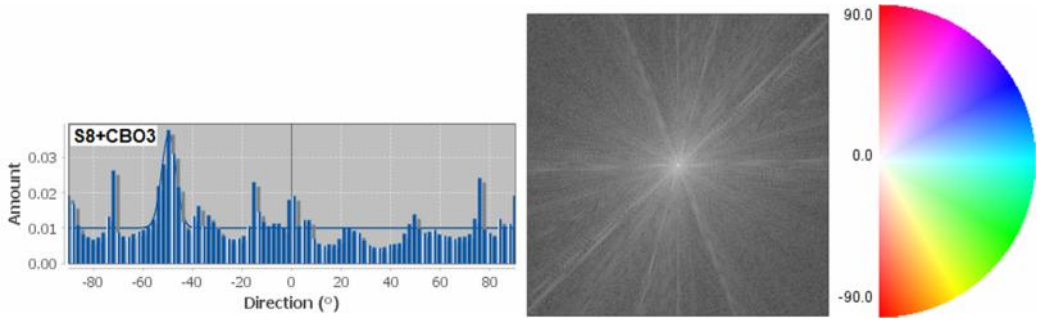
S8+CBO3
Amount
0.03
0.02
0.01
0.00
-80 -60 -40 -20 0 20 40 60 80
Direction (°)
90.0
0.0
-90.0

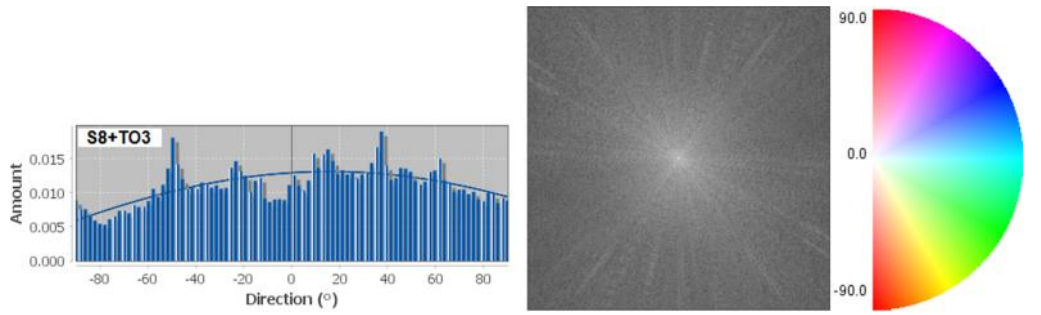
S8+TO3
Amount
0.015
0.010
0.005
0.000
-80 -60 -40 -20 0 20 40 60 80
Direction (°)
90.0
0.0
-90.0

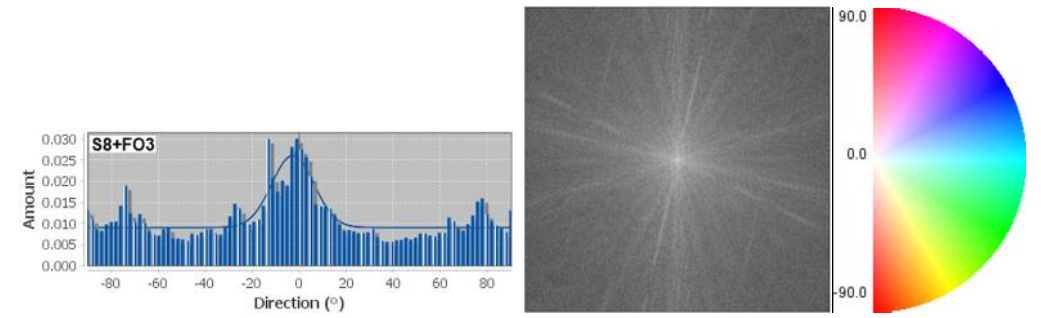
S8+FO3
Amount
0.030
0.025
0.020
0.015
0.010
0.005
0.000
-80 -60 -40 -20 0 20 40 60 80
Direction (°)
90.0
0.0
-90.0

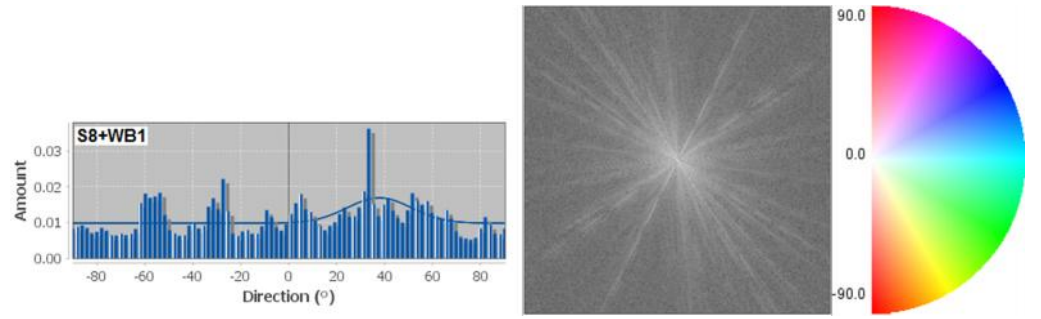
S8+WB1
Amount
0.03
0.02
0.01
0.00
-80 -60 -40 -20 0 20 40 60 80
Direction (°)
90.0
0.0
-90.0

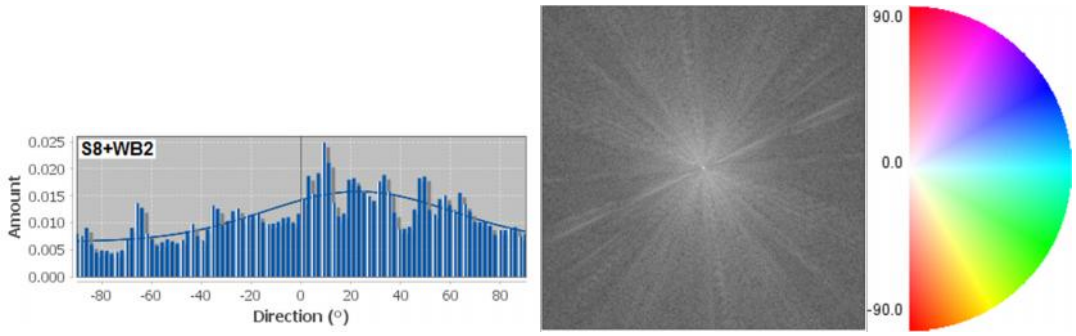
S8+WB2
Amount
0.025
0.020
0.015
0.010
0.005
0.000
-80 -60 -40 -20 0 20 40 60 80
Direction (°)
90.0
0.0
-90.0

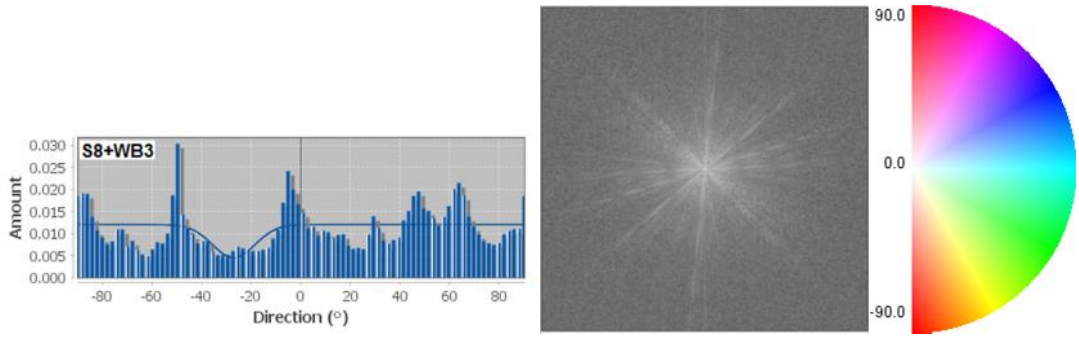
S8+WB3
Amount
0.030
0.025
0.020
0.015
0.010
0.005
0.000
-80 -60 -40 -20 0 20 40 60 80
Direction (°)
90.0
0.0
-90.0

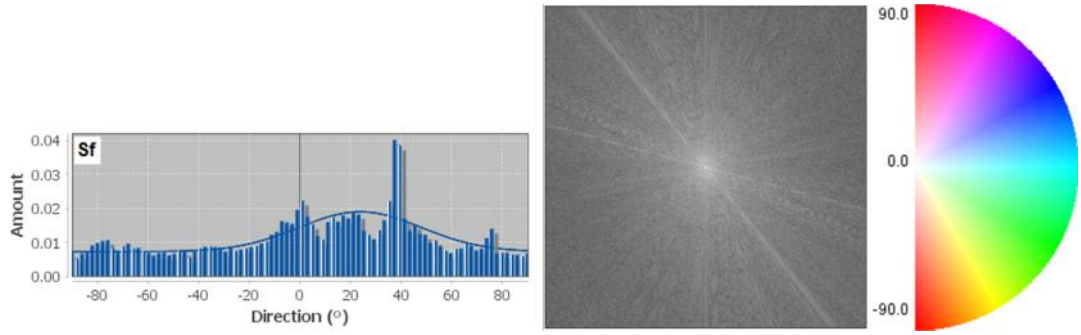
Sf
Amount
0.04
0.03
0.02
0.01
0.00
-80 -60 -40 -20 0 20 40 60 80
Direction (°)
90.0
0.0
-90.0

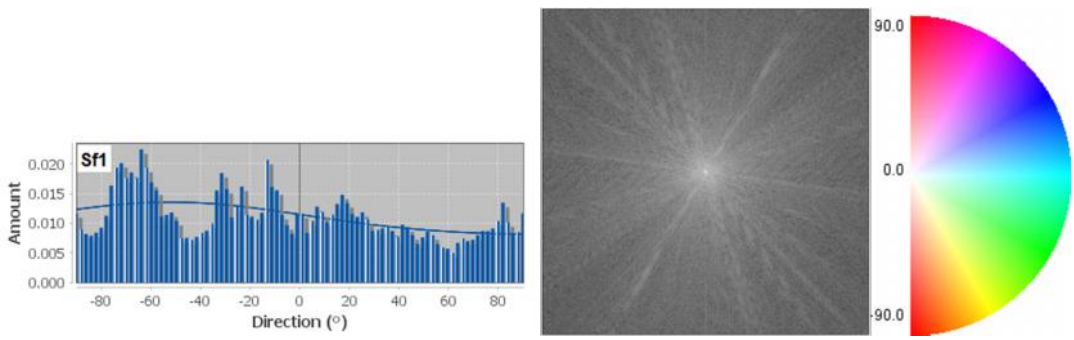
Sf1
Amount
0.020
0.015
0.010
0.005
0.000
-80 -60 -40 -20 0 20 40 60 80
Direction (°)
90.0
0.0
-90.0

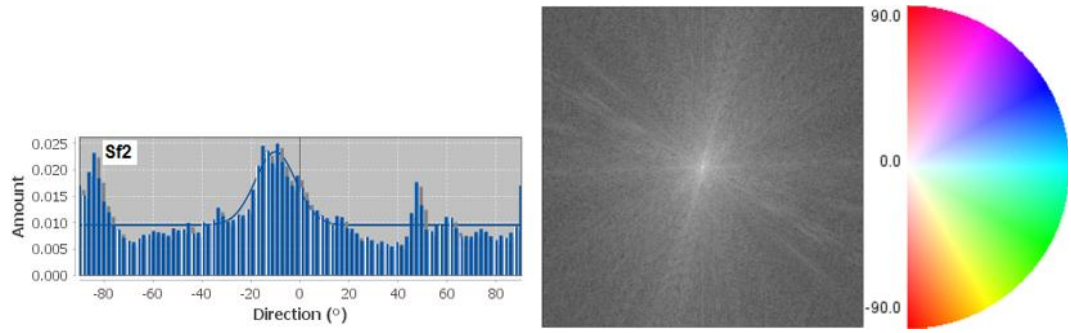
Sf2
Amount
0.025
0.020
0.015
0.010
0.005
0.000
-80 -60 -40 -20 0 20 40 60 80
Direction (°)
90.0
0.0
-90.0

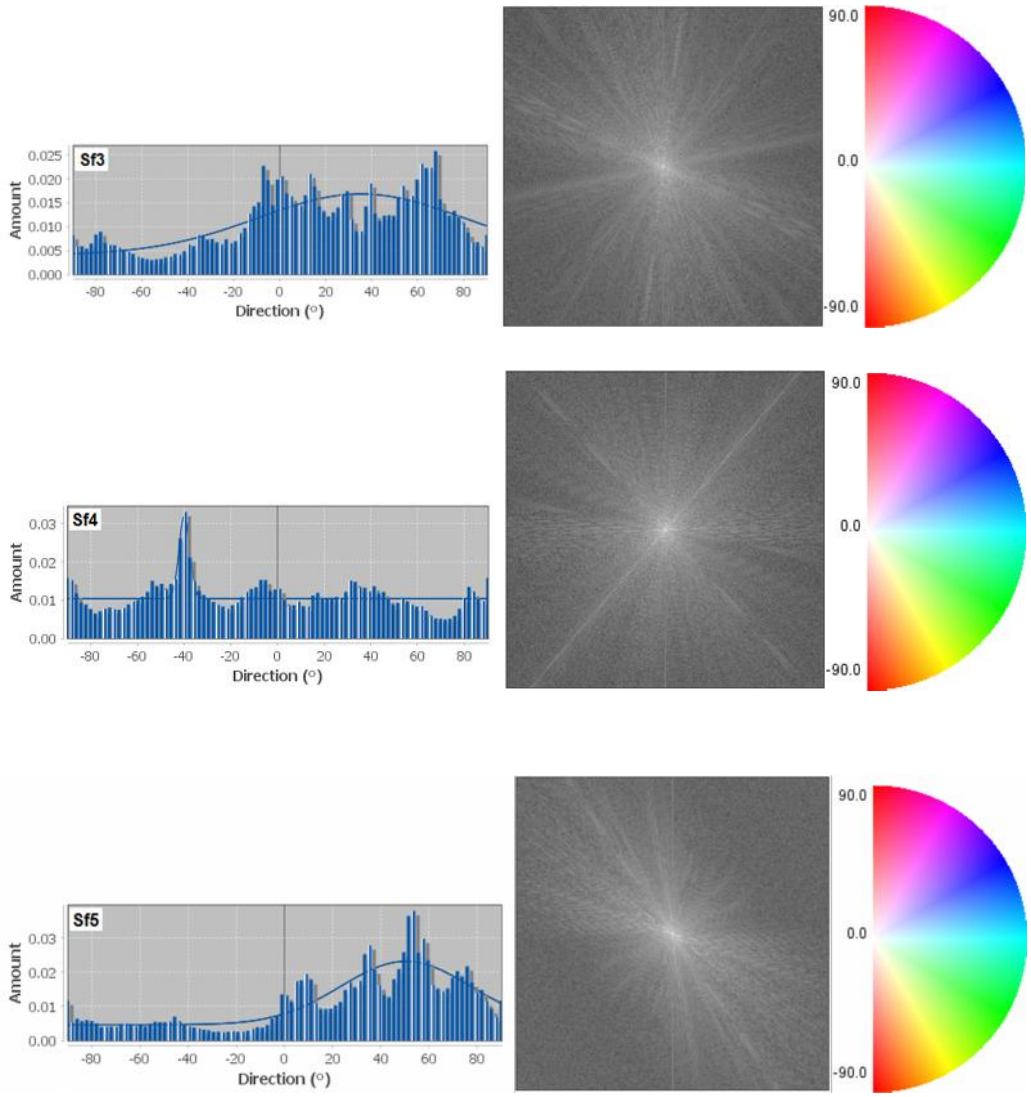

Directionality histograms **2D-FFT**

Figure (4.16): Directionality histogram, and 2D-FFT for samples in all the parts.

Appendix C

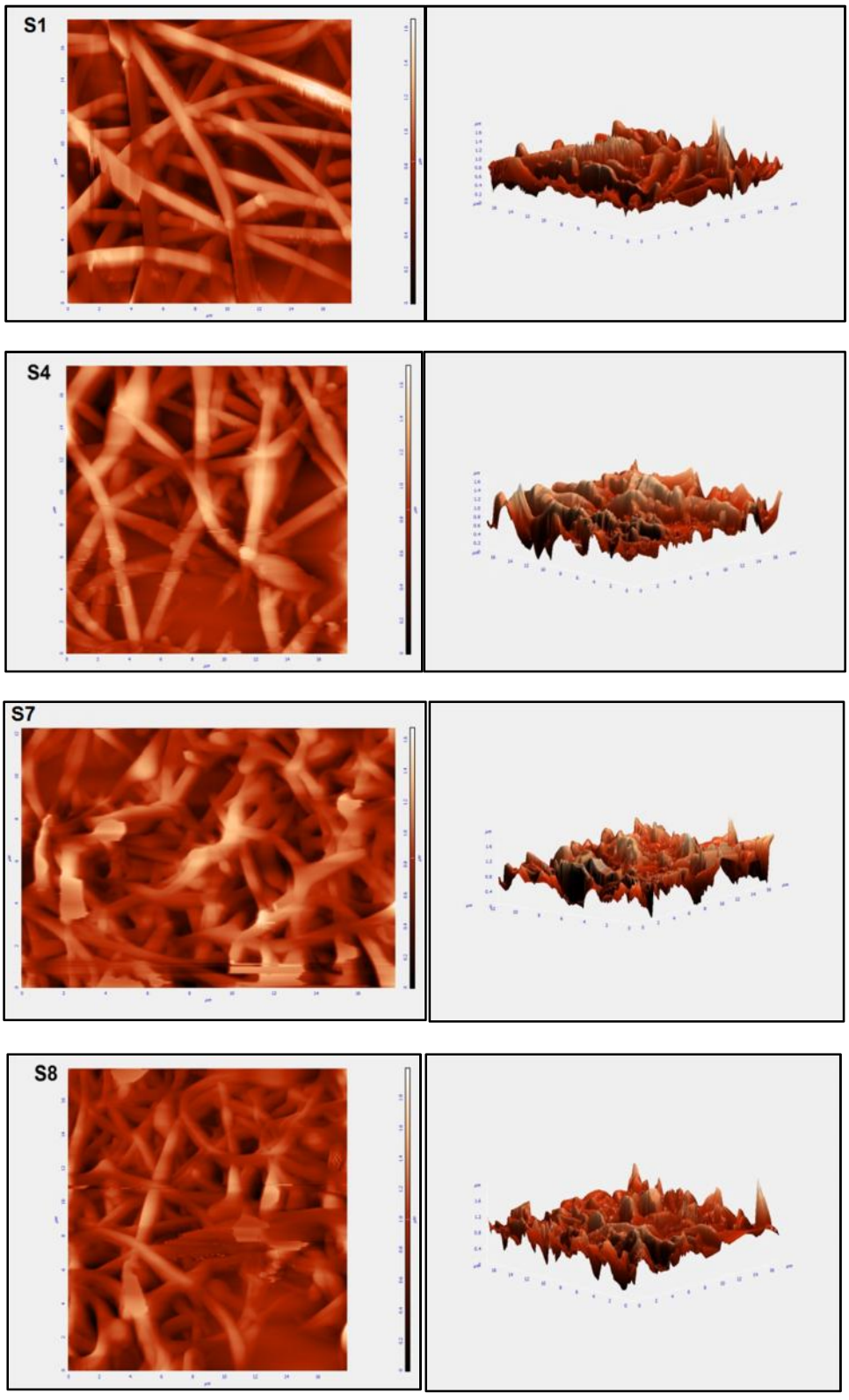

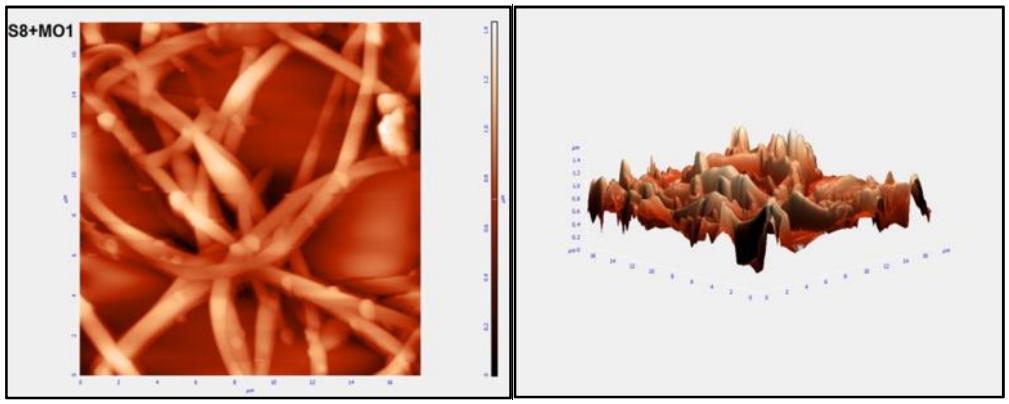
S8+MO1

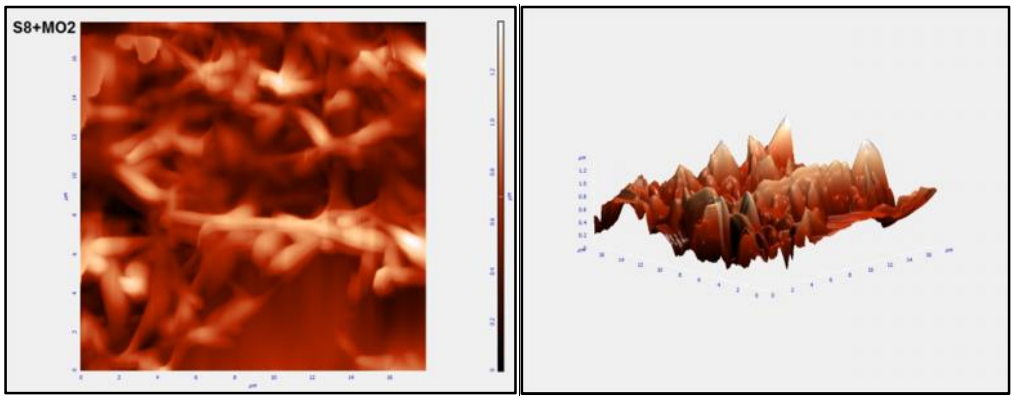
S8+MO2

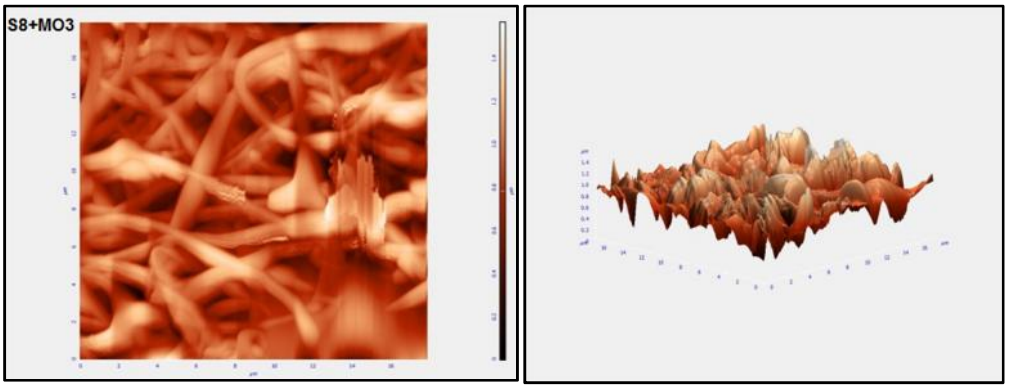
S8+MO3

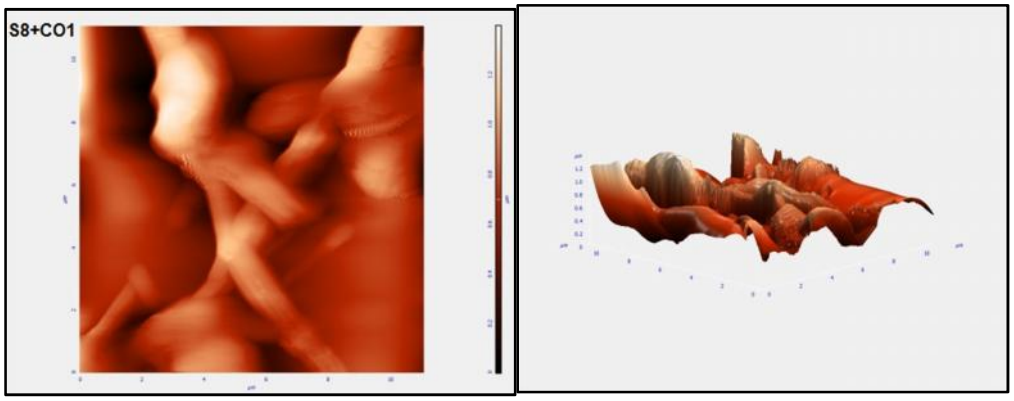
S8+CO1

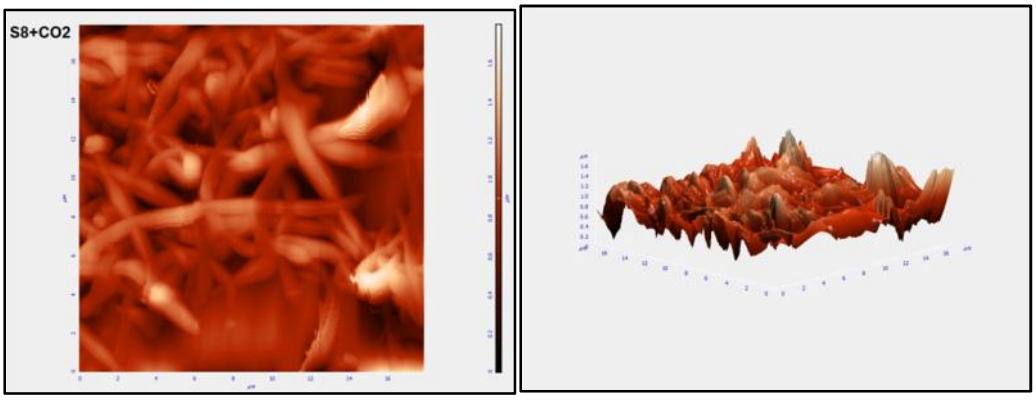
S8+CO2

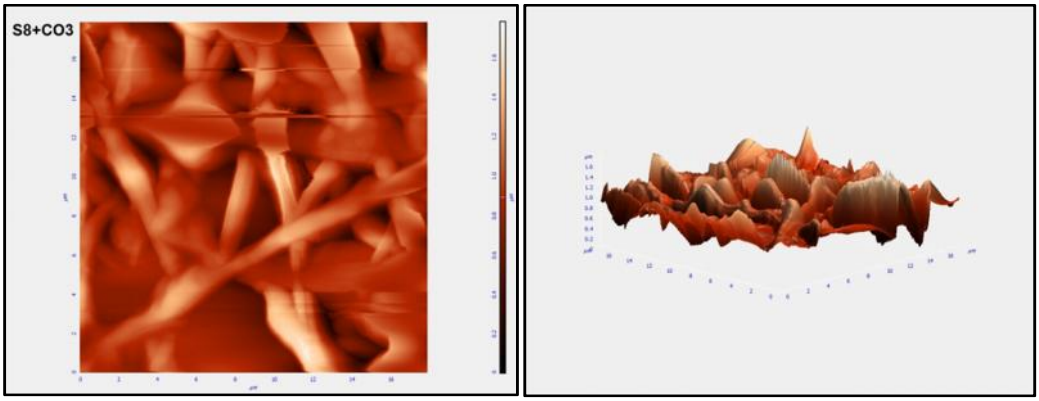
S8+CO3

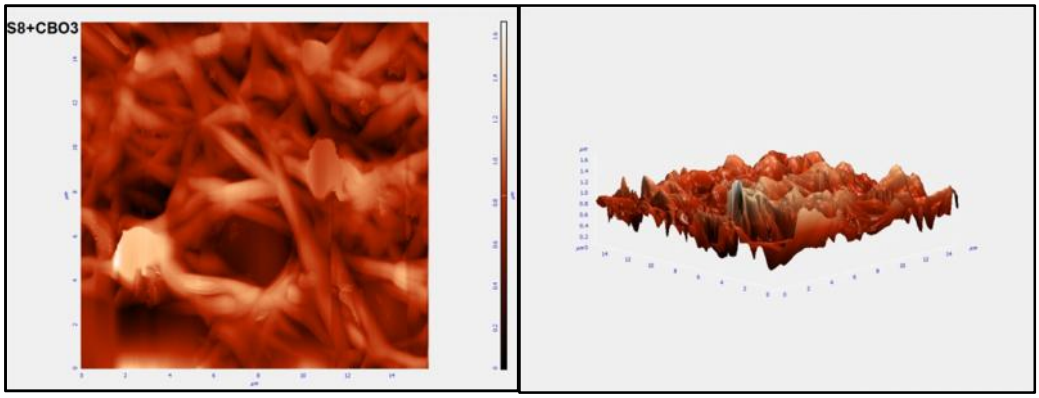
S8+CBO3

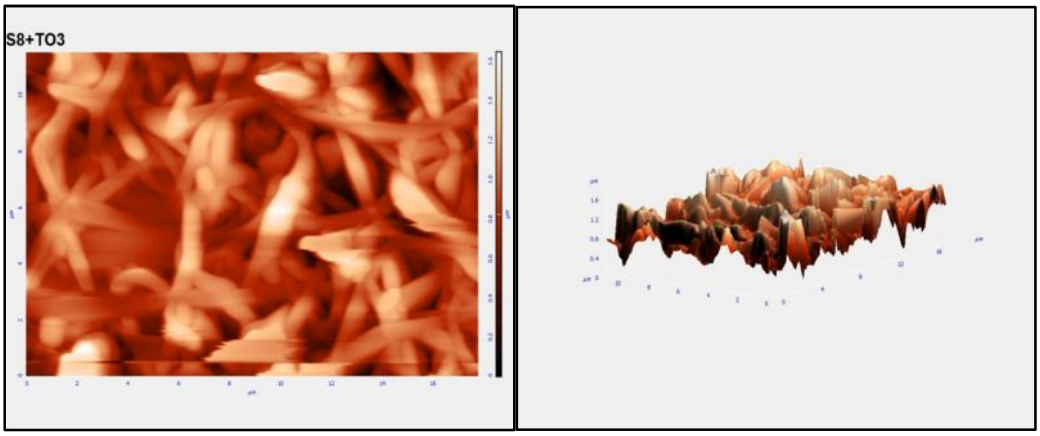
S8+TO3

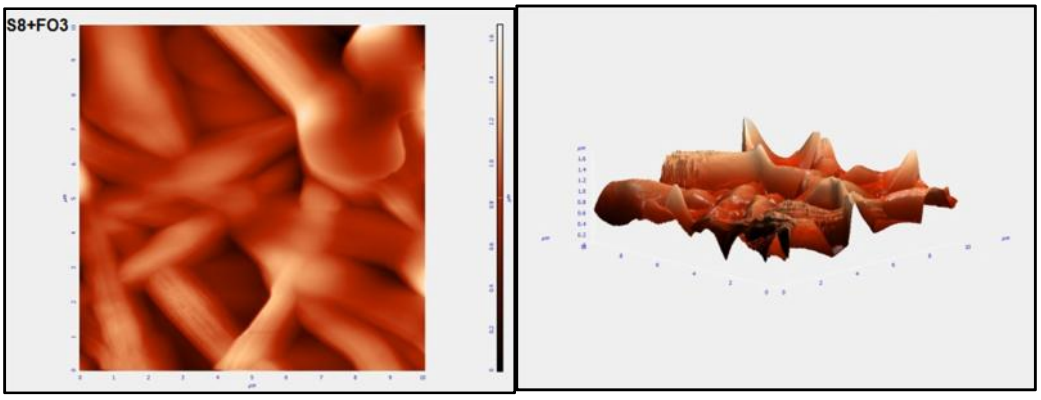
S8+FO3

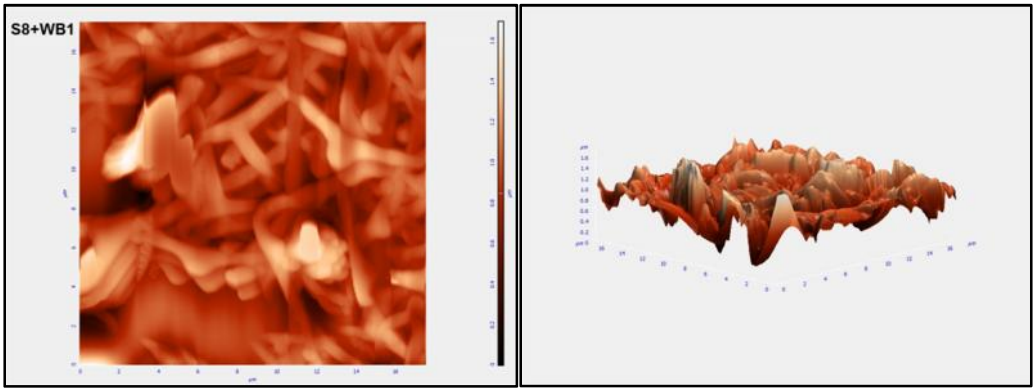
S8+WB1

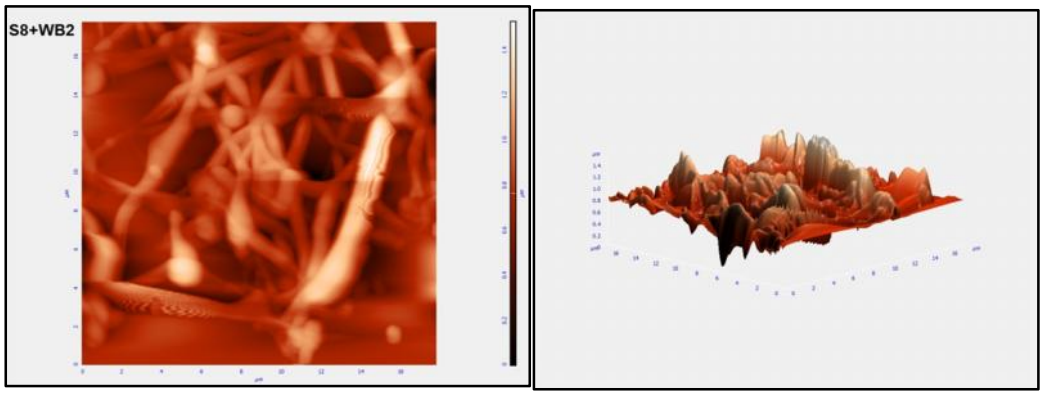
S8+WB2

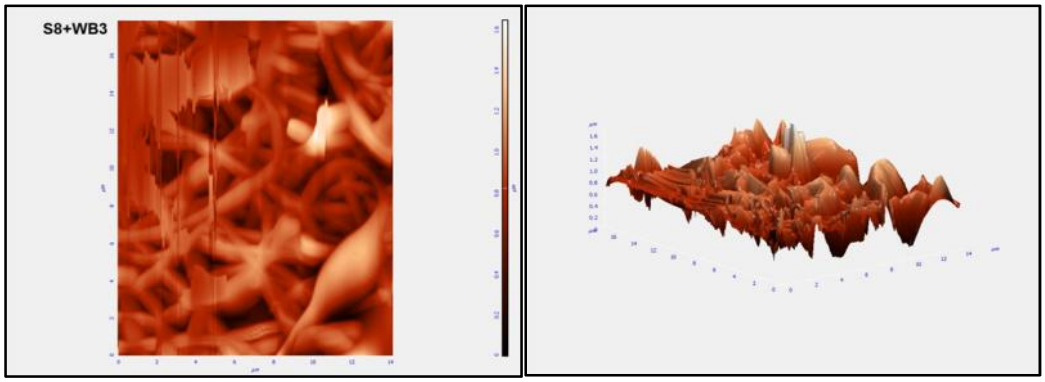
S8+WB3

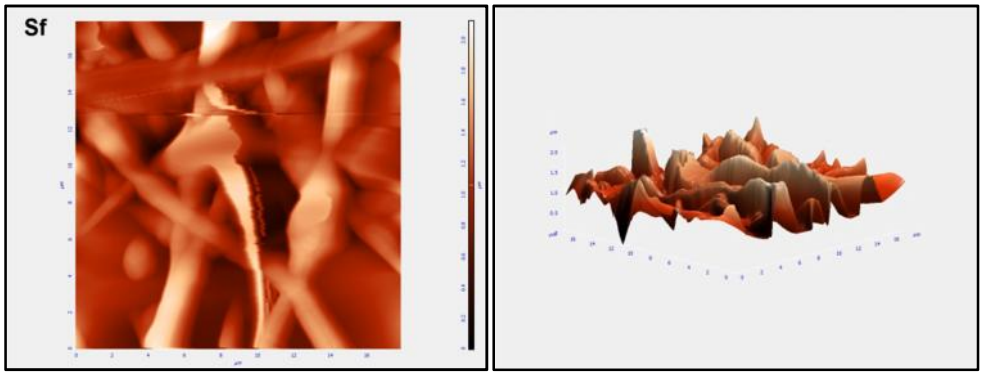

2D **3D**

Figure (4.18): Atomic force microscopy test (2D) and (3D) images for the samples in all parts.

Appendix D

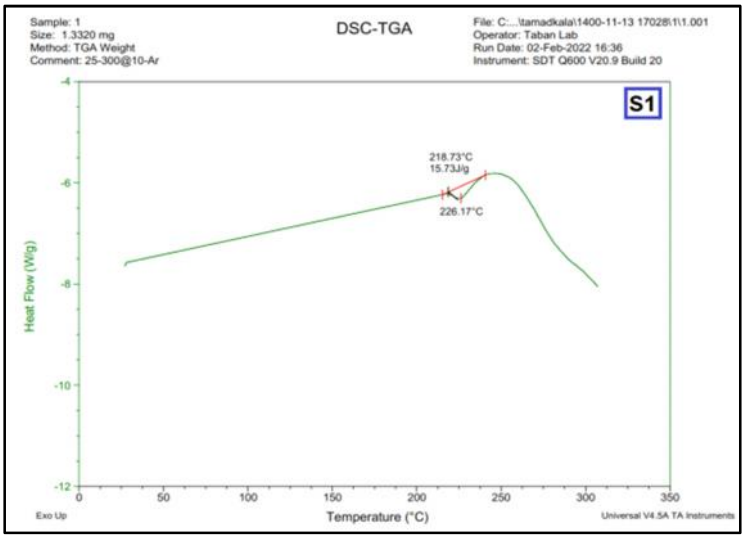
Sample: 1
Size: 1.3320 mg
Method: TGA Weight
Comment: 25-300@10-Ar
DSC-TGA
File: C:...\tamadkala\1400-11-13 17028\1\1.001
Operator: Taban Lab
Run Date: 02-Feb-2022 16:36
Instrument: SDT Q600 V20.9 Build 20
S1
218.73°C
15.73J/g
226.17°C
Heat Flow (W/g)
Temperature (°C)
Exo Up
Universal V4.5A TA Instruments

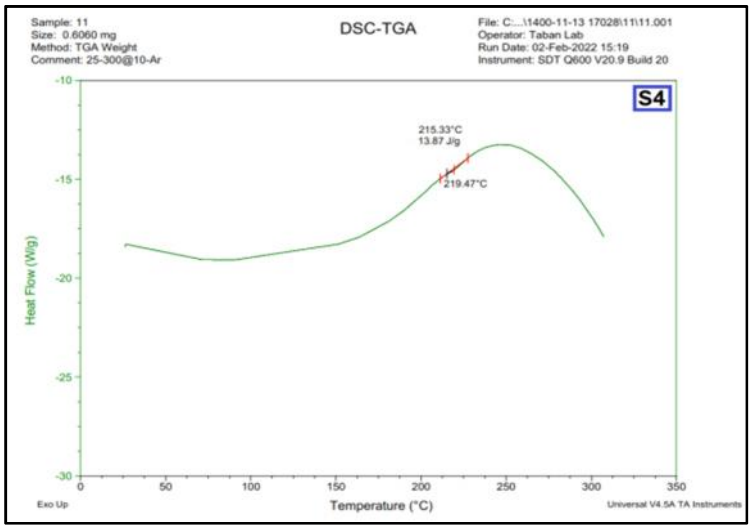
Sample: 11
Size: 0.6060 mg
Method: TGA Weight
Comment: 25-300@10-Ar
DSC-TGA
File: C:...\1400-11-13 17028\11\11.001
Operator: Taban Lab
Run Date: 02-Feb-2022 15:19
Instrument: SDT Q600 V20.9 Build 20
S4
215.33°C
13.87 J/g
219.47°C
Heat Flow (W/g)
Temperature (°C)
Exo Up
Universal V4.5A TA Instruments

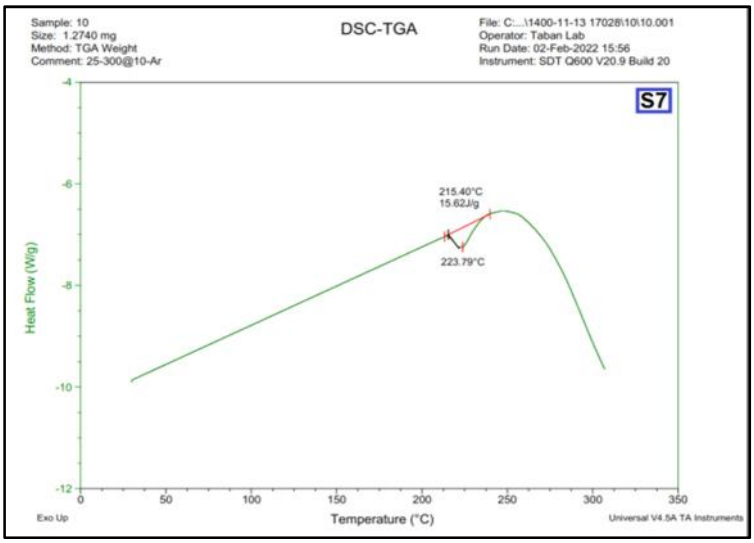
Sample: 10
Size: 1.2740 mg
Method: TGA Weight
Comment: 25-300@10-Ar
DSC-TGA
File: C:...\1400-11-13 17028\10\10.001
Operator: Taban Lab
Run Date: 02-Feb-2022 15:56
Instrument: SDT Q600 V20.9 Build 20
S7
215.40°C
15.62J/g
223.79°C
Heat Flow (W/g)
Temperature (°C)
Exo Up
Universal V4.5A TA Instruments

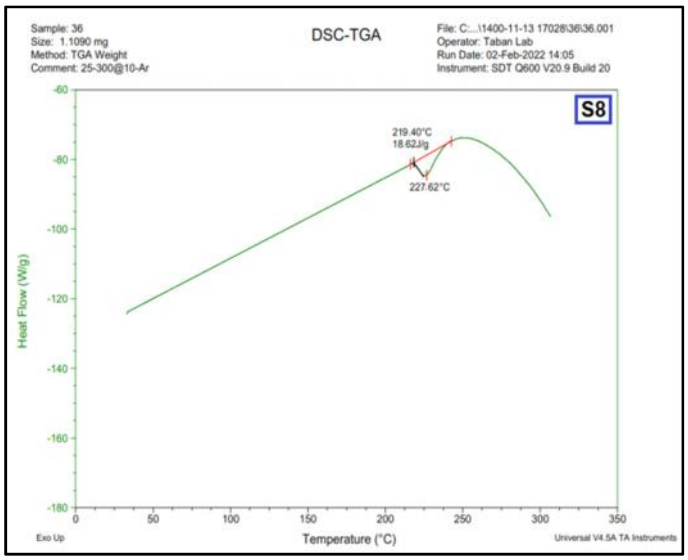
Sample: 36
Size: 1.1090 mg
Method: TGA Weight
Comment: 25-300@10-Ar
DSC-TGA
File: C:...\1400-11-13 17028\36\36.001
Operator: Taban Lab
Run Date: 02-Feb-2022 14:05
Instrument: SDT Q600 V20.9 Build 20
S8
219.40°C
18.62J/g
227.62°C
Heat Flow (W/g)
Temperature (°C)
Exo Up
Universal V4.5A TA Instruments

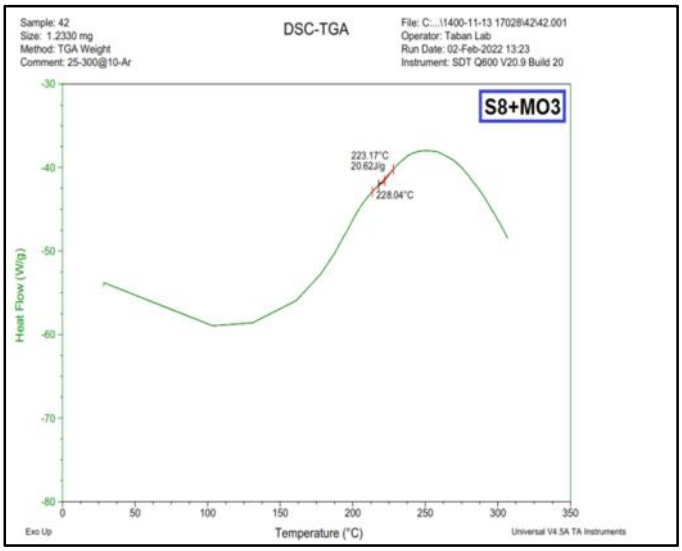
Sample: 42
Size: 1.2330 mg
Method: TGA Weight
Comment: 25-300@10-Ar
DSC-TGA
File: C:...\1400-11-13 17028\42\42.001
Operator: Taban Lab
Run Date: 02-Feb-2022 13:23
Instrument: SDT Q600 V20.9 Build 20
S8+MO3
223.17°C
20.62J/g
228.04°C
Heat Flow (W/g)
Temperature (°C)
Exo Up
Universal V4.5A TA Instruments

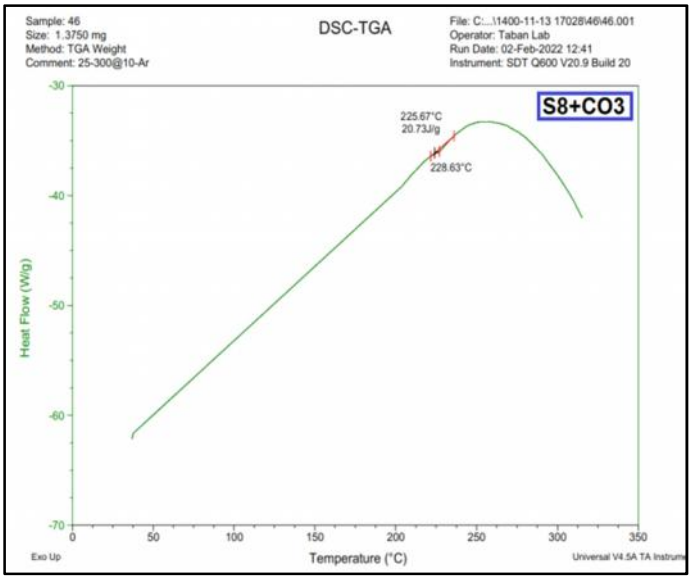
Sample: 46
Size: 1.3750 mg
Method: TGA Weight
Comment: 25-300@10-Ar
DSC-TGA
File: C:...\1400-11-13 17028\46\46.001
Operator: Taban Lab
Run Date: 02-Feb-2022 12:41
Instrument: SDT Q600 V20.9 Build 20
S8+CO3
225.67°C
20.73J/g
228.63°C
Heat Flow (W/g)
Temperature (°C)
Exo Up
Universal V4.5A TA Instrume

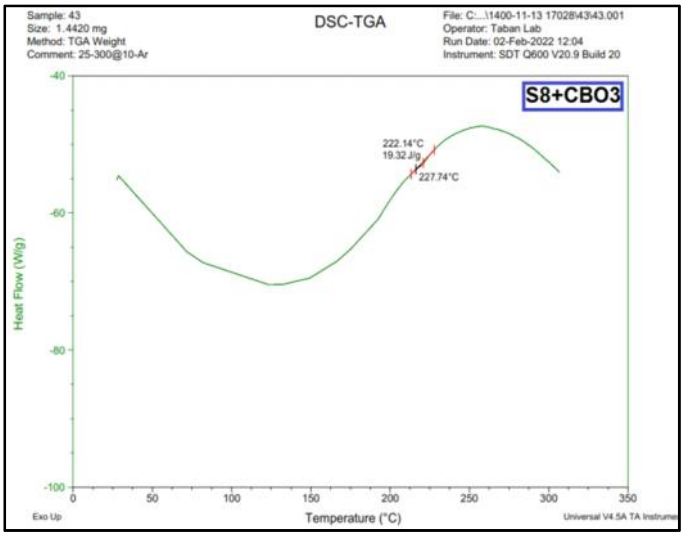
Sample: 43
Size: 1.4420 mg
Method: TGA Weight
Comment: 25-300@10-Ar
DSC-TGA
File: C:...\1400-11-13 17028\43\43.001
Operator: Taban Lab
Run Date: 02-Feb-2022 12:04
Instrument: SDT Q600 V20.9 Build 20
S8+CBO3
222.14°C
19.32 J/g
227.74°C
Heat Flow (W/g)
Exo Up
Temperature (°C)
Universal V4.5A TA Instrume

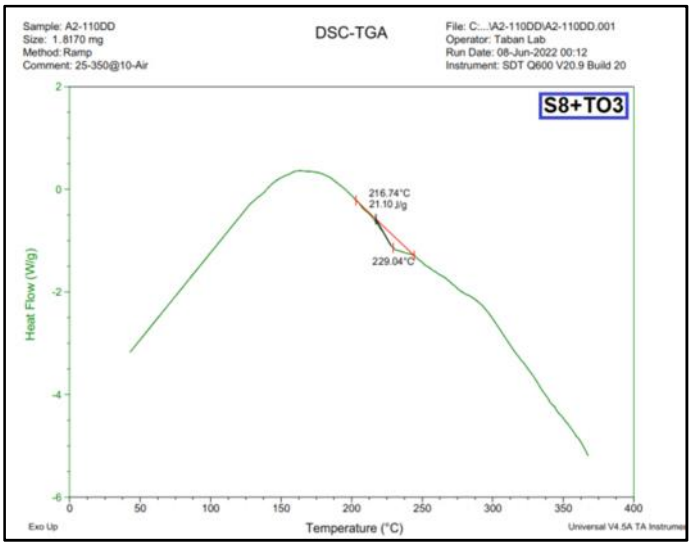
Sample: A2-110DD
Size: 1.8170 mg
Method: Ramp
Comment: 25-350@10-Air
DSC-TGA
File: C:...\A2-110DD\A2-110DD.001
Operator: Taban Lab
Run Date: 08-Jun-2022 00:12
Instrument: SDT Q600 V20.9 Build 20
S8+TO3
216.74°C
21.10 J/g
229.04°C
Heat Flow (W/g)
Exo Up
Temperature (°C)
Universal V4.5A TA Instrume

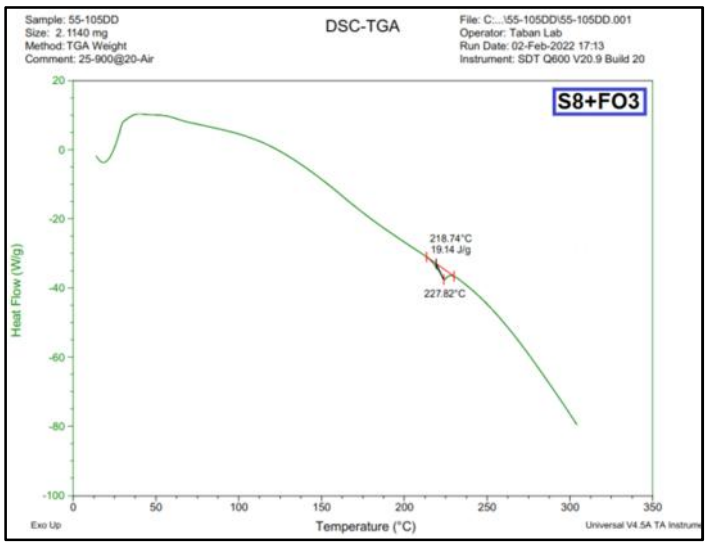
Sample: 55-105DD
Size: 2.1140 mg
Method: TGA Weight
Comment: 25-900@20-Air
DSC-TGA
File: C:...\55-105DD\55-105DD.001
Operator: Taban Lab
Run Date: 02-Feb-2022 17:13
Instrument: SDT Q600 V20.9 Build 20
S8+FO3
218.74°C
19.14 J/g
227.82°C
Heat Flow (W/g)
Exo Up
Temperature (°C)
Universal V4.5A TA Instrume

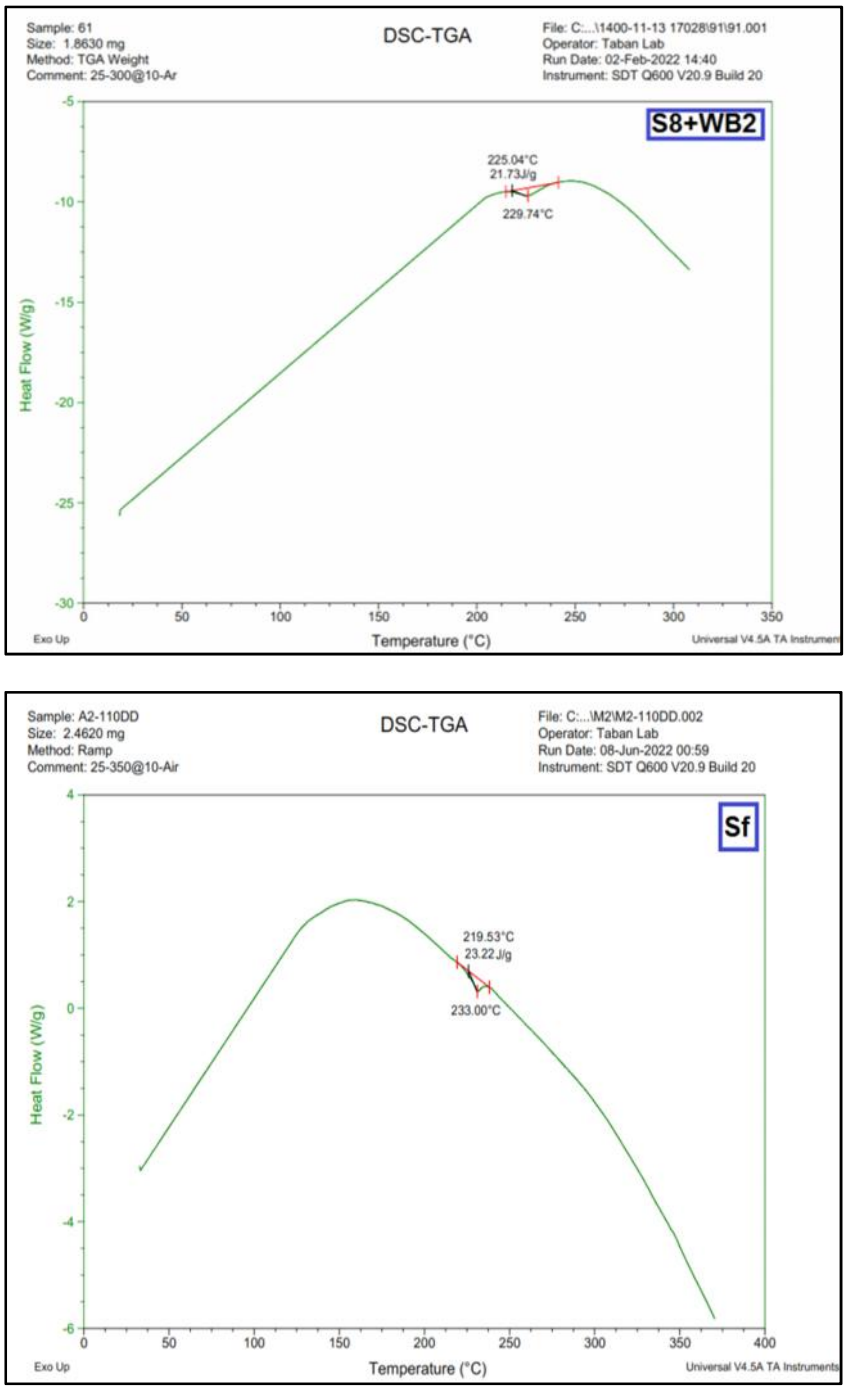

Figure (4.23): DSC curves of samples in all parts.

الخلاصة

في الوقت الحاضر ، تستخدم المواد البوليمرية على نطاق واسع في تطوير عبوات الطعام. خاصة عند زيادة الطلب على جودة وسلامة الغذاء. لذلك كان من الضروري تطوير استراتيجيات تغليف فعالة لإطالة العمر الافتراضي للأغذية. وفي الوقت نفسه ، ركز مجال التعبئة والتغليف على إنتاج مواد وظيفية قادرة على الوصول إلى مزيد من الحماية مثل تثبيط نمو الكائنات الحية الدقيقة ، ومقاومة الأكسدة ، والاستقرار ضد المخاطر البيئية. باستخدام تقنية جديدة الغزل الكهربائي

لذا فإن استخدام طبقة طلاء وظيفي قائم على أساس حيوي على طبقة بوليمرية كمواد لتغليف المواد الغذائية يمكن أن يكون طريقة محتملة لتوفير هذه الحماية للأطعمة.

وبذلك كان الهدف الرئيسي في هذه الدراسة الحالية هو استخدام مواد طبيعية صديقة للبيئة ومذيبات غير سامة لغرض الاستدامة وتقليل استهلاك المواد الاصطناعية. وهكذا تم تحضير ثلاثة أجزاء في هذه الأطروحة. يتكون الجزء الأول من استخدام النشا (STA) وصمغ بذور حب الرشاد (CSM) كمصدر جديد للجزيئات الحيوية الكبيرة والبوليمرات الطبيعية التي لفتت الانتباه في تغليف المواد الغذائية كمزيجين منفصلين مع PVA (البولي فينيل الكحول) الذي يستخدم كمساعد في القدرة على الغزل الكهربائي .

بعد ذلك ، تم دمج المزيجين من (PVA:ST:CSM) في نسب حجميه مختلفة وتم اختيار النسبة الحجمية الافضل (40:30:30) بناءا على أعلى زاوية تماس والتي تعتبر العينة الأساسية لتحضير الجزء الثاني من هذه الدراسة وبعدها تضاف مواد التقويه من الزيوت الأساسية مثل ((زيت المورينجا (MO) ، زيت الهيل (CO) ، زيت برعم القرنفل (CBO) ، زيت الزعتر (TO) ، وزيت الحلبة (FO)) بتركيزات مختلفة (1,5, 10%) بالاضافة الى مسحوق لحاء شجرة الجوز (WB) بنسب وزنية مختلفة (0.3,0.5, 0.7%) وتم فحصها بالمجهر الإلكتروني (FESEM) وفحص قابلية التبلل بالإضافة إلى الاختبارات البيولوجية مثل النشاط المضاد للبكتيريا والنشاط المضاد للأكسدة.

وبناءً على هذه النتائج تم اختيار أفضل نسبة من هذه الإضافات والتي تتمثل ب (10%) من الزيوت الأساسية و (0.5%) من مسحوق لحاءشجرة الجوز (WB). واستخدمت هذه النسب لتحضير الجزء الثالث من هذه الدراسة والذي يمثل المزيج النهائي ودُرست الخصائص التركيبية

والفيزيائية له وذلك عن طريق اجراء الفحص المجهري الإلكتروني (FESEM) واختبار قابلية البلل وفحص (FTIR) وفحص (DSC) وفحص الخشونة السطحية (AFM) وفحص (UV) وفحص حيود الأشعة السينية (XRD) وفحص الاستقرارية الحرارية (TGA). بالإضافة إلى الاختبارات البيولوجية مثل النشاط المضاد للبكتيريا والنشاط المضاد للأكسدة والنشاط المضاد للفطريات واختبار للشد النانوي.

وبينت النتائج زيادة قيمة زاوية التماس (WCA) من (74.049-105.358º) للعينة الأساسية والنهائية على التوالي. بينما زاد متوسط قطر الالياف النانوية من (86.873 - 277.302 nm) وزادت خشونة سطحها اي معامل الخشونة من (159.012- 210.046 nm) للعينة الأساسية والنهائية على التوالي .بالإضافة إلى ذلك ، يتكون شكل العينة النهائية من هياكل متعددة الطبقات يمكن أن تملأ مسلم الأغشية ، وبالتالي تؤثر على نفاذية الهواء لحصيرة الالياف النانوية والتي يمكن اعتبارها مجدية لتطبيقات تغليف المواد الغذائية.

بينما أظهرت نتائج FTIR وجود تداخل فيزيائي فقط بين المكونات ولم تحدث اي تفاعلات كيميائية.

اما بالنسبة للخصائص البيولوجية بينت ان الألياف النانوية للعينة الأساسية لا تمتلك خصائص مضادة للبكتيريا ومضادة للفطريات ، بينما اظهرت الألياف النانوية التي تحتوي على جميع الإضافات نشطًا مضادًا للبكتيريا حوالي (20%) ضد (S. aureus) و (37%) ضد (E. coli) ونشطا مضادا للفطريات ضد بكتيريا (candida) حوالي (18%).

بالإضافة إلى ذلك ، أدى دمج جميع الإضافات في العينة الأساسية إلى تحسين مضادات الأكسدة للألياف النانوية المتولدة. وكانت كمية تثبيط الألياف النانوية للعينة الاساسية (37٪) وزادت إلى (55%) للعينة النهائية. وقد لوحظت زيادة في معامل المرونة من اختبار الشد النانوي أدت الى زيادة قوة الشد وهذه الخصائص الميكانيكية من الخصائص الضرورية للتغليف الفعال للاحتفاظ بشكله تحت تحميل الطعام وأثناء تخزينه.

واخيرا تم دراسة توافقية الالياف الناتجة من خلال تعبئة الفواكه والخضروات المختلفة في عبوات بلاستيكية وإغلاقها بواسطة الالياف النانوية للعينة النهائية واخرى بدونها. وابقائها لمدة زمنية محددة والتي تمثلت بعشرة أيام في درجة حرارة الغرفة.

بعد هذه الفترة استنتج أن الفواكه والخضروات المغلفة بواسطة الالياف النانوية أظهرت نضارة أفضل مقارنة بتلك التي لا تحتوي على ألياف نانوية. وبالتالي بينت جميع نتائج الاختبارات التي تم إجراؤها ، أن الالياف النانوية النهائية تمتلك ما يكفي من الخواص المورفولوجية والتركيبية والبيولوجية والميكانيكية والفيزيائية لاستخدامها في تغليف المواد الغذائية.

جمهورية العراق
وزارة التعليم العالي والبحث العلمي
جامعـــــــــة بابـــــــــل
كليـــــــــة هنـــــــــدسة المواد
قسم البوليمرات والصناعات البتروكيمياوية

تحضير وتوصيف ألياف نانوية بتقنية الغزل الكهربائي مضادة للبكتريا لتطبيقات تغليف المواد الغذائية

رسالة

مقدمه إلى قسم هندسة البوليمر والصناعات البتروكيمياوية في
كلية هندسة المواد/ جامعة بابل
وهي جزء من متطلبات نيل درجة الدكتوراه فلسفة في هندسة المواد/البوليمر

من قبل

رسل محمد عبد الرضا فليح

بإشراف

أ.د. هناء جواد كاظم

أ.د. علي عبد الامير الزبيدي

٢٠٢٢م

١٤٤٤ هـ